MA 80-27,I

REPORT NO.   UMTA-MA-06-0100-80-4

IMPROVED DESIGN OF TUNNEL SUPPORTS:
VOLUME 1 - SIMPLIFIED ANALYSIS FOR GROUND-STRUCTURE INTERACTION IN TUNNELING

Charles W. Schwartz
Herbert H. Einstein

MASSACHUSETTS INSTITUTE OF TECHNOLOGY
Department of Civil Engineering
Cambridge MA   02139

JUNE 1980
FINAL REPORT

Prepared for

1. Report No. UMTA-MA-06-0100-80-4	2. Government Accession No.	3. Recipient's Catalog No.

4. Title and Subtitle IMPROVED DESIGN OF TUNNEL SUPPORTS: VOLUME 1 - SIMPLIFIED ANALYSIS FOR GROUND- STRUCTURE INTERACTION IN TUNNELING	5. Report Date June 1980
	6. Performing Organization Code

7. Author's) C.W. Schwartz, H. H. Einstein	8. Performing Organization Report No. DOT-TSC-UMTA-80-27.I

9. Performing Organization Name and Address Massachusetts Institute of Technology* Department of Civil Engineering Cambridge, MA 02139	10. Work Unit No. (TRAIS) UM048/R0720
	11. Contract or Grant No. DOT-TSC-1489
	13. Type of Report and Period Covered

12. Sponsoring Agency Name and Address U.S. Department of Transportation Urban Mass Transportation Administration Office of Technology Development & Deployment Office of Rail and Construction Technology Washington DC 20590	Final Report (Vol. 1) January 1978-August 1979
	14. Sponsoring Agency Code

16. Abstract

It is doubtful that the complex interrelationships among the nearly countless variables in any real tunneling problem can ever be rigorously analyzed, even using the most sophisticated numerical techniques. As an alternative approach, the simplified method focuses on the essential elements of very complicated physical phenomena in order to isolate the major factors that have an overriding influence on support loads. These factors are as follows:

1) relative stiffness of the support and ground mass
2) spatial lag or delay of support construction behind tunnel face
3) yielding of ground mass as its shear strength is exceeded.

Using these factors, the intent of Volume 1 is to provide an analysis in which accentuated computational ease, coupled with sufficient accuracy, makes the simplified method a valuable and effective design tool.

This is the first of five volumes published on the Improved Design of Tunnel Supports. The Executive Summary of the five-volume report was published in December, 1979 (Report No. UMTA-MA-06-0100-79-15).

The remaining final reports published in this five-volume series are:

Volume 2 - Aspects of Yielding in Ground-Structure Interaction
Volume 3 - Finite Element Analysis of the Peachtree Center Station in Atlanta
Volume 4 - Tunneling Practices in Austria and Germany
Volume 5 - Empirical Methods in Rock Tunneling -- Review and Recommendations

17. Key Words Tunneling, Support Design, Ground-Structure Interaction	18. Distribution Statement DOCUMENT IS AVAILABLE TO THE PUBLIC THROUGH THE NATIONAL TECHNICAL INFORMATION SERVICE, SPRINGFIELD, VIRGINIA 22161

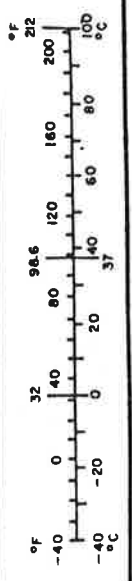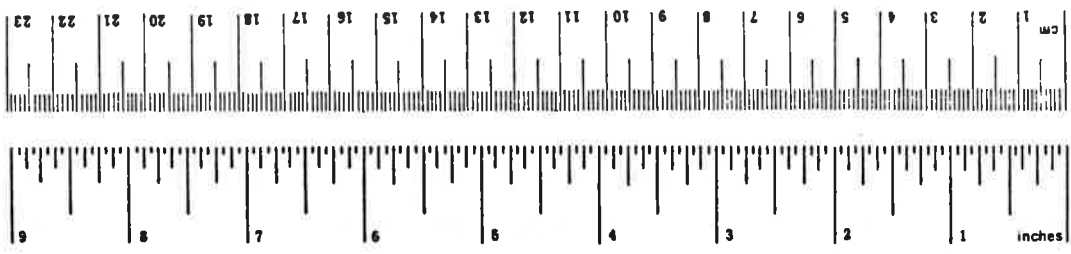| 19. Security Classif. (of this report) UNCLASSIFIED	20. Security Classif. (of this page) UNCLASSIFIED	21. No. of Pages 450	22. Price

PREFACE

This report is the first of five publications (the Executive Summary of this five-volume report was published in December, 1979) which included the results of an extensive research effort by the Massachusetts Institute of Technology (MIT) to improve the design methodologies available to tunnel designers. The contract DOT-TSC-1489, was funded by the U.S. Department of Transportation (DOT) and was sponsored by the Urban Mass Transportation Administration's (UMTA) Office of Rail and Construction Technology. The contract was monitored by the Transportation Systems Center (TSC) Construction and Engineering Branch.

This report deals with a simplified analysis for ground-structure interaction in tunneling, which is necessary because of the indeterminate relationships which describe the realm of tunneling parameters. Using a few major factors that have an overriding influence on the support loads, the intent was to provide an analysis which accentuated computational ease, coupled with sufficient accuracy to make the simplified method a valuable and effective tool.

METRIC CONVERSION FACTORS

Approximate Conversions to Metric Measures

Symbol	When You Know	Multiply by	To Find	Symbol
	LENGTH			
in	inches	*2.5	centimeters	cm
ft	feet	30	centimeters	cm
yd	yards	0.9	meters	m
mi	miles	1.6	kilometers	km
	AREA			
in²	square inches	6.5	square centimeters	cm²
ft²	square feet	0.09	square meters	m²
yd²	square yards	0.8	square meters	m²
mi²	square miles	2.6	square kilometers	km²
	acres	0.4	hectares	ha
	MASS (weight)			
oz	ounces	28	grams	g
lb	pounds	0.45	kilograms	kg
	short tons (2000 lb)	0.9	tonnes	t
	VOLUME			
tsp	teaspoons	5	milliliters	ml
Tbsp	tablespoons	15	milliliters	ml
fl oz	fluid ounces	30	milliliters	ml
c	cups	0.24	liters	l
pt	pints	0.47	liters	l
qt	quarts	0.95	liters	l
gal	gallons	3.8	liters	l
ft³	cubic feet	0.03	cubic meters	m³
yd³	cubic yards	0.76	cubic meters	m³
	TEMPERATURE (exact)			
°F	Fahrenheit temperature	5/9 (after subtracting 32)	Celsius temperature	°C

*1 in = 2.54 (exactly). For other exact conversions and more detailed tables, see NBS Misc. Publ. 286, Units of Weights and Measures, Price $2.25, SD Catalog No. C13.10:286.

Approximate Conversions from Metric Measures

Symbol	When You Know	Multiply by	To Find	Symbol
	LENGTH			
mm	millimeters	0.04	inches	in
cm	centimeters	0.4	inches	in
m	meters	3.3	feet	ft
m	meters	1.1	yards	yd
km	kilometers	0.6	miles	mi
	AREA			
cm²	square centimeters	0.16	square inches	in²
m²	square meters	1.2	square yards	yd²
km²	square kilometers	0.4	square miles	mi²
ha	hectares (10,000 m²)	2.5	acres	
	MASS (weight)			
g	grams	0.035	ounces	oz
kg	kilograms	2.2	pounds	lb
t	tonnes (1000 kg)	1.1	short tons	
	VOLUME			
ml	milliliters	0.03	fluid ounces	fl oz
l	liters	2.1	pints	pt
l	liters	1.06	quarts	qt
l	liters	0.26	gallons	gal
m³	cubic meters	35	cubic feet	ft³
m³	cubic meters	1.3	cubic yards	yd³
	TEMPERATURE (exact)			
°C	Celsius temperature	9/5 (then add 32)	Fahrenheit temperature	°F

°F -40   0   32   80   98.6   120   160   200   212 °F
°C -40 -20   0   20   37   40   60   80   100 °C

TABLE OF CONTENTS

TABLE OF CONTENTS (CONTINUED)

TABLE OF CONTENTS (CONTINUED)

LIST OF ILLUSTRATIONS

LIST OF ILLUSTRATIONS (CONTINUED)

LIST OF ILLUSTRATIONS (CONTINUED)

LIST OF TABLES

1. INTRODUCTION

Tunnel construction is undeniably an expensive endeavor. Recent bids for a 4325 ft. long section of twin mined tunnels for the Red Line subway extension in Boston were in excess of $47 million, or over $5400 per foot of tunnel. Support of these tunnels represented a substantial portion--25%--of this total cost. In general, the cost of the tunnel supports will be an even larger portion of the total project costs than these Red Line figures would indicate; a survey by Tse (1979) found that the ratio of support costs to total costs averaged 30-35% for tunnels in urban environments and up to 40% for deep-lying tunnels in mountainous regions. Clearly there is a great economic incentive for developing more efficient and less costly tunnel support designs.

A significant number of empirical and analytical methods for the design of tunnel supports are readily available today. Many of the more sophisticated analytical methods, like finite element analysis, can handle ground and support characteristics of great complexity, provided the appropriate input information is available. Empirical methods, on the other hand, bypass this need for accurate and detailed input information by directly relating the support requirements to easily measured ground properties or to qualitative geologic

1

descriptions; however, this approach usually results in a substantial and indeterminable amount of overdesign. Both approaches have applications to which they are best suited, but there exists a definite need for a third type in which limited quantitative data could be interpreted quickly and simply within a rational analytical framework. These simpler analytical methods would supplement the empirical design methods when more detailed geotechnical information is available and would permit the designer to rapidly investigate a range of possible support alternatives. They could, for example, incorporate information obtained from the exploration program into the design for the initial supports and the preliminary design of the final supports; more important, these methods could aid in the evaluation of monitoring measurements and adaptation of the initial supports during construction.

The purpose of the research reported here has been to develop this third type of simplified, design-oriented method for determining the loads on tunnel supports. Naturally, since the range of tunneling conditions encountered in practice and the different design and construction methods devised to deal with them are so diverse, some limitations must be imposed to make the problem tractable. Accordingly, the simplified analysis method developed herein is generally intended for circular tunnels with closed-ring primary support systems in ground masses that can for practical

purposes be treated as time-independent continua. The method is also restricted to tunnels that are excavated full-face under free air at depths greater than about two tunnel diameters. Many types of practical tunneling situations satisfy these requirements and are amenable to analysis by the simplified method; examples include--but are not limited to--tunnels in soil, heavily jointed rock, and massive rock formations supported with circular steel ribs, prefabricated segmented liners, and continuous shotcrete.

It is doubtful that the complex interrelationships among the nearly countless variables influencing the ground-structure interaction around a tunnel can ever be rigorously analyzed, even using the most sophisticated numerical techniques. As an alternative approach, the simplified analysis method reduces this very complicated physical phenomenon to its essential elements, the few major factors that have an overriding influence on the support loads. The three major factors explicitly considered in the analysis are: (1) the relative stiffnesses of the support and the ground mass, (2) the spatial lag or delay of support construction behind the tunnel face, and (3) the yielding of the the ground mass as its shear strength is exceeded. The influence of each of these variables on the support loads is studied in detail, and the investigation of their combined effects forms the foundation for the simplified analysis method.

3

Since one of the criteria for judging the effectiveness of any design-oriented analytical tool is that it be easy to use, the development of the simplified method is geared toward hand calculations on desk top or pocket programmable calculators rather than numerical solutions on large central computers. Accordingly, the method is based on simple, closed-form, plane strain continuum solutions. Since these solutions cannot model all of the complex ground-structure interaction phenomena around the tunnel, however, finite element numerical analyses will be used extensively as research tools in the development of the simplified method. Although the high costs and the input requirements of these finite element techniques in a real tunneling situation often make them impractical for design use, they can be productively applied in the idealized research environment to derive correction factors for the effects of variables that cannot be considered directly in the simple closed-form solutions. Two of these correction factors are incorporated in the simplified analysis method.

The development of the method follows a logical, step-by-step progression. The effects of relative support stiffness are investigated in Section 2, followed by the treatment of the support delay effect in Section 3 and the influence of ground yielding in Sections 4 and 5. The combined effects of these three variables are also analyzed in Section 5,

4

leading to the outline of the simplified method in Section 6. Finally, in order to verify the accuracy of the simplified analysis method, it is applied to five representative tunnel projects reported in the literature in which the actual support loads were measured during construction. The details of these cases and the conclusions from the comparisons are also presented in Section 6.

Before proceeding to the detailed development of the method, a short but necessary digression is convenient at this point in order to introduce the important conceptual tool ·of characteristic curves as background for what follows. These characteristic curves, which are old engineering aids frequently used around the beginning of the century and since reintroduced in tunneling by Rabcewicz (1973), Peck (1969), and Lombardi (1973), will be used extensively in the following sections to describe the general ground-structure interaction around a tunnel. As shown in Figure 1.1, characteristic curves are simply pressure vs. displacement relations for the ground mass and the tunnel support. The ground characteristic curve is developed by first assuming that an unlined tunnel exists in the undisturbed ground mass; this opening has an internal pressure, P_I, equal to the in situ ground stress. Upon gradual reduction of the internal pressure (i.e., unloading), inward radial displacement, u, of the tunnel wall occurs, and the plot of the internal pressure vs. displacement is the ground characteristic curve.
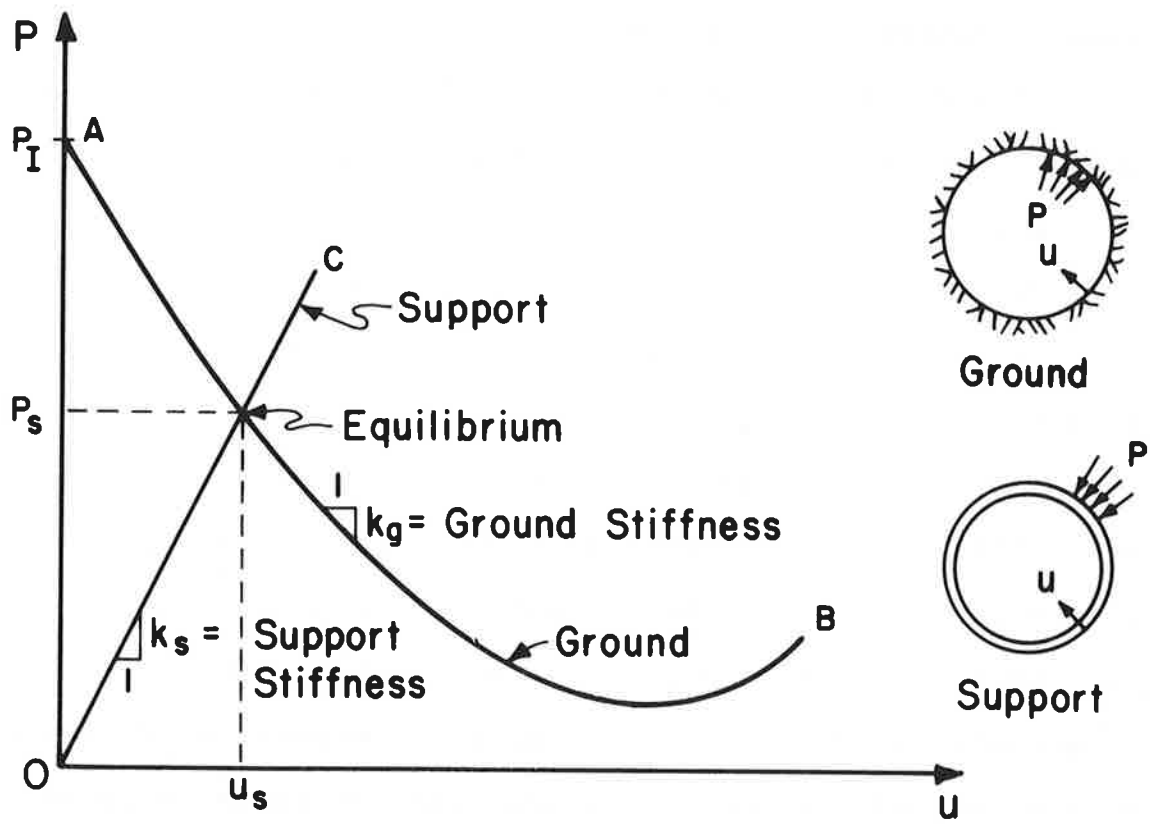
FIGURE 1.1. CHARACTERISTIC CURVES

In an analogous manner, the support characteristic curve is based on the displacements that develop as the external pressure on the support is gradually increased. The point at which the ground and support characteristic curves intersect is the equilibrium point (see Figure 1.1); P_s will be the tunnel support load, and u_s will be the support displacement.

Since the characteristic curves are pressure vs. displacement relations, the slopes of the curves will be functions of the stiffnesses of the ground mass and the cunnel support, as shown in Figure 1.1. The equilibrium point will be strongly influenced by these stiffnesses. This phenomenon is the subject of the next section.

2. RELATIVE STIFFNESSES OF SUPPORT AND GROUND

2.1 QUALITATIVE EFFECT OF RELATIVE STIFFNESS

The interaction between a tunnel support and the sur-
rounding ground mass is analogous to the behavior of any
indeterminate composite structure. The elements of the com-
posite system share in resisting the applied load (the
excavation-induced ground stresses in the tunneling problem)
and the load is apportioned to each element on the basis
of its stiffness relative to the other elements in the
system. Thus the relative stiffnesses of the ground and the
tunnel support are important variables influencing the equi-
librium support loads. A relatively stiff support will
provide a larger share of the composite resistance of the
ground-support system and as a result will "attract" a larger
load than will a relatively flexible support.

The concept of relative stiffness is particularly easy
to visualize using characteristic curves. Since stiffness
is defined as the amount of load required to induce a unit
deformation in a body, the stiffness of the ground or the
support is simply the slope of its characteristic curve,
i.e., the slope of its load-deformation curve. A steep
characteristic curve, or a large load per unit deformation,
corresponds to a stiff tunnel support or ground mass.

9

The effect of two different support stiffnesses on the final support load is shown in Figure 2.1. As expected, the equilibrium pressure for the stiff (steep characteristic curve) support is considerably larger than that for the flexible (flat characteristic curve) support.
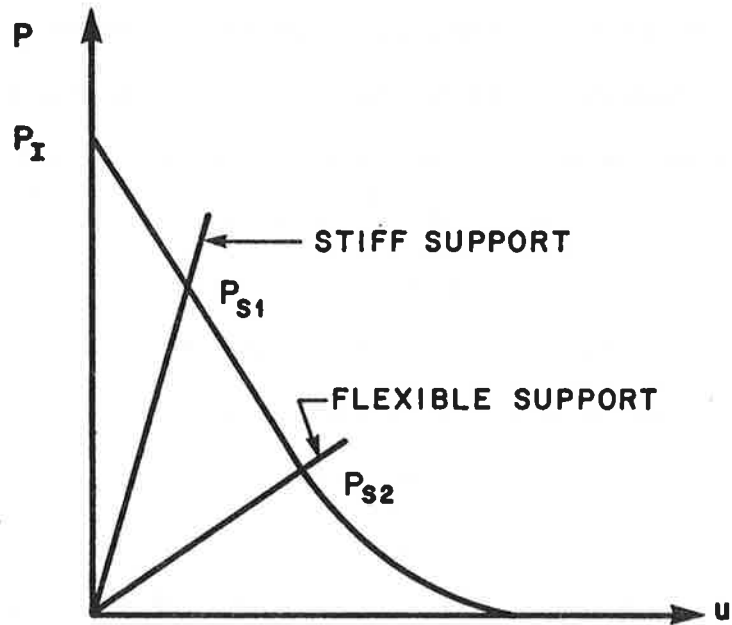
FIGURE 2.1. EFFECT OF RELATIVE STIFFNESS--CHARACTERISTIC CURVES

Not all of the effects of relative stiffness can be demonstrated using characteristic curves, though. The characteristic curve representation of the overall ground and support behavior is based on the tacit assumption of isotropic or uniform stress conditions; thus, it cannot be used to study the change of shape of the support or the accompanying bending moments which occur when the lateral ground stress ratio, K, is different from 1. The effects of support

10

stiffness on these shape changes and moments have been
lucidly described by Peck (1969), who showed that an ideally
flexible support in a non-uniform stress field will deform
until the stresses acting on the support are uniform (no
bending moment can occur). An ideally rigid support will
not change its shape and will have to support the original
non-uniform stress fields (large bending moments can occur--
see Figure 2.2).
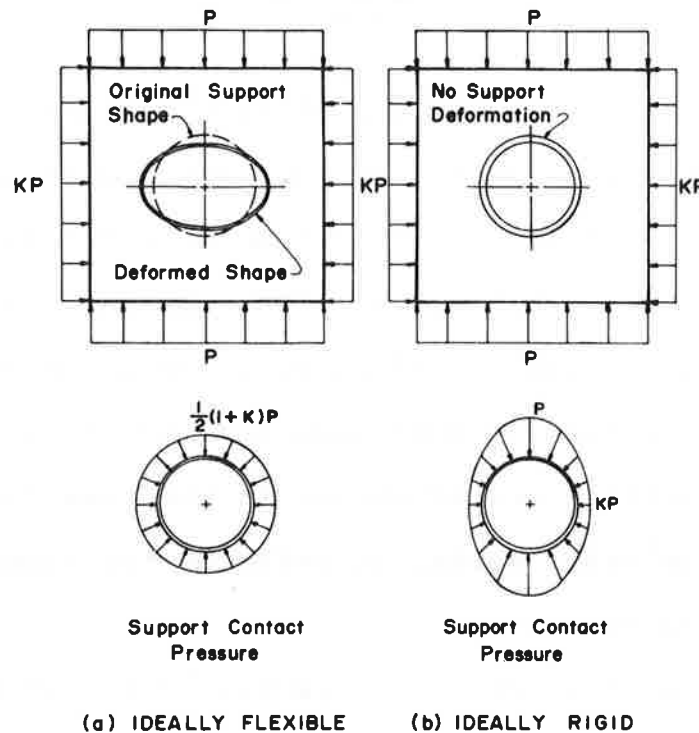
FIGURE 2.2. EFFECT OF RELATIVE SUPPORT STIFFNESS ON
SHAPE CHANGE OF OPENING

11

2.2 DIMENSIONLESS STIFFNESS RATIOS

The relative stiffnesses of the ground mass and the tunnel support can be conveniently expressed by two dimensionless parameters, the compressibility and flexibility ratios. The derivation of these parameters is outlined in Figure 2.3; a more detailed derivation, complete with discussion and a critique of other formulations for these ratios reported in the literature, can be found in Appendix A.

The compressibility ratio, C^*, is defined as:

$$C^* = \frac{ER(1-\nu_s^2)}{E_s A_s (1-\nu^2)} \qquad (2.1)$$

in which E, ν and E_s, ν_s are the elastic constants for the ground and support, A_s is the average cross-sectional area of the support per unit length of tunnel, and R is the tunnel radius. The compressibility ratio is a measure of the relative stiffness of the ground-support system under a uniform or symmetric loading condition (horizontal ground stress equal to the vertical ground stress in the free field--see Figure 2.3a); in other words, it reflects the circumferential stiffness of the system.

The flexibility ratio, F^*, is similarly defined as:

$$F^* = \frac{ER^3(1-\nu_s^2)}{E_s I_s (1-\nu^2)} \qquad (2.2)$$
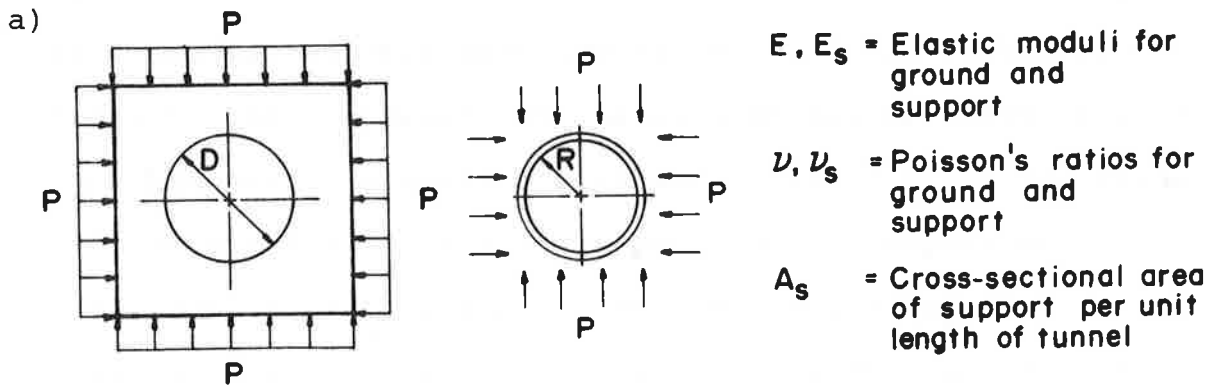
12

a)

E, E_s = Elastic moduli for ground and support

ν, ν_s = Poisson's ratios for ground and support

A_s = Cross-sectional area of support per unit length of tunnel

$$\frac{P}{\Delta D/D} \propto \frac{E}{(1-\nu^2)} \qquad \frac{P}{\Delta D/D} = \frac{E_s A_s}{(1-\nu_s^2)R}$$

$$C^* = \text{Compressibility Ratio} = \frac{ER(1-\nu_s^2)}{E_s A_s(1-\nu^2)}$$

b)

I_s = Moment of inertia of support per unit length of tunnel
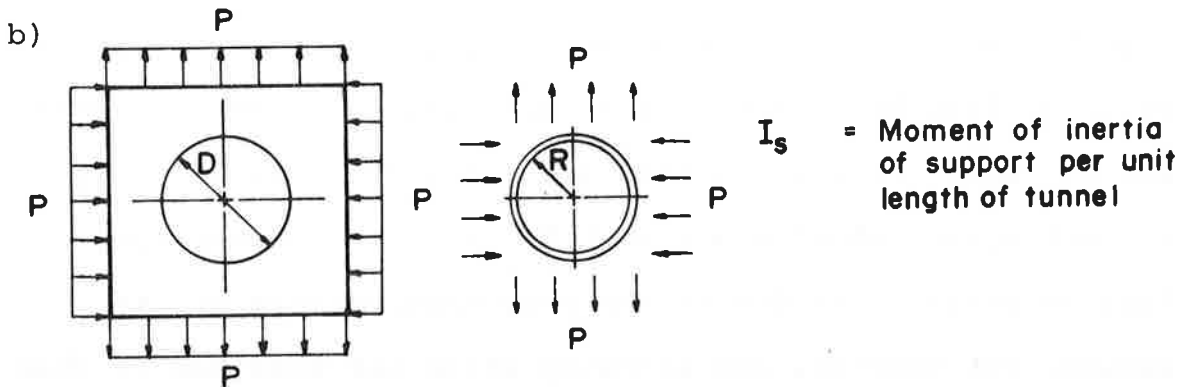
$$\frac{P}{\Delta D/D} \propto \frac{E}{(1-\nu^2)} \qquad \frac{P}{\Delta D/D} \propto \frac{E_s I_s}{(1-\nu_s^2)R^3}$$

$$F^* = \text{Flexibility Ratio} = \frac{ER^3(1-\nu_s^2)}{E_s I_s(1-\nu^2)}$$

FIGURE 2.3. DIMENSIONLESS STIFFNESS RATIOS

13

in which I_s is the moment of inertia of the tunnel support
per unit length of tunnel. The flexibility ratio is a
measure of the relative stiffness of the ground-support
system under an antisymmetric loading condition (horizontal
ground stress equal to but of opposite sign of the vertical
ground stress in the free field--see Figure 2.3b); in other
words, it reflects the "flexural" stiffness of the system.

The ranges of the compressibility ratio for some com-
mon primary support systems are illustrated in Figure 2.4.
In this figure, only practical combinations of support sys-
tems and ground types are considered; for example, steel
liner plates in massive rock formations would obviously
have a much higher compressibility ratio than those shown in
Figure 2.4, but this support and ground combination is rarely
found in practice. For practical tunneling situations, the
dividing line between soil and rock tunnels is at C^* approx-
imately equal to 1.0. Steel ribs-and-lagging is the only
support system which spans both the soil and rock ranges;
this versatility is due to the many combinations of rib
weight, rib spacing, and blocking which are possible in this
system.

It is very difficult to determine typical values of
the flexibility ratio for many common support systems since
F^* depends so strongly on construction details. For example,
segmented cast iron liners may be relatively stiff--low F^*--
if the joints are tightly bolted, or they may approach

14
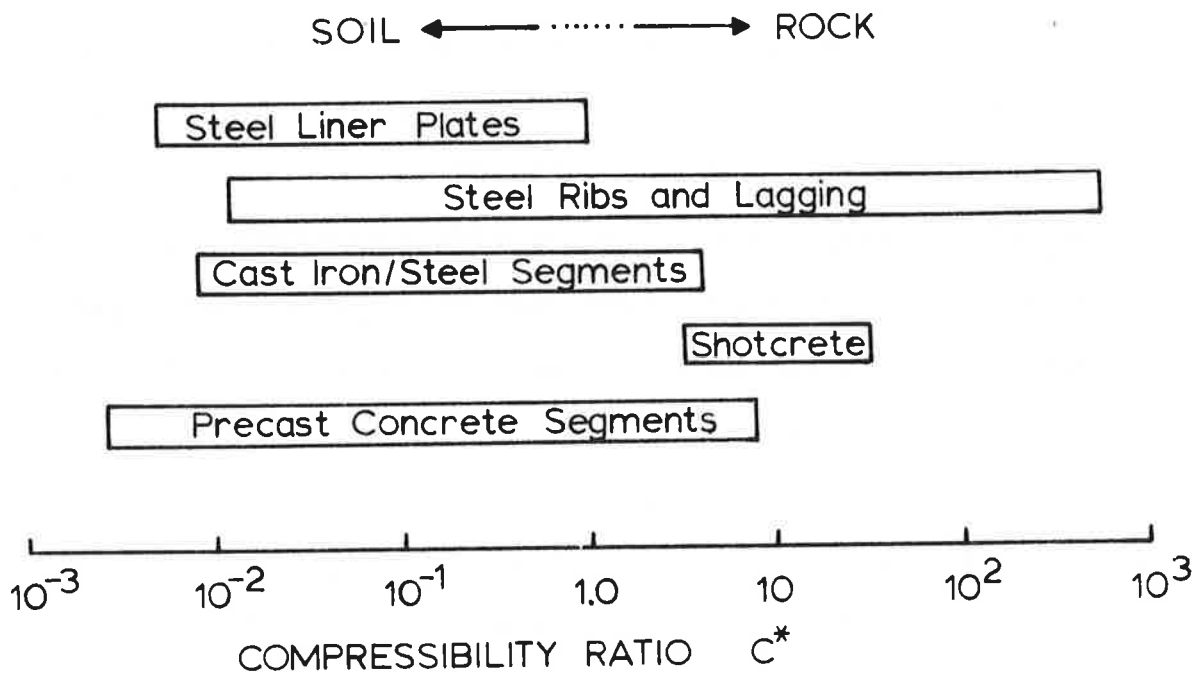
FIGURE 2.4. RANGES OF C* FOR COMMON SUPPORT SYSTEMS

complete flexibility--F^* approaching infinity--if the joints
are unbolted and articulated. Generally, F^* will be greater
than 10 for even the stiffest support systems.

In addition to quantifying the relative stiffnesses
of the ground mass and the support, the compressibility
and flexibility ratios also serve as the starting point in
the derivation of simple, closed-form analyses of the re-
lationships between tunnel support loads and relative stiff-
ness.

15

2.3 DEVELOPMENT OF THE RELATIVE STIFFNESS SOLUTIONS

Since the relative stiffness of the ground to the support is such a major factor influencing the ground-structure interaction around a tunnel, the first step in the development of any simplified tunnel design procedure will be to devise some analytical tools that directly relate support forces and displacements to the support and ground stiffnesses. By applying the theory of elasticity, it is possible to develop closed-form solutions, termed "relative stiffness solutions," which relate the support forces and displacements to the dimensionless compressibility and flexibility ratios. Several of these solutions have been published in the literature, and two new solutions, which are more appropriate for the tunneling problem, are derived here.

The principal assumptions and limitations, either implied or explicitly stated, in all of these relative stiffness solutions are:

1) The tunnel is an elastically lined cylindrical cavity. The detailed implementation of this assumption varies among the solutions, however; the support may be treated as a thick walled cylinder, as an inextensible (i.e., incompressible) thin shell, or as an extensible thin shell.

2) The ground mass is homogeneous, isotropic, and linearly elastic.

16

3) The ground mass is infinite in extent; or, at the very least, the tunnel is located at sufficient depth that the proximity of the ground surface has negligible effect--generally, at depths greater than two tunnel diameters (Duns and Butterfield, 1971; Peck, Hendron and Mohraz, 1972).

4) There is a negligible variation of ground stresses with depth. However, the vertical and horizontal ground stresses need not be equal.

5) The ground mass and tunnel support are in a state of plane strain.

6) One of two limiting conditions exists at the interface between the support and the ground: a) there is "full slip" between the ground and the support, i.e., there is no shear stress transfer at the interface, or b) there is "no slip" between the ground and the support, i.e., there is full shear stress transfer at the interface.

The original relative stiffness solution was developed by Burns and Richard (1964) for buried culverts under one dimensional (quasistatic) blast overloads. Similar ideas had been formulated earlier by Schmid (1931) and Voellmy (1937). Burns and Richard's solution employs extensible (i.e., compressible) shell theory to model the cylindrical tunnel support. The derivation treats both full-slip or no-slip conditions at the ground-support interface. However,

17

the lateral free-field ground stresses are restricted to a
fixed function of the vertical stresses and Poisson's ratio
(i.e., $\sigma_h = \frac{\nu}{1-\nu} \sigma_v$). Hoeg (1968) extended the Burns and
Richard solution by making the lateral and vertical stresses
independent of each other. He also approximated the effect
of a narrow soft ground zone near the interface and the ef-
fect of tensile stresses in the ground. Hoeg's solution for
the full-slip condition unfortunately contains an error,
though; the shear stressess at the interface between the
ground and the support do not reduce to zero as they should
for this case. Dar and Bates (1974) further refined the
relative stiffness solution by treating the support as a
thick walled cylinder. Their derivation, for the no-slip
case only, produces expressions for the stress distribution
in the support. The differences between Dar and Bates's
and Burns and Richard's solutions become significant only
for quite thick liners (e.g., thickness equal to 20% of the
tunnel radius); for practical support thicknesses these dis-
crepancies are negligible.

Although all of the above-mentioned relative stiffness
solutions are theoretically correct (except for Hoeg's
full-slip derivation) and reasonably accurate in the cases
for which they are intended (culverts and tunnels under sur-
charge or blast pressure loadings), significant errors arise
when these same solutions are applied to the tunneling
problem. One cause of this discrepancy lies in the

18

assumptions for the loading conditions. The surface over-pressure loading, or "external loading" condition, implies that the tunnel opening has been excavated and supported before the loads corresponding to the free field stresses are applied (Figure 2.5a). While this loading condition is correct for backfilled culverts and for tunnels subjected to blast overloads, it does not adequately represent the actual "excavation unloading" condition that occurs during tunneling. In this case (Figure 2.5b), the tunnel opening is excavated and simultaneously supported after the loads corresponding to the free field stresses have already been applied. The tunnel is constructed in an initially stressed ground mass. Choosing the assumption of external loading instead of excavation unloading may lead to computed support forces that are excessively conservative (Mohraz et. al., 1975).

Morgan (1961) attempted a relative stiffness solution incorporating the correct excavation unloading condition for tunnels, but he made a serious error in his derivation by assuming that $\sigma_r + \sigma_\theta$ = constant in the ground mass. Muir Wood (1975) corrected this mistake, but he also erred in another part of the derivation when he ignored the effect of the in situ shear stresses at the ground-support inter-face. In a subsequent discussion, Curtis (1975) corrected all of these errors and gave the final solution, but his derivation is not straightforward and is restricted to

19

(a) EXTERNAL LOADING
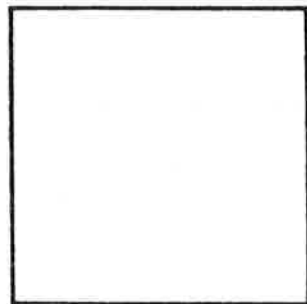
1) Unstressed
Ground Mass
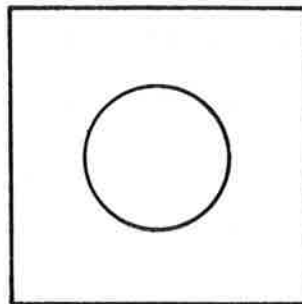
2) Excavate Tunnel
Install Liner
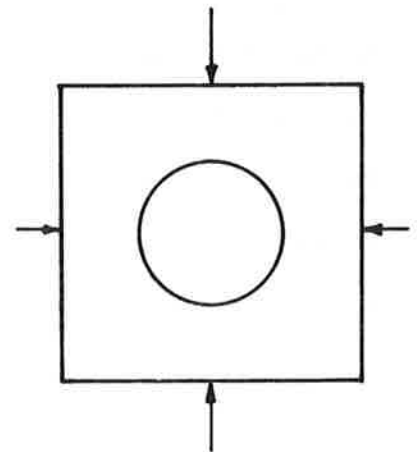
3) Apply Stresses

(b) EXCAVATION UNLOADING
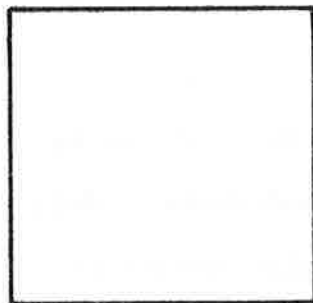
1) Unstressed
Ground Mass
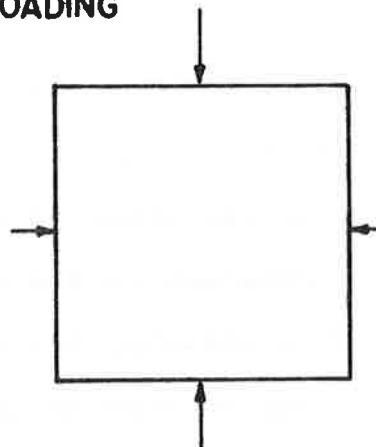
2) Apply In Situ
Stresses
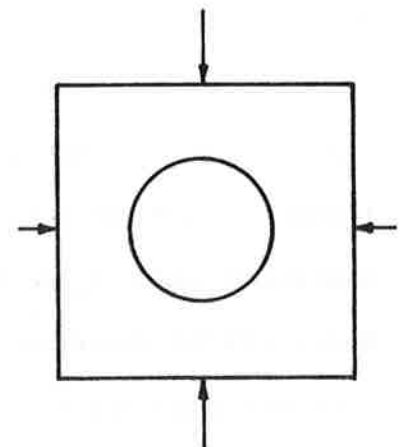
3) Excavate Tunnel
Install Liner

FIGURE 2.5.   LOADING CONDITIONS: EXCAVATION UNLOADING VS.
EXTERNAL LOADING

inextensible supports (i.e., incompressible or $C^* = 0$); thus, Curtis's solution is limited to tunnels in very soft grounds.

A very recent dissertation by Ranken (1978) contains several solutions for compressible tunnel supports under excavation unloading conditions. These solutions are similar to the derivations outlined in the next section. Details of Ranken's solutions are discussed further in Appendix A.

2.4 RELATIVE STIFFNESS SOLUTION REVISED FOR EXCAVATION UNLOADING CONDITIONS

The derivation follows the original logic of Burns and Richard (1964). The ground mass is postulated to be an infinite, elastic, homogeneous, isotropic medium with an initial vertical stress P equal to the vertical ground stress at the centerline of the tunnel and with an initial horizontal stress KP. The tunnel support is treated as an elastic shell in which both flexural and circumferential deformations are considered. (i.e., extensible shell theory is employed). Both the ground and the support are assumed to be in a state of plane strain. The notation used in the solution is illustrated in Figure 2.6.

The relative stiffness of the ground mass to the tunnel support is incorporated into the solution through the use of the two dimensionless parameters, the compressibility and flexibility ratios, defined in Section 2.2.

The derivation of the revised relative stiffness solution follows three basic steps:

21
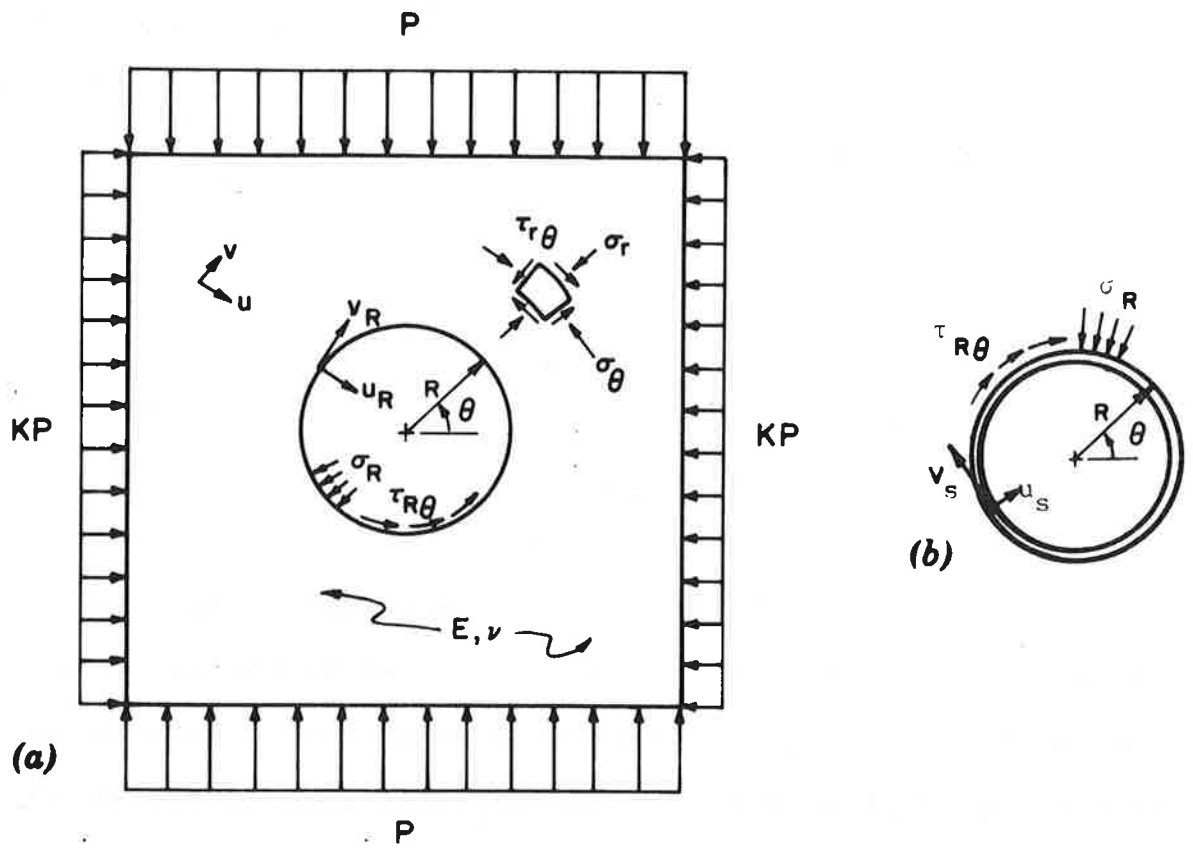
FIGURE 2.6.   NOTATION FOR RELATIVE STIFFNESS SOLUTIONS

1. Derive the initial displacement field in the ground mass due to the in situ stresses.

2. Derive the total stress and incremental displacement fields in the ground mass after excavation and the contact stresses at the ground-support interface. The incremental displacement field is the displacement field for a circular hole in the ground under an external loading condition minus the displacements due to in situ stresses. The "full-slip" or "no-slip" boundary conditions at the ground—support interface are also considered in Step 2 and lead to two different solutions.

3. Compute the internal support forces induced by the contact stresses at the ground-support interface.

Details of the derivation for each of the three steps are given in Appendix A. Only the final equations for the support forces and displacements for the full-slip and no-slip cases are given below. For the full-slip case:

$$\frac{T}{PR} = \frac{1}{2}(1+K)(1-a_0^*) + \frac{1}{2}(1-K)(1-2a_2^*)\cos 2\theta \qquad (2.3a)$$

$$\frac{M}{PR^2} = \frac{1}{2}(1-K)(1-2a_2^*)\cos 2\theta \qquad (2.3b)$$

$$\frac{u_s E}{PR(1+\nu)} = \frac{1}{2} (1+K) a_0^* - (1-K) [(5-6\nu) a_2^* - (1-\nu)] \cos 2\theta$$

$$(2.3c)$$

$$\frac{v_s E}{PR(1+\nu)} = \frac{1}{2} (1-K) [(5-6\nu) a_2^* - (1-\nu)] \sin 2\theta \qquad (2.3d)$$

in which:

$$a_0^* = \frac{C^* F^* (1-\nu)}{C^* + F^* + C^* F^* (1-\nu)} \qquad (2.3e)$$

$$a_2^* = \frac{(F^*+6)(1-\nu)}{2F^*(1-\nu) + 6(5-6\nu)} \qquad (2.3f)$$

C^*, F^* given in Equations 2.1 and 2.2

For the no-slip case:

$$\frac{T}{PR} = \frac{1}{2} (1+K)(1-a_0^*) + \frac{1}{2}(1-K)(1+2a_2^*)\cos 2\theta \qquad (2.4a)$$

$$\frac{M}{PR^2} = \frac{1}{4} (1-K)(1-2a_2^*+2b_2^*)\cos 2\theta \qquad (2.4b)$$

$$\frac{u_s E}{PR(1+\nu)} = \frac{1}{2}(1+K)a_0^* + \frac{1}{2}(1-K)[4(1-\nu)b_2^* - 2a_2^*]\cos 2\theta$$

$$(2.4c)$$

$$\frac{v_s E}{PR(1+\nu)} = -(1-K)[a_2^* + (1-2\nu)b_2^*]\sin 2\theta \qquad (2.4d)$$

in which:

$$a_0^* = \frac{C^* F^* (1-\nu)}{C^* + F^* + C^* F^* (1-\nu)} \qquad (2.4e)$$

$$\hat{b} = \frac{(6+F^*)C^*(1-\nu) + 2F^*\nu}{3F^* + 3C^* + 2C^* F^* (1-\nu)} \qquad (2.4f)$$

$$b_2^* = \frac{C^*(1-\nu)}{2[C^*(1-\nu) + 4\nu - 6\hat{b} - 3\hat{b}C^*(1-\nu)]} \qquad (2.4g)$$

$$a_2^* = \hat{b}b_2^* \qquad (2.4h)$$

C^*, F^* given in Equations 2.1 and 2.2

25

This revised relative stiffness solution can be readily programmed on a small calculator, as documented in Appendix A, or expressed graphically, as is done in the next section.

2.5 APPLICATION OF THE RELATIVE STIFFNESS SOLUTION TO TYPICAL GROUND AND SUPPORT CHARACTERISTICS

The purpose of this section is to provide the reader with values of thrust, moment and displacement for ground and support characteristics that are typical of soft ground and hard rock tunnels. At the same time, it will be possible to discuss the effect of the different loading conditions and of the different support types and dimensions.

2.5.1 Ground and Support Parameters

As shown in Figures 2.7 through 2.12 the following parameters were varied to investigate the effect of ground and support characteristics on support thrust, moment and displacement:

1) relative stiffness: $E/E_s = 10^{-4}$ to 1; $t/R = 0.01$ to 0.075, t = average support thickness; corresponds to $C^* \cong 0.001$ to 100.0, $F^* \cong 2.0$ to 1.2×10^7

2) Poisson's ratio of the medium: $\nu = 0.0$ to 0.5

3) ratio of lateral to vertical stress: $K = 0.0$ to 4.0

4) boundary conditions at the support-ground interface: no-slip and full-slip

5) loading conditions: excavation unloading vs. external loading

26
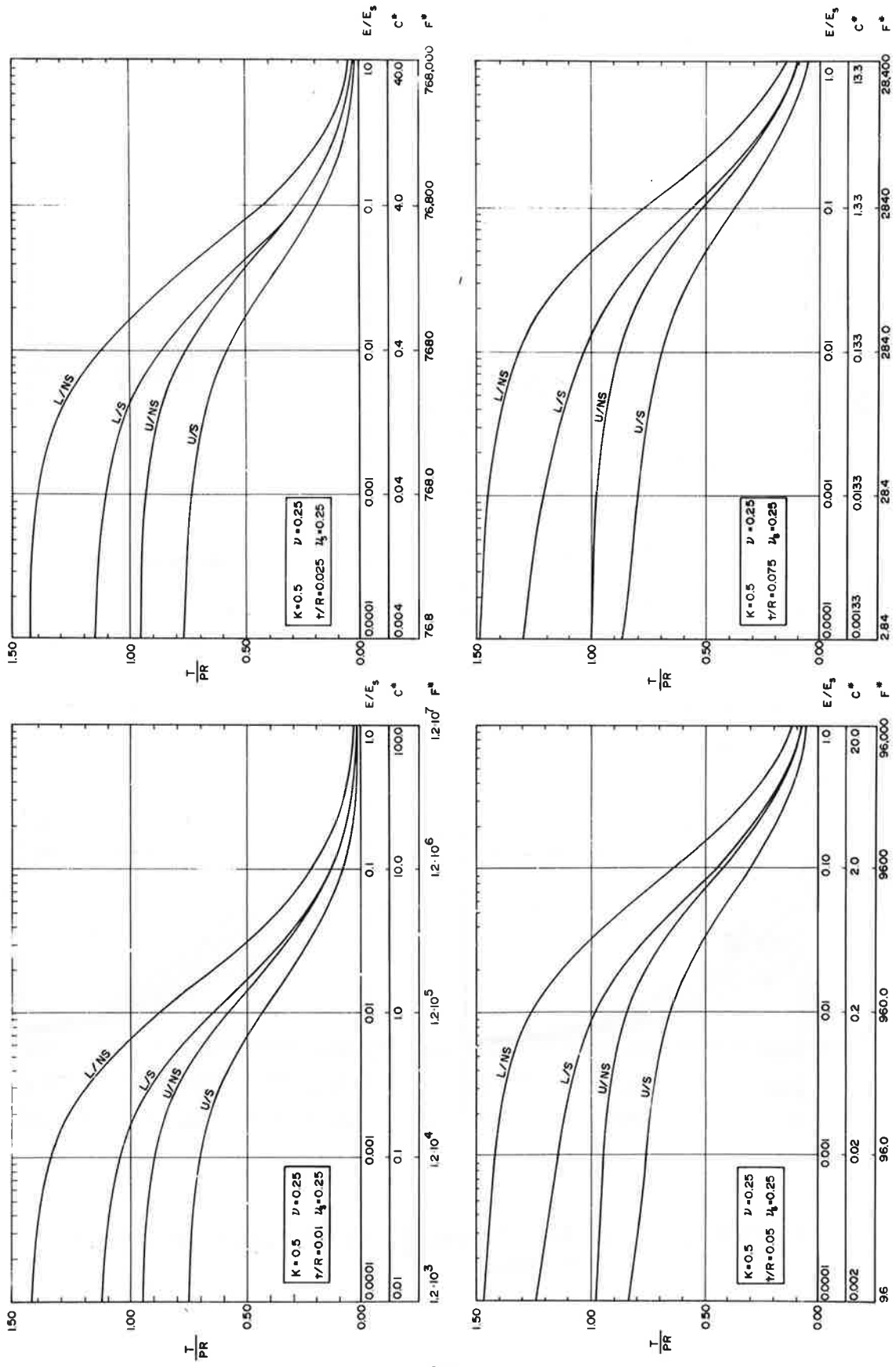
FIGURE 2.7. SUPPORT THRUST COEFFICIENT AT TUNNEL SPRINGLINE

27
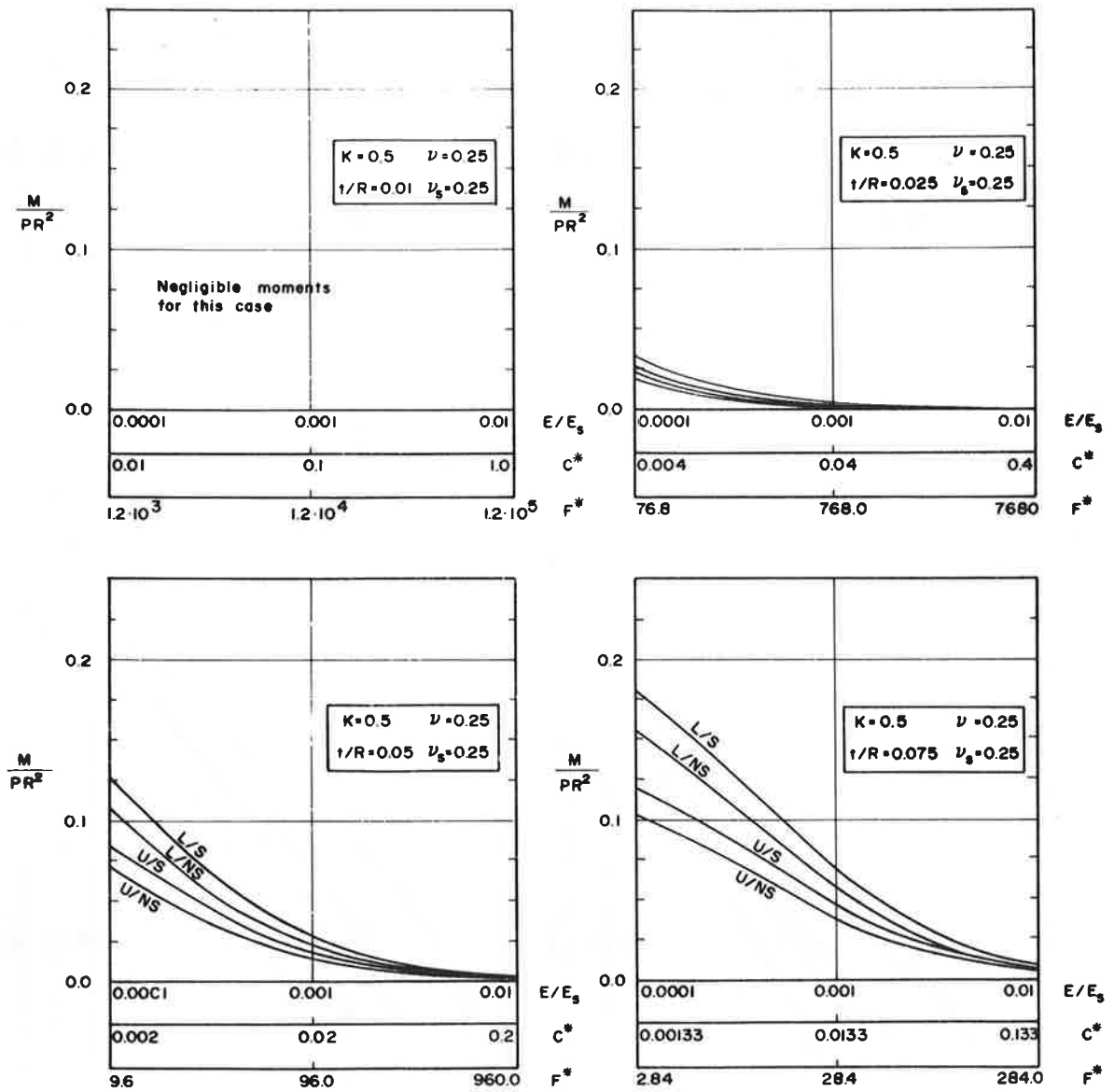
FIGURE 2.8.   SUPPORT MOMENT COEFFICIENT AT TUNNEL
SPRINGLINE
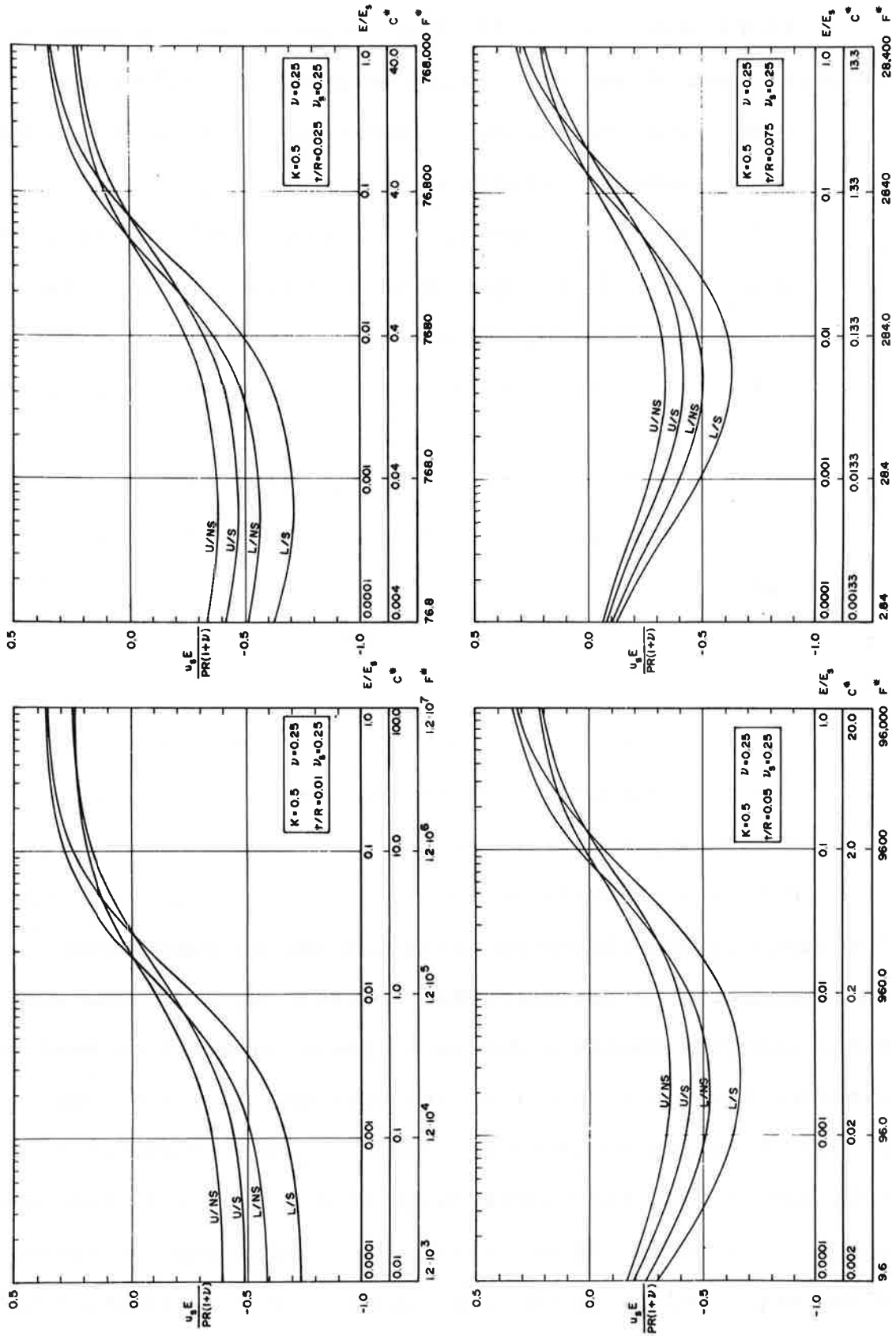
FIGURE 2.9. SUPPORT DISPLACEMENT COEFFICIENT AT TUNNEL SPRINGLINE (Inward is Positive)

29

In Figures 2.7 - 2.12, the following key is used to identify each of the four relative stiffness solutions:

L/NS external loading condition, no-slip at ground-support interface (Hoeg, 1968)

L/S external loading, full-slip (Peck et al., 1972)

U/NS excavation unloading condition, no-slip at ground-support interface (revised solution)

U/S excavation unloading, full-slip (revised solution)

Although the ground and support parameters can be in the entire range mentioned above and shown in Figures 2.7 - 2.12, most practical combinations of the parameters will occur in more limited ranges. Representative ranges of E/E_s are:

Steel or cast iron supports in soft ground: 10^{-4} to 10^{-3}

Concrete supports in soft ground: 10^{-3} to 10^{-2}

Steel supports in rock: 10^{-2} to 10^{-1}

Concrete supports in rock: 10^{-2} to 1

The range of the thickness ratio t/R can be considered to represent: 1) prefabricated concrete or cast iron elements and cast-in-place concrete liners in small to medium diameter tunnels (10-20') at the high end ($t/R = 0.075$); 2) cast-in-place concrete in medium to large diameter tunnels (20-30') in the middle range ($t/R = 0.05$); 3) fabricated steel liner plates or steel sets in a wide range of tunnel diameters (10-30') in the low ranges ($t/R = 0.025$ and 0.01).

30

Shotcrete in medium to large diameter tunnels would also fall in this last category.

It should be emphasized at this point that it is not necessary to work with the assumption (on which the curves in Figures 2.7 - 2.9 are based) of a uniformly thick support; the relative stiffness solutions can treat any cross-sectional shape of the support. Figure 2.10 shows a comparison of two support cross-sections having equal areas but different shapes. Varying the cross-sectional shape has only a slight influence on the support thrusts, but the effects on the support moments and displacements are more significant.

2.5.2 Discussion of Results

The first part of this discussion will consider the effects of all parameter variations for the excavation unloading condition only while the second part will be devoted to a comparison of these results with those obtained using the external loading condition in the original relative stiffness solution.

Effects of Relative Stiffness, Poisson's Ratio and Stress Ratio K

The results of varying the relative stiffnesses of the support and the ground are presented in Figures 2.7 - 2.9. Increasing the relative stiffness of the support by decreasing E/E_s or increasing t/R increases the support thrust and moment. This is intuitively expected since stiffer supports contribute more resistance to the combined ground-support system. Also unsurprising is the result that

31
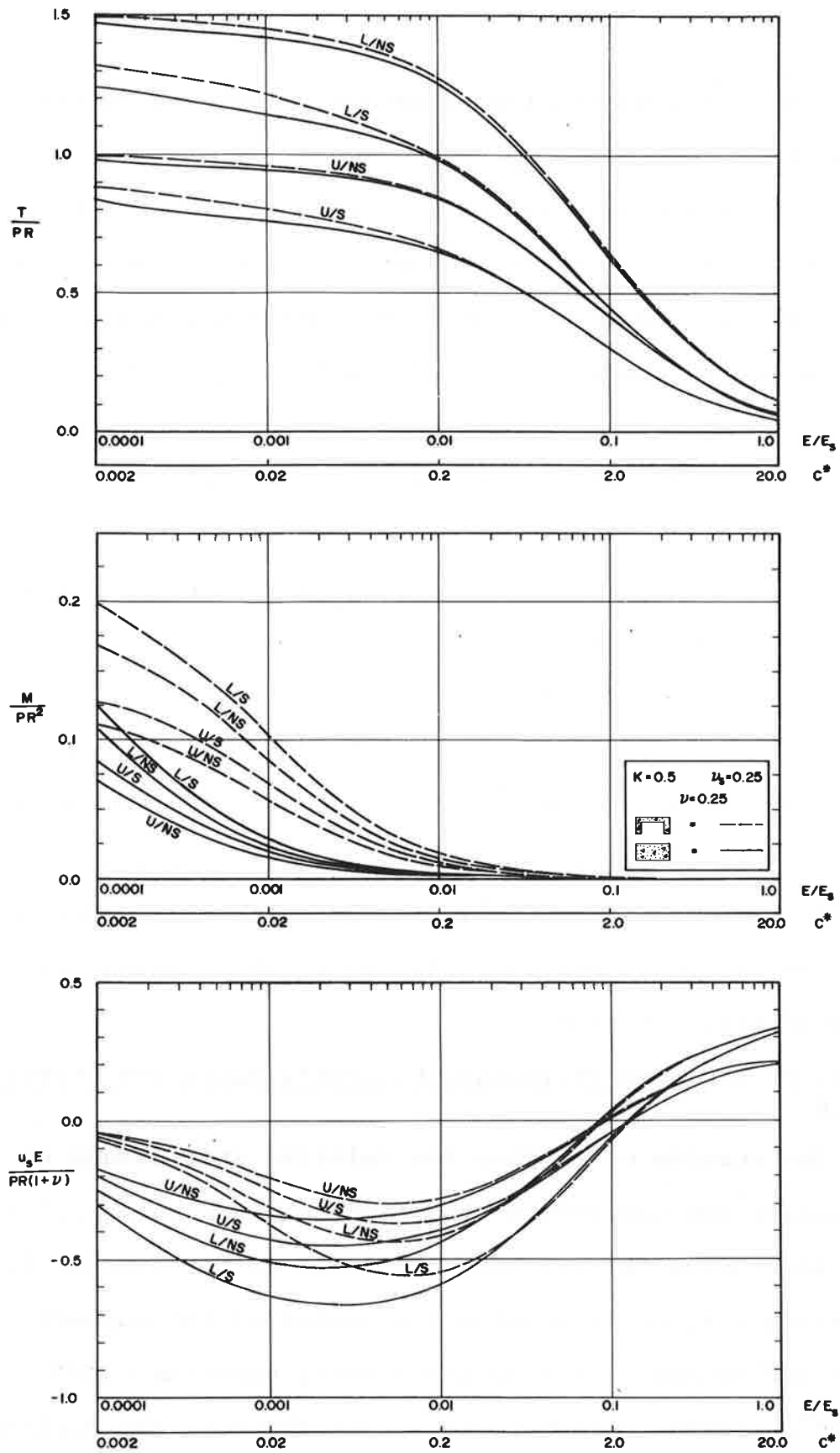
FIGURE 2.10.   EFFECT OF DIFFERENT SUPPORT CROSS-SECTIONS

32

very flexible supports are not subject to any moments; as indicated by the values for E/E_s and t/R shown in the figures, this condition will occur in most rock tunnels. The effect of the relative support stiffness on the support displacements is somewhat more complex however. At very low support stiffnesses $(E/E_s > 0.1)$ the tunnel is essentially unsupported and the net displacements are inward (positive). As the relative support stiffness increases $(E/E_s$ decreases), the support begins to pick up load and resist the inward ground movement. "Ovalling" of the support will also occur when $K \neq 1$ (see also Peck, 1969); for the $K = 0.5$ conditions depicted in Figure 2.9, the support forms a lying ellipse and the net springline displacements are outward (negative) when $C^* < \sim 2.0$. Further support stiffness increases are accompanied by increased bending stiffness which eventually restrains some of the "ovalling" of the support and decreases the outward movement at the springlines. Finally, for an ideally rigid support no displacements and maximum thrust and moment occur.

The effects of the relative stiffness variations confirm statements made in the literature by Peck (1969) and intuitive predictions, particularly in the extreme cases of ideally flexible and ideally rigid supports. It is important to notice that most practical tunnels in soil will fall into the high thrust and moderate moment ranges[1] while rock tunnels will usually lie in the moderate thrust

---

[1] In terms of the dimensionless thrust and moment coefficients.

33

and low moment ranges, based on the representative stiffness values discussed in the previous section. One has to remember, however, that the supports considered here are continuous and that articulation (as would occur with some segmented supports) will substantially decrease the support bending moments.

The effects of Poisson's ratio, ν, of the ground mass on the support behavior is shown in Figure 2.11 for two cases: a relatively stiff support ($E/E_s = 0.001$, $t/R = 0.05$) and a relatively flexible support ($E/E_s = 0.1$, $t/R = 0.05$). Increasing Poisson's ratio decreases the support thrust slightly, although this effect is somewhat more pronounced for the stiff support under the external loading condition. Moments and displacements are influenced very little by the value of ν.

Figure 2.12 shows the effect of varying the stress ratio K. As expected, for K = 1 the thrust is equal to the hoop load and no moments occur. As K decreases, the springline thrust decreases and the moments and negative springline displacements (expansion) increase for the relatively stiff support considered in the figure. The opposite behavior occurs for K greater than one. Interestingly, both the full-slip and no-slip conditions produce practically the same moments and displacements over the entire range of K-values. However, the thrust in the full-slip case deviates considerably from that in the no-slip case;

34
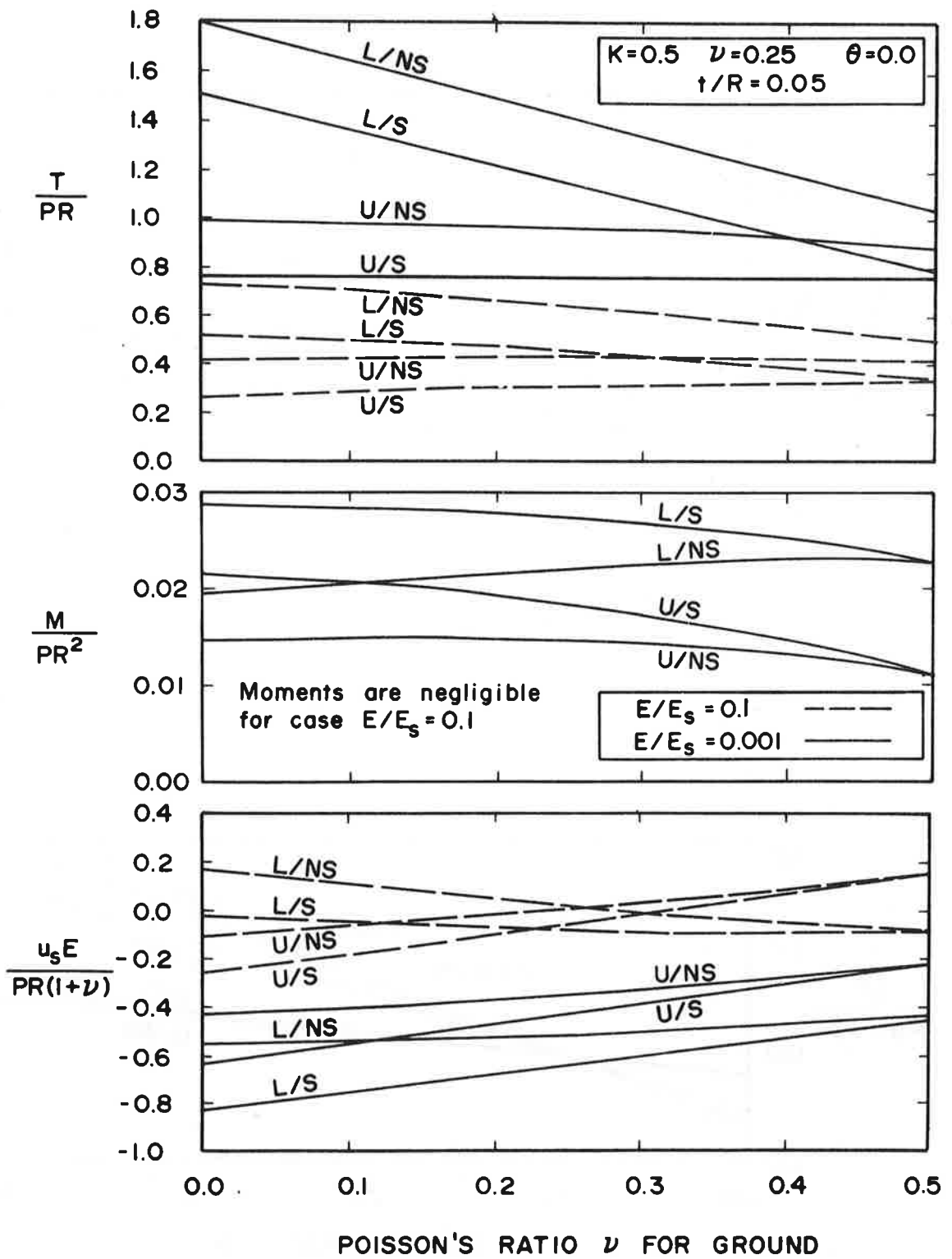
FIGURE 2.11. EFFECT OF POISSON'S RATIO ON SPRINGLINE
SUPPORT FORCES AND DISPLACEMENTS

35
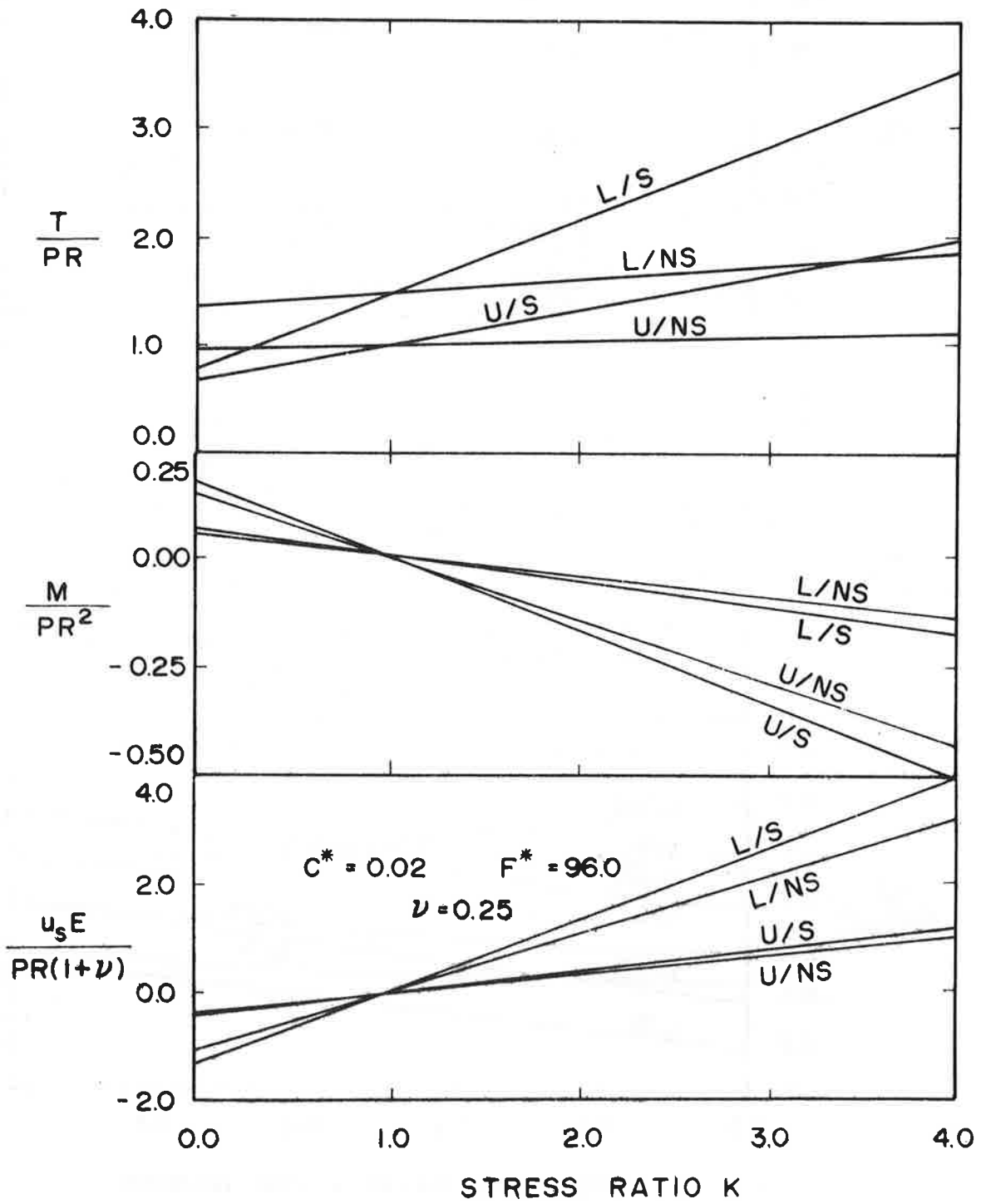
FIGURE 2.12.   EFFECT OF LATERAL STRESS RATIO ON SPRINGLINE
SUPPORT FORCES AND DISPLACEMENTS

furthermore, in the no-slip case the thrust is approximately constant for the entire K-range. In the no-slip case there is a significant transfer of shear stresses from the ground to the support that appears to be responsible for the insensitivity of the support thrust to the lateral stress ratio. Practically, this implies that the thrust coefficient for shotcrete supports that are interlocked with the ground (e.g., blasted rock tunnels) is not significantly influenced by the in situ stress conditions.

Effect of Slip at Interface

Figures 2.7 - 2.9 clearly illustrate the effects of shear slippage at the ground-support interface on the spring-line forces and displacements. When K < 1 (as it is in the figures), the slippage reduces the springline thrusts and increases the springline moments and displacements. At the crown and invert, the thrust, moments, and displacements are all increased by the slippage of the interface (for K < 1). The differences between the full-slip and no-slip solutions depend strongly upon K; for the special case of K = 1, the two solutions are identical.

In reality, of course, the ground mass will have only a limited shear capacity at the support interface. For certain combinations of relative support stiffness and lateral stress ratio this shear capacity will be exceeded and the

no-slip relative stiffness solutions will no longer be valid. The values of C^*, F^*, and K that produce this condition can be determined approximately through a limiting equilibrium analysis of the stresses at the ground-support interface.

The shear and normal stresses acting over one quadrant of the tunnel support (Equations A.39b and A.39a from the no-slip solution in Appendix A) can be integrated to give the total shear and normal forces, $S_{R\theta}$ and N_R:

$$S_{R\theta} = \frac{1}{2} PR(1-K)(1+6a_2^* - 2b_2^*) \qquad (2.5)$$

$$N_R = \frac{1}{2} PR(1+K)(1-a_0^*)\frac{\pi}{2} \qquad (2.6)$$

in which a_0^*, a_2^*, and b_2^* are given by Equation (2.4). If ϕ_w and c_w are the friction angle and cohesion between the ground mass and the tunnel wall, full slip will not occur as long as:

$$S_{R\theta} - N_R \tan\phi_w - c_w \left[\frac{\pi R}{2} \right] < 0 \qquad (2.7)$$

Tattersall et al. (1955) performed tests on the friction between precast concrete tunnel liners and London clay and suggested the following values for c_w and $\tan\phi_w$:

38

Condition at Interface	c_w	$\tan\phi_w$
Dry	5 psi	0.34
Wet	3.5	0.13
Soft Soap Lubrication	0.04	0

For tunnels at normal depths, the wall cohesion c_w will be much smaller than the stresses at the interface and may be safely neglected.

The ranges of K and ϕ_w for which the no-slip assumption is valid (based on Equation 2.7 with $c_w = 0$) are shown in Figure 2.13 for three support stiffnesses. Many common tunneling situations will lie in the no-slip domain. Nevertheless, even in the cases in which the no-slip assumption is valid, the deviations between the no-slip and full-slip solutions are small; these deviations are a function of the lateral stress ratio, K, and range from 0 - 40% for support thrusts and from 0 - 20% for support moments and displacements.

Effects of Loading Conditions

All of the results of the relative stiffness solutions that have been presented in Figures 2.7 - 2.9 show clearly that external loading conditions yield design parameters that are 50 to 100% less favorable than those for excavation unloading. Table 2.1 shows the results from the relative stiffness solutions for the limiting case of ideally rigid supports. The external loading condition is always more severe. In addition, the differences between no-slip and

39
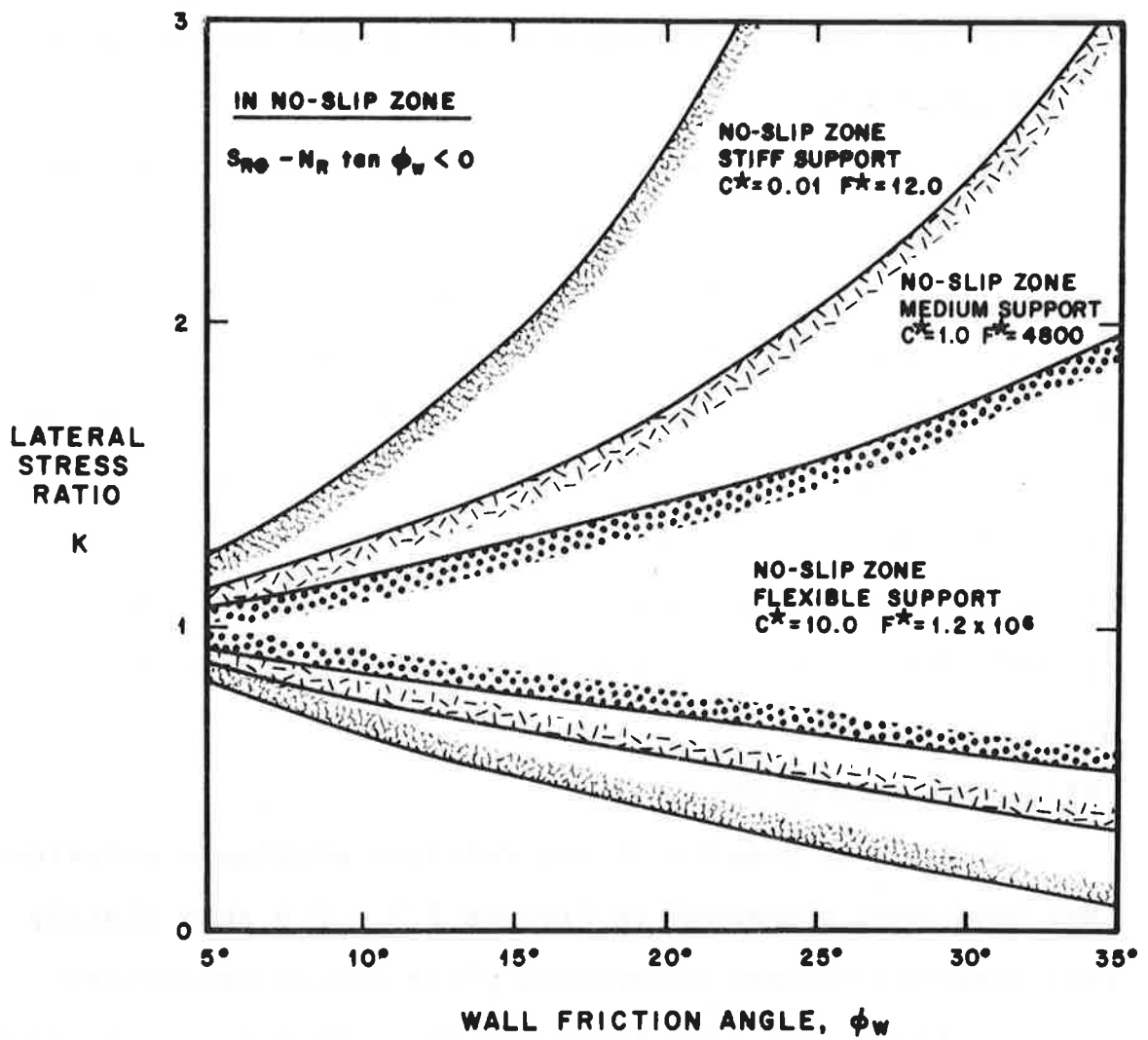
FIGURE 2.13.   DOMAINS IN WHICH NO-SLIP ASSUMPTION IS VALID

40

TABLE 2.1. SPRINGLINE THRUST AND MOMENT COEFFICIENTS FOR A PERFECTLY RIGID SUPPORT, $C^* = F^* = 0$.

Solution	$\nu = 0.10$		$\nu = 0.25$		$\nu = 0.48$	
	$\frac{T}{PR}$	$\frac{M}{PR^2}$	$\frac{T}{PR}$	$\frac{M}{PR^2}$	$\frac{T}{PR}$	$\frac{M}{PR^2}$
Excavation Unloading, Full Slip	0.898	0.148	0.893	0.143	0.877	0.127
Excavation Unloading, No Slip	1.00	0.125	1.00	0.125	1.00	0.125
External Loading, Full Slip	1.55	0.205	1.34	0.214	1.03	0.245
External Loading, No Slip	1.70	0.173	1.50	0.188	1.26	0.241

full-slip boundary conditions are greater in the external

loading case. This is due to the fact that more load is

transferred to the support in the external loading case and

thus the no-slip boundary condition, which "attracts" more

load to the support, has a greater effect.

2.6 COMPARISON OF ANALYTICAL PREDICTIONS WITH MEASURED LOADS

The validity of the revised relative stiffness solution,

or of any analysis of tunnel support behavior, can only be

established through careful comparisons of the analytical

predictions with measured support loads in the field. Without

these comparisons, the mathematical derivations remain

nothing more than elegant academic exercises. For reasons

which will be discussed at some length in the next several

chapters, it would be premature to make any comparisons

at this point between predicted and measured loads for the

excavation unloading solutions. However, it is appropriate

here to make these comparisons for the external loading solu-

tions.

Good agreement between the predicted and measured sup-

port loads is expected in the external loading cases for

two main reasons. First, the relative stiffness of the ground

to the support is the sole major variable in external loading

situations; other factors such as ground movement prior to

support construction, ground yielding, etc. (all of which

will be treated later) have only a minor influence on the

42

support loads. Second, most of the assumptions in the relative stiffness solutions--the plane strain assumption in particular--are reasonably satisfied in external loading situations. The only limitation to these comparisons is the scarcity of field data for tunnels under this loading condition.

Several researchers have conducted experiments on small, scale model tunnels subjected to external pressure loadings. Hoeg (1968) performed an elegant series of tests in which he measured the radial contact stresses acting upon steel cylinders embedded in Ottawa sand. The cylinders were of various stiffnesses, ranging from near-rigid inclusions to very flexible thin-walled shells ($t/R = 0.025$). The measured contact stresses were generally within 30% of the values calculated using the relative stiffness solution, but the detailed distribution of the stresses around the circumference was non-symmetric and irregular because of variations in the bedding conditions at the cylinder wall.

Duns and Butterfield (1971) summarize much of the experimental work that has been done on small scale models in sand. Their principal conclusions from this work are:

1) There is "tolerably" good agreement between the theoretical predictions (from the relative stiffness solutions) and the experimental data.

43

2) The nonlinear relationship between the ground
    modulus and the average level of applied stress
    should be considered in order to improve the
    accuracy of the theoretical predictions.

3) The relationship between the support thrust and
    the applied external pressure is essentially linear.

4) The support moments vary nonlinearly with the
    applied external pressure, largely because
    moments are more sensitive to the local stress-
    dependent variations of the ground modulus.

The best field data for large-scale tunnels under
external loading conditions is from the Garrison Dam project
in North Dakota (see Chapter 6 for more details). A total
of eight tunnels, ranging in diameter from 22 to 36 feet,
run through the earth dam. During construction, two instru-
mented sections in one of these tunnels were excavated and
supported before the dam embankment was built; thus the
increase in support loads induced by the embankment surcharge
corresponds to an external loading condition. A comparison
between the measured and calculated support load increments
at the springlines and crown for the two instrumented tunnel
sections is shown in Figure 2.14. In this figure, the
calculated thrust coefficients are illustrated as shaded
bands; the limits of the bands correspond to the no-slip and
full-slip extremes in the external loading relative stiffness
solutions. The agreement between the measured and calculated

44
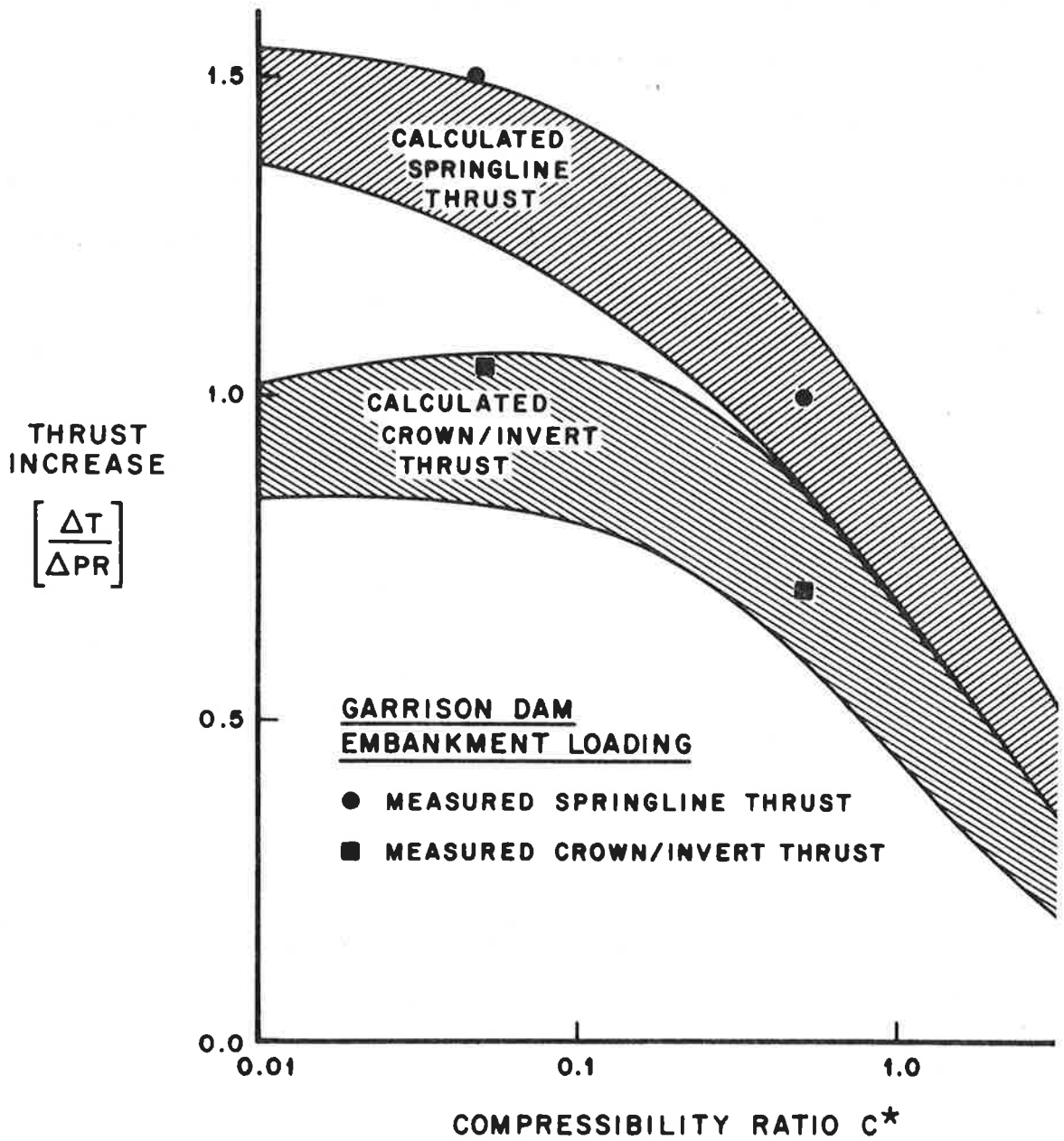
FIGURE 2.14. COMPARISON OF CALCULATED AND MEASURED SUPPORT
THRUSTS FOR GARRISON DAM TUNNELS--EXTERNAL
LOADING CASE

45

thrusts is quite close. The field data exhibit the expected trend of decreasing thrust with increasing support compressibility (as predicted by the relative stiffness solutions), and the calculated thrusts are very close in magnitude to the measured quantities.

Although the physical model and field data substantiate the accuracy of the external loading relative stiffness solutions, verification of the excavation unloading cases requires the consideration of other factors influencing the ground-structure interaction around the face of an advancing tunnel. These other factors will be investigated in the next three sections.

3. DELAY OF SUPPORT CONSTRUCTION BEHIND THE FACE OF AN ADVANCING TUNNEL

3.1 QUALITATIVE DESCRIPTION

An explicit assumption in the relative stiffness solutions presented in Section 2 is that both the ground and the support are everywhere in a state of plane strain. The subtle and more restrictive implicit assumption for the excavation unloading case--the case for tunnels--is that the tunnel is simultaneously excavated and supported along its entire length in one step. Neither of these assumptions accurately reflects the complicated ground-structure inter-action around the face of an advancing tunnel and, as a result, the relative stiffness solutions for the excavation unloading condition must be modified before they can accurately predict the support loads.

A good overview of the actual patterns of stress changes and ground movements around the face of an advancing tunnel can be gained by considering a typical cycle in the tunnel construction sequence. Figure 3.1a shows the conditions existing around the tunnel immediately preceding a new increment or "round" of excavation. The excavation of the previous round has been completed, the support has been installed, and a temporary, short-term equilibrium has been attained. Notice that, as is often the case in real tunnels, the support in Figure 3.1a does not extend

47

(a) BEFORE NEW ROUND OF EXCAVATION:

Unsupported

Support segment

Tunnel face

Advance
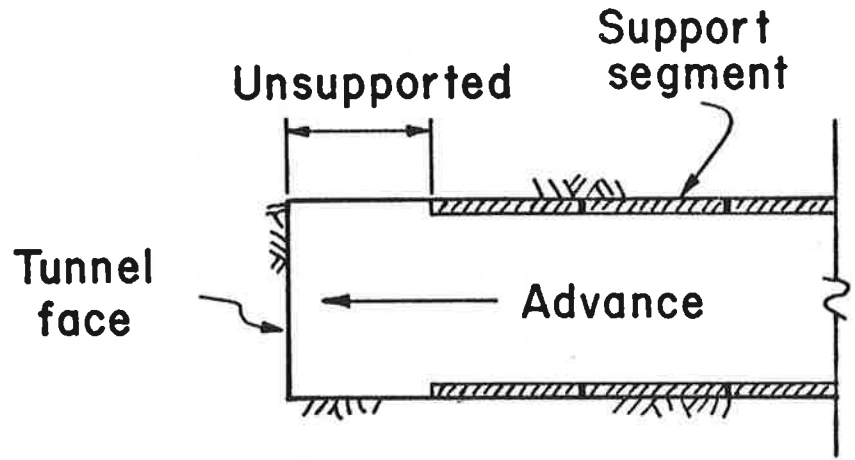
(b) AFTER NEW ROUND OF EXCAVATION:

Load redistribution

Ground movement

Install next support segment

New round of excavation
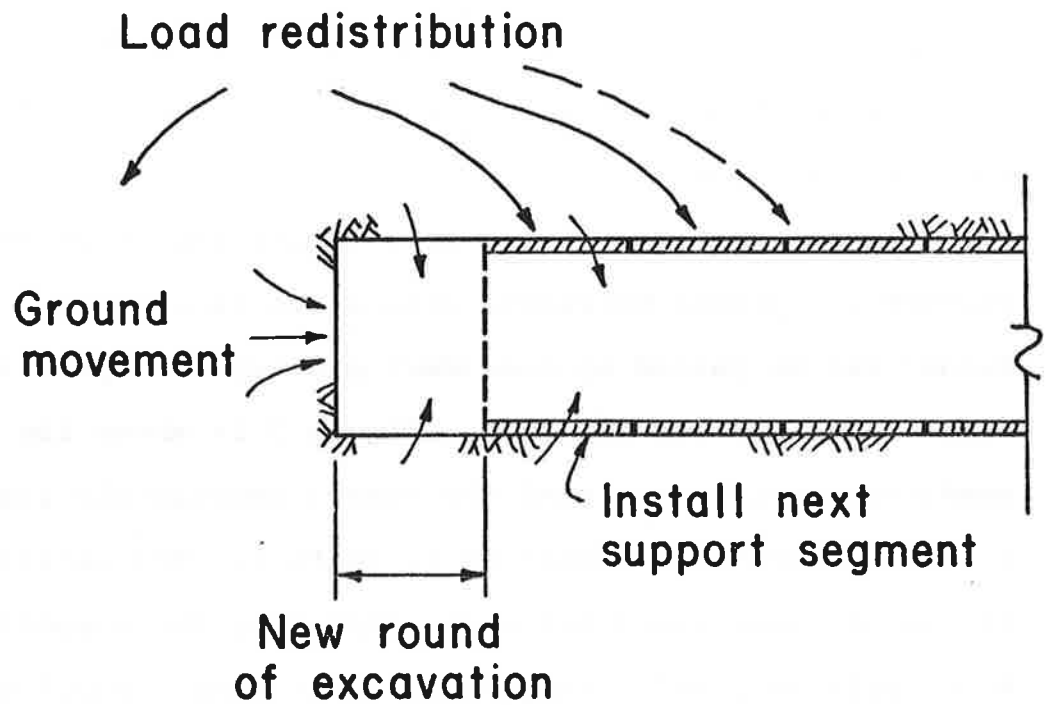
FIGURE 3.1.   GROUND MOVEMENT AND LOAD REDISTRIBUTION
RESULTING FROM TUNNEL EXCAVATION

48

completely to the tunnel face. The length of this spatial lag or "delay" of the support installation depends on the ground type and on the details of the construction procedure. These factors also control the face support, if required; in this example, the face is assumed to be unsupported.

The changes that occur around the tunnel after a new round of excavation are shown in Figure 3.1b. The removal of ground up to the new face causes a change in the stress field or a load redistribution around the tunnel. Most of this redistributed load is transferred to the tunnel support --both to the support already in place and onto the newly installed section--but a significant portion is also transferred to the unexcavated ground ahead* of the face. Concurrently, this redistribution of load induces a pattern of movements within the ground mass. Behind* the face and around the excavated section these movements toward the opening are predominantly radial. In the region immediately ahead of the face the combination of the stress increase due to load redistribution and the stiffness decrease due to the removal of the longitudinal support (the excavated ground) at the new face causes both longitudinal and radial ground displacements. These radial displacements ahead of the face may be a sizeable fraction (20-30% or more) of the eventual

*Definitions: Ahead of the Face - The unexcavated zone into which the tunnel is advancing.
                Behind the Face - The region including and surrounding the already-excavated section of the tunnel.

49

total radial ground movement around the tunnel.

Three distinct behavioral regions can be identified along the longitudinal axis of the tunnel. Far ahead of the face is an undisturbed zone in which the natural state of the ground has not yet been affected by the excavation. Within a region extending approximately 1-2 tunnel diameters ahead of and behind the face, the load redistribution resulting from the excavation produces stress changes and movements in the ground; this region is termed the 3-D transition zone after the three-dimensional pattern of movements that develops within it. Eventually, a zone is reached in which the excavation at the face has no further influence. This region is usually called the plane strain zone.

If the ground mass surrounding the tunnel does not squeeze (creep) or swell with time, the only way that any ground-structure interaction--and therefore any support loads--can develop is if the support is constructed within the 3-D transition zone. The support must be installed close enough to the face that further advances of the tunnel result in additional ground movements and support deformations; otherwise, if the support construction is delayed until the ground mass has stabilized and movements have ceased, the support loads will be nil. Of course, any time-dependent (squeezing or swelling) ground deformations will add another component to the ground-structure interaction regardless of

the support delay, but only the time-independent or short-term interaction will be treated here.

The extreme case for the short-term ground-structure interaction occurs when the tunnel is excavated and simultaneously supported along its entire length, as is assumed in the relative stiffness solutions. This extreme,naturally, is unrealistic. A real tunnel is alternately excavated and supported in small increments, and significant ground movements can develop before the support is installed. These movements, which are largely a function of the support delay, substantially reduce the eventual loads on the tunnel supports.

The effects of support delay on the ground-structure interaction and the resulting tunnel support loads can be easily represented using characteristic curves. Figure 3.2a shows the typical variation of the radial displacement of the ground at the tunnel wall as a function of the distance from the tunnel face for a case in which the support construction lags one tunnel radius behind the face. The ground movements begin at approximately 1-2 radii ahead of the face and increase very rapidly near the face. By the time the support is constructed, the ground has already deformed by an amount u_o. This movement corresponds to a partial unloading of the ground mass prior to support; any further movements of the ground will cause deformations and internal forces

51
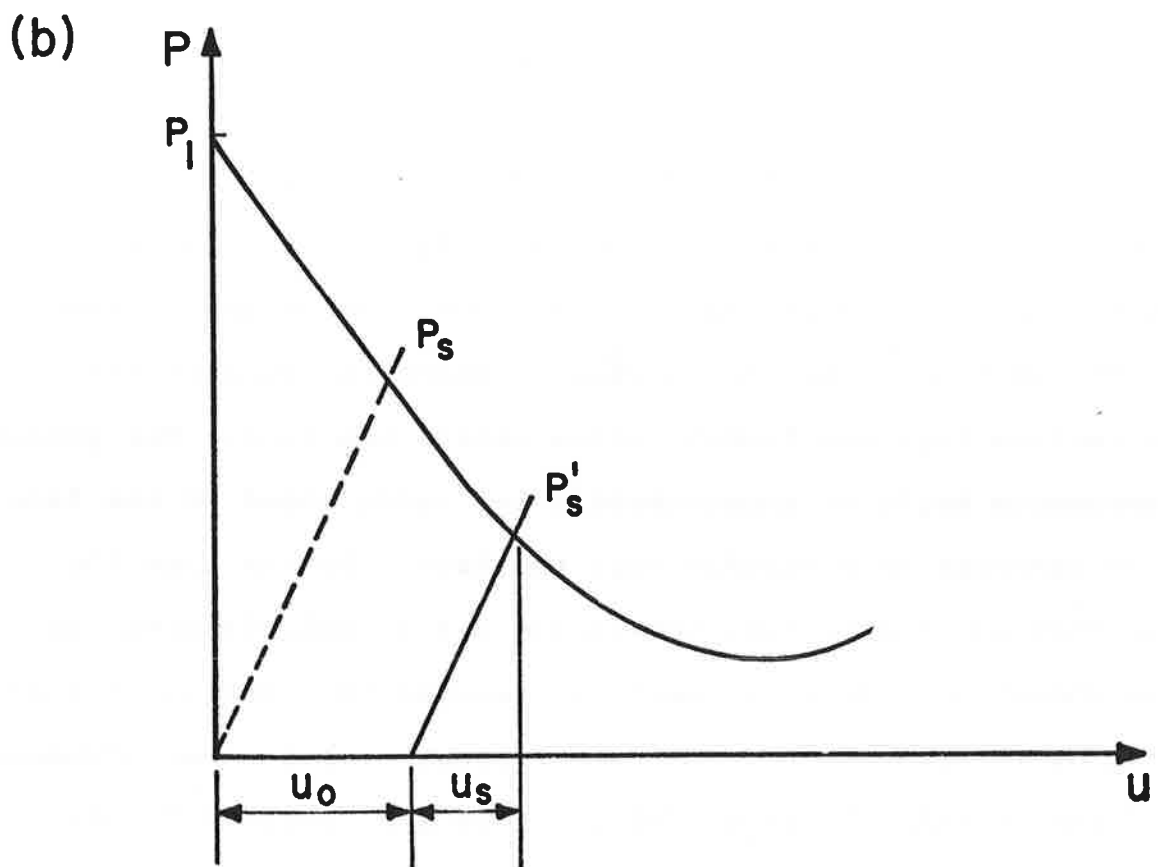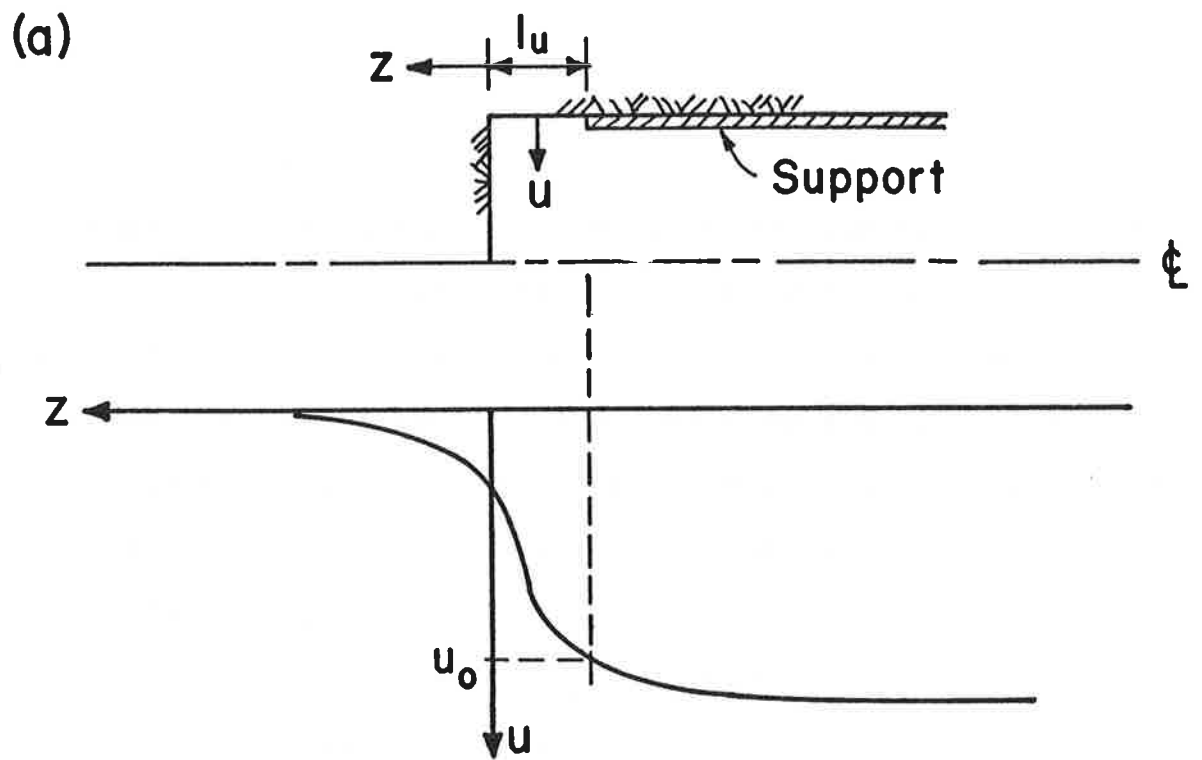
FIGURE 3.2 EFFECT OF SUPPORT DELAY ON SUPPORT LOADS

in the tunnel support. This partial unloading of the ground mass is shown by the characteristic curves in Figure 3.2b. Simultaneous excavation and support of the tunnel (as assumed in the relative stiffness solutions) would give an equilibrium support pressure equal to P_s, while the one-radius support delay results in the reduced equilibrium pressure, P_s', and in increased ground displacements (see also Peck, 1969). The ground movements that occur prior to support construction have the effect of shifting the origin of the support characteristic curve to the right by an amount u_0.

Clearly, any variable having this important an impact on the support loads must be explicitly considered in the design calculations. The remainder of this chapter will describe techniques for quantifying the effect of support delay.

3.2 FINITE ELEMENT ANALYSES OF ADVANCING TUNNELS

To study in more detail the effects of delayed construction of the tunnel support, the behavior of the ground mass around the face of the advancing tunnel must be quantitatively analyzed. Unfortunately, this problem is not amenable to simple, closed-form analyses like the relative stiffness solutions in Section 2; the problem must instead be solved numerically using techniques like the finite element method. These numerical solutions will, in general, be three-dimensional and nonlinear.

Several researchers have already applied numerical techniques to the problem of the advancing tunnel. Most of their effort has been spent on analyzing unsupported tunnels. Descoeudres (1974), using a very coarse three-dimensional finite element mesh, studied the influence of the lateral in situ stress ratio, K, on the crown, springline, and face displacements in an unlined tunnel. He considered both elastic and elastic-perfectly plastic ground behavior in his analyses. Daemen and Fairhurst (1972) restricted their finite element analyses to the case of an unsupported tunnel in an axisymmetric (i.e., K=1) stress field and focused their investigation on the effects of strain-softening ground behavior. Hocking (1976), using boundary element methods, studied the relationships between K and the stress concentrations around the face of an unsupported tunnel in an elastic ground mass.

Ranken and Ghaboussi (1975) have performed the most extensive series of finite element analyses for advancing tunnels. Their study, restricted to the case of isotropic or K=1 in situ stresses, investigated the behavior of both lined and unlined tunnels in elastic and elastic-perfectly plastic ground masses. The incremental excavation and support of the tunnel was simulated in the calculations, with the support "construction" occurring either immediately at the face or at a spatial delay of one tunnel radius behind

54

the face. Ground properties (E=5000-15000 psi, ϕ=0-30°, c=14-37 psi) and support (1' thick concrete) in their analyses were representative for soft ground tunnels. Although Ranken and Ghaboussi's study brings out many of the important features of the ground-structure interaction, it is nevertheless difficult to draw from their results any general quantitative conclusions or recommendations that could be profitably applied to actual tunnel design.

The behavior near the face of a tunnel can also be studied using scale models. Abel and Lee (1973) determined the stresses and displacements around unlined model tunnels in acrylic plastic, concrete, and granite.

The numerical analysis of the behavior of an advancing tunnel can be simplified considerably if certain limiting assumptions are made. The dimension of the problem can be reduced from three to two if axial symmetry can be assumed; however, this requires that : (a) the tunnel section is circular, (b) the in situ lateral stress ratio, K, is equal to 1, (c) the variation of the in situ stresses with depth is negligible, (d) the tunnel is deep lying (i.e., the proximity of the ground surface has an insignificant effect on the tunnel's behavior), and (e) any inhomogeneities in the ground are symmetric about the tunnel's centerline. The complexity of the problem can be further reduced if the ground mass can be assumed to behave linearly elastically. It should be noted that this assumption simplifies but does not eliminate the

55

nonlinearity of the analysis; the incremental advance of the tunnel--i.e., the incremental change in the geometry--is a form of nonlinearity inherent in the problem. Assuming linearly elastic ground behavior does ease the numerical solution, though, and greatly aids the interpretation of the results.

Of course, these simplifications in the analysis do have several drawbacks. The assumption of axial symmetry eliminates any possibility of studying the bending moments in the tunnel support since these moments only develop when $K \neq 1$. This limitation is not too serious, though, because these moments are quite small for all but the most rigid of the common support systems.[1] Furthermore, the critical moments in the support are more often due to factors like inadequate blocking or incomplete grouting than to overall bending under nonuniform stresses.

More serious drawbacks attend the assumption of linearly elastic ground behavior, however. A tunnel in a truly elastic ground mass doesn't need any support--it is stable at zero internal pressure--so the issue of support delay is irrelevant. Unfortunately, though, truly elastic ground masses are

---

[1]Based on the numbers from the relative stiffness solutions in Chapter 2, the eccentricity of the support thrust--i.e., the ratio of moment to thrust--is less than 15% of the tunnel radius for even the most rigid concrete supports.

the exception, and as a rule some yielding will occur. The fact that ground yielding adversely affects support loads has long been known; this concept underlies Terzaghi's pioneering development of arching theory, for example. The problem is that support delay and ground yielding are coupled (as will be explained in Section 5) and considering both simultaneously will mask the individual effects of each. Therefore, the balance of this chapter will concentrate just on implications of support delay for elastic ground masses, and the complexities of ground yielding will be added later in Sections 4 and 5.

3.2.1 Description of the Elastic Finite Element Analyses

In order to determine the quantitative effect of support delay on support loads, a series of elastic, axisymmetric finite element analyses were performed. These analyses simulate the step-by-step advance of the tunnel by deactivating ground elements and activating support elements at appropriate stages of the calculations. The distance behind the face at which the support elements are "constructed" (i.e., activated) is the major variable in the analyses.

The finite element program ADINA was used for all the analyses in this dissertation. ADINA (Automatic Dynamic Incremental Nonlinear Analysis) is a general purpose, nonlinear, three-dimensional analysis program developed by Prof. K.J. Bathe of the MIT Mechanical Engineering Department as a

further development of the SAP IV and NONSAP programs
(Bathe, 1976, 1977). It offers a variety of element types
and constitutive models that are useful in geotechnical
analyses. Although irrelevant for the analyses in this
chapter, both material and geometric nonlinearities can be
treated, and an iteration algorithm is available to ensure
accuracy in nonlinear solutions. A feature in ADINA that is
particularly attractive for the analysis of underground
structures is the "birth/death" option in which individual
elements can be activated or deactivated during the cal-
culations. Simulation of the incremental advance of the face
of a tunnel is thus possible by deactivating each "round"
of ground elements sequentially.

The element mesh used for the analyses is shown in
Figure 3.3 Because of the assumption of axial symmetry,
two-dimensional elements can be used to study the behavior
near the tunnel face; the mesh in Figure 3.3 represents a
one-radian "slice" along the tunnel axis. Extending 10
tunnel radii in the longitudinal (z-axis) direction,
and 6 radii in the radial (y-axis) direction, the mesh
is an assemblage of 114 elements and 225 nodes with a total
of 402 degrees of freedom. The isotropic (i.e., $\sigma_x = \sigma_y = \sigma_z = P$)
in situ ground stresses are applied as nodal loads at the
boundaries of the mesh before any "excavation" takes place.
Sequential excavation of the ground and the installation of
the support elements is simulated by deactivating elements
at appropriate stages of the calculations, using the "birth/

58
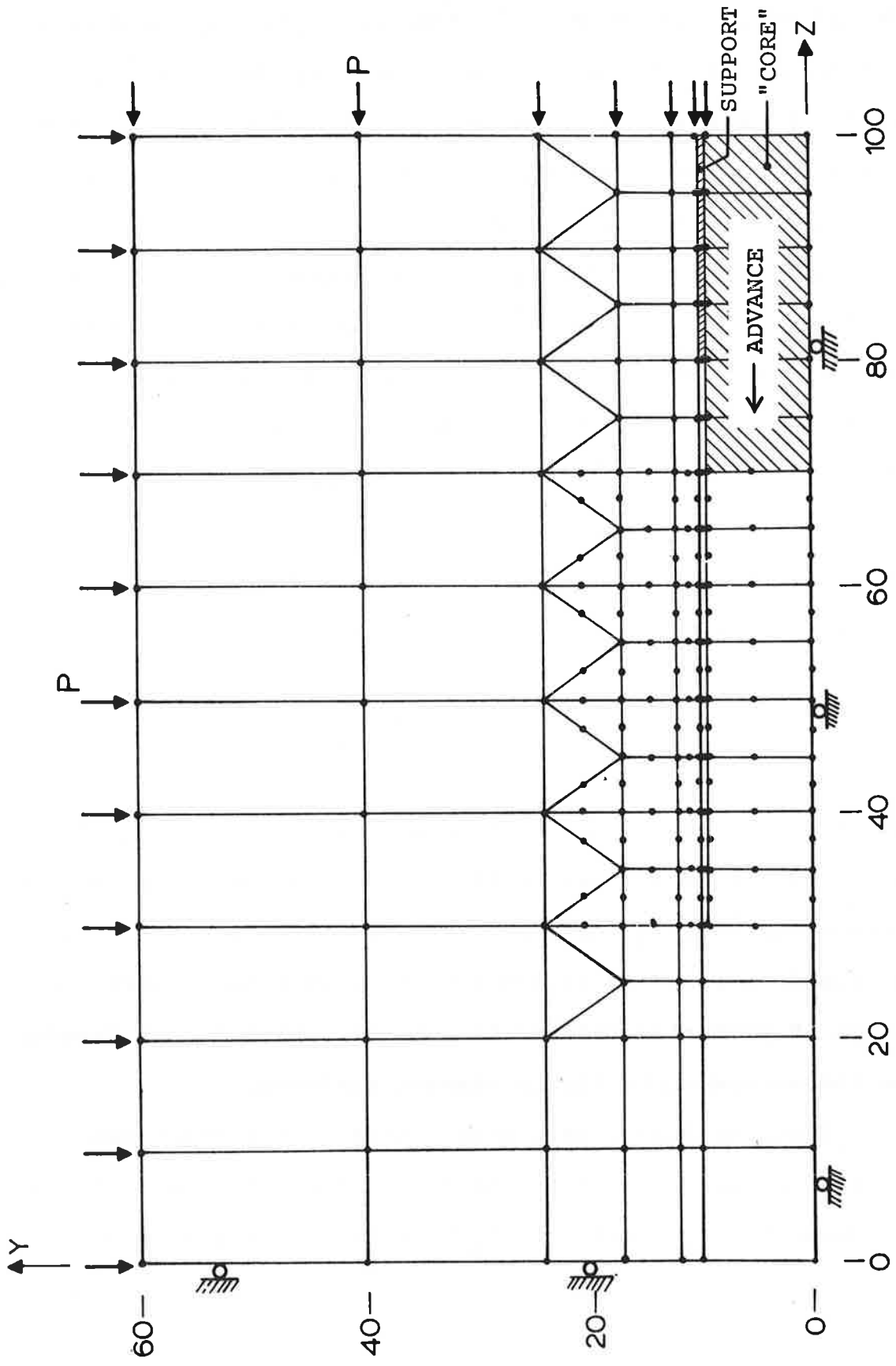
FIGURE 3.3. MESH FOR AXISYMMETRIC FINITE ELEMENT ANALYSES

death" option in ADINA. Fourteen excavation steps were per-
formed in most of the analyses, but only the data from the
last 6 to 8 steps are considered valid. The first 6 to 8
steps, although necessary, are adversely affected by the
proximity of the mesh boundary.

The parameters for all of the analyses are summarized
in Table 3.1. The analyses are grouped into five cases:
cases 1, 2A and 2B have ground moduli (E, ν) that are
reasonable for soft ground tunnels, case 4 represents a
tunnel in moderate quality rock, and case 3 can be considered
as a tunnel in either very stiff soil or very soft rock.
The support moduli (E_s, ν_s) and thicknesses (t) are typical
values for precast concrete liner elements. It should be
remembered, however, that it is not the individual stiff-
nesses of the ground and support in each case that is im-
portant, but rather their relative stiffness. This relative
stiffness is expressed by the compressibility ratio, C*,
which varies from 0.045 to 10.0 and spans the range for most
common tunneling situations. The flexibility ratio, F*,
varies from 161.0 to 48,000 but it is of minor importance
since it primarily relates to moments, which do not develop
in the axisymmetric finite element analyses.

Three analyses, each with a different support delay,
were executed for each of the five cases. The support delay
is defined by the distance L_d between the tunnel face and

60

TABLE 3.1.   PROPERTIES FOR ELASTIC FINITE ELEMENT ANALYSES

Case	Radius R	Ground Properties		Support Properties			C^*	F^*
		E	ν	E_s	ν_s	t		
1	10 Ft.	15000 psi	0.30	1.94×10^6 psi	0.30	6.9 in.	0.134	484.0
2A	10	5000	0.48	1.94×10^6	0.30	6.9	0.0528	191.0
2B	10	5000	0.30	1.94×10^6	0.30	6.9	0.0447	161.0
3	10	1.5×10^5	0.15	3.0×10^6	0.15	6.0	1.0	4800
4	10	1.5×10^6	0.15	3.0×10^6	0.15	6.0	10.0	48,000

the midpoint of the leading support ring (see Figure 3.4a).
Values for L_d of 0.25, 0.75, and 1.25 times the tunnel radius
were used in the finite element analyses. Other researchers,
most notably Ranken and Ghaboussi (1975), have chosen the
unsupported distance L_u (Figure 3.4a) between the face and
the leading edge of the support as their measure of the sup-
port delay. Certain inadequacies arise from this measure of
the delay, however; the round length (i.e., the length of
the support ring) also influences the support loads.[1]
Using the distance to the midpoint of the support ring, L_d,
as the measure of the support delay largely eliminates these
problems and is therefore the preferred choice.

Although the definition of the support delay length
in the finite element analyses is straightforward, the
interpretation of L_d in an actual tunneling sequence is more
subtle. Within each "round" or increment of advance in the
finite element simulation, the ground is "excavated" and
the support "constructed" simultaneously; as shown in Figure
3.4a, L_d is constant throughout every step of the analysis.
The complication in the actual tunneling sequence is that the
excavation and support construction do not take place

---

[1]See, for example, Ranken and Ghaboussi's analyses of
different excavation sequences. (Ranken and Ghaboussi,
1975, Section 4.4.1)
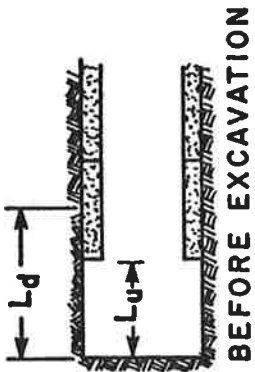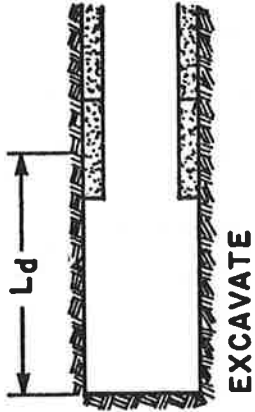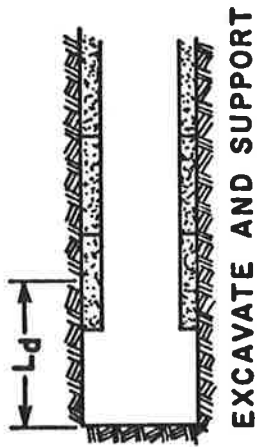
FIGURE 3.4   DEFINITION OF SUPPORT DELAY LENGTH

simultaneously and, as a consequence, L_d is not constant. As depicted in Figure 3.4b, L_d is longer just after excavation (Step 2A) than just before (Step 1). Since the time-independent ground-structure interaction is assumed to occur instantaneously upon excavation, this longest value for L_d is the correct one and the one that corresponds to the delay length in the finite element analyses.

3.2.2 Results from the Analyses

The pertinent data from the elastic axisymmetric finite element analyses are summarized in Figures 3.5 through 3.9 for each of the five cases. These figures depict the variation of the following quantities with distance from the tunnel face:

1) the radial ground displacement, u, at the tunnel wall (i.e., at r = R), expressed in dimensionless form as $\frac{uE}{PR(1+\nu)}$;

2) the longitudinal ground displacement, w, along the centerline of the tunnel, expressed in dimensionless form as $\frac{wE}{PR(1+\nu)}$; and

3) the circumferential thrust, T, in the support, expressed in dimensionless form as $\frac{T}{PR}$.

In principle, the dimensionless expressions for the radial ground displacement and circumferential support thrust have upper limits; $\frac{uE}{PR(1+\nu)}$ will equal 1.0 when the tunnel is completely unsupported, and $\frac{T}{PR}$ will equal 1.0 when the support carries the full overburden load P. Although there is no corresponding upper limit for the longitudinal ground displacements, they are also expressed dimensionlessly for convenience and consistency.

Some general trends can be readily traced in the data in Figures 3.5 through 3.9. In all of the cases, the radial ground movements begin approximately 2 to 3 tunnel radii ahead of the face. These movements quickly

65
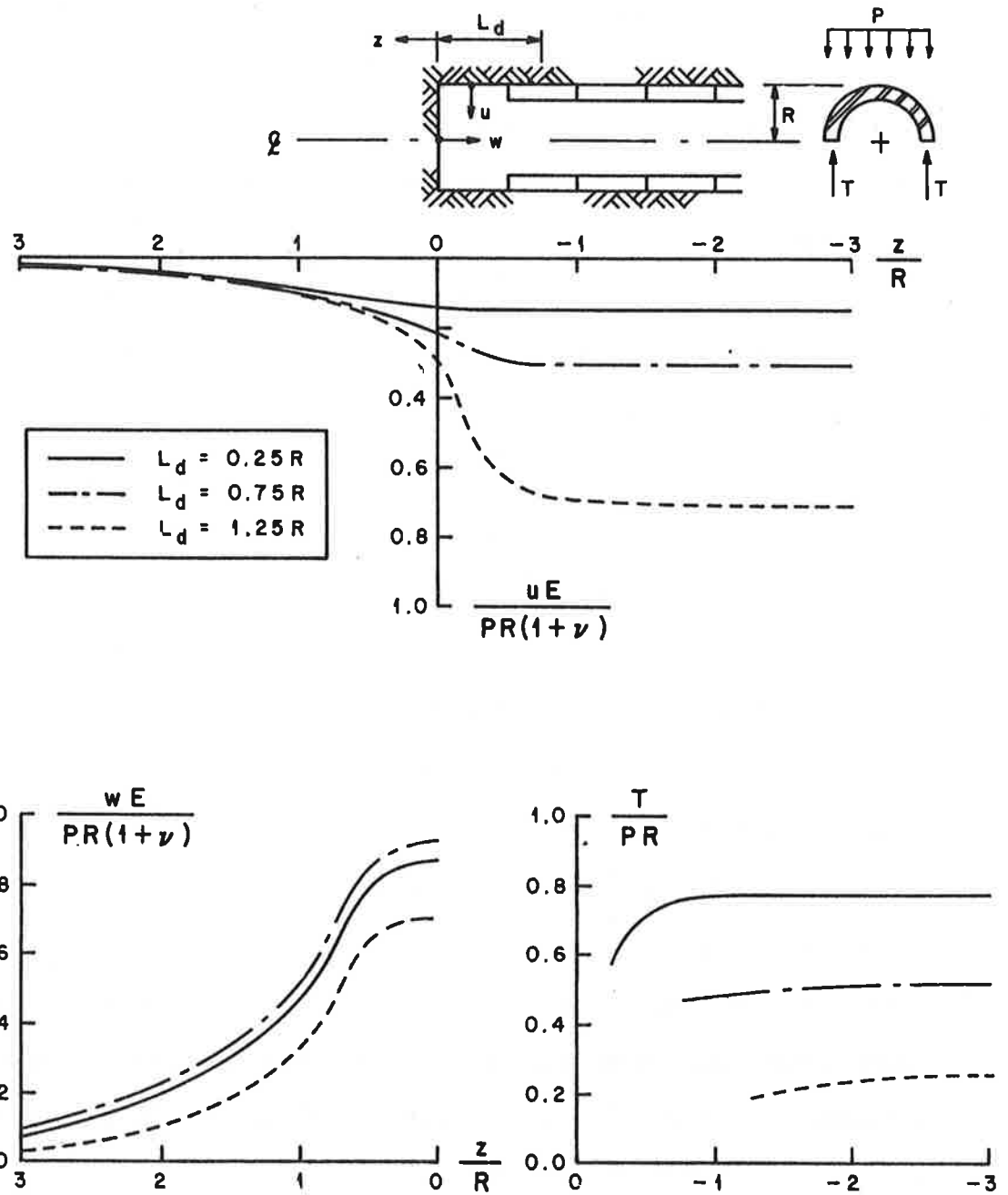
FIGURE 3.5. RESULTS FROM ELASTIC FINITE ELEMENT ANALYSES--
CASE 1 (SOFT GROUND)

66
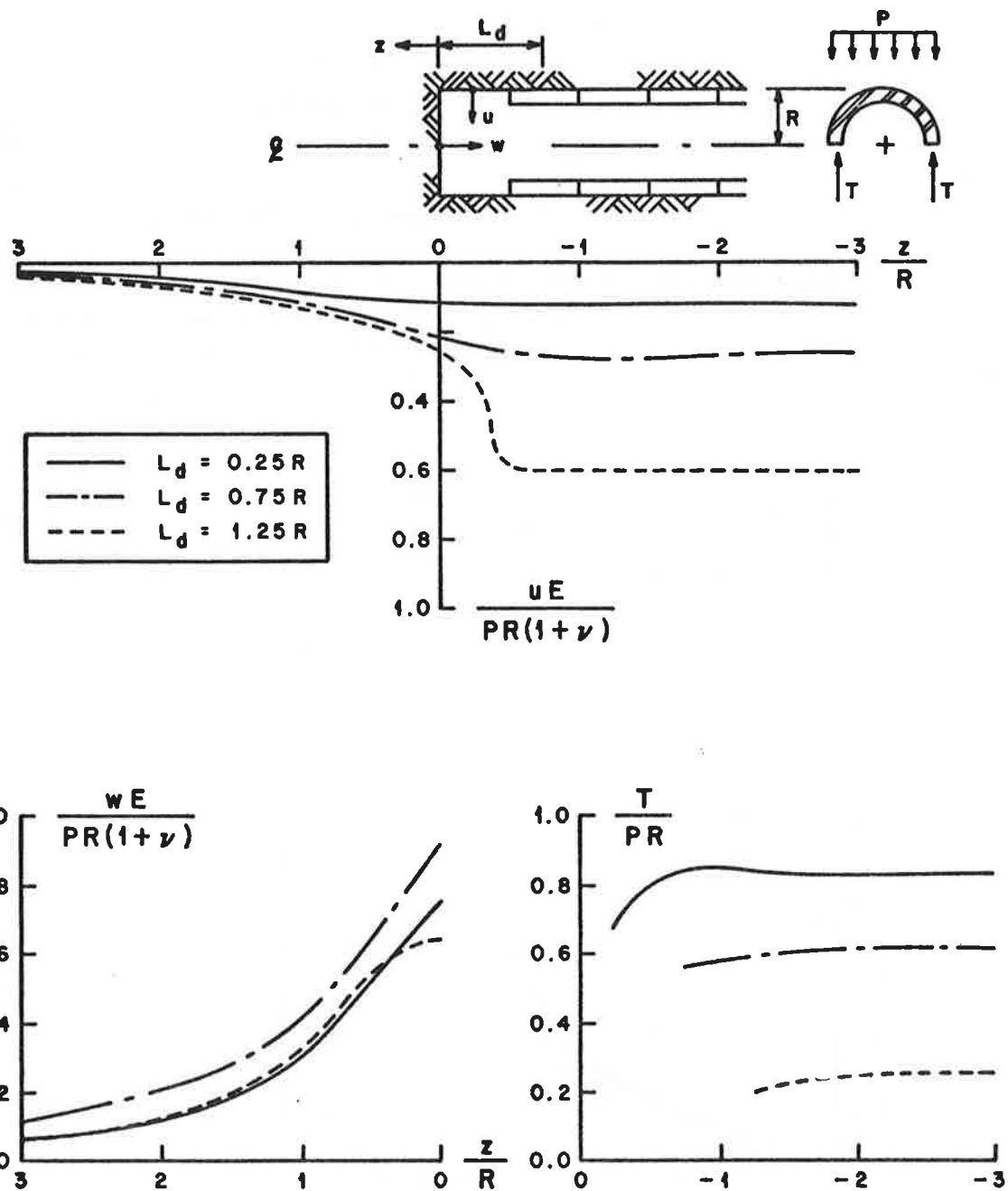
FIGURE 3.6. RESULTS FROM ELASTIC FINITE ELEMENT ANALYSES--
CASE 2A (SOFT GROUND)
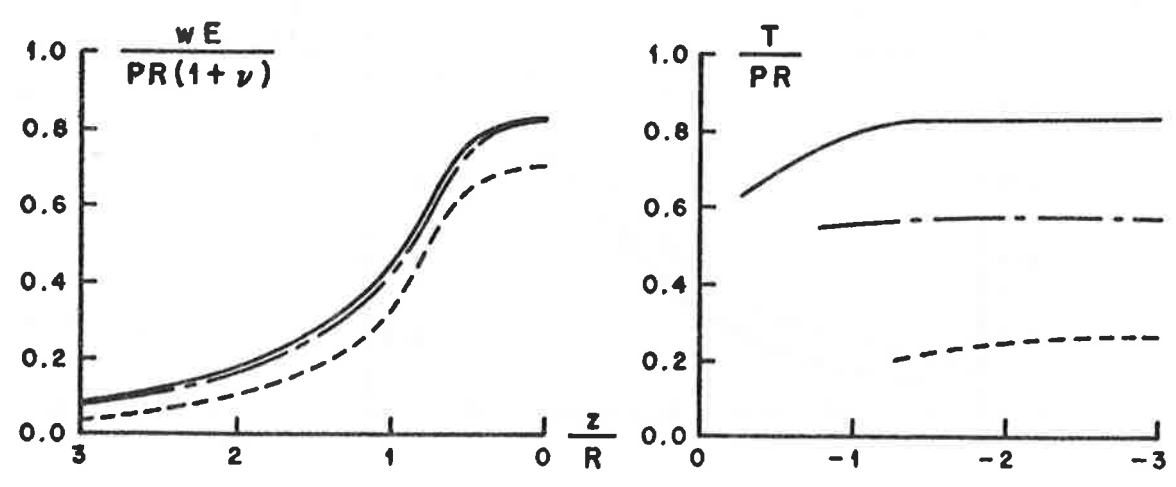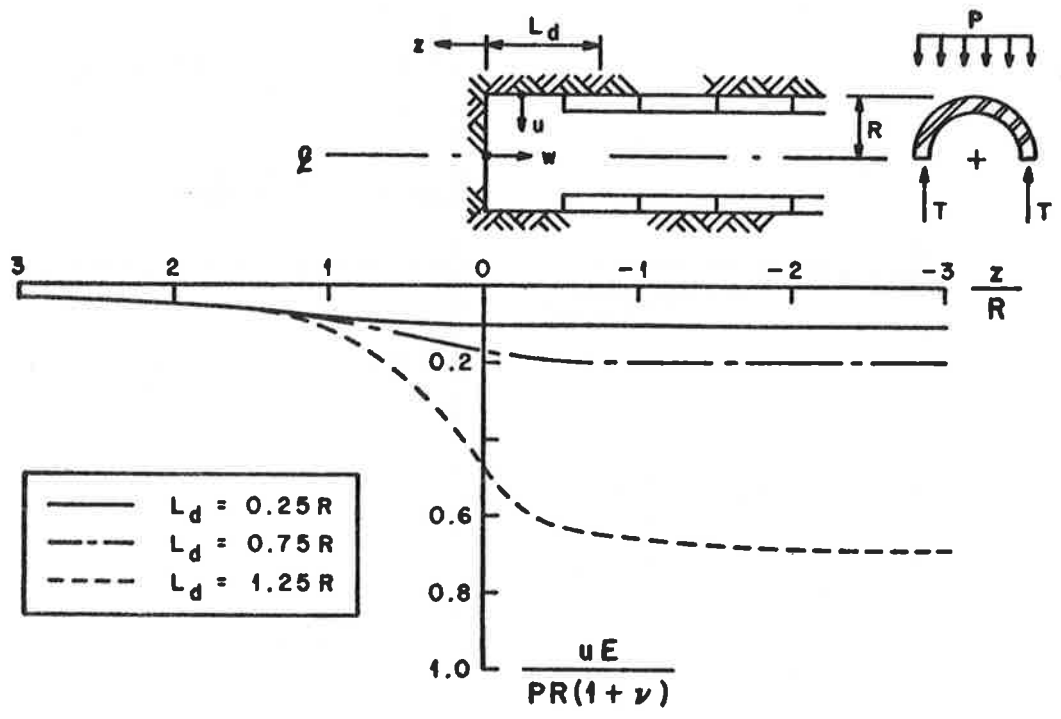
FIGURE 3.7.   RESULTS FROM ELASTIC FINITE ELEMENT ANALYSES--
CASE 2B (SOFT GROUND)

68
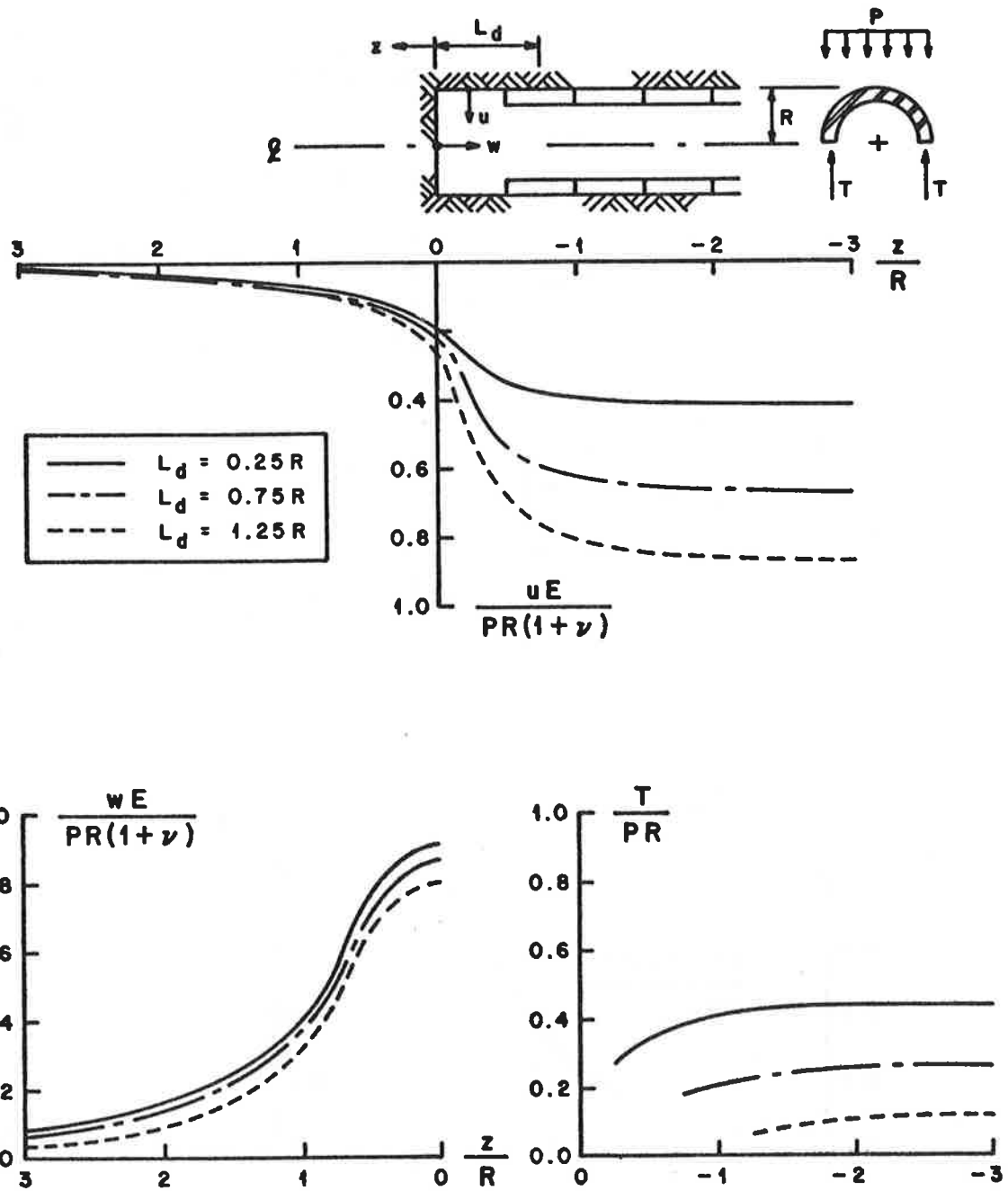
FIGURE 3.8.   RESULTS FROM ELASTIC FINITE ELEMENT ANALYSES--
CASE 3 (STIFF SOIL/SOFT ROCK)

69
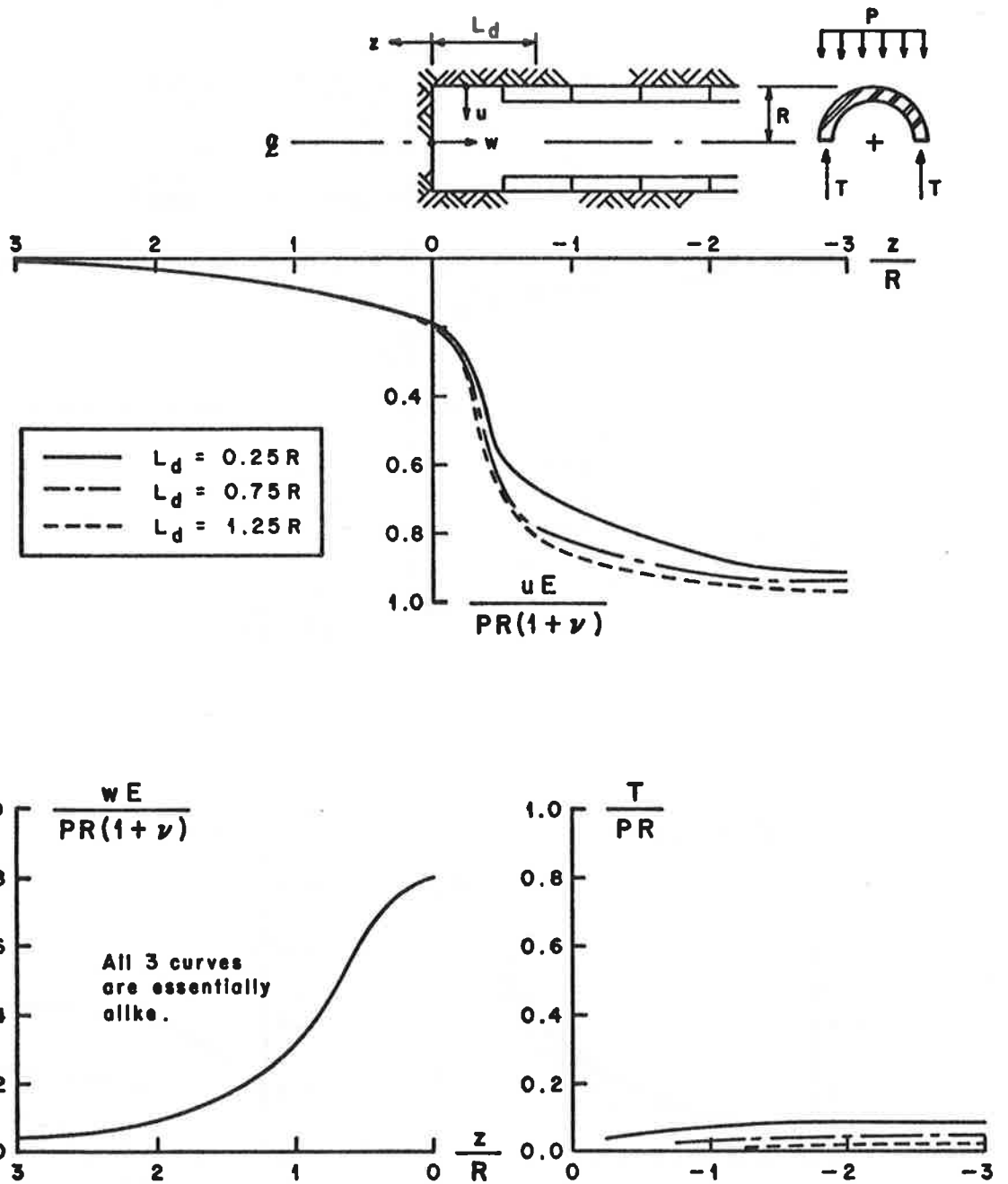
FIGURE 3.9.   RESULTS FROM ELASTIC FINITE ELEMENT ANALYSES--
CASE 4   (ROCK)

70

increase near the tunnel face, with larger movements prevailing in the analyses with the longer support delays. A large portion of the radial displacements in the soft ground cases 1, 2A, and 2B occurs ahead of the face; the installation of the support and the rapid development of support thrust quickly arrests further ground movements and constant (i.e., plane strain) conditions are soon attained. The final radial displacement coefficient $\frac{uE}{PR(1+\nu)}$ ranges from 0.1 to 0.7. At the other extreme, the relatively less stiff support in the hard rock case 4 is not as effective in restraining the radial ground displacements. A smaller fraction to the total movement takes place ahead of the face, constant or plane strain conditions are reached much later, and the final radial displacement coefficients are much larger, approaching close to 1.0

The longitudinal ground displacements, $\frac{wE}{PR(1+\nu)}$, at the centerline of the tunnel also begin at approximately 3 tunnel radii ahead of the face and increase sharply for $\frac{z}{R}$ less than 1. These longitudinal movements are of the same order of magnitude as the radial ground movements at the tunnel wall. The support delay length has a relatively minor influence on the longitudinal ground displacements and, in fact, in the hard rock case 4 the three curves for $\frac{L_d}{R}$ equal to 0.25, 0.75, and 1.25 are indistinguishable.

The variation of the support thrust $\frac{T}{PR}$ with distance from the tunnel face is not great, as indicated in Figures

71

3.5 through 3.9. Most of the thrust develops in the leading support ring during the first round of advance after installation; subsequent advances of the face increase the support thrust only slightly. In some of the analyses, particularly those with stiff supports and short delays, "arching" in the longitudinal direction induces local stress and thrust concentrations near the leading edge of the support (see, for example, case 2A with L_d = 0.25R in Figure 3.6). Decreasing the support stiffness or increasing the support delay length lessens these stress concentrations and also substantially reduces the final support thrusts.

It must be noted here that the support thrust curves in Figures 3.5 through 3.9 are based on the average thrust in each support ring. Within each ring the circumferential stresses vary with longitudinal distance, as illustrated in Figure 3.10.

The final values for the radial ground displacements and circumferential support thrusts are summarized in Table 3.2 for the five cases. These values were calculated after constant (plane strain) conditions had been reached. Generally, this occurred at a distance of 1.5 tunnel radii behind the leading edge of the support. Also included in Table 3.2 are the values for the support thrust calculated from the relative stiffness solution in Section 2. As expected, the thrusts from this solution, which does not consider any support delay, are significantly larger than the thrusts from the finite element analyses.

72
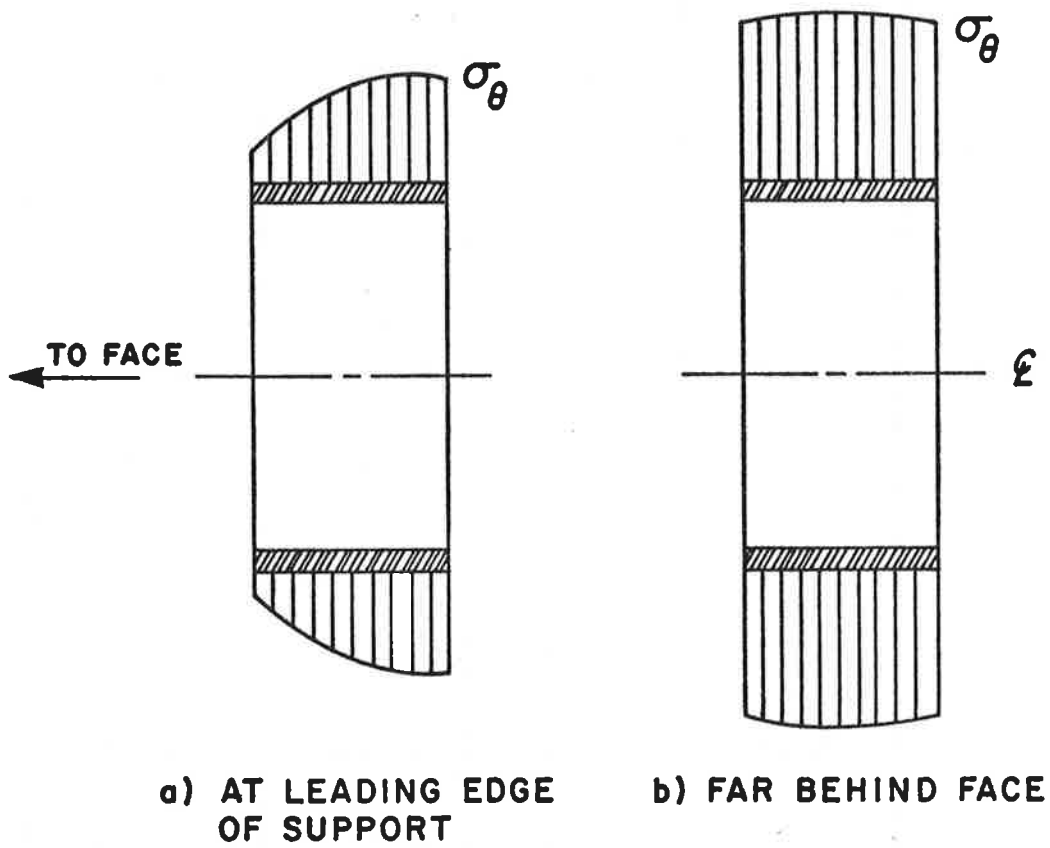
FIGURE 3.10. VARIATION OF CIRCUMFERENTIAL STRESS ALONG
INDIVIDUAL SUPPORT RINGS

TABLE 3.2   RESULTS FROM ELASTIC FINITE ELEMENT ANALYSES

Case	$\left[\dfrac{T}{PR}\right]^{*}_{RSS}$	$\dfrac{L_d}{R}$	$\dfrac{T}{PR}$	$\dfrac{uE}{PR(1+\nu)}$
1	0.914	0.25	0.77	0.15
		0.75	0.51	0.30
		1.25	0.25	0.72
2A	0.973	0.25	0.84	0.13
		0.75	0.61	0.31
		1.25	0.27	0.61
2B	0.970	0.25	0.83	0.12
		0.75	0.58	0.21
		1.25	0.28	0.69
3	0.541	0.25	0.44	0.42
		0.75	0.27	0.67
		1.25	0.13	0.87
4	0.105	0.25	0.086	0.91
		0.75	0.052	0.95
		1.25	0.027	0.99

*Thrust calculated from relative stiffness
 solution (Section 2)

74

The curves in Figures 3.5 through 3.9, while capturing the essential features of the behavior around the tunnel, do not successfully isolate the effects of the primary variable in the analyses, the support delay length L_d. The influence of the support delay is masked somewhat by the different relative support stiffnesses in the five cases. In order to highlight the effects of the support delay, the final values for the radial ground displacements and circumferential support thrusts (given in Table 3.2) are plotted in Figures 3.11 and 3.12 as functions of the dimensionless delay length L_d/R. These figures show quite dramatically the influence of support delay: increasing L_d/R from 0.25 to 1.25 increases the radial ground displacements in the different cases from 10 to 700 percent and correspondingly reduces the support thrusts by approximately 70 percent.

3.3 CORRECTION FACTORS FOR SUPPORT DELAY

Finite element analyses such as the ones described in the preceding section are powerful research tools for confirming our qualitative understanding of the ground-structure interaction around an advancing tunnel and for calculating the quantitative effect that variables like support delay have on the tunnel support loads. Nevertheless, because of their high costs and their need for high quality input data, finite element methods are often impractical to use for tunnel support design. As already

75
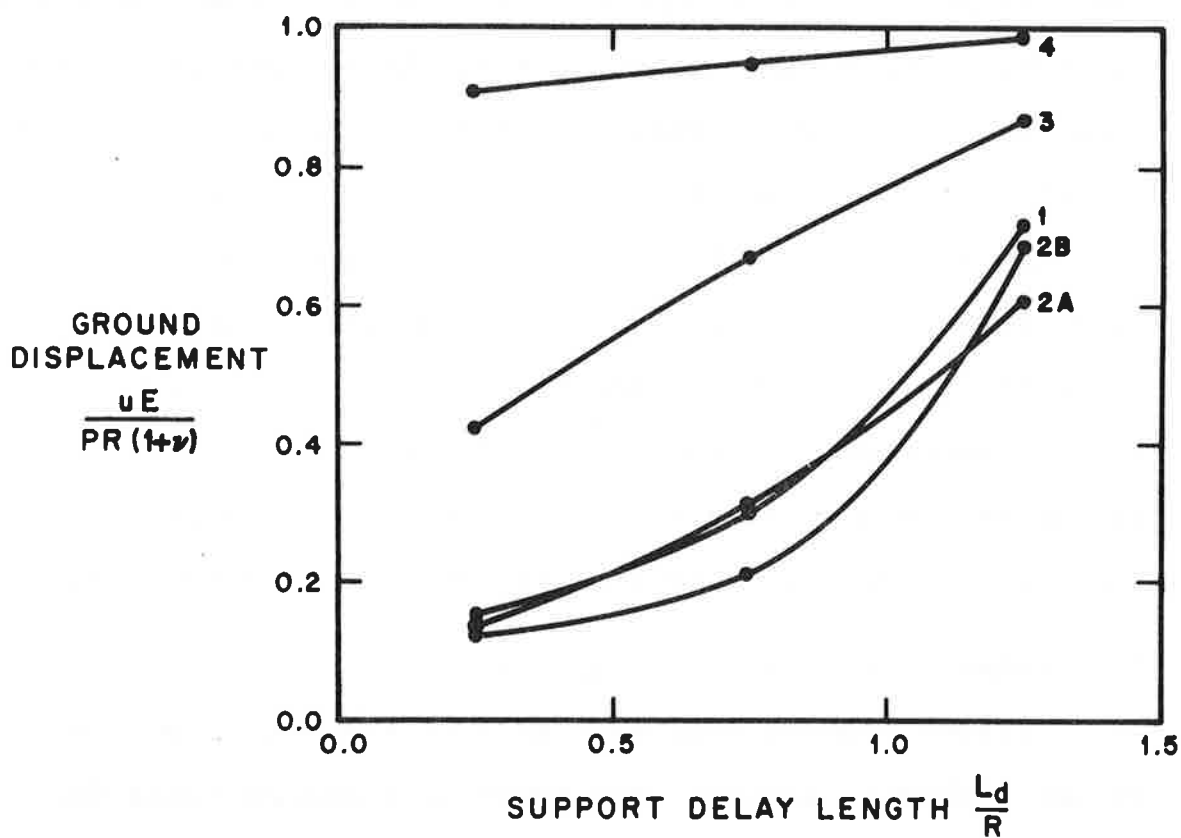
FIGURE 3.11. EFFECT OF SUPPORT DELAY ON RADIAL GROUND DISPLACEMENT

76
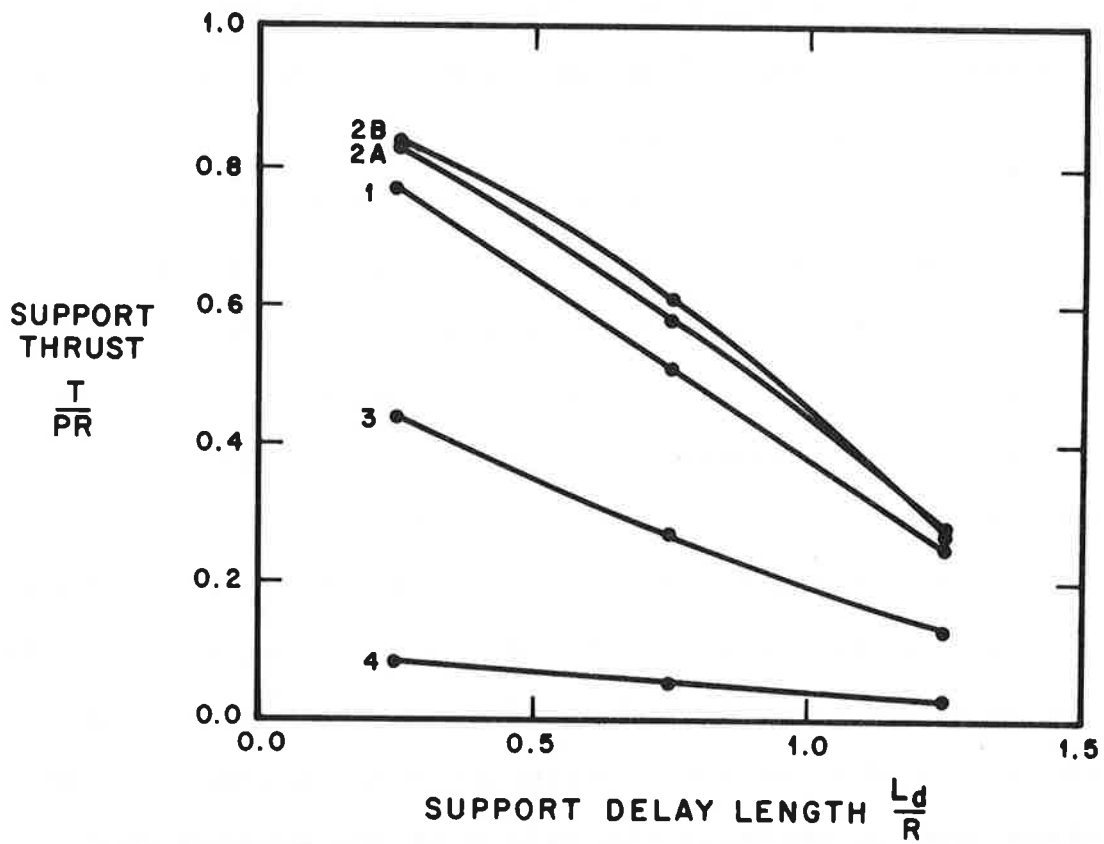
FIGURE 3.12.   EFFECT OF SUPPORT DELAY ON CIRCUMFERENTIAL
SUPPORT THRUST

77

described in Section 1, a more practical approach for the development of a practical design aid is to use the finite element method to derive correction factors that can be coupled with simpler design-oriented analytical methods like the relative stiffness solutions in Section 2. These correction factors would serve to incorporate into the design the effects of variables that cannot be considered directly in the simpler analytical methods.

An example of a correction factor for the effect of support delay is outlined in Figure 3.13. The general variation of the radial ground displacement with distance from the tunnel face and the effects of support delay on the equilibrium support loads have already been qualitatively described in Section 3.1. The important points to recall are: (1) the ground at the tunnel wall has already moved radially by an amount u_o by the time the support is installed at distance L_d behind the face (Figure 3.13a), and (2) the effect of u_o on the equilibrium support loads can be visualized by shifting the origin of the support characteristic curve to the right by an amount u_o (Figure 3.13b).[1] The net effect of the support delay is to reduce the support

[1] Any other "pre-support" ground movements would be added to u_o and would shift the support characteristic curve even further to the right. A source for these other pre-support movements might be an incompletely grouted tail void behind a shield, for example. As can be easily shown, if this pre-support movement equals u_o' it can be included in the support delay factor λ_d by subtracting u_o'/u_f from Eq. 3.1.

$$u_O = F(L_d)$$
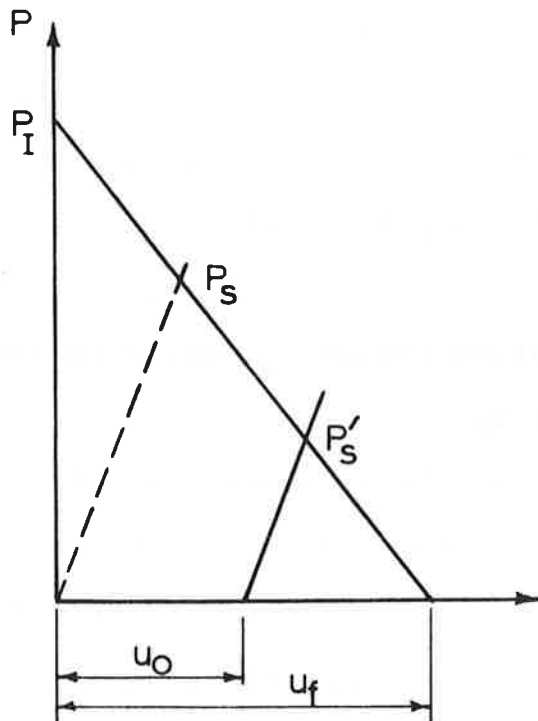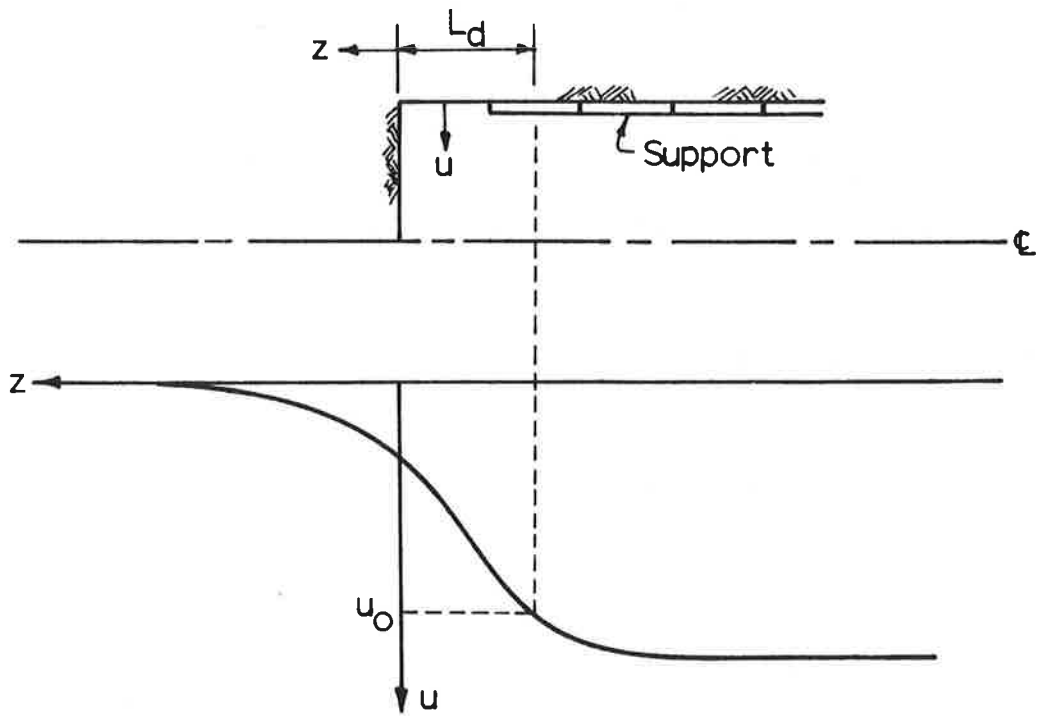
$$\frac{P'_S}{P_S} = \frac{u_f - u_O}{u_f} = \lambda_d$$

FIGURE 3.13.   DERIVATION OF CORRECTION FACTOR FOR SUPPORT DELAY

load from P_s to P_s' . If, as shown in Figure 3.13, the ground is linearly elastic, the ground characteristic curve is a straight line and the reduced support load P_s' can be determined by simple geometry:

$$\frac{P_s'}{P_s} = \frac{u_f - u_o}{u_f} \equiv \lambda_d \tag{3.1}$$

It follows, then, that:

$$P_s' = P_s \lambda_d \tag{3.2}$$

The quantity P_s represents the support load calculated from an analysis -- like the plane strain relative stiffness solution in Section 2 -- that does not consider any support delay, and λ_d is the multiplicative correction factor for the effect of the delay. Since u_o is a function of the delay length L_d, the correction factor λ_d, which depends on u_o, is also a function of L_d.

The idea of an approximate treatment for the support delay effect is not new. Daemen and Fairhurst (1972), following a chain of logic slightly different from that outlined in Figure 3.13, derived an approximate solution for the support delay effect that is of a form similar to Eq. (3.1):

80

$$\frac{P_s'}{P} = \chi \left[1 + \frac{E(1+\nu_s)\left[(1-2\nu_s) + (1-t/R)^2\right]}{E_s(1+\nu)(2-t/R)(t/R)} \right]^{-1}$$

(3.3)

in which   P = in situ stress (isotropic)

           P_s' = support load (reduced for support delay)

E, ν, E_s, ν_s = elastic properties for ground and support

           t = support thickness

           R = tunnel radius

           $\chi = \dfrac{u_f - \hat{u}_o}{u_f}$ (note similarity with Eq. 3.1)

           $\hat{u}_o$ = radial displacement at leading edge of support, obtained from an axisymmetric finite element analysis for an unlined tunnel.

           u_f = total radial displacement for an un-supported tunnel.

81

Daemen and Fairhurst correctly point out that the value of χ (which is very similar to the factor λ_d in Eq. 3.1) is crucial to their analysis. Determining χ requires knowledge of the radial ground displacement $\hat{u}_o$ at the leading edge of the support, and calculation of this displacement is possible only through the use of numerical techniques like finite element methods. Daemen and Fairhurst suggest that only one finite element solution, an axisymmetric elastic solution for an unsupported tunnel, is needed to calculate χ (see Figure 3.14); this general relationship for χ would then hold for all supported tunnels and all support delays.

Since Daemen and Fairhurst do not present any data substantiating their approximate analysis, it is interesting to compare the results from their solution with the support loads calculated from the elastic axisymmetric analyses of Section 3.2. This comparison is made in Table 3.3. The values for the support thrust calculated from Daemen and Fairhurst's approximate solution and from the finite element analyses are reasonably close for the fully supported (i.e., $L_d/R = 0.25$ or $L_u/R = 0$) cases, but the errors from the approximate analysis become intolerable as the support delay is increased. For L_d/R equal to 0.75 and 1.25, Daemen and Fairhurst's approximate solution overestimates the support loads by up to 84 percent (Table 3.3).

82
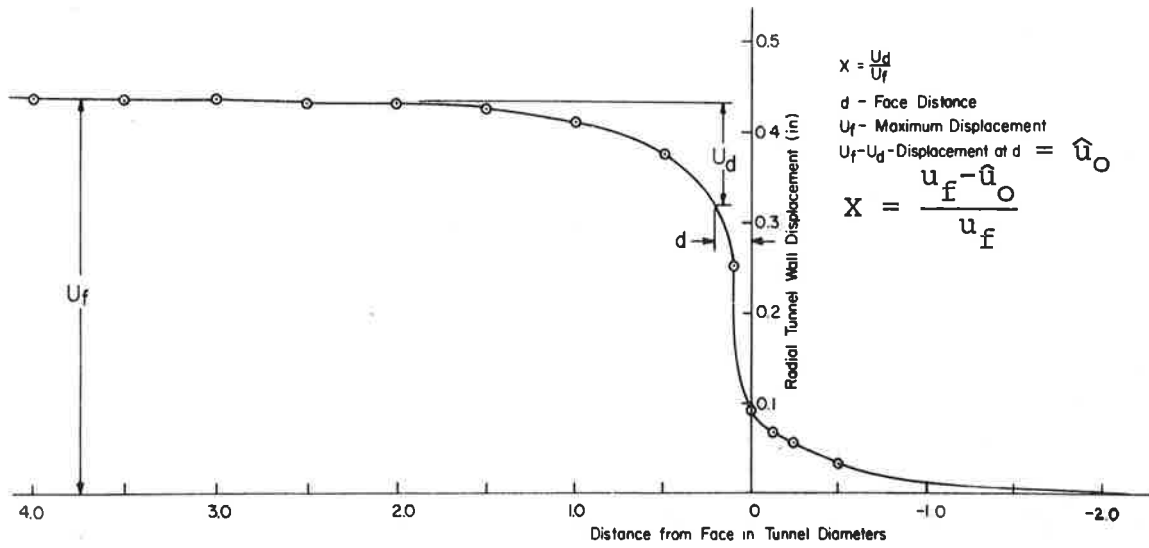
FIGURE 3.14.   RADIAL GROUND DISPLACEMENT VS. DISTANCE FROM FACE
FOR AN UNLINED ELASTIC TUNNEL (FROM DAEMEN AND
FAIRHURST, 1972)

83

TABLE 3.3. COMPARISON OF DAEMEN AND FAIRHURST'S APPROXIMATE ANALYSIS WITH RESULTS FROM ELASTIC FINITIE ELEMENT ANALYSES

Case	$\frac{L_d}{R}$	$\frac{L_u}{R}$	$\left[\frac{T}{PR}\right]$ From Elastic Finite Element Analysis (Table 3.2)	$\left[\frac{T}{PR}\right]$ From Daemen and Fairhurst's Analysis (Eq. 3.3)[1]	Error in Daemen and Fairhurst's Analysis (Percent)
1	0.25	0	0.77	0.70	9
	0.75	0.50	0.51	0.12	76
	1.25	1.00	0.25	0.043	83
2A	0.25	0	0.84	0.75	11
	0.75	0.50	0.61	0.12	80
	1.25	1.00	0.27	0.046	83
2B	0.25	0	0.83	0.74	11
	0.75	0.50	0.58	0.12	79
	1.25	1.00	0.28	0.046	84
3	0.25	0	0.44	0.42	5
	0.75	0.50	0.27	0.070	74
	1.25	1.00	0.13	0.026	80
4	0.25	0	0.086	0.083	3
	0.75	0.50	0.052	0.014	73
	1.25	1.00	0.027	0.0051	81

[1]Note that $\frac{T}{PR}$ equals $\frac{P'_s}{P_s}$ in Equation 3.3

There are two main reasons for the errors in the approximate solution, and both of them concern the method for determining χ. First, χ is directly dependent upon $\hat{u}_o$, the radial ground displacement at the leading edge of the support; however, choosing the leading edge of the support as the point for evaluating the ground displacement is completely arbitrary. Considering the steep displacement gradients around the tunnel face, computing $\hat{u}_o$ at the tail end of the support ring or at midlength (probably the best choice) would give much different values for χ. Second, the u vs. z relationship from the unsupported analysis (Figure 3.14) used to compute $\hat{u}_o$ and χ is not correct for a supported case. The curves in Figures 3.5 through 3.9 clearly show that installing a support alters the u vs. z relationship not only around the support but also ahead of the face. The "one curve applies to all" approach for calculating $\hat{u}_o$ and χ is incorrect and, as a result, Daemen and Fairhurst's technique cannot be used as a general design tool.

The problems associated with the determination of χ in Daemen and Fairhurst's formulation will also apply to the calculation of λ_d in Eq. (3.1). It will be difficult to compute with accuracy the value of u_o upon which λ_d so heavily depends. However, the form of Eq. (3.1) suggests an alternate approach for determining λ_d.

Instead of deriving λ_d from the uncertain values of the radial displacements u_o and u_f, λ_d can be backfigured directly from the ratio P_s'/P_s. While it is true that in a real design problem the ratio P_s'/P_s is unknown and is in fact the quantity one is trying to determine, enough values for P_s'/P_s have been obtained from the finite element analyses in Section 3.2 that a general relationship between P_s'/P_s and L_d, and therefore between λ_d and L_d, can be derived, at least for a limited range of L_d. This general relationship can then be used in actual design calculations.

In the finite element analyses, the circumferential support thrust, T_{FE}, is uniquely related to the reduced support load, P_s', in Eq. (3.1); similarly, the thrust from the excavation unloading relative stiffness solution, T_{RSS}, corresponds to P_s, the unreduced support load. Thus, λ_d equals the ratio T_{FE}/T_{RSS}.

The values of T_{FE}/T_{RSS} for the cases analyzed in Section 3.2 are plotted in Figure 3.15 as a function of the dimensionless delay length L_d/R. Although there is some small scatter in the data from the different cases, the trend of the λ_d vs. L_d relation can be expressed with reasonable accuracy by a straight line (based on a least-squares fit for the data) of the form:

$$\lambda_d = \frac{T_{FE}}{T_{RSS}} = 0.98 - 0.57\left(\frac{L_d}{R}\right) \tag{3.4}$$

86
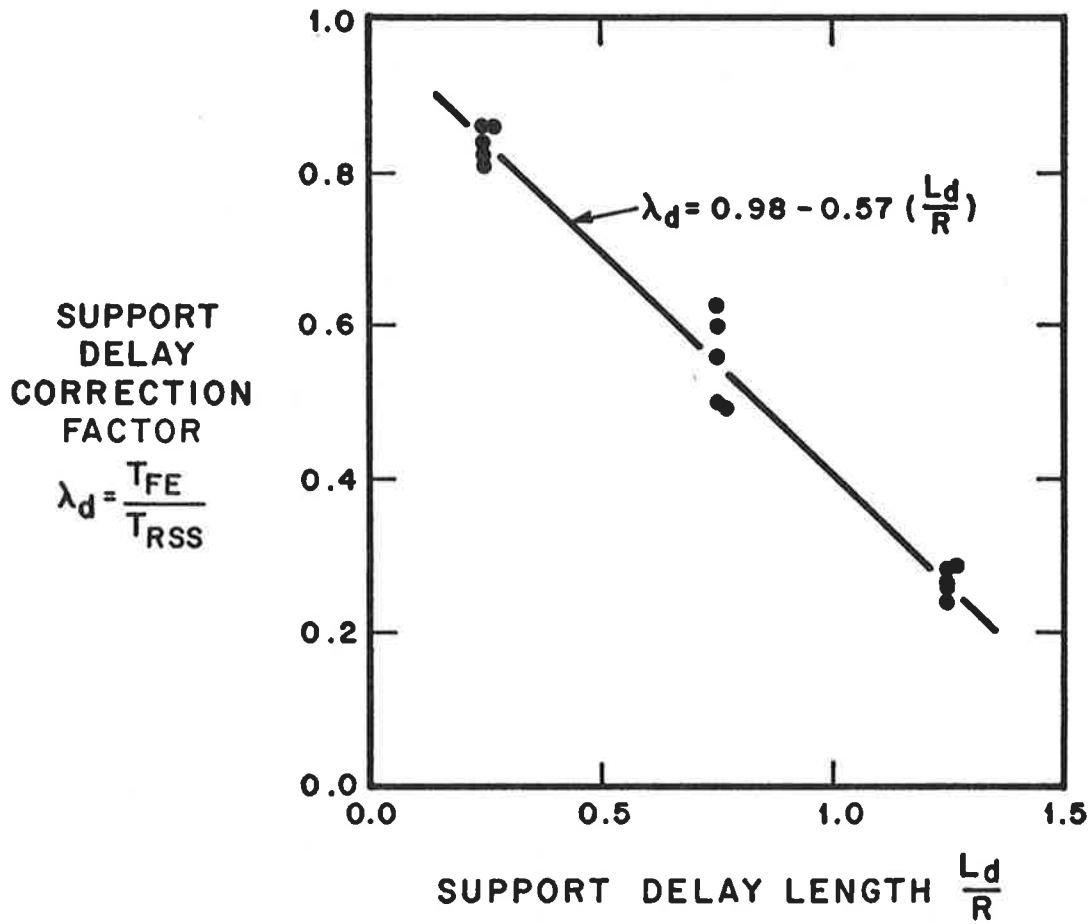
FIGURE 3.15.   SUPPORT DELAY CORRECTION FACTOR

87

Based on physical considerations, λ_d varies between the extremes of 1.0 (no support delay effect) and 0 (full support delay effect); as a result, L_d/R in Eq. (3.4) is limited to values greater than 0 (approximately) and less than 1.7. Actually, Eq. (3.4) is really valid for only a more limited range of L_d/R, since the analyses from which the data in Figure 3.15 were taken only consider delay lengths of 0.25, 0.75, and 1.25 times the tunnel radius. Applying Eq. (3.4) to cases in which L_d/R is less than 0.15 or more than about 1.5 will probably give erroneous results. This limitation is not serious, though, since the delay lengths most commonly encountered in actual tunnels lie within the range of L_d/R for which Eq. (3.4) is valid.

For Eq. (3.4) to be of truly general value, at least for tunnels in elastic ground masses, it must be insensitive to the two other major variables affecting the support loads: (1) the lateral stress ratio K, and (2) the relative support stiffness. The influence of K will be discussed in detail in the next section, but the insensitivity of λ_d to variations in the relative support stiffness (as expressed by the compressibility ratio C^*) for K = 1 conditions is clearly demonstrated by the data from the elastic axisymmetric finite element analyses. As shown in Figure 3.16 for delay lengths of 0.25R, 0.75R, and 1.25R, λ_d varies insignificantly for values of the compressibility ratio, C^*, between 0.045 and 10.0. Stiff supports (small

88
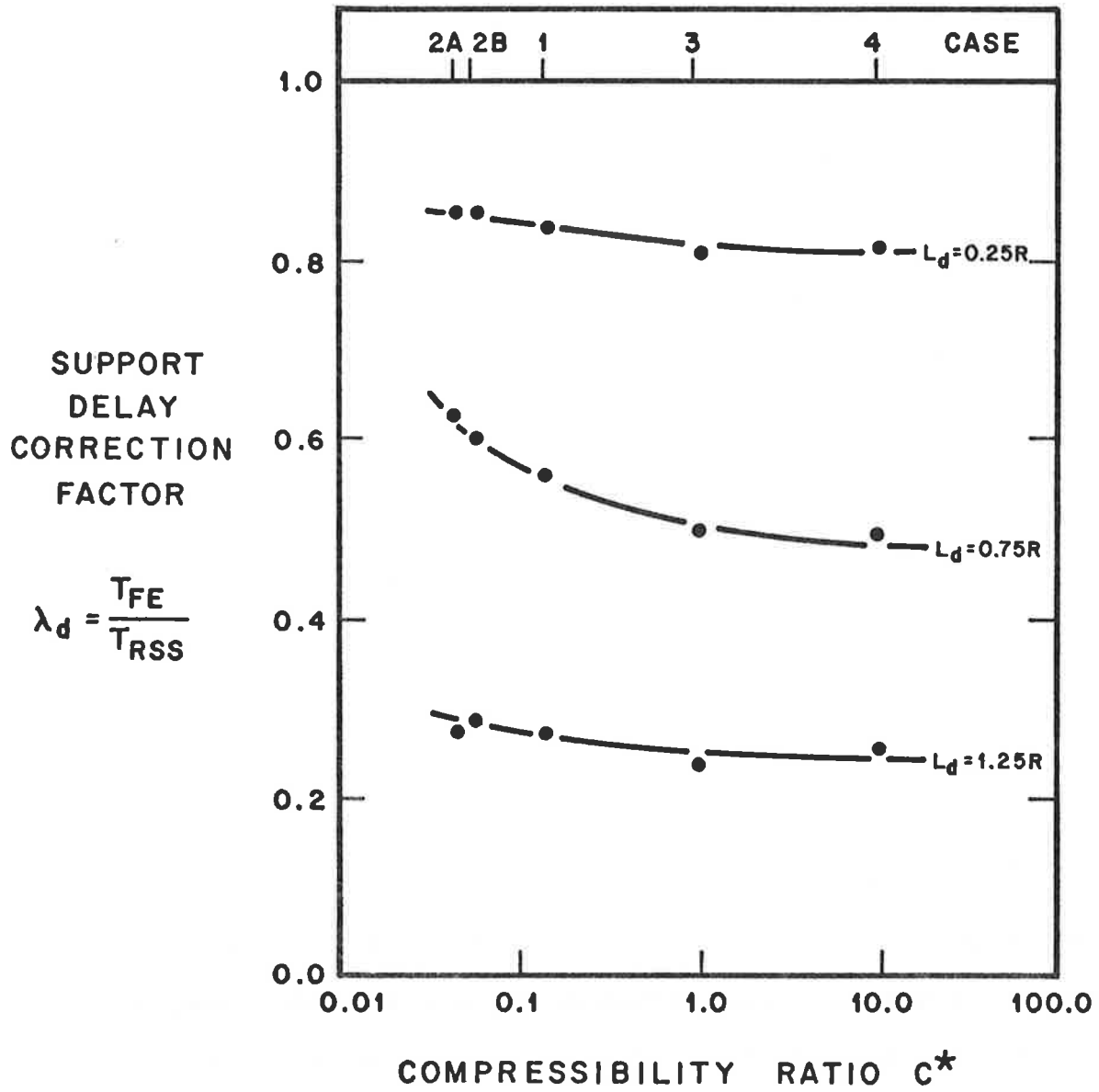
FIGURE 3.16.   EFFECT OF COMPRESSIBILITY RATIO ON SUPPORT
DELAY FACTOR

89

C^*) give slightly higher values for λ_d, especially in the medium delay ($L_d = 0.75R$) cases.

3.4 EFFECT OF SUPPORT DELAY UNDER NONAXISYMMETRIC STRESS CONDITIONS

All of the preceding discussion in this chapter, besides having been restricted to tunnels in elastic ground masses, has also been limited to cases in which the in situ stresses in the ground are axisymmetric (i.e., $K = 1$). This is a rather atypical stress condition in tunneling, so before any general relationship like Eq. (3.4) for the support delay effect can be used in design, the influence of the lateral stress ratio K must be investigated. This is the purpose of this section.

The material that follows is intended to parallel the development in the preceding section of this chapter. First, the support delay correction factor, λ_d, for the support thrusts is derived for $K \neq 1$ conditions, and next, the sensitivity of this factor to variations in the relative support stiffness is studied. In addition, since nonuniform support loads develop for $K \neq 1$ conditions, a second correction factor, λ_d^*, is derived to account for the effect of support delay on the bending moments in the support.

In the preceding sections, the effects of the support delay for $K = 1$ conditions could be quantitatively determined using finite element methods that simulated the step-

by-step construction of an advancing tunnel. The restriction of $K = 1$ meant that these finite element analyses could be axisymmetric, and the dimension of the problem was therefore reduced from three to two. Relaxing the restriction of $K = 1$ destroys this axial symmetry of the problem and, as a result, a full three-dimensional finite element analysis must be performed for the $K \neq 1$ case. Three-dimensional analyses are very expensive and time-consuming, and even for research purposes they are generally impractical. Fortunately, though, a simpler approximate technique, based on ideas similar to those presented by Panet (1976) and by Laabmayr and Swoboda (1978), can be employed to study the interrelationship between support delay and stress state and to derive the correction factors λ_d and λ_d^* for $K \neq 1$ conditions.

3.4.1   Approximate Analysis of Support Delay Effect

As already described, the most important effect of support delay is that movement takes place in the ground mass before the support is constructed. This movement mobilizes some of the resistance of the ground and thereby reduces the load that the support must carry. In the axisymmetric finite element analyses in Section 3.2, these movements were an intrinsic part of the simulation of the incremental tunnel construction. However, it is also possible to artificially incorporate (at least approximately) these "pre-support" movements, which are directly related

91

to the support delay length L_d, into a plane strain analysis.

These "pre-support" ground movements can be treated in a plane strain analysis in two ways. Panet (1976 -- see also Panet and Guellec, 1974) suggests that the tunnel can be initially modeled as an unlined opening with an internal pressure equal to the in situ ground stresses (Figure 3.17a). Before the support is installed, the internal pressure is reduced by a fraction α and the ground moves radially inward by an amount u_o; the support is then installed and the internal pressure is reduced to zero. Laabmayr and Swoboda (1978), on the other hand, advocate a slightly different approach. In their system, the ground mass is initially unperforated (Figure 3.17b). Before the tunnel is excavated and the support is installed, the elastic modulus within the "core" region -- i.e., the region within the eventual tunnel perimeter -- is reduced by a fraction β (they use $\beta = 0.5$) and the ground moves radially inward by an amount u_o at $r = R$; the support is then activated and the core region is simultaneously "excavated" by reducing the modulus to zero. The two methods are equivalent when K equals one, but when K is different from one, the internal pressure in Panet's model must also be nonuniform and the method breaks down somewhat. Laabmayr and Swoboda's method, on the other hand, works equally well for all values of K and is therefore the preferred choice.
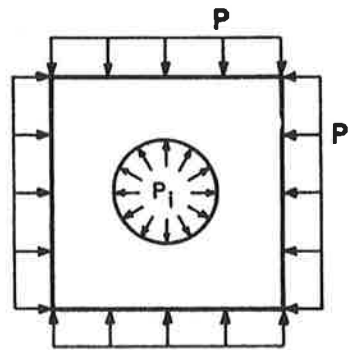
i) Initial Conditions : $P_i = P$
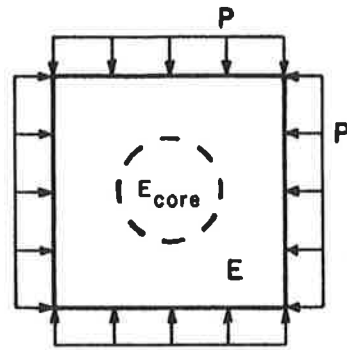
i) Initial Conditions : $E_{core} = E$
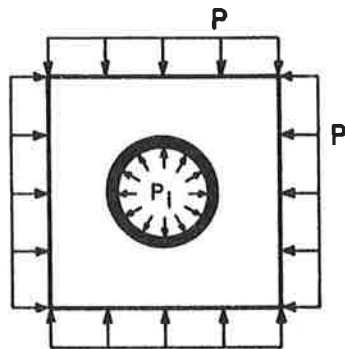
ii) $P_i = (1-\alpha)P$
Install Support
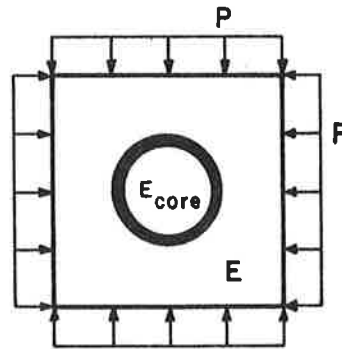
ii) $E_{core} = (1-\beta)E$
Install Support
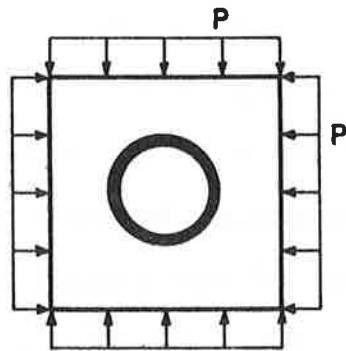
iii) $P_i = 0$
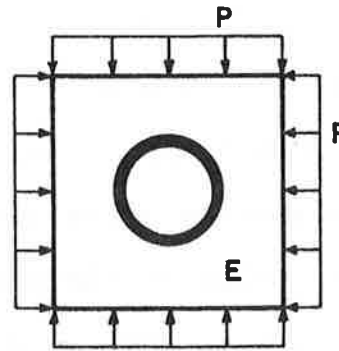
iii) $E_{core} = 0$

A) PANET

B) LAABMAYR and SWOBODA

FIGURE 3.17.   METHODS FOR SIMULATING SUPPORT DELAY IN PLANE
STRAIN ANALYSES

93

In conceptual terms, Laabmayr and Swoboda's reduction
of the core modulus to simulate the behavior near the tun-
nel face is quite reasonable.[1] In an actual tunnel
(Figure 3.18a) the ground movements are a function of dis-
tance from the face, z; by the time the support is in-
stalled at a distance L_d behind the face, total ground move-
ments equal to u_o have already occurred. In the plane strain
approximation (Figure 3.18b) the ground movements are now a
function of the core modulus factor, β; at a core modulus
reduction of β_d, total ground movements equal to u_o have
again occurred. The effect of u_o on the support loads will
be roughly the same regardless of its cause, and as a conse-
quence the core modulus reduction factor β should be
roughly correlated with the support delay length L_d. (The
exact relationship between β and L_d is derived later in
this chapter.) Of course, the detailed distributions of
the stresses and displacements in Laabmayr and Swoboda's
plane strain approximation will not match those in the
real tunneling situation, but the essential feature of the
support delay -- the overall movement of the ground prior
to support -- will be adequately simulated by the core
modulus reduction.

[1]Lombardi (1973) has used a similar technique.

94
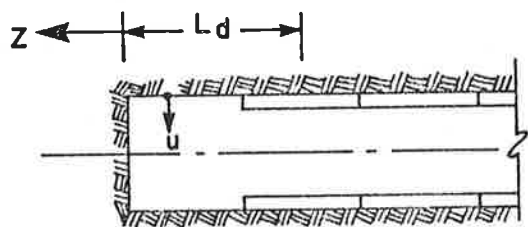
a) ACTUAL TUNNEL
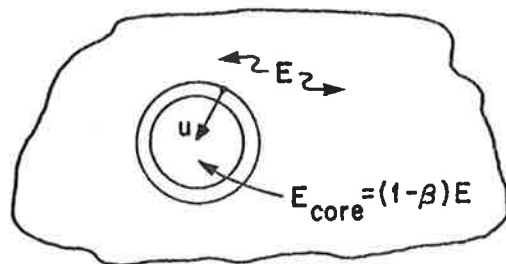
b) PLANE STRAIN APPROXIMATION
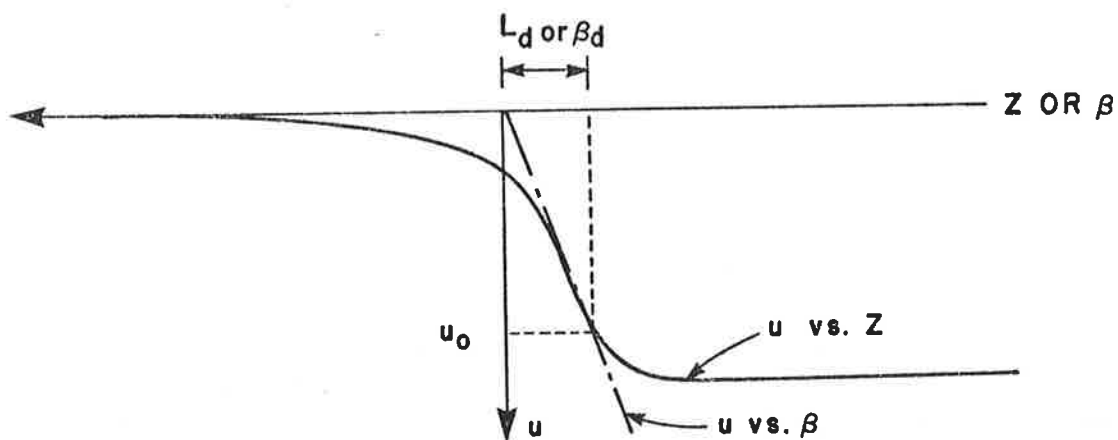
c) RADIAL GROUND DISPLACEMENTS

FIGURE 3.18.   CONCEPTUAL INTERPRETATION FOR SIMULATING
SUPPORT DELAY WITH CORE MODULUS REDUCTION

95

A closed-form plane strain solution that incorporates Laabmayr and Swoboda's approximation for the support delay has been developed; the detailed derivation is presented in Appendix B. This solution is very similar to the relative stiffness solutions described in Section 2. The major difference in the new solution is that, instead of deriving the initial ground displacements u_I and v_I from the in situ stresses in the unperforated ground mass, the initial ground movements are now based on the stresses existing in the ground mass after the modulus in the core region has been partially reduced. All subsequent steps in the derivations for the two solutions are the same. For simplicity, only the full-slip boundary condition at the ground-support interface is considered herein; although the no-slip condition may in fact be more appropriate in certain cases, the differences in the support loads calculated from the two (full-slip vs. no-slip) solutions would be small (see Section 2).

The support thrust and moment coefficients from the delayed support solution are (see Appendix B for details):

$$\frac{T}{PR} = \frac{1}{2}(1+K)(1-a_o^*) + \frac{1}{2}(1-K)(1-2a_2^*)\cos2\theta \qquad (3.5)$$

$$\frac{M}{PR^2} = \frac{1}{2}(1-K)(1-2a_2^*)\cos2\theta \qquad (3.6)$$

96

in which: $\quad a_o^* = \dfrac{C^*(1-\nu) - A_1(1+C^*/F^*)}{C^*(1-\nu) + 1 + C^*/F^*}$ $\qquad$ (3.7a)

$$a_2^* = \dfrac{(F^*+6)(1-\nu) + A_2[1+4(2-3\nu)]}{2F^*(1-\nu) + 6(5-6\nu)} \qquad (3.7b)$$

$$C^* = \dfrac{ER(1-\nu_s^2)}{E_sA_s(1-\nu^2)} \qquad (3.7c)$$

$$F^* = \dfrac{ER^3(1-\nu_s^2)}{E_sI_s(1-\nu^2)} \qquad (3.7d)$$

$$A_1 = \dfrac{(1-\mu)(1-2\nu)}{[1 + \mu(1-2\nu)]} \qquad (3.7e)$$

$$A_2 = \dfrac{(\mu-1)[1+\mu(3-4\nu)]}{[(1+\mu)^2(3-4\nu) + 4\mu(1-2\nu)^2]} \qquad (3.7f)$$

$$\mu = \dfrac{1}{1 - \beta} \qquad (3.7g)$$

$$(1-\beta) = \dfrac{E_{core}}{E} \qquad (3.7h)$$

97

The factor β represents the fraction by which the core modulus is reduced before support installation.

3.4.2   Support Delay Correction Factors for K ≠ 1

The support delay correction factor for the support thrusts, λ_d, is derived for the K ≠ 1 case in the same way as for K = 1 conditions.   Recalling the definition of λ_d for the case of K = 1 (see Eq. 3.4):

$$\lambda_d = \frac{T_{FE}}{T_{RSS}} \qquad (3.8)$$

in which T_{FE} is the thrust from the axisymmetric finite element analysis with support delay and T_{RSS} is the thrust from the relative stiffness solution without support delay, the definition of λ_d for the case of K ≠ 1 can be analogously defined as:

$$\lambda_d = \frac{T_{\beta \neq 0}}{T_{RSS}} = \frac{T_{\beta \neq 0}}{T_{\beta = 0}} \qquad (3.9)$$

in which $T_{\beta \neq 0}$ and $T_{\beta = 0}$ (which equals T_{RSS}) are calculated from the approximate plane strain solution for the support delay (Eq. 3.5).   A similar factor, λ_d^*, for the support moments can be derived from Eq. (3.6) and is defined as:

$$\lambda_d^* = \frac{M_{\beta \neq 0}}{M_{RSS}} = \frac{M_{\beta \neq 0}}{M_{\beta = 0}} \qquad (3.10)$$

The variations of λ_d and λ_d^* with β for the case of $K = 0.5$ are illustrated in Figures 3.19 and 3.20 for several values of Poisson's ratio, ν.

The core modulus reduction factor β is directly related, of course, to the support delay length L_d. This relationship can now be derived from the two expressions for λ_d, Eqs. (3.4) and (3.9), which are equal when $K = 1$. Solving these two equations together with Eq. (3.5) for the support thrusts gives the following expression for β:

$$\beta = \frac{2(1-\nu)[0.02 + 0.57\left(\frac{L_d}{R}\right)]}{2(1-\nu) - 0.98 + 0.57\left(\frac{L_d}{R}\right)}$$

(3.11)

Using the relations in Eqs. (3.9) and (3.10), it is possible to investigate the sensitivity of the support delay correction factors λ_d (for support thrust) and λ_d^* (for support moments) to variations of the lateral stress ratio K and the relative support stiffness (expressed by the dimensionless ratios C^* and F^*). A parametric study was performed with the following values for the variables:

1) lateral stress ratio K ranging between 0 and 5

2) compressibility ratio C^* ranging between 0.01 and 100.0

3) flexibility ratio F^* equal to $1200C^*$ unless otherwise stated (corresponds to t/R of 0.1)
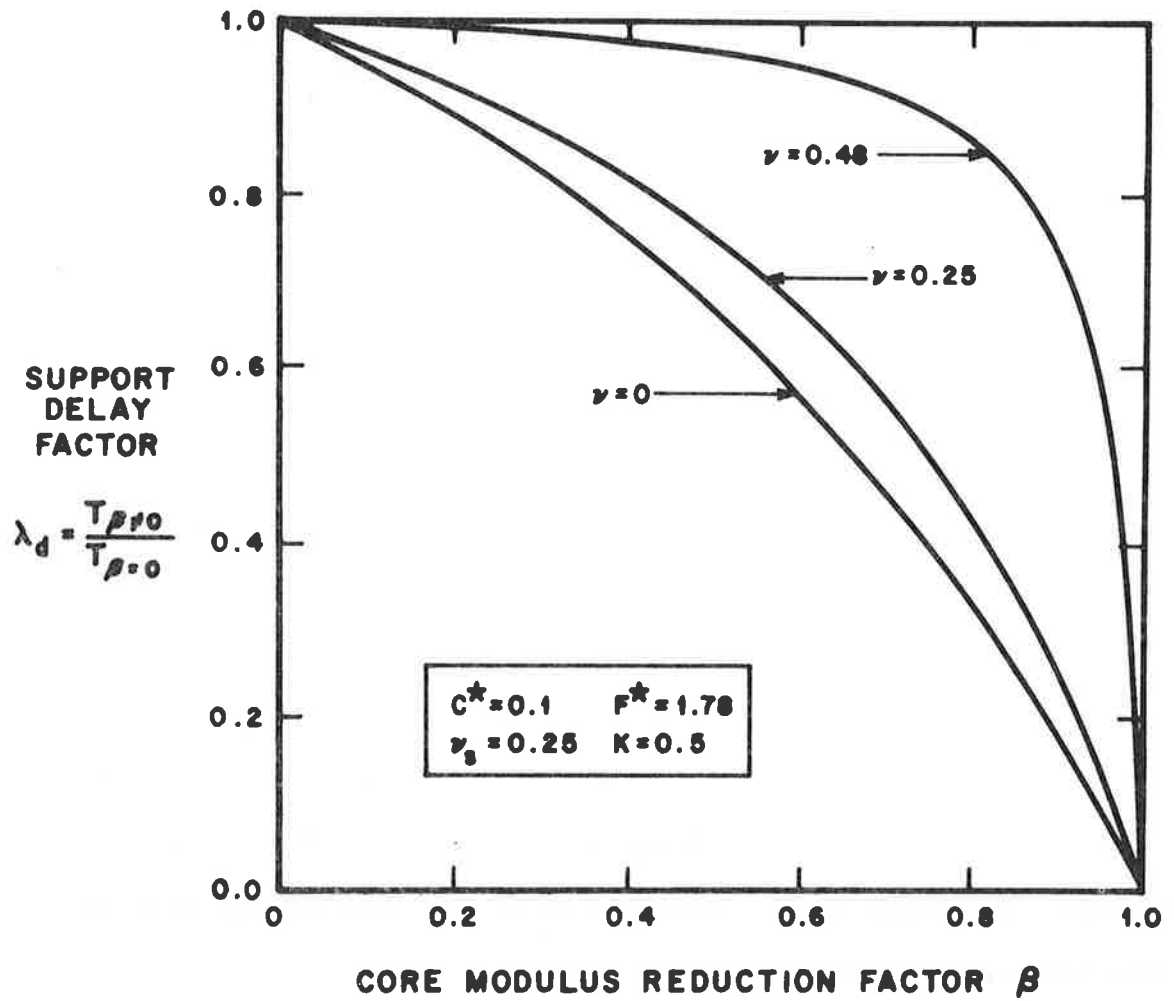
FIGURE 3.19.   DELAY FACTOR FOR SUPPORT THRUSTS
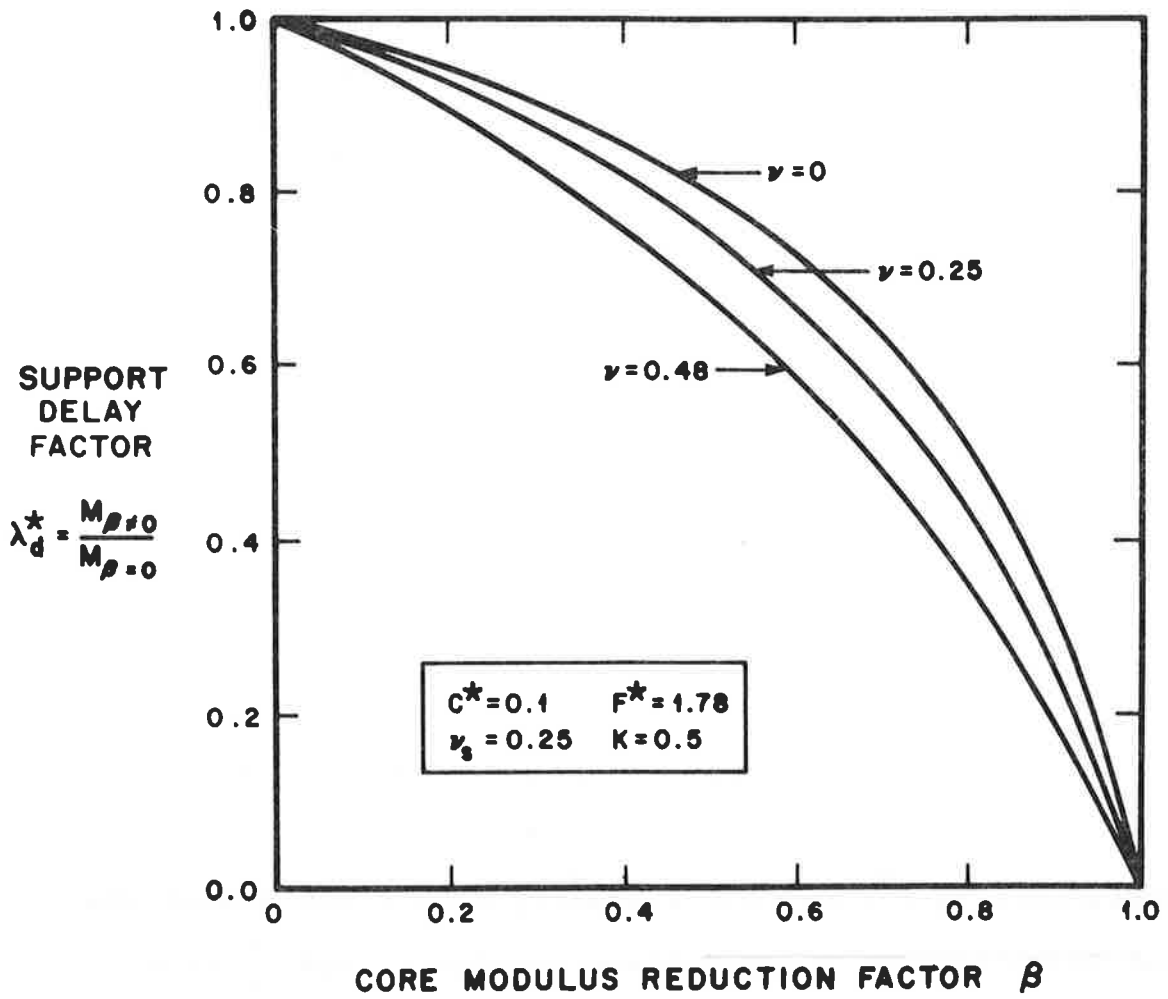
FIGURE 3.20.   DELAY FACTOR FOR SUPPORT MOMENTS

101

The results from this parametric study are shown in Figure 3.21 ror values for β of 0.2 and 0.8. The curves in this figure, together with those in Figures 3.19 and 3.20, lead to the following simple conclusions about the support delay correction factors λ_d and λ_d^*:

1) λ_d and λ_d^* are independent of K for fixed C^*, F^*, ν, and β (Figure 3.21a). This conclusion is most significant, because it confirms the general validity of λ_d as derived from the axisymmetric elastic finite element analyses for K = 1 (Eq. 3.4)

2) λ_d and λ_d^* are independent of C^* and F^* for fixed K, ν, and β (Figure 3.21b). This also confirms the findings in Section 3.3 for K = 1.

3) λ_d equals λ_d^* when $\nu = 0.25$

4) Increasing ν increases λ_d and decreases λ_d^*; furthermore, λ_d is more sensitive to ν than is λ_d^* (see Figures 3.19 and 3.20).

Variations in C^*, F^*, and K equally affect the numerators and denominators in the definitions for λ_d and λ_d^* (Eqs. 3.9 and 3.10) -- hence conclusions (1) and (2) above. The only variable other than the support delay that influences λ_d and λ_d^* is ν, and this influence is shown in Figures 3.19 and 3.20 to be slight except for values of ν near 0.5.

b)

$\lambda_d = \dfrac{T_{\beta \neq 0}}{T_{\beta = 0}}$

$\overset{\star}{\lambda_d} = \dfrac{M_{\beta \neq 0}}{M_{\beta = 0}}$

$\beta = 0.2$

$\beta = 0.8$

K = 0.5
$\nu = 0.25$

$\beta = 0.2$

$\beta = 0.8$

1.0

0.5

0.0
1.0

0.5

0.0

0.01 0.1   1.0   10.0 100.0

COMPRESSIBILITY RATIO C*

a)

$\lambda_d = \dfrac{T_{\beta \neq 0}}{T_{\beta = 0}}$

$\overset{\star}{\lambda_d} = \dfrac{M_{\beta \neq 0}}{M_{\beta = 0}}$

$\beta = 0.2$

$\beta = 0.8$

C = 0.1
F = 1.78
$\nu = 0.25$

$\beta = 0.2$

$\beta = 0.8$

1.0

0.5

0.0
1.0

0.5

0.0

0   1   2   3   4   5

LATERAL STRESS RATIO K
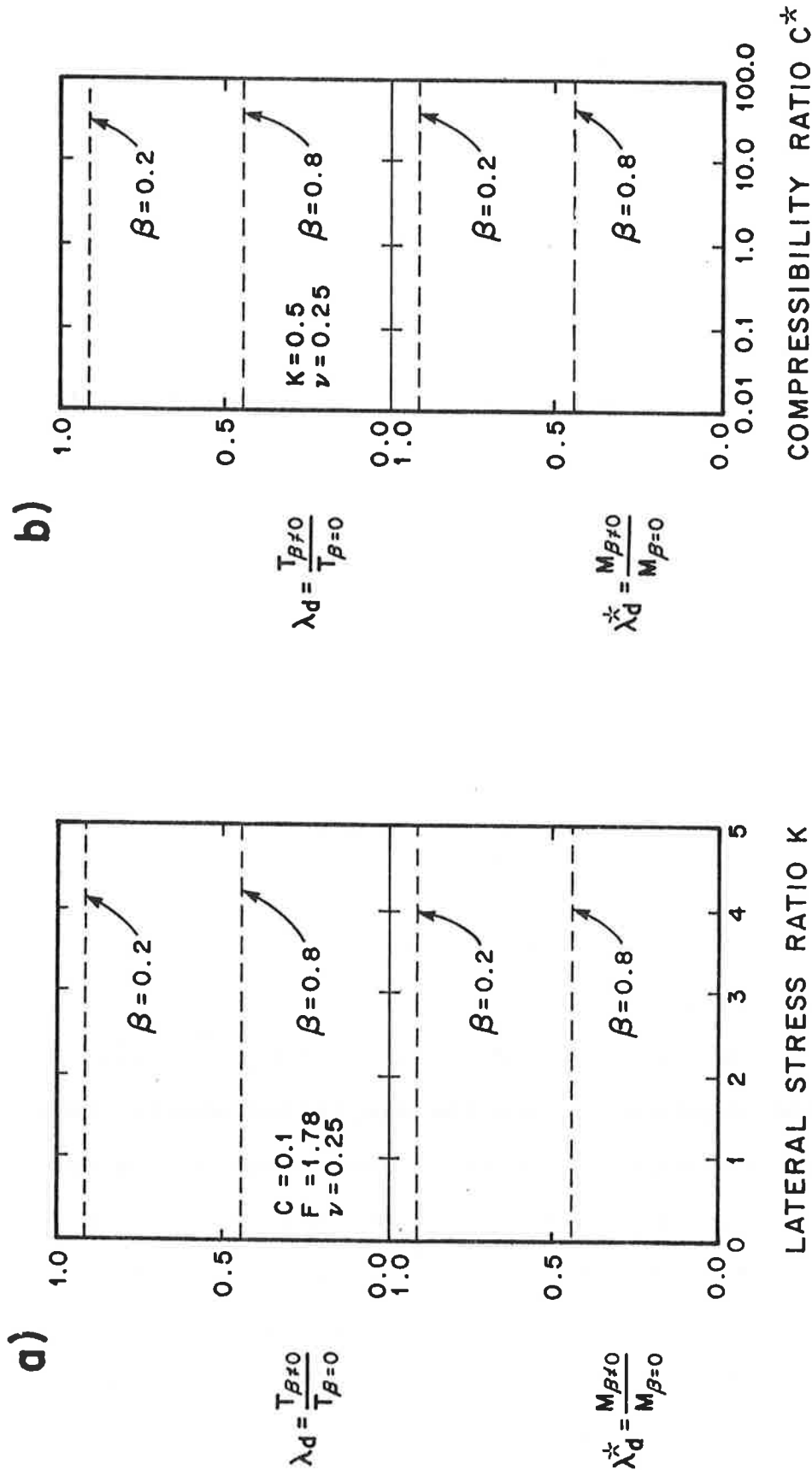
FIGURE 3.21. PARAMETRIC STUDY--EFFECTS OF LATERAL STRESS RATIO AND SUPPORT COMPRESSIBILITY ON DELAY FACTORS λ_d AND $\overset{\star}{\lambda_d}$

103

3.5 SUMMARY

In practice, the support in a tunnel is usually con-
structed at a point some distance behind the tunnel face.
As a result of this support delay, the ground mass deforms
and mobilizes some of its resistance before the support
becomes active, thus reducing the load that the support must
eventually sustain. These effects of the support delay can
be analyzed using finite element methods that simulate the
step-by-step advance of the tunnel. The results from these
finite element analyses in turn can be used to backfigure
correction factors (like λ_d in Eq. 3.4) that can be used
in conjunction with simpler design-oriented analytical tech-
niques (like the relative stiffness solutions in Section 2)
which cannot directly include the support delay effect. For
tunnels in elastic ground masses, the support delay correc-
tion factor λ_d depends primarily upon the support delay
length, only slightly on the relative support stiffness,
and not at all on the lateral in situ stress ratio.

The behavior of the ground mass surrounding a real
tunnel is more complicated than the simplified elastic model
presented in this chapter, however. Longer support delays
will lead to larger movements and higher stresses in the
grounds; at some point, the strength of the ground mass
will be exceeded, and it will yield and behave nonlinearly.
This yielding of the ground mass is the subject of the
next two sections.

104

4. BEHAVIOR OF YIELDING GROUND MASSES SURROUNDING TUNNELS

4.1 INTRODUCTION

The derivation of the relative stiffness solutions in Section 2 and the investigation into the effects of support delay in Section 3 were both limited to the case of linearly elastic ground behavior. In general, this simplifying assumption will not be true for real ground masses. As the ground deforms and stresses are redistributed and concentrated during excavation of the tunnel, the strength of the ground will be exceeded and the ground mass will begin to behave nonlinearly. This ground yielding will have a significant effect upon the ground-structure interaction and upon the tunnel support loads.

The purpose of this section is first to describe in conceptual terms the effects of yielding on the ground characteristic curve. Then, some simple analytical tools for describing this nonlinear ground behavior will be presented. The treatment of ground yielding in this section is brief and is intended as background for the numerical investigations that follow in Section 5; a more general discussion of the yielding ground behavior around a tunnel can be found in Volume 2 of this report. In that volume, the stress conditions and failure mechanisms in the ground mass are reviewed qualitatively, the principal factors influencing the ground failure and yielding are identified, and attempts are made to clarify particular aspects of this behavior that are sometimes confused or neglected.

105

Since the behavior of the yielding ground mass itself is the principal concern of this section, the detailed influence of the tunnel support will be temporarily ignored; the support will be treated simply as an internal pressure. The actual interaction between the yielding ground and the tunnel support will be investigated in Section 5. The discussion in this section will serve as the conceptual foundation for that investigation.

4.2 QUALITATIVE DESCRIPTION OF GROUND BEHAVIOR

The excavation of a tunnel results in a partial or complete unloading of the initially stressed ground mass. The stages in this unloading behavior can be conceptually illustrated by using the idealized load-displacement curve, the ground characteristic curve. The ground characteristic curve shown in Figure 4.1 has been developed by first assuming that an unlined tunnel exists in the undisturbed ground mass. This opening has an initial internal pressure, P_I, equal to the in situ ground stress. Upon gradual reduction of the internal pressure (i.e., unloading), inward radial displacement, u, of the tunnel wall occurs. The plot of internal pressure versus radial displacement is the ground characteristic curve.

There are three main stages of the unloading behavior: (1) As the internal cavity pressure is gradually reduced, the ground first responds elastically; the characteristic

106
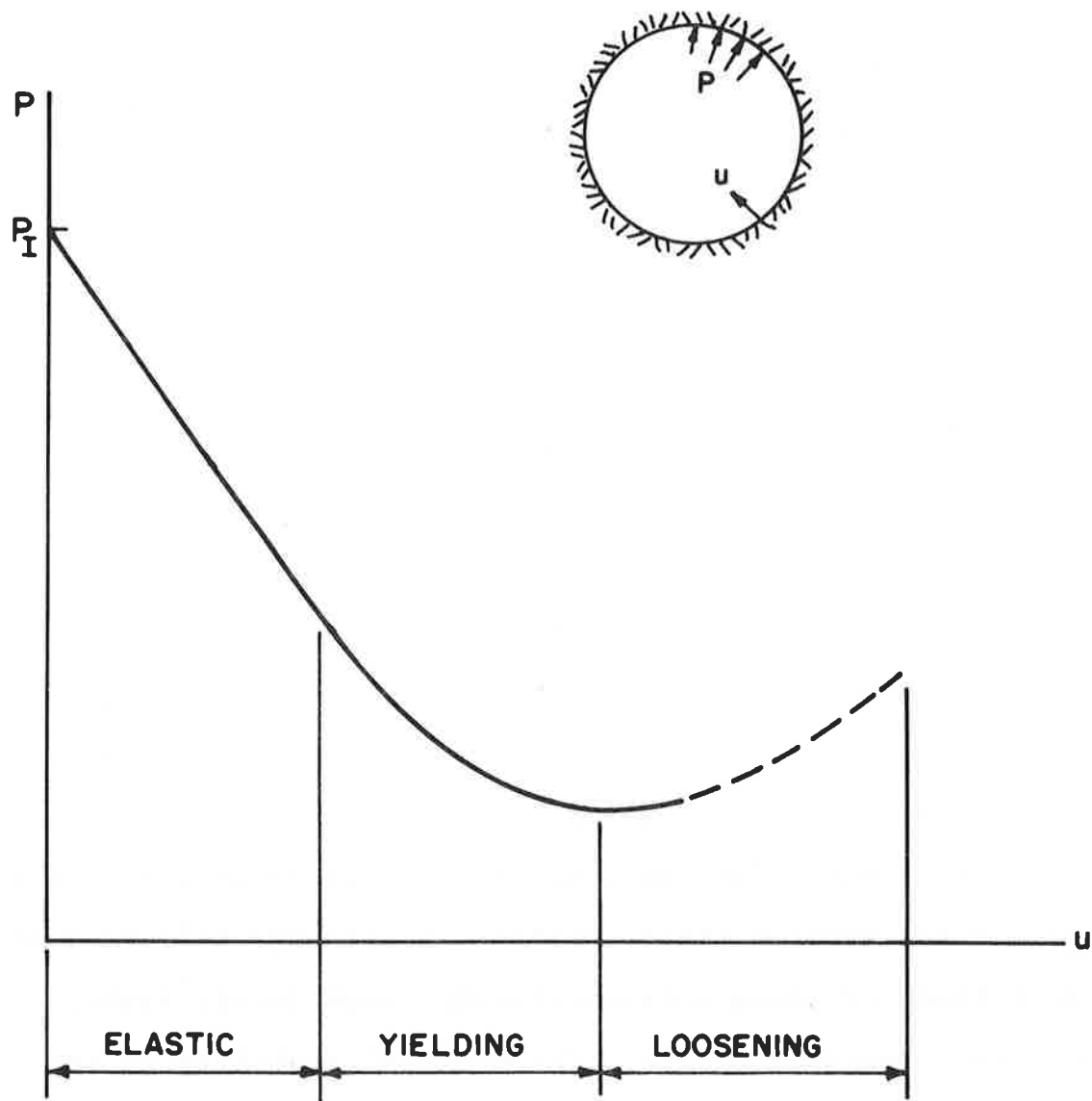
FIGURE 4.1.   GROUND CHARACTERISTIC CURVE

107

curve is linear during this stage. (2) At some point, yielding begins as the shear strength of the ground is exceeded at the cavity wall; the characteristic curve becomes distinctly nonlinear during this stage. (3) Finally, under some conditions continued deformations may lead to an unstable situation in which the internal cavity pressure must be increased to maintain a given ground displacement; the characteristic curve sweeps upward in this loosening stage.

True elastic behavior is generally limited to intact rock or homogeneous soil deposits over a limited stress range. Layered soils and discontinuous rock masses can often be approximated by an anisotropic elastic medium for small stress changes. If the ground mass were truly elastic over all stress ranges, the ground characteristic curve would be a straight line and the opening would be stable even at zero internal pressure.

Yielding occurs as soon as the failure strength of the ground is exceeded either within a continuous soil mass or rock block or along a discontinuity (rock joint, fault, or other weakness plane). The eventual stability of the opening depends heavily on the post-failure behavior of the ground mass. Cavities in perfectly plastic or strain hardening grounds with a cohesive strength component will always stabilize at zero internal pressure, although the concomitant radial displacements of the cavity wall may be

very large. Severely strain softening ground, on the other hand, will require a positive internal pressure or counter-stress to maintain stability. The loosening range of the ground characteristic curve is commonly associated with this strain softening ground behavior (this is discussed in considerable detail in Volume 2 of this report).

Many geologic materials of interest in tunneling <u>dilate</u> as they fail; that is, the post-failure strains cause an increase in the material's volume. The degree of dilatancy exhibited by a given material depends upon many factors: the strength parameters (particularly the friction angle), confining stress, level of shear strains, and joint geometry and roughness (for rock masses) are some examples. Dilatancy merits special mention in the tunneling problem because it alters the shape of the ground charcteristic curve in both the yielding and loosening ranges. Because of dilatancy, the ground within the yielded zone will increase in volume. To accommodate this volume increase, the tunnel wall must move radially inward. Therefore, if it is assumed that the extent of the yielded zone is the same for a given internal cavity pressure regardless of whether or not dilatancy develops,[1] the radial displacements at the wall of a tunnel

[1]In Section 4.3 it will be shown that, for plane strain axisymmetric conditions around a tunnel, the radius of the yielded zone and the stress distributions within it are theoretically independent of the strains for elastic-perfectly-plastic yield rules.

in a strongly dilatant ground mass will be larger than those for a tunnel in a ground that does not dilate as it yields. These larger displacements at a given internal cavity pressure mean that dilatancy "flattens" the ground characteristic curve, as shown in Figure 4.2. Dilatancy exaggerates the effects of ground yielding and lessens the effects of loosening.

Regardless of the detailed past-failure behavior of the ground mass, though, the most important effect of ground yielding is the nonlinearity it imparts to the ground characteristic curve. The nonlinear curve always lies above the straight-line curve for the elastic case, and as a consequence, a larger support pressure is needed in yielding or "weak" ground masses to maintain a given ground displacement.

4.3 PLASTICITY SOLUTIONS FOR GROUND CHARACTERISTIC CURVE

Whereas Section 4.2 has been limited to a strictly qualitative description of the yielding ground behavior around a tunnel, the remaining sections will be devoted to the development of some simple analytical tools for studying this behavior quantitatively. Specifically, several analytical formulations for the characteristic curve of a yielding ground mass will be described and some indices
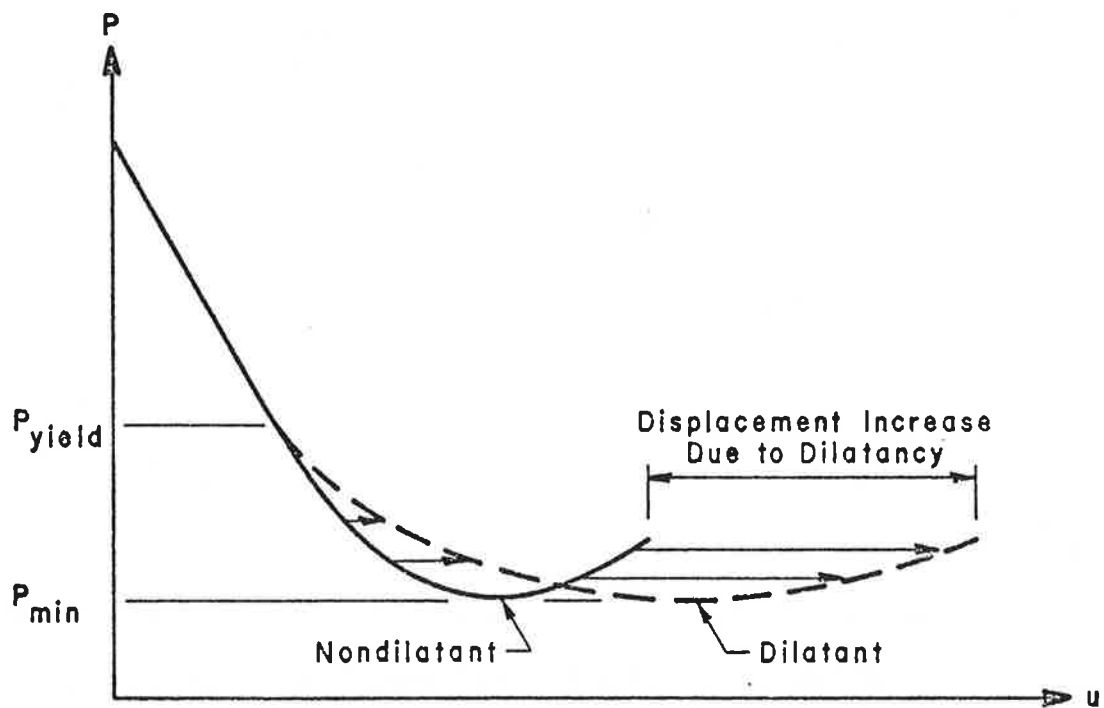
FIGURE 4.2   EFFECT OF DILATANCY ON THE GROUND CHARACTERISTIC
CURVE

111

for quantifying the overall ground strength around the tunnel will be derived.

Characteristic curves have been a very useful conceptual tool for relating the internal tunnel support pressure to the radial ground displacement. They were employed in Section 2 to qualitatively describe the influence of the relative support stiffness on the support loads and in Section 3 to describe and approximately analyze the reduction of these loads caused by support delay. Characteristic curves will be used again in Chapter 5 to develop a design-oriented analysis for support loads that will include the effects of ground yielding. Before this can be done, though, the nonlinear characteristic curve for the yielding ground mass must be expressed in an analytical form.

Many simple closed-form solutions have been derived for the problem of a cylindrical tunnel in a yielding ground mass. These solutions, which are all based on plasticity theory and relatively simple constitutive models, relate the stresses (and usually the displacements) in the yielding ground mass to the internal pressure in the cavity. In order to simplify the problem enough for it to be solved, the analyses all assume most of the following highly idealized conditions:

    (1)   plane strain

    (2)   homogeneous, isotropic, and infinite ground mass

3) in situ lateral stresses equal to the in situ

   vertical stresses -- i.e., K = 1 (variously called

   axisymmetric, uniform, or hydrostatic stress

   conditions in the literature)

4) no variation of ground stresses with depth

5) a cylindrical unlined tunnel cavity with a uni-

   form internal pressure

6) elastic-perfectly plastic strength models for

   the ground, governed by simple yield criteria

   like the Mohr-Coulomb rule.

Some of the solutions in the literature relax one or two

of these restrictions slightly. Of course, no actual

tunnel would satisfy any of these assumptions precisely;

as in any engineering analysis, reality rarely matches

the ideal model. Nevertheless, if the engineer is aware

of the restrictions inherent in the idealization and if

he takes care that these assumptions are not excessively

violated, the analytical solutions can produce acceptable

practical results.

   The plasticity solutions published in the literature

for the tunneling problem can be grouped into two major

categories, with four subcategories in the latter:

   (a) Solutions for stresses but no displacements

   (b) Solutions for stresses and displacements; dis-

       placements derived from the assumption of:

(1) Zero total volume change in the yielded zone ($\Delta V^T = 0$)

(2) Empirically determined coefficient for the total volume change in the yielded zone ($\Delta V^T/\Delta V = -\bar{\varepsilon}_V$

(3) Zero plastic volumetric strain in the yielded zone ($\varepsilon_V^{\overset{P}{}} = 0$)

(4) Plastic strains derived from the associated plastic flow rule.

The next few subsections will describe some of the most frequently cited solutions in each category. Because of widely varying notations and forms for the equations, none of the published derivations will be reproduced intact here. Instead, new derivations, which follow much of the same logic as the published solutions, are presented; these new derivations are of necessity brief, but because of their consistent notation and coherent overall logic they clearly point out the similarities and differences between the different types of solutions and the rational progression from one to the next. Derivations relying heavily on particular published solutions are so noted in the text.

The following derivations are all based on assumptions (1) - (6) previously itemized. The notation used throughout the derivations is as follows:

a	tunnel radius
b	radius of the yielded zone
c	cohesion
E	Young's modulus of elasticity
E'	plane strain elastic modulus $= \dfrac{E}{1 - \nu^2}$
F	yield function
K	in situ lateral stress ratio
N_ϕ	frictional strength coefficient $= \dfrac{1+\sin\phi}{1-\sin\phi}$
P	vertical in situ stress at tunnel axis
P_b	radial stress at the boundary of the yielded zone (i.e., at r=b)
P_s	internal (support) pressure in tunnel
r	radial distance from tunnel axis
u	radial ground displacement (positive toward tunnel)
u_a, u_b	radial ground displacements at r = a,b
u_I	initial radial ground displacement
V	volume of yielded zone (per unit length of tunnel)
ΔV	increase in volume of yielded zone (per unit length of tunnel)
ε_r, ε_{re}, ε_{rp}	total, elastic, plastic radial strains
ε_θ, $\varepsilon_{\theta e}$, $\varepsilon_{\theta p}$	total, elastic, plastic tangential strains
ε_V, ε_{Ve}, ε_{VP}	total, elastic, plastic volumetric strains

115

$\bar{\varepsilon}_V$	average volumetric strain in yielded zone
$\Delta\varepsilon_V$	change in volumetric strain
$\dot{\varepsilon}_{rp}, \dot{\varepsilon}_{\theta p}$	radial and tangential plastic strain rate components
$\dot{\lambda}$	proportionality factor for plastic strain rates
ν	Poisson's ratio (for plane stress)
ν'	Poisson's ratio for plane strain $= \dfrac{\nu}{1-\nu}$
ϕ	friction angle
σ_r, σ_θ	radial, tangential stresses.

All stresses and strains are positive when compressive; displacements are positive when toward the tunnel.

A. Stresses But No Displacements

Since knowledge of the ground displacements is essential to the investigation of the ground-structure interaction of the tunnel, the solutions in this category are of limited value. However, these solutions do represent some of the earliest attempts at analyzing the tunneling problem. Fenner (1938), Westergaard (1940) Morrison and Coatts (1955), and Kastner (1962) all derive the solution for the stresses around a tunnel in a Mohr-

116

Coulomb material. Savin (1970) presents an extensive compilation of solutions derived by Russian researchers; his book also contains the only analytical solution for $K \neq 1$ stress conditions (for a Von Mises material).[1]

Although none of the above solutions give expressions for the displacements in the ground mass, the stress distributions are independent of the strains and therefore are of general validity. For the case of a tunnel in an elastic-perfectly plastic ground mass governed by a Mohr-Coulomb yield criterion (the most common two-dimensional yield criterion for many geologic materials), the derivation for the stress distributions is straightforward. Equilibrium in both the yielded and elastic zones requires that the stresses satisfy the relation (for axisymmetric or $K = 1$ conditions):

$$\frac{d\sigma_r}{dr} + \frac{\sigma_r - \sigma_\theta}{r} = 0 \qquad (4.4)$$

The boundary conditions for the problem are:

$$\sigma_r = P_s \quad \text{at} \quad r = a \qquad (4.5a)$$

$$\sigma_r = P \quad \text{at} \quad r = \infty \qquad (4.5b)$$

---

[1] Savin also gives expressions for the displacements in this solution. The derivation for this condition is not general, however; it is restricted to particular patterns of yielding that completely surround the tunnel.

In the elastic zone $b \leq r \leq \infty$, the stresses are given by the familiar expressions (see Jaeger and Cook, 1976, for example):

$$\sigma_r = P - (P - P_b) \left(\frac{b}{r}\right)^2 \tag{4.6a}$$

$$\sigma_\theta = P + (P - P_b) \left(\frac{b}{r}\right)^2 \tag{4.6b}$$

in which P_b is the radial stress at the boundary between the elastic and yielded zones. This stress can be found from the condition that at $r = b$ the elastic stresses must satisfy the Mohr-Coulomb yield criterion, which requires that:

$$\sigma_\theta = N_\phi \sigma_r + \sigma_u \tag{4.7}$$

Substituting (4.6) into (4.7) and solving for P_b at $r = b$:

$$P_b = \frac{2P - \sigma_u}{N_\phi + 1} \tag{4.8}$$

The stresses in the elastic zone are then given as:

$$\sigma_r = P - \left[\frac{P(N_\phi - 1) + \sigma_u}{N_\phi + 1}\right] \left(\frac{b}{r}\right)^2 \tag{4.9a}$$

118

$$\sigma_\theta = P + \left[\frac{P(N_\phi - 1) + \sigma_u}{N_\phi + 1} \right] (\frac{b}{r})^2 \qquad (4.9b)$$

The stresses in the yielded zone $a \le r \le b$ can be determined by substituting the yield function (4.7) into the equilibrium equation (4.4) and solving for σ_r, subject to the boundary condition (4.5a):

$$\sigma_r = (P_s + \frac{\sigma_u}{N_\phi - 1}) (\frac{r}{a})^{N_\phi - 1} - \frac{\sigma_u}{N_\phi - 1} \qquad (4.10a)$$

and then, from the yield criterion (4.7):

$$\sigma_\theta = N_\phi (P_s + \frac{\sigma_u}{N_\phi - 1}) (\frac{r}{a})^{N_\phi - 1} - \frac{\sigma_u}{N_\phi - 1} \qquad (4.10b)$$

The radius of the yielded zone, b, is obtained from the requirement that the radial stress in the elastic zone equal the radial stress in the yielded zone at $r = b$. Equating (4.9a) and (4.10a) and solving for b:

$$b = a \left[\frac{2}{N_\phi + 1} \quad \frac{P + \frac{\sigma_u}{N_\phi - 1}}{P_s + \frac{\sigma_u}{N_\phi - 1}} \right]^{\frac{1}{(N_\phi - 1)}} \qquad (4.11)$$

B.1 Stresses and Displacements, Zero Total Volume Change in Yielded Zone

In order to determine the radial displacements at the tunnel wall, some assumption must be made about the

119

post-failure deformations in the ground. Perhaps the simplest assumption is that the total volume of the yielded zone remains constant. Deere et al. (1969), Newmark (1969), and Daemen (1975) have all derived solutions for this condition.

The steps in this type of derivation are: (1) find the radius of the yielded zone, b; (2) determine the elastic radial displacement u_b at b; and (3) calculate the radial displacement u_a at the tunnel wall from u_b and the condition of constant total volume in the yielded zone. The stresses in the ground mass and the radius of the yielded zone are the same as in the preceding section (Eqs. 4.9 - 4.11). Calculation of the elastic displacements at the boundary of the yielded zone requires use of the elastic strain-displacement-stress relationships, which are:

$$\varepsilon_r = \frac{du}{dr} = \frac{1}{E'}(\sigma_r - \nu'\sigma_\theta) \qquad (4.12a)$$

$$\varepsilon_\theta = \frac{u}{r} = \frac{1}{E'}(\sigma_\theta - \nu'\sigma_r) \qquad (4.12b)$$

Using the elastic stresses given in (4.9), the second of these equations can be solved for u directly:

$$u = \frac{r}{E'}[P(1-\nu') + (1+\nu')(P-P_b)(\frac{b}{r})^2] \qquad (4.13)$$

120

However, this expression for u includes not only the displacements due to the excavation of the tunnel but also the initial displacements due to the in situ stresses (i.e., Eq. 4.13 is for the external loading condition described in Section 2). This second component of the displacements, u_I, must be subtracted from (4.13):

$$u = \frac{r}{E'} [P(1-\nu') + (1+\nu') (P-P_b) (\frac{b}{r})^2] - u_I \qquad (4.14)$$

The initial displacement u_I can be determined from the requirement that u go to zero as r approaches infinity. Therefore:

$$u_I = \frac{Pr(1-\nu')}{E'} \qquad (4.15)$$

and then, considering expression (4.8) for P_b, the radial ground displacements (4.14) are:

$$u = \frac{(1+\nu')}{E'} \left[\frac{P(N_\phi-1) + \sigma_u}{N_\phi + 1} \right] \frac{b^2}{r} \qquad (4.16)$$

and at r = b:

$$u_b = \frac{(1+\nu')}{E'} \left[\frac{P(N_\phi-1) + \sigma_u}{N_\phi + 1} \right] b \qquad (4.17)$$

121

The condition of constant volume of the yielded zone requires that:

$$\pi(b^2 - a^2) = \pi[(b - u_b)^2 - (a - u_a)^2] \tag{4.18}$$

which, if small displacements are assumed, reduces to the approximate relation:

$$u_a \cong (\frac{b}{a}) \, u_b \tag{4.19}$$

Combining (4.17) and (4.19) gives the final expression for the radial displacement at the tunnel wall:

$$u_a = \frac{(1 + \nu')}{E'} \left[\frac{P(N_\phi - 1) + \sigma_u}{N_\phi + 1} \right] \frac{b^2}{a} \tag{4.20}$$

in which b, the radius of the yielded zone, is given by (4.11).

B.2 Stresses and Displacements, Empirically Determined Coefficient For Total Volume Change in Yielded Zone

This solution is the generalization of the constant volume derivation; it incorporates the well-known fact that many geologic materials dilate as they yield. The total increase in volume of the yielded zone (per unit length of tunnel), ΔV, is expressed as:

$$\Delta V = -\overline{\varepsilon}_v \, V \cong -\overline{\varepsilon}_v \, \pi(b^2 - a^2) \tag{4.21}$$

in which $\bar{\epsilon}_v$ is the empirically determined average volumetric strain in the yielded zone (positive $\bar{\epsilon}_v$ implies volumetric compression). Equation (4.18) then becomes:

$$\pi(b^2-a^2) = \pi[(b-u_b)^2 - (a-u_a)^2] - \Delta V \qquad (4.22)$$

Therefore, for small displacements:

$$u_a \cong (\frac{b}{a}) u_b + \frac{\Delta V}{2\pi a} \qquad (4.23)$$

and, from (4.17):

$$u_a = \frac{(1+\nu')}{E'} \left[\frac{P(N_\phi-1) + \sigma_u}{N_\phi + 1} \right] \frac{b^2}{a} - \frac{\bar{\epsilon}_v(b^2-a^2)}{2a} \qquad (4.24)$$

in which b, the radius of the yielded zone, is given by (4.11). The stresses in the ground mass are still given by (4.9) and (4.10).

Several researchers have derived solutions similar to the one above and have made recommendations regarding the proper value of $\bar{\epsilon}_v$ to use in the analysis. Daemen and Fairhurst (1973) claim that $\bar{\epsilon}_v$ usually ranges between -0.01 and -0.05 (recall that negative values for $\bar{\epsilon}_v$ imply volumetric expansion) but offer no substantiating evidence. Labasse (1949) backfigured a value of -0.1 from displacement measurements in a tunnel through weak schist,

123

but his calculations were highly approximate. Vesic (1972) and Baligh (1976), in derivations for the very similar problem of cavity expansion, express $\bar{\varepsilon}_v$ as an empirically-determined (based on laboratory tests) function of the average octohedral normal stress in the yielded zone; this type of formulation requires an iterative solution.

Following what might be termed a hybrid approach, Ladanyi (1974) derives $\bar{\varepsilon}_v$ from the theoretical associated plastic flow rule (more on this later); however, he recognizes that the associated flow rule often overestimates the post-failure dilatancy (he cites tests by himself and Nguyen Don, 1970, as substantiating evidence) and states that $\bar{\varepsilon}_v$ should be calculated by applying the flow rule to only a limited portion of the post-failure strains (e.g., strains up to three times the failure strain). His recommendations for $\bar{\varepsilon}_v$ for the Mohr-Coulomb yield criterion (he also derives a solution incorporating the Fairhurst parabolic criterion) are:

$$\bar{\varepsilon}_v = \frac{2(\frac{u_b}{b})(\frac{b}{a})^2}{[(\frac{b}{a})^2 - 1][1 - \frac{1}{2 \sin \phi \ln (b/a)}]} \quad \text{for } \frac{b}{a} \lesssim \sqrt{3}$$

(4.25a)

$$\bar{\varepsilon}_v = \frac{2(\frac{u_b}{b})(\frac{b}{a})^2}{[(\frac{b}{a})^2 - 1](1 - \frac{1}{1.1 \sin \phi})} \quad \text{for } \frac{b}{a} \gtrsim \sqrt{3}$$

(4.25b)

124

in which u_b and b are given by Eqs. (4.17) and (4.11). For

E' = 10,000 psi, ν' = 0.25, ϕ = 30°, c = 0, a = 100 in.,

P = 100 psi, P_s = 20 psi (reasonable values for a soft

ground tunnel), b = 158 in., u_b = 0.99 in., $\frac{b}{a}$ = 1.58 < $\sqrt{3}$

and (4.25a) gives $\bar{\varepsilon}_v$ = - 0.018.

B.3 Stresses and Displacements, Zero Plastic Volumetric Strain in the Yielded Zone

Neither of the two types of derivations for the

ground displacements described above has explicitly consid-

ered the actual stress and strain distributions within

the yielded zone. These distributions can be treated in

the analysis provided some rule is assumed for calculating

the plastic strain increments; one of the simplest of

these rules is that the plastic component ε_{vp} of the

volumetric strain is everywhere zero within the yielded

zone. Daemen (1975) and Kennedy and Lindberg (1978b)

have derived solutions to the tunneling problem for this

condition. Hobbs (1966) also solves this problem with

the additional assumption of a reduced elastic modulus in

the yielded zone (he uses laboratory tests to determine

the amount of the reduction).

The following derivation is adapted from Kennedy

and Lindberg (1978a, 1978b). The stresses in the ground

mass are the same as given earlier in (4.9) and (4.10),

the radius of the yielded zone is given by (4.11), and

the displacements in the elastic region are expressed by

125

(4.16). The total strains in the yielded zone are obtained from the relations:

$$\varepsilon_r = \frac{du}{dr} = \varepsilon_{re} + \varepsilon_{rp} = \frac{1}{E'}(\sigma_r - \nu'\sigma_\theta) + \varepsilon_{rp} \tag{4.26a}$$

$$\varepsilon_\theta = \frac{u}{r} = \varepsilon_{\theta e} + \varepsilon_{\theta p} = \frac{1}{E'}(\sigma_\theta - \nu'\sigma_r) + \varepsilon_{\theta p} \tag{4.26b}$$

The plastic strain components ε_{rp} and $\varepsilon_{\theta p}$ are assumed to satisfy the condition:

$$\varepsilon_{vp} = \varepsilon_{rp} + \varepsilon_{\theta p} = 0 \tag{4.27}$$

Note that (4.27) implies that the ground is nondilatant. Using relations (4.26) and (4.27) for the strains and (4.10) for the stresses, the total strains in the yielded zone are expressed as:

$$\varepsilon_r = \frac{du}{dr} = \frac{1}{E'}\left[(1-\nu'N_\phi)\left(\frac{\sigma_u}{N_\phi - 1} + P_s\right)\left(\frac{r}{a}\right)^{N_\phi - 1} - (1-\nu')\frac{\sigma_u}{N_\phi - 1}\right] - \varepsilon_{\theta p} \tag{4.28a}$$

$$\varepsilon_\theta = \frac{u}{r} = \frac{1}{E'}\left[(N_\phi - \nu')\left(\frac{\sigma_u}{N_\phi - 1} + P_s\right)\left(\frac{r}{a}\right)^{N_\phi - 1} - (1-\nu')\frac{\sigma_u}{N_\phi - 1}\right] + \varepsilon_{\theta p} \tag{4.28b}$$

126

The condition of strain compatibility requires that:

$$r \frac{d\varepsilon_\theta}{dr} + (\varepsilon_\theta - \varepsilon_r) = 0 \qquad (4.29)$$

Substituting (4.28) into (4.29) gives:

$$r \frac{d\varepsilon_{\theta p}}{dr} + 2 \varepsilon_{\theta p} + \frac{(N_\phi^2 - 1)}{E'} (\frac{\sigma_u}{N_\phi - 1} + P_s)(\frac{r}{a})^{N_\phi - 1} = 0$$

$$(4.30)$$

which can be solved using the boundary condition that $\varepsilon_{\theta p}$ vanish at the radius of the yielded zone, $r = b$. The solution is:

$$\varepsilon_{\theta p} = \frac{N_\phi - 1}{E'} (\frac{\sigma_u}{N_\phi - 1} + P_s)\left[(\frac{b}{a})^{N_\phi + 1} (\frac{r}{a})^{-2} - (\frac{r}{a})^{N_\phi - 1}\right] = 0$$

$$(4.31)$$

From (4.28b) and (4.31), the radial ground displacement at the tunnel wall is determined as:

$$u_a = \frac{a}{E'}\left[(N_\phi - 1)(\frac{\sigma_u}{N_\phi - 1} + P_s)(\frac{b}{a})^{N_\phi + 1} + (1 - \nu')P_s\right] \qquad (4.32)$$

However, this expression for u_a includes not only the displacements due to the excavation of the tunnel but also the initial (elastic) displacements due to the in situ stresses. The initial displacement at the tunnel wall can be obtained from (4.15):

127

$$(u_I)_a = \frac{Pa(1-\nu')}{E'} \tag{4.33}$$

Subtracting this from (4.32) gives the net or excavation-induced radial displacement of the tunnel wall:

$$u_a = \frac{a}{E'} \left[(N_\phi - 1)(\frac{u}{N_\phi - 1} + P_s)(\frac{b}{a})^{N_\phi + 1} - (1-\nu')(P-P_s) \right]$$

$$\tag{4.34}$$

in which b, the radius of the yielded zone, is given by (4.11)

B.4 Stresses and Displacements, Plastic Strains Derived From the Associated Flow Rule

In this class of solutions, the ground displacements in the yielded zone are derived rigorously (in terms of plasticity theory) from the elastic and plastic strain components. The elastic strains are calculated as usual from the elastic stress-strain relations (4.12); the plastic strains are obtained from the associated plastic flow rule. Hendron and Aiyer (1972) have derived several of these solutions; in addition to elastic-perfectly plastic strength behavior, they consider various types of strength and stiffness degradation in the yielded zone. Panet (1976) has also derived the solution for a material with a strain softening cohesive strength component. Kennedy and Lindberg, after having first derived the basic

128

solution for the case of a linear Mohr-Coulomb yield criterion (Kennedy and Lindberg, 1978a), have solved the problem for a nonlinear failure envelope by dividing the ground into a set of concentric rings and assuming a piecewise linear failure envelope, i.e., a separate linear failure rule within each ring (Kennedy and Lindberg, 1978b).

The following derivation is adapted from Kennedy and Lindberg's (1978a) solution for the elastic-perfectly plastic case with a linear yield function; it closely parallels the preceding derivation for solution B.3.[1] The stresses in the ground mass are the same as those given earlier in (4.9) and (4.10), the radius of the yielded zone is given by (4.11), and the displacements in the elastic region are expressed by (4.16). The total strains in the yielded region are obtained from relations (4.26) in the preceding derivation. However, now the plastic strain components ε_{rp} and $\varepsilon_{\theta p}$ are derived from the associated plastic flow rule:

---

[1] Hendron and Aiyer's (1972) solution for the elastic-perfectly plastic case gives the same final results as Kennedy and Lindberg's solution. However, Hendron and Aiyer derived their solution in a general form in which the specific constitutive model for the yielded zone -- e.g., elastic-perfectly plastic, various types of strain softening, or elastic modulus reduction -- can be included as one of the last steps in the derivation. As a consequence, the logic in their solution is more convoluted than the less general but more straightforward formulation by Kennedy and Lindberg.

$$\dot{\epsilon}_{rp} = \dot{\lambda} \, \frac{\partial F_{MC}}{\partial \sigma_r} \qquad (4.35a)$$

$$\dot{\epsilon}_{\theta p} = \dot{\lambda} \, \frac{\partial F_{MC}}{\partial \sigma_\theta} \qquad (4.35b)$$

in which $\dot{\epsilon}_{rp}$, $\dot{\epsilon}_{\theta p}$ are the plastic strain rates, $\dot{\lambda}$ is a proportionality factor, and F_{MC} is the Mohr-Coulomb yield function:

$$F_{MC} = \sigma_\theta - N_\phi \sigma_r - \sigma_u = 0 \qquad (4.36)$$

Therefore:

$$\dot{\epsilon}_{rp} = -\dot{\lambda} N_\phi \qquad (4.37a)$$

$$\dot{\epsilon}_{\theta p} = \dot{\lambda} \qquad (4.37b)$$

and:

$$\frac{\dot{\epsilon}_{rp}}{\dot{\epsilon}_{\theta p}} = \frac{\epsilon_{rp}}{\epsilon_{\theta p}} = -N_\phi \qquad (4.38)$$

or:

$$\epsilon_{rp} = -N_\phi \, \epsilon_{\theta p} \qquad (4.39)$$

Note that (4.37) requires:

$$\varepsilon_{rp} + \varepsilon_{\theta p} = (1-N_\phi) \; \varepsilon_{\theta p} \qquad (4.40)$$

which in general is not equal to zero -- i.e., the material is not incompressible. In fact, for ϕ greater than 0, N_ϕ is greater than 1, and (4.40) indicates that the material is dilatant (i.e., $\varepsilon_{rp} + \varepsilon_{\theta p} < 0$). Using relations (4.26) and (4.39) for the strains and (4.10) for the stresses, the total strains in the yielded zone are expressed as:

$$\varepsilon_r = \frac{du}{dr} = \frac{1}{E'}\left[(1-\nu'N_\phi) (\frac{\sigma_u}{N_\phi-1} + P_s)(\frac{r}{a})^{N_\phi-1}\right. \qquad (4.41a)$$

$$\left. - (1-\nu') \; \frac{\sigma_u}{N_\phi-1} \right] - N_\phi \varepsilon_{\theta p}$$

$$\varepsilon_\theta = \frac{u}{r} = \frac{1}{E'}\left[(N_\phi-\nu') (\frac{\sigma_u}{N_\phi-1} + P_s)(\frac{r}{a})^{N_\phi-1}\right. \qquad (4.41b)$$

$$\left. - (1-\nu') \; \frac{\sigma_u}{N_\phi-1} \right] + \varepsilon_{\theta p}$$

Substituting (4.41) into the strain compatibility relation (4.29) gives:

$$\frac{u\varepsilon_{\theta p}}{dr} + \frac{(1+N_\phi)}{r} \; \varepsilon_{\theta p} + \frac{1}{E'}\left[\frac{(N_\phi^2-1)}{a}(\frac{\sigma_u}{N_\phi-1} + P_s)(\frac{r}{a})^{N_\phi-2} \right] = 0$$

$$(4.42)$$

131

which can be solved using the boundary condition that $\varepsilon_{\theta p}$ vanish at the radius of the yielded zone, $r = b$. The solution is:

$$\varepsilon_{\theta p} = \frac{N_\phi^2 - 1}{2N_\phi E'} \left(\frac{\sigma_u}{N_\phi - 1} + P_s\right)\left[(\frac{b}{a})^{N_\phi - 1}(\frac{b}{r})^{N_\phi + 1} - (\frac{r}{a})^{N_\phi - 1}\right]$$

(4.43)

From (4.28b) and (4.43), the radial ground displacement at the tunnel wall is determined as:

$$u_a = \frac{a}{E'}\left[\frac{N_\phi^2 - 1}{2N_\phi} - (\frac{\sigma_u}{N_\phi - 1} + P_s)(\frac{b}{a})^{2N_\phi}\right.$$

(4.44)

$$\left. - (\frac{N_\phi^2 - 1}{2N_\phi} - N_\phi + \nu')(\frac{\sigma_u}{N_\phi - 1} + P_s) - (1-\nu')\frac{\sigma_u}{N_\phi - 1}\right]$$

The initial elastic displacements at the tunnel wall due to the in situ stresses (4.33) must be subtracted from the displacements given by (4.44). The net or excavation induced radial displacement of the tunnel wall is then;

$$u_a = \frac{a}{E'}\left[\frac{N_\phi^2 - 1}{2N_\phi} (\frac{\sigma_u}{N_\phi - 1} + P_s)(\frac{b}{a})^{2N_\phi}\right.$$

(4.45)

$$\left. -(\frac{N_\phi^2 - 1}{2N_\phi} - N_\phi + \nu')(\frac{c_u}{N_\phi - 1} + P_s) - (1-\nu')(\frac{\sigma_u}{N_\phi - 1} + P_s)\right]$$

in which b, the radius of the yielded zone, is given by (4.11).

132

The characteristic curves calculated from the four different solutions for typical soft ground properties are plotted in Figure 4.3. The constant volume solution B.1 will always give the smallest ground displacements and the associated flow rule plasticity solution B.4, the largest. As shown in the figure, assuming zero plastic volume strains in the yielded zone gives only slightly larger ground movements than assuming zero total volume change (solution B.3 vs. B.1). The formulation incorporating the empirical volume change coefficient, solution B.2, gives intermediate values for the ground displacements, depending on the particular value for the coefficient.

Choosing which of the above formulations to use for a practical problem depends largely upon the expected behavior of the ground mass. If there is reason to believe that little volume change will occur during yielding, (as might happen in an undrained clay, for example), then the constant-volume solution B.1 should be used; on the other hand, if much dilatancy is likely (as in a dense sand for example) then the associated flow rule solution B.4 should give better results. Practically, though, the associated flow rule overestimates the dilatancy for most geologic materials, particularly if yielding is extensive, and one of the less dilatant solutions B.1, B.2 (with small $\bar{\epsilon}_V$), or B.3 will produce a more realistic

Graph showing P (psi) on vertical axis from 0 to 100, and u (in.) on horizontal axis from 0 to 12. Parameter box:

$E' = 10,000\,psi$ $N_\phi = 3$
$\nu' = 0.50$ $\sigma_u = 20\,psi$
$P = 100\,psi$ $FY = 0.45$
$a = 100\,inches$

See Text for Descriptions
of Solutions B.1 - B.4

Curves labeled B.1, B.2 ($\bar{\epsilon}_v = -.01$), B.3, B.4
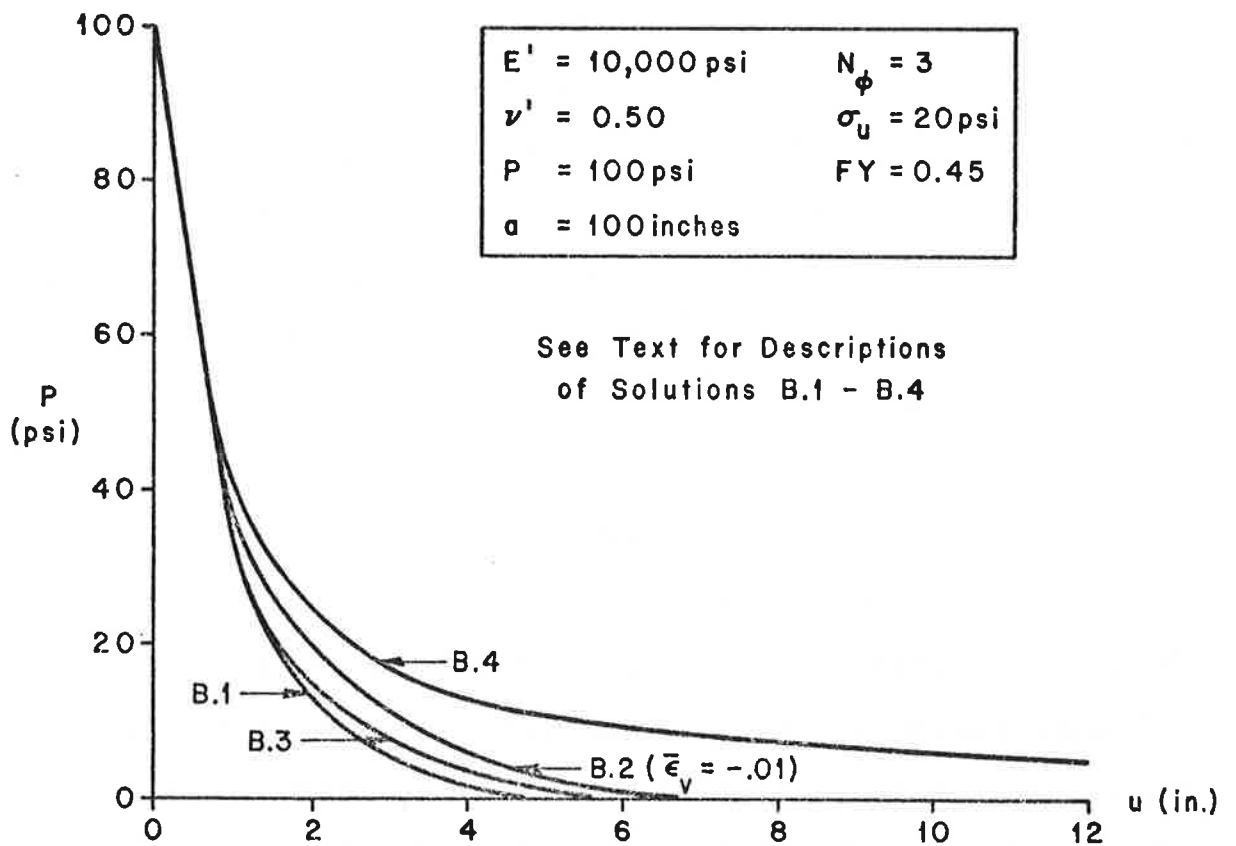
FIGURE 4.3   GROUND CHARACTERISTIC CURVES CALCULATED FROM
DIFFERENT PLANE STRAIN SOLUTIONS

134

ground characteristic curve.

4.4 YIELD INDICES FOR GROUND MASSES

In the analysis for tunnels in yielding ground masses it is convenient to have some method for quantifying the total ground strength. The tunnel designer will then know whether to expect no yielding or large amounts of yielding in the ground mass around his project. The problem with quantifying the total ground strength, however, is that most ground masses have two strength components, cohesive and frictional, that are expressed by the parameters c and ϕ (or by σ_u and N_ϕ), but neither one of these parameters alone is an adequate measure of the total ground strength. The problem is further complicated because the relative importance of each component changes with depth; cohesive strength is generally more important in shallow tunnels than in deep-lying ones. The solution to this problem is to develop a "yield index" that accounts for both cohesive and frictional ground strength under the specific stress conditions around tunnels at various depths. This index would indicate the potential for ground yielding around a tunnel.

One idea for a yield index that quickly comes to mind is the radius of the yielded zone around the tunnel. This radius was given earlier in Equation (4.11) for the simplified case of plane strain conditions and a Mohr-

135

Coulomb strength rule. All of the important factors would be included in a yield index based on this radius: it combines the cohesive and frictional ground strength components, it works equally well for shallow (but deeper than about 2 diameters) and deep tunnels, and it is approximately related to the actual stress conditions around the opening. Nevertheless, there are several complications that make the radius of the yielded zone unsuitable for the yield index. The radius of the yielded zone b is a direct function of the internal cavity or support pressure, P_s (see Eq. 4.11); for given ground strength properties, anything from zero to extensive ground yielding may develop, depending upon P_s. This difficulty could be overcome by calculating b for the specific P_s in the tunnel. However, the specific support pressure P_s in an actual tunnel is a function of the support properties (e.g., relative stiffness and support delay) as well as the ground properties; the yield index, which is intended solely as a measure of the ground strength, should be independent of the support properties if possible. Even this difficulty could be overcome, though, by arbitrarily setting P_s equal to zero, thereby making the radius of the yielded zone a function only of the overburden pressure and ground strength properties. Unfortunately, this too is unsatisfactory. Besides being completely arbitrary, it gives bad results in certain applications. For example, setting P_s equal

136

to zero in a tunnel in a cohesionless ground will produce
an infinite yielded zone regardless of the friction angle
(see Eq. 4.11); a yield index based on the radius of the
yielded zone could not distinguish between $\phi = 0$ and $\phi = 50°$
in this case, even though this distinction would have
severe implications for the actual supported (i.e., $P_s \neq 0$)
tunnel.

A better approach, and the one that will be used
herein, is to base the yield index on the conditions at
which yielding first occurs in the ground mass for $K = 1$
in situ stress conditions. If P_s is the internal
pressure at which yielding commences at the tunnel wall
(i.e., the pressure at which b = a in Eq. 4.11), then the
"first-yield" (FY) index is defined as:

$$FY \equiv \frac{P_s}{P} \qquad (4.46)$$

This FY index has several distinct advantages for quanti-
fying the potential for yielding around the tunnel. First,
it satisfies all of the basic requirements for a yield
index: it combines the cohesive and frictional ground
strength components and it is a function of the actual
stress conditions around a tunnel at any depth. Second,
FY varies between the convenient limits of 0 and 1: FY = 0
means that the ground mass remains completely elastic
even at zero support pressures, while FY = 1 implies

137

that the ground mass has zero strength (i.e., reducing P_s even slightly from the in situ ground stress P induces yielding in the ground mass). And third, FY has a very real practical significance: if the calculated support pressure P_s for the actual tunnel support is high enough so that $\frac{P_s}{P}$ is greater than FY, the designer will know that no ground yielding will develop around the tunnel.

The FY index can be easily derived for a variety of simple yield functions. All that is required is to find the internal support pressure which gives elastic stresses at the tunnel wall (for $K = 1$ conditions) that just satisfy the yield criterion. The elastic principal stresses at the tunnel wall can be expressed as:

$$\sigma_1 = \sigma_\theta = 2P - P_s \tag{4.47a}$$

$$\sigma_2 = \sigma_z = P_z \tag{4.47b}$$
$$= \nu(\sigma_r + \sigma_\theta) = 2\nu P \text{ for plane strain}$$

$$\sigma_3 = \sigma_r = P_s \tag{4.47c}$$

Note that these relations for σ_1 and σ_3 satisfy the condition that $\sigma_1 + \sigma_3 = 2P$ (constant) for a circular opening in $K = 1$ in situ conditions.[1] For the Mohr-Coulomb yield

[1]See Bjorkman and Richards (1976) for a theoretical discussion of this point.

138

criterion (see Eq. 4.7), these elastic stresses at the tunnel wall must satisfy the following relation at the instant of yielding:

$$2P - P_s = N_\phi P_s + \sigma_u \qquad (4.48)$$

and the FY index for the Mohr-Coulomb criterion is then given by:

$$(FY)_{MC} = \frac{P_s}{P} = \frac{2 - \sigma_u/P}{N_\phi + 1} \qquad (4.49)$$

Another simple yield criterion that is frequently used in geotechnical analyses is the Drucker-Prager yield function (Drucker and Prager, 1952). This criterion, which can be thought of as a generalized Mohr-Coulomb rule for three-dimensional stress states, is expressed as:

$$F_{DP} = J_2^{1/2} - \alpha J_1 - k = 0 \qquad (4.50)$$

in which J_1 = first invariant of the deviatoric stress tensor

$$J_1 = \sigma_1 + \sigma_2 + \sigma_3 \qquad (4.51a)$$

J_2 = second invariant of the deviatoric stress tensor

139

$$J_2 = \frac{1}{6}[(\sigma_1 - \sigma_2)^2 + (\sigma_2 - \sigma_3)^2 + (\sigma_1 - \sigma_3)^2] \qquad (4.51b)$$

α, k = yield parameters (material constants)

This yield criterion will be used in the elasto-plastic finite element analyses described in Section 5. For the initiation of yielding under this yield rule, the stresses at the tunnel will must satisfy the relation (substitute Eq. 4.47 into 4.50):

$$\frac{1}{\sqrt{6}}[(2P - P_s - P_z)^2 + 4(P - P_s)^2 + (P_z - P_s)^2]^{1/2} - \alpha(2P + P_z) - k = 0$$

$$(4.52)$$

which , when simplified, gives the first-yield index:

$$(FY)_{DP} = \frac{P_s}{P} = 1 - \left[\left(\frac{P_z}{P}\right)^2 \left(\alpha^2 - \frac{1}{3}\right) + 2\frac{P_z}{P}\left(\frac{1}{3} + 2\alpha^2 + \frac{\alpha k}{P}\right)\right.$$
$$\left. + \left(2\alpha + \frac{k}{P}\right)^2 - \frac{1}{3}\right]^{1/2}$$

$$(4.53)$$

For plane strain conditions, $P_z = 2\nu P$ and:

$$(FY)_{DP} = 1 - \left[4\nu^2\left(\alpha^2 - \frac{1}{3}\right) + 4\nu\left(\frac{1}{3} + 2\alpha^2 + \frac{\alpha k}{P}\right) + \left(2\alpha + \frac{k}{P}\right)^2 - \frac{1}{3}\right]^{1/2}$$

$$(4.54)$$

140

A third yield function that is sometimes used is the
three dimensional Von-Mises criterion:

$$F_{VM} = J_2 - \frac{\sigma_u^2}{3} = 0 \tag{4.55}$$

in which J_2 is defined as in (4.51b) and σ_u is the uniaxial
(i.e., unconfined) compressive strength. The FY index
for this case is obtained by substituting (4.47) into (4.55)
and simplifying:

$$(FY)_{VM} = 1 - \frac{1}{\sqrt{3}} \left[(\frac{\sigma_u}{P})^2 - 1 + 2(\frac{P_z}{P}) - (\frac{P_z}{P})^2 \right]^{1/2} \tag{4.56}$$

For plane strain conditions, $P_z = 2\nu P$ and:

$$(FY)_{VM} = 1 - \frac{1}{\sqrt{3}} \left[(\frac{\sigma_u}{P})^2 - 1 + 4\nu - 4\nu^2 \right]^{1/2} \tag{4.57}$$

The derivation of the FY index for the ground strength
concludes the general description of the behavior of yield-
ing ground masses around tunnels. Ground yielding imparts
a nonlinearity to the ground characteristic curve; conse-
quently, a support pressure higher than that in an

141

equivalent linearly elastic case is required to maintain
a given ground movement. Factors like dilatancy and loosen-
ing also affect the post-yield nonlinearity of the ground
mass. The yielding ground behavior under axisymmetric
(K=1) stress conditions can be modeled analytically by
plane strain elasto-plastic solutions; several types of
these solutions have been summarized in this chapter.
The principles behind these solutions can also be used
to derive indices, like the "first-yield" (FY) index, for
the composite (cohesive plus frictional) strength of the
ground mass surrounding the tunnel.

The next step in the investigation of tunnel support
loads in yielding ground masses is to add the effects of
the support itself into the analysis. The additional com-
plexities that result -- especially the coupling of the
effects of relative support stiffness, support delay, and
ground yielding -- are the subject of the next chapters.

5. INCREASE IN SUPPORT LOADS
CAUSED BY GROUND YIELDING

5.1 QUALITATIVE DESCRIPTION

Yielding in the ground mass surrounding a tunnel sig-nificantly changes the nature of the ground's behavior and its interaction with the tunnel support. The discussion in Section 4 demonstrated that the ground characteristic curve becomes nonlinear as yielding develops and that this nonlinear curve always lies above the straight-line curve for the elastic case. As a consequence, a larger support pressure is needed in yielding or "weak" ground masses to maintain a given ground displacement.

Determining the precise increase in support loads caused by ground yielding is somewhat difficult, however. Complexities arise because the effects of ground yielding are coupled with the effects of relative support stiffness (Section 2) and support delay (Section 3). As illustrated in Figure 5.1, a relatively flexible support with a long delay (support characteristic curve AB in the figure) will intersect the ground characteristic curve well within the nonlinear range and the yielding of the week ground mass will increase the support load by ΔP_{AB}. A much stiffer support with the same support delay (curve AC) would suffer the even more substantial support load increase ΔP_{AC}. At the

143
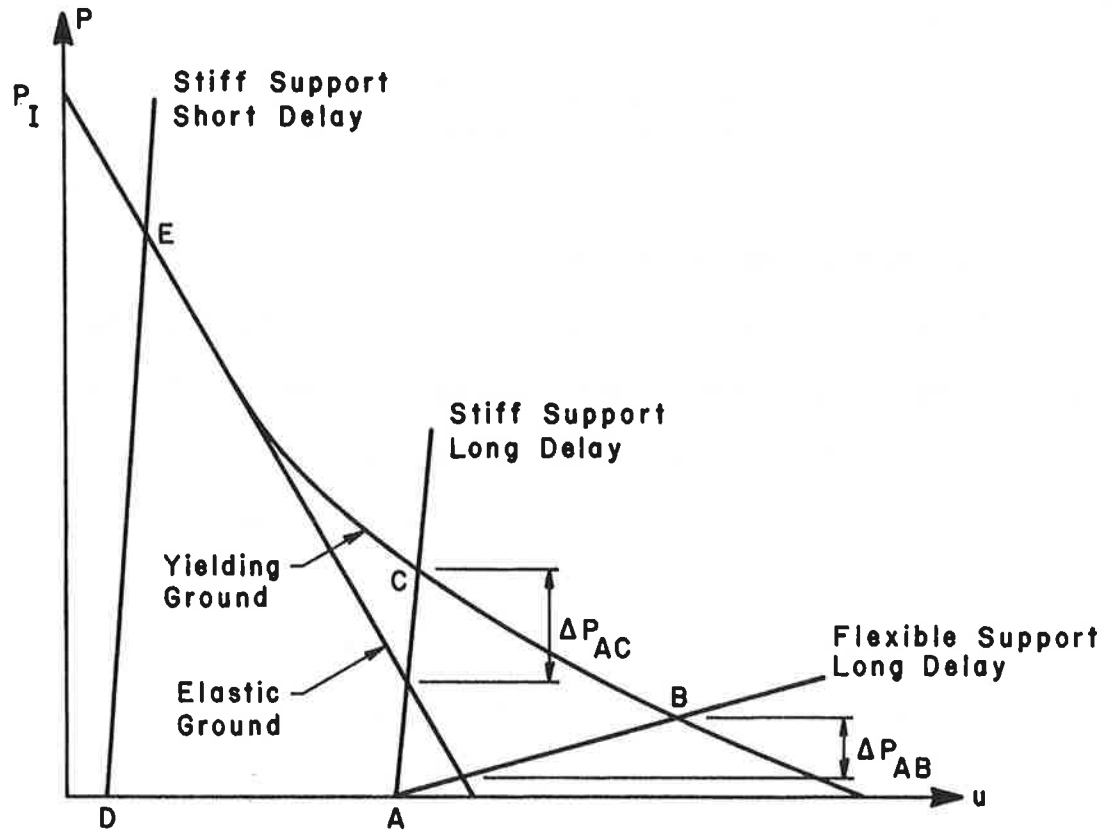
FIGURE 5.1. COUPLED EFFECTS OF GROUND YIELDING, SUPPORT
STIFFNESS, AND SUPPORT DELAY ON SUPPORT LOADS.

other extreme, however, decreasing the support delay of

the relatively stiff support (curve DE in Figure 5.1)

will cause it to intersect the same ground character-

istic curve in the initial linear or elastic range; the

ground will not have deformed enough for yielding to

develop and the weakness of the ground mass will not

have any bearing on the support loads in this case. Thus,

144

it is not just the weakness of the ground mass alone but the combination of the ground and support properties that determines the increase in support loads caused by ground yielding.

Since in some circumstances ground yielding can substantially increase the support loads, the strength of the ground mass must be considered explicitly in the design calculations. The remainder of this chapter will describe the quantitative impact that ground yielding has on support loads and will present simple techniques for incorporating the coupled effects of ground yielding, relative support stiffness, and support delay into the design analysis.

5.2 ELASTO-PLASTIC FINITE ELEMENT ANALYSES OF ADVANCING TUNNELS

In Section 3, finite element methods were employed to study the forces that developed in a tunnel support as the tunnel advanced through a linearly elastic ground mass. The problem is only slightly more complicated if the ground is treated as an elasto-plastic continuum; thus, after some small modifications the same finite element techniques can be used to simulate the step-by-step construction of a tunnel in a yielding ground mass. These finite element analyses will now be truly nonlinear in the conventional sense -- that is, in addition to the nonlinear geometry of the problem (the incremental advance of the tunnel), the constitutive equations for the ground mass will be

145

nonlinear.[1]

As already pointed out in Section 3.2, the numerical analysis of the behavior of an advancing tunnel can be simplified considerably if the dimensions of the problem can be reduced from three to two by assuming axial symmetry. This assumption requires that:

(1) the tunnel section is circular at all stages of construction

(2) the in situ lateral stress ratio, K, is equal to 1.

(3) the variation of the in situ stresses over the depth of the tunnel is negligible

(4) the tunnel is deep enough that the proximity of the ground surface has an insignificant effect on the tunnel behavior (generally, depths greater than 2 tunnel diameters -- more if extensive yielding develops -- are sufficient).

(5) any inhomogeneities in the ground are symmetric about the tunnel's centerline.

One of the drawbacks of this axial symmetry assumption is that it eliminates any possibility of studying

---

[1]Daemen and Fairhurst (1972), Descoeudres (1974), and Ranken and Ghaboussi (1975) have all performed elasto-plastic finite element studies of the ground behavior around the face of a tunnel. However, only Ranken and Ghaboussi considered supported tunnels and only they simulated the step-by-step tunnel construction. For more details, see Section 3.2.

the bending moments in the tunnel support since these moments only develop when $K \neq 1$. This limitation is not too restrictive, though, because for most common support systems the critical support moments are small and usually due to local factors like inadequate blocking or grouting. A related and more serious limitation of the axial symmetry assumption is that it requires the in situ ground stresses to be axisymmetric or $K = 1$. This represents a very special case for a yielding ground mass because when $K = 1$ the in situ shear stresses in the ground are zero. In order to simplify the problem, though, this special case will be assumed for the present analyses. The additional complexities arising from $K \neq 1$ stress conditions will be considered separately in Section 5.4.

5.2.1 Description of the Axisymmetric Elasto-Plastic Finite Element Analyses

In order to determine the quantitative effect of ground yielding on support loads, a series of axisymmetric elasto-plastic finite element analyses were performed. These analyses, which are very similar to those for tunnels in elastic ground masses described in Section 3.2, simulate the step-by-step advance of the tunnel through a yielding ground mass. The principal variables in the analyses are the strength parameters for the ground, the support delay, and the relative support stiffness.

147

The element mesh used for the analyses is the same as that shown earlier in Figure 3.3. The mesh for the elasto-plastic analyses is in all respects identical to that used for the elastic analyses in Section 3.

The input parameters for the axisymmetric elasto-plastic analyses are summarized in Table 5.1. The eight cases, which except for their strength properties are identical to the corresponding elastic cases in Section 3, are grouped into two major categories. Cases 1, 2A, and 2B represent soft ground tunnels. The ground's elastic modulus for these cases varies between 5000 and 15000 psi, and the in situ ground stresses correspond to a depth of about 100 feet. The second group, cases 4A through 4E, represents tunnels in moderate quality rock masses. These five cases, in which the ground's elastic modulus is held constant at 1.5×10^6 psi but the strength properties are varied, are intended to isolate the effects of ground yielding. The rock cases 4A - 4E are assumed to be located twice as deep as the soft ground tunnels, at a depth of approximately 200 feet. Since these two groups of cases bracket most common tunneling situations, no elasto-plastic analyses were performed for the intermediate case 3 in Section 3.

The values for the support moduli (E_s, ν_s) and thicknesses (t) are typical for precast concrete liner

148

TABLE 5.1. PROPERTIES FOR AXISYMMETRIC ELASTO-PLASTIC FINITE ELEMENT ANALYSES

Case	In Situ Stress P	Ground Properties				Support Properties[1]			Stiffness Ratios[2]		Strength Index[3] FY
		E	ν	c	ϕ	E_s	ν_s	t	C^*	F^*	
1	83.3psi	15000psi	0.30	0.1psi	35°	1.94×10^6 psi	0.30	6.9 in.	0.134	484.0	0.43
2A	83.3	5000	0.48	16.7	0	1.94×10^6	0.30	6.9 in.	0.0528	191.0	0.80
2B	83.3	5000	0.30	0.1	25	1.94×10^6	0.30	6.9 in.	0.0447	161.0	0.58
4A	166.7	1.5×10^6	0.15	8.68	16.1	3.0×10^6	0.15	6.0 in.	10.0	48,000	0.67
4B	166.7	1.5×10^6	0.15	10.4	19.1	3.0×10^6	0.15	6.0 in.	10.0	48,000	0.61
4C	166.7	1.5×10^6	0.15	40.9	16.1	3.0×10^6	0.15	6.0 in.	10.0	48,000	0.49
4D	166.7	1.5×10^6	0.15	17.4	30	3.0×10^6	0.15	6.0 in.	10.0	48,000	0.41
4E	166.7	1.5×10^6	0.15	26.0	40.9	3.0×10^6	0.15	6.0 in.	10.0	48,000	0.23

[1] Tunnel Radius = 10 ft. in all cases

[2] Compressibility (C^*) and Flexibility (F^*) ratios are defined in Section 2

[3] The First Yield (FY) Strength Index is defined in Section 4; in this table, it is based on the Mohr-Coulomb yield criterion. (See footnote in text.)

elements. The compressibility ratio C^*, which expresses the relative support stiffness, varies between 0.045 and 10.0 and spans the range for most common tunneling situations. The flexibility ratio, F^*, varies from 161 to 48,000 but it is of minor importance since it primarily relates to support moments, which do not develop in the axisymmetric finite element analyses.

The ground strength properties for the soft ground cases 1, 2A, and 2B range from purely cohesive (Case 2A -- $c = 16.7$ psi, $\phi = 0$) to near-purely frictional (Case 1 -- $c = 0.1$ psi, $\phi = 35°$). The values of the strength parameters in these three cases are reasonable for soft grounds like clays, sands, and glacial tills. In the rock cases 4A - 4E, the strength parameters are varied over a wide range ($c = 8.68 - 40.9$ psi, $\phi = 16.1° - 40.9°$) in order to highlight the effects of ground yielding. The values of the strength parameters chosen for these analyses are consistent with strength properties backfigured from observed slope failures in "soft to jointed, hard rock" masses with varying degrees of disturbance (e.g., from blasting) and weathering (see Hoek and Bray, 1974, Figure 70). In all of the rock and soft ground cases, the combined cohesive and frictional strength of the ground mass can be quantified by the "first-yield" (FY) strength index developed in

150

Section 4;[1] as indicated in Table 5.1, this index for the overall strength of the ground mass ranges from 0.43 to 0.80 for the soft ground cases 1, 2A, and 2B and from 0.23 to 0.67 in the rock cases 4A - 4E.

An elastic-perfectly plastic constitutive model for the ground behavior was used in all of the analyses. Yielding is governed by the Drucker-Prager yield criterion for three-dimensional stress states (see Bathe, 1976, for details of its implementation in ADINA):

$$F_{DP}(\sigma_1, \sigma_2, \sigma_3) \; = \; J_2^{\frac{1}{2}} \; - \; \alpha \; J_1 \; - \; k \; = \; 0 \qquad\qquad (5.1)$$

in which J_1 = first invariant of the deviatoric stress tensor

$$= \; \sigma_1 \; + \; \sigma_2 \; + \; \sigma_3$$

---

[1]Recalling the development in Section 4, the first-yield (FY) strength index is defined for K = 1, plane strain stress conditions as the internal support pressure at which ground yielding first occurs divided by the in situ ground pressure. The FY strength index can be calculated from simple elasto-plastic closed-form solutions. FY varies between the limits of 0 (elastic ground -- no yielding develops even when the internal support pressure is zero) and 1 (ground has zero strength -- yielding develops when stresses deviate even slightly from uniform in situ conditions).

$$J_2 \; = \; \text{second invariant of the deviatoric stress}$$

tensor

$$J_2 \; = \; \frac{1}{6} \left[(\sigma_1 - \sigma_2)^2 + (\sigma_1 - \sigma_3)^2 + (\sigma_2 - \sigma_3)^2 \right]$$

$$\alpha, k \; = \; \text{yield parameters}$$

$$\sigma_1, \sigma_2, \sigma_3 \; = \; \text{principal stresses}$$

The Drucker-Prager yield criterion can be thought of as the three-dimensional generalization of the two-dimensional Mohr-Coulomb yield function. The yield parameters α and k can be related to the more familiar Mohr-Coulomb strength parameters c and ϕ in certain special cases. For example, for c and ϕ determined from conventional triaxial compression tests[1] ($\sigma_1 = \sigma_{axial}$, $\sigma_2 = \sigma_3 = \sigma_{confining}$), the values of α and k are given by (Bathe, 1976):

----

[1]Triaxial extension tests ($\sigma_1 = \sigma_2 = \sigma_{confining}$, $\sigma_3 = \sigma_{axial}$) generally give values for c and ϕ different from those in the triaxial compression test; the relations between α and ϕ and between k and c for the extension test can be shown to equal:

$$\alpha \; = \; \frac{2 \sin \phi}{\sqrt{3} \; (3 + \sin \phi)}$$

$$k \; = \; \frac{(6c) \cos \phi}{\sqrt{3} \; (3 + \sin \phi)}$$

c, ϕ from triaxial extension tests.

The values for α and k should be the same for both types of tests if the tested material really does follow the Drucker-Prager yield law.

$$\alpha = \frac{2 \sin \phi}{\sqrt{3} \ (3-\sin\phi)} \tag{5.2a}$$

$$k = \frac{(6c) \ \cos\phi}{\sqrt{3} \ (3-\sin\phi)} \tag{5.2b}$$

The values of α and k calculated from these equations, using the values for ϕ and c given in Table 5.1, are summarized in Table 5.2. For purely cohesive or $\phi = 0$ strength properties, the Drucker-Prager yield criterion in Eq. (5.1) is equivalent to the Von Mises yield function:

$$F_{VM}(\sigma_1, \sigma_2, \sigma_3) = J_2 - \frac{\sigma_0^2}{3} = 0 \tag{5.3}$$

in which σ_0 = yield stress in simple compression

$$= 2c$$

The associated flow rule is used to calculate the plastic strain increments in all cases.

In addition to the relative support stiffness and the ground strength properties, the support delay was varied in the finite element analyses. Support delay lengths (L_d) of 0.25, 0.75, and 1.25 times the tunnel radius (R) were investigated in cases 1 and 2A; in cases 2B and 4A - 4E, only the bracketing values of L_d/R equal to 0.25 and 1.25 were treated.

153

TABLE 5.2. DRUCKER-PRAGER YIELD PARAMETERS FOR THE FINITE
ELEMENT ANALYSES

Case	Mohr-Coulomb Yield Parameters		Drucker-Prager Yield Parameters	
	ϕ	c	α	k
1	35°	0.1 psi	0.273	0.0168 psi
2A	0	16.7	0	2.77
2B	25	0.1	0.189	0.175
4A	16.1	8.68	0.118	1.53
4B	19.1	10.4	0.141	1.84
4C	16.1	40.9	0.118	7.20
4D	30	17.4	0.231	3.00
4E	40.9	26.0	0.322	4.19

5.2.2 Results from the Analyses

Since yielding of the ground mass is one of the most important features of this series of finite element analyses, it is interesting to look first at the extent of the yielded zone in each of the eight cases. The shapes and sizes of the yielded zones for the soft ground cases 1, 2A, and 2B are illustrated in Figure 5.2. In case 1, the strongest case (smallest FY, equal to 0.43), the yielded zone in the analysis with the short support delay (L_d = 0.25R) is very small, extending about one-quarter of a tunnel radius into the ground mass in the very local region at the center of the face. The other extreme occurs in case 2A, the weakest case (largest FY, equal to 0.8), with the long support delay (L_d = 1.25R). In this case yielding is quite extensive, with the yielded zone extending longitudinally about 2 radii ahead of the face and radially a maximum of 1.5 radii beyond the tunnel wall. The influence of both support delay and ground strength on ground yielding is quite clear in Figure 5.2. Increasing the support delay length or decreasing the ground strength (increasing FY) leads to progressively larger yielded zones. Intermediate amounts of yielding develop in cases 1 and 2A for the other support delays and in case 2B (FY = 0.58) at all values of L_d. In all of these soft ground cases, yielding primarily develops ahead of the face and around the unsupported section of

155

KEY

$L_d = 0.25R$

$L_d = 0.75R$

$L_d = 1.25R$
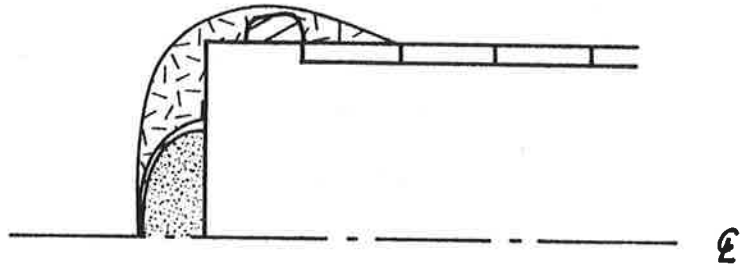
CASE 1 (FY=0.43)

CASE 2A (FY=0.80)

L_d

R
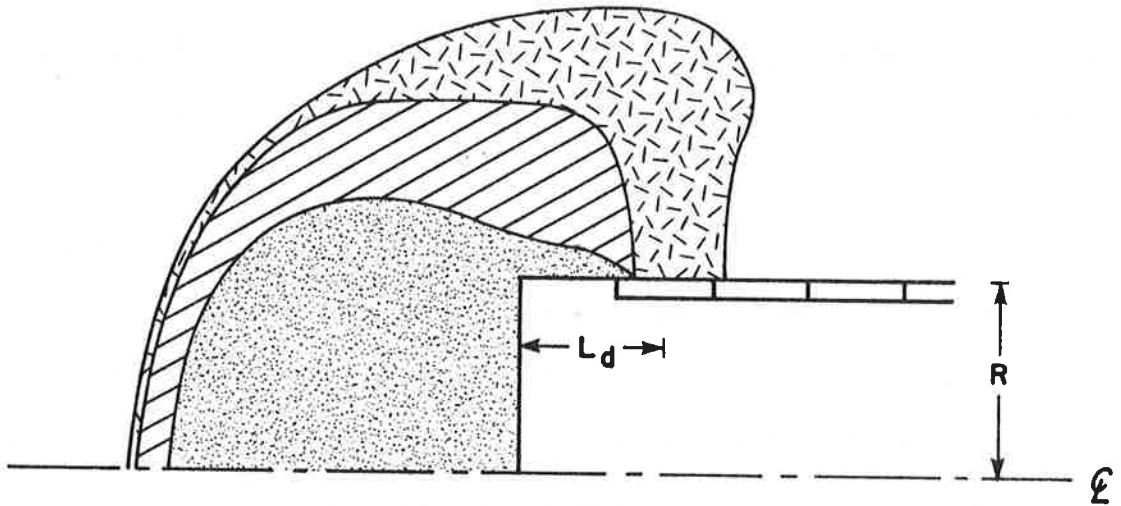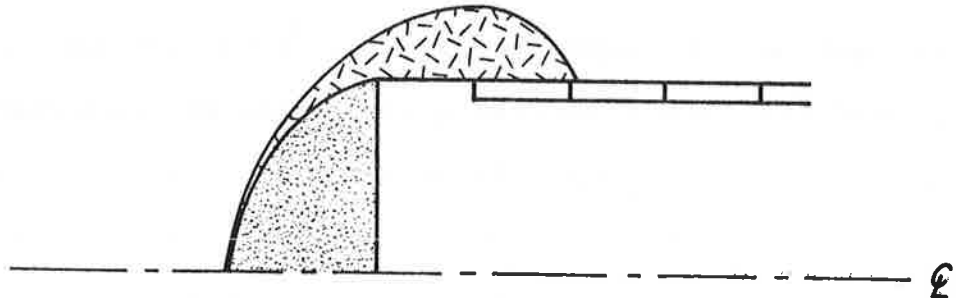
CASE 2B (FY=0.58)

FIGURE 5.2 EXTENT OF THE YIELDED ZONE--CASES 1, 2A, AND 2B.

156

the tunnel; the installation of the tunnel support provides a radial counterstress to the ground mass that essentially "reloads" the ground, causing a return to elastic ground behavior and the "collapse" of the yielded zone.

The extent of the yielded zones for the rock cases 4A through 4E are shown in Figure 5.3. These cases are alike in all respects but the ground strength. The most extensive yielding develops in the weakest case, 4A, with L_d = 1.25R; the yielded zone extends longitudinally about 1.25 radii ahead of the face and radially approximately 1.25 radii beyond the tunnel wall. As in the soft ground cases, the size of the yielded zone decreases as the strength increases. Yielding in the strongest case, 4E, is confined to the very local region at the center of the tunnel face. In contrast to the soft ground cases, however, the amount of yielding in the rock cases 4A - 4E does not increase dramatically with increasing support delay. The yielded zone in the weak case 4A is only slightly larger when L_d = 1.25R than it is when L_d = 0.25R; in the relatively strong cases 4D and 4E the differences in the yielded zones for the two support lengths become insignificant. The reason for this phenomenon is that the relatively flexible supports in the rock cases have a much smaller influence on the ground behavior in general than do the relatively stiff supports in the soft ground tunnels. As a result, changing the support properties --

157

KEY

▦ $L_d = 0.25R$

▨ $L_d = 1.25R$
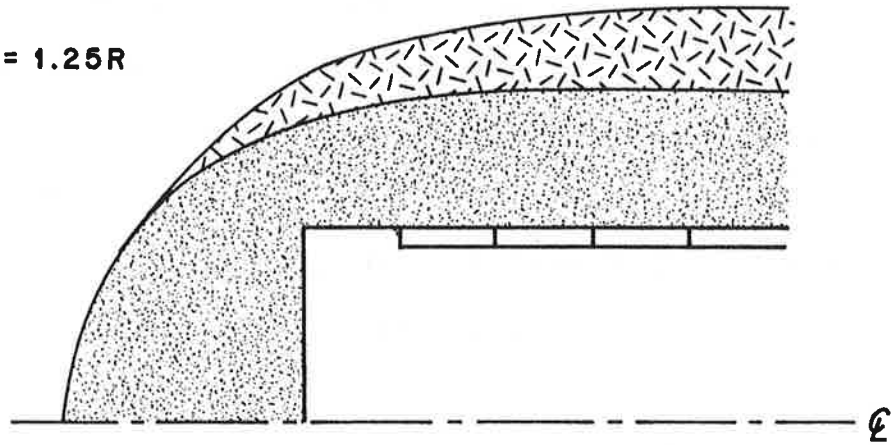
CASE 4A (FY=0.67)
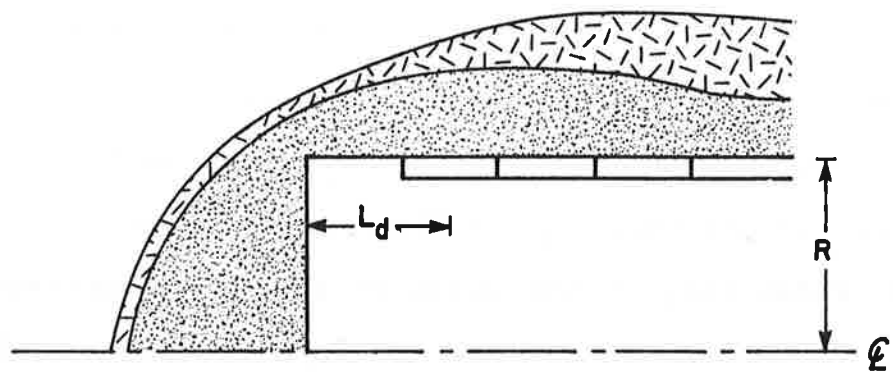
CASE 4B (FY=0.61)

FIGURE 5.3.   EXTENT OF THE YIELDED ZONE--CASES 4A-4E.

158

YIELDED ZONES FOR L_d=0.25R AND
L_d=1.25R ARE NEARLY IDENTICAL

CASE 4C (FY=0.49)

YIELDED ZONES FOR L_d=0.25R
AND L_d=1.25R ARE IDENTICAL

CASE 4D (FY=0.41)

YIELDED ZONES FOR L_d=0.25R
AND L_d=1.25R ARE IDENTICAL
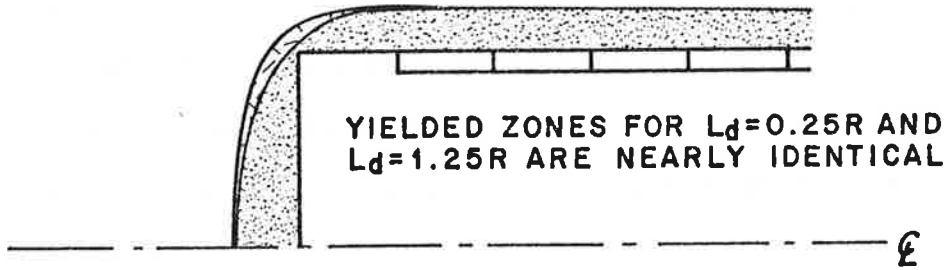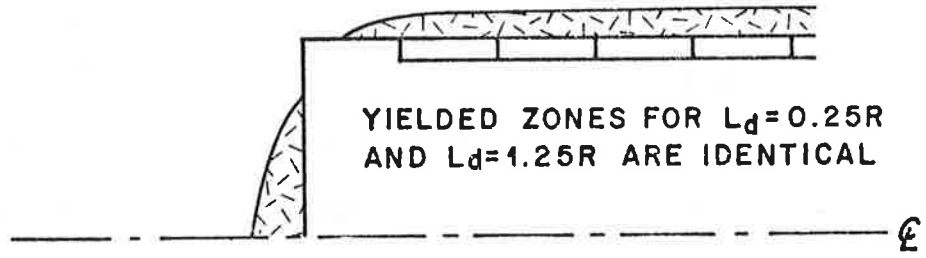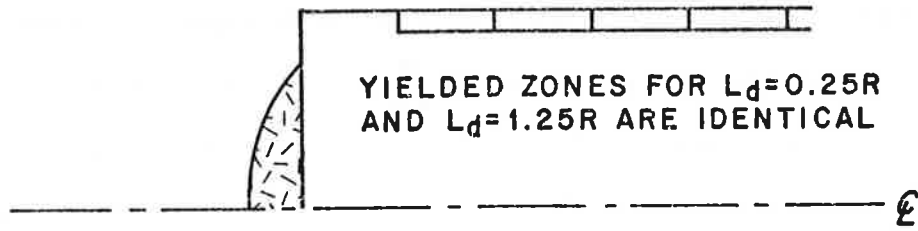
CASE 4E (FY=0.23)

FIGURE 5.3.   EXTENT OF THE YIELDED ZONE--CASES 4A-4E (CONT.)

like the support delay -- has only a minor influence on the ground behavior in cases 4A - 4E. Another consequence of the flexible supports in these cases is that the yielded zone no longer "collapses" after the support is installed, as it did in the soft ground cases 1, 2A, and 2B; the support no longer reloads the ground enough to reverse the yielding.

The pertinent quantitative results from the axisymmetric elasto-plastic finite element analyses are summarized in Figures 5.4 through 5.6 for cases 1, 2A, and 2B, in Figure 5.7 for cases 4A - 4E with $L_d = 0.25R$, and in Figure 5.8 for cases 4A - 4E with $L_d = 1.25R$. These figures depict the variation of the following quantities with distance from the tunnel face: (1) the radial ground displacement, u, at the tunnel wall (i.e., at r=R), expressed in dimensionless form as $\frac{uE}{PR(1+\nu)}$; (2) the longitudinal ground displacement, w, along the centerline of the tunnel, expressed in dimensionless form as $\frac{wE}{PR(1+\nu)}$; and (3) the circumferential thrust, T, in the support, expressed in dimensionless form as $\frac{T}{PR}$. As in the elastic cases considered in Section 3, the dimensionless circumferential thrust coefficient has a theoretical upper limit of 1.0, which occurs when the support sustains the full overburden pressure P. However, in the elasto-plastic analyses the dimensionless radial displacement coefficient

160
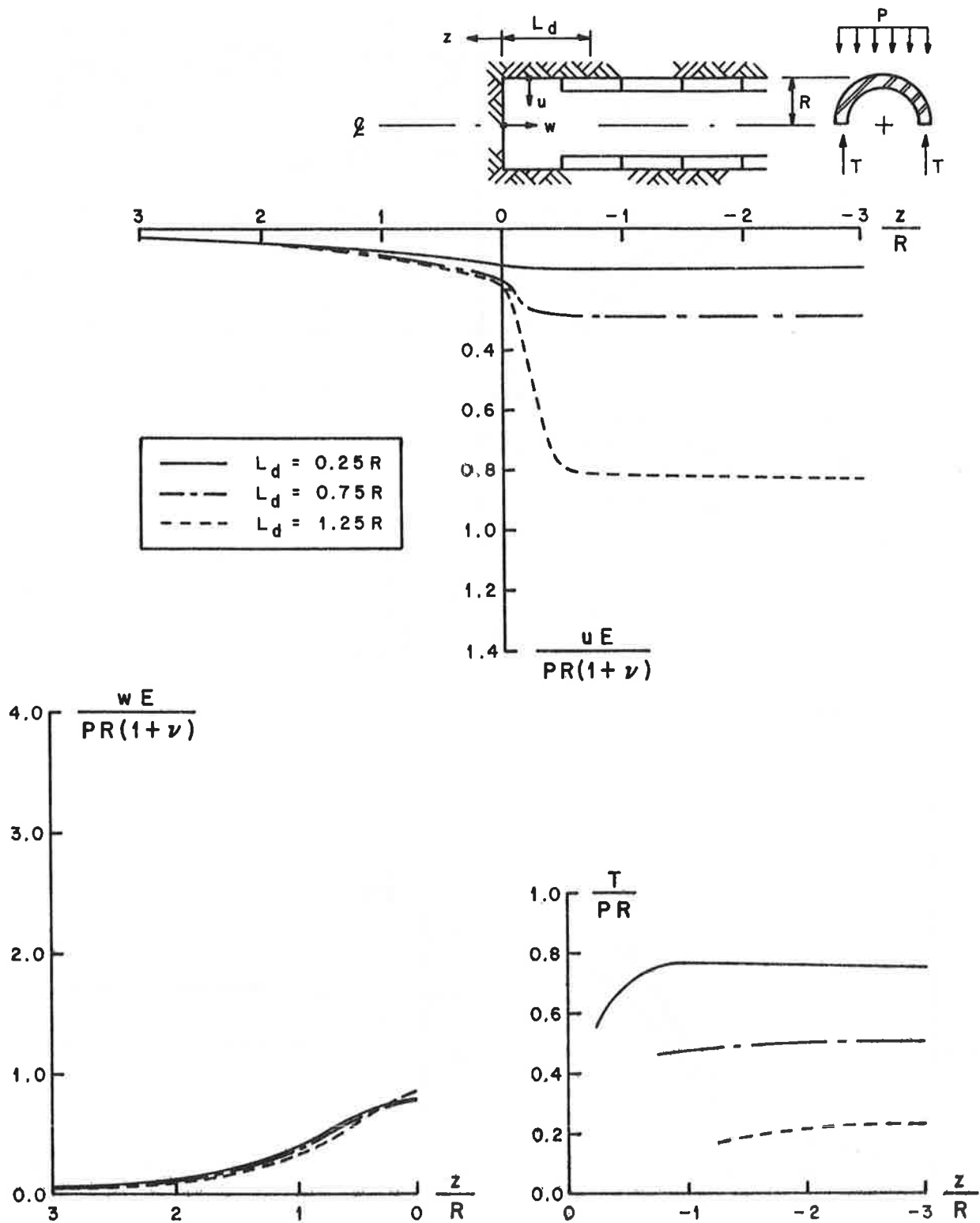
FIGURE 5.4.   RESULTS FROM AXISYMMETRIC ELASTO-PLASTIC FINITE
ELEMENT ANALYSES--CASE 1.

161
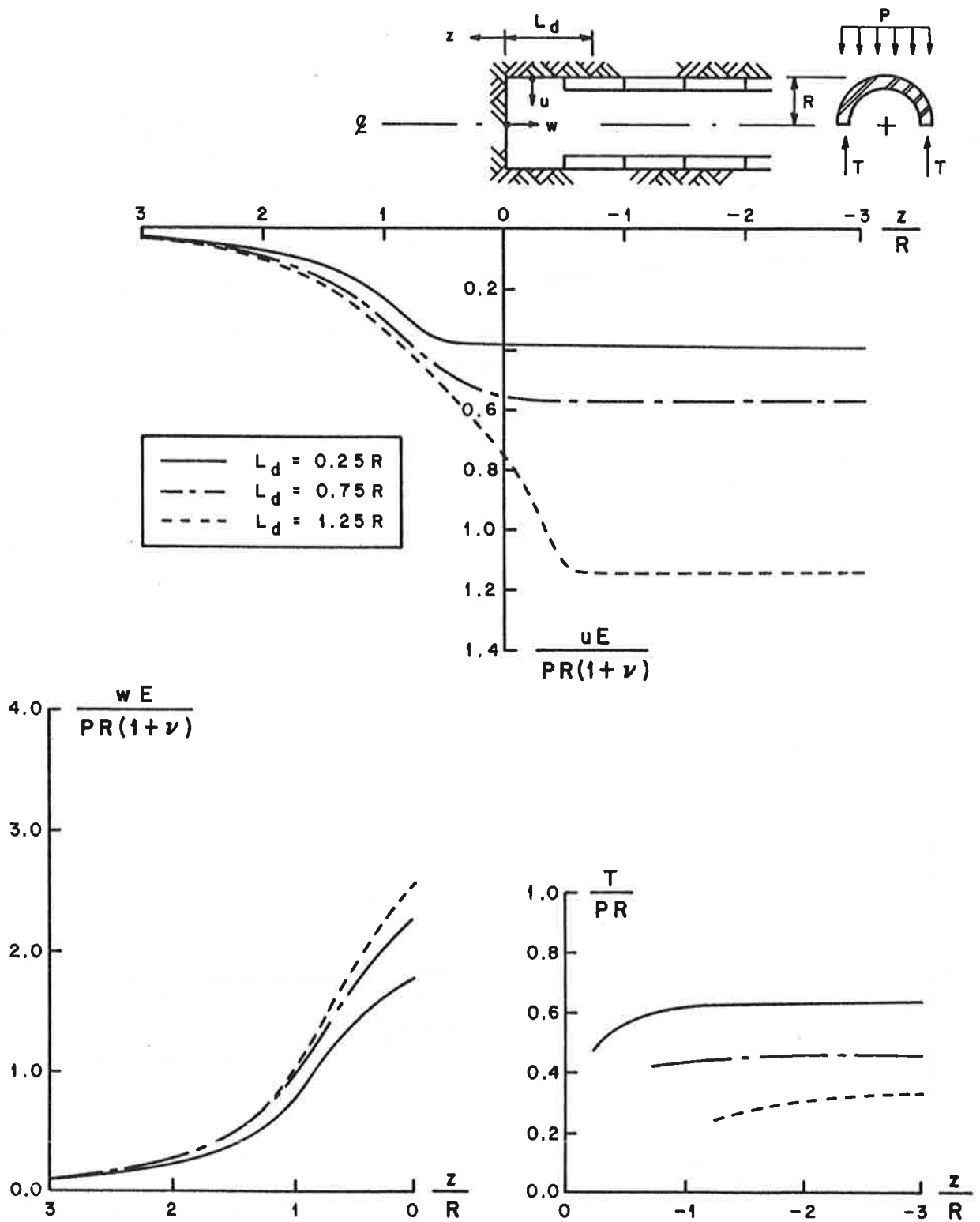
FIGURE 5.5.   RESULTS FROM AXISYMMETRIC ELASTO-PLASTIC FINITE
ELEMENT ANALYSES--CASE 2A.

162
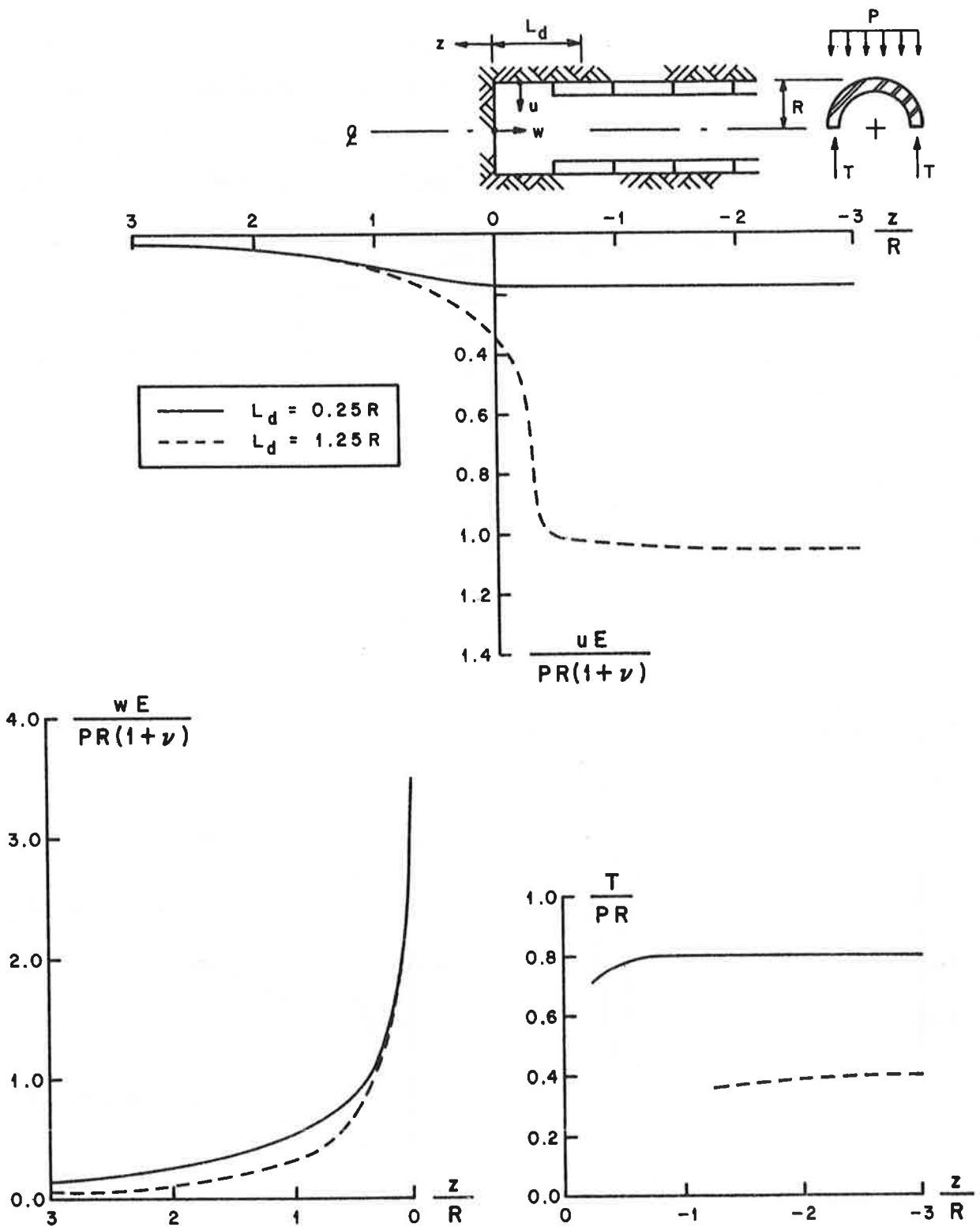
FIGURE 5.6.   RESULTS FROM AXISYMMETRIC ELASTO-PLASTIC FINITE
ELEMENT ANALYSES--CASE 2B.

163
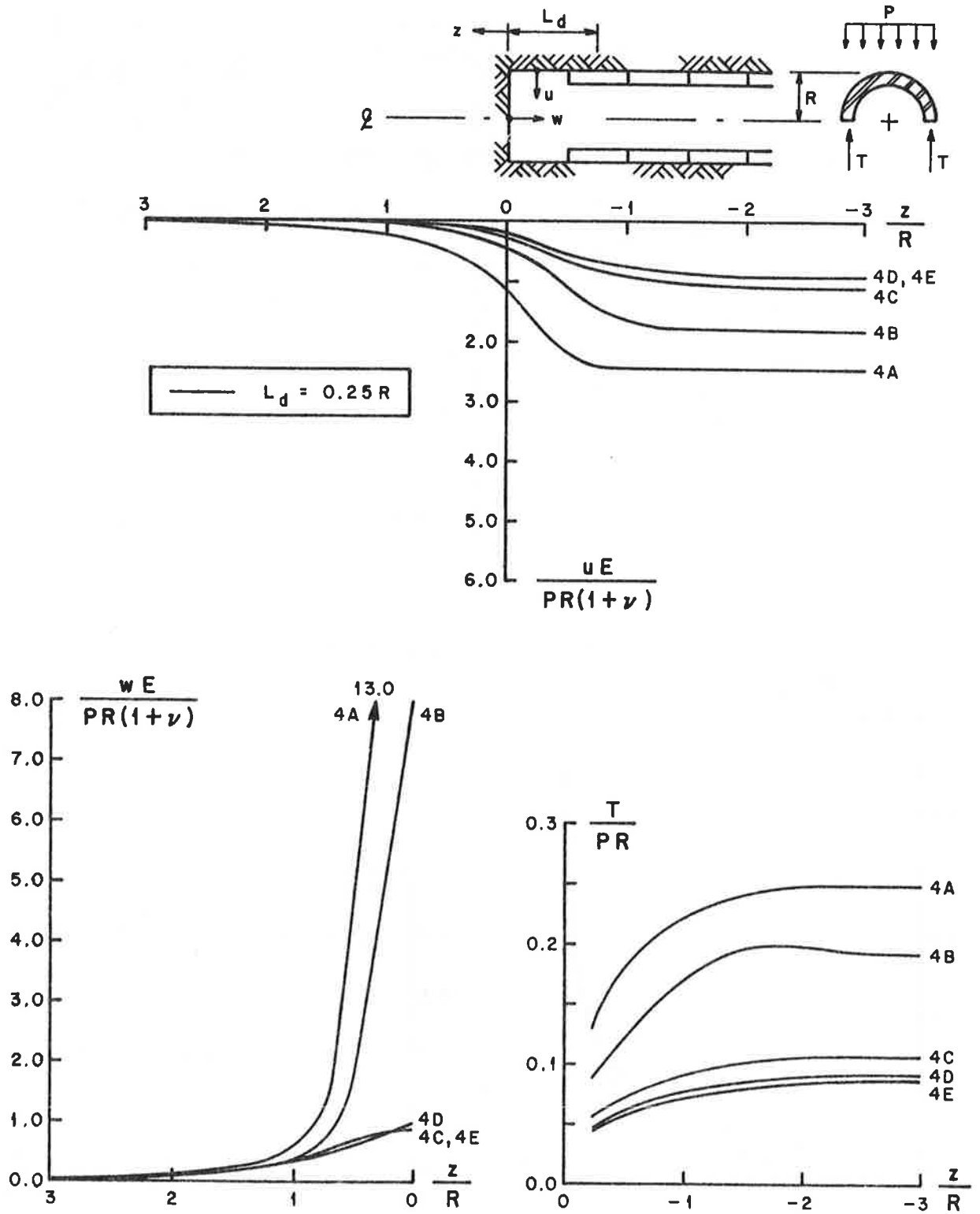
FIGURE 5.7.   RESULTS FROM AXISYMMETRIC ELASTO-PLASTIC FINITE
ELEMENT ANALYSES--CASES 4A-4E, $L_d = 0.25R$

164
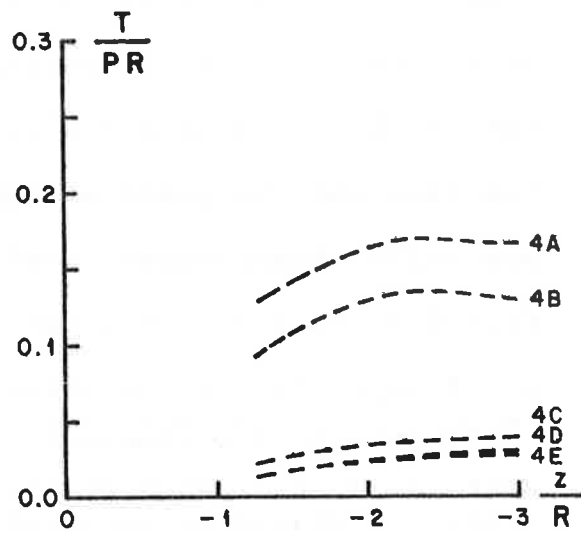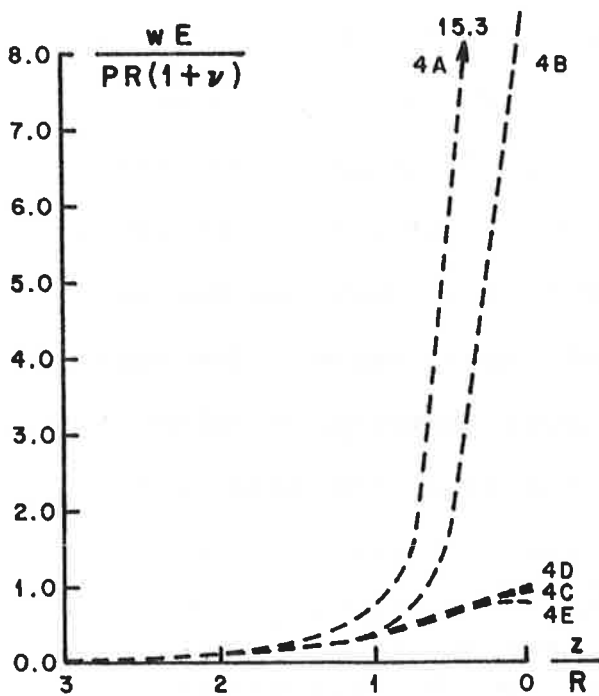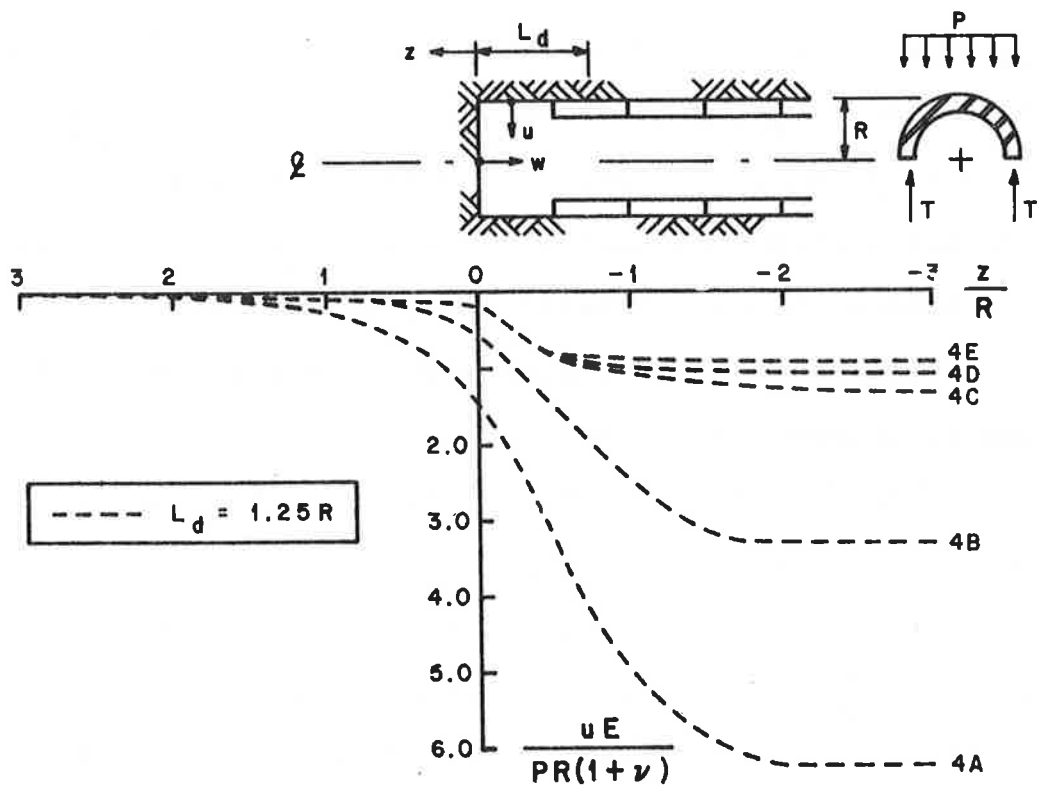
FIGURE 5.8.   RESULTS FROM AXISYMMETRIC ELASTO-PLASTIC FINITE
ELEMENT ANALYSES--CASES 4A-4E, L_d = 1.25R

165

$\frac{uE}{PR(1+\nu)}$ no longer has an upper limit and, in fact, the variation in $\frac{uE}{PR(1+\nu)}$ is so large that the data for cases 4A - 4E (Figures 5.7 and 5.8) must be plotted to a scale different from that used for cases 1, 2A, and 2B (Figures 5.4 through 5.6).[1] Nevertheless, it is still convenient to express the displacements and thrusts in terms of the dimensionless coefficients.

The general character of the data in Figures 5.4 through 5.8 is similar to that of the elastic analyses in Chapter 3. In all of the cases, the radial ground movements, $\frac{uE}{PR(1+\nu)}$, begin approximately 2 to 3 tunnel radii ahead of the face. Nearly all of the total radial movement takes place ahead of the face in the soft ground cases 1, 2A, and 2B with the short support delay (Figures 5.4 - 5.6 with L_d = 0.25R); as the support delay is increased in these cases, a progressively smaller fraction of the total movement occurs ahead of the face (from 20 to 60% for L_d = 1.25R) and a larger portion develops between the face and the point of support installation. The maximum radial displacement coefficients, ranging in value from 0.13 to 1.2, are attained soon after the relatively stiff supports are installed in the soft ground. In the

---

[1] Although the displacement coefficients, $\frac{uE}{PR(1+\nu)}$, for the rock cases are generally larger than for the soft ground cases, it should be realized that the absolute displacements in the rock are still much smaller. This seeming discrepancy is a result of the normalization of the data in the displacement coefficient.

rock cases 4A - 4E (Figures 5.7 and 5.8), on the other
hand, the relatively less stiff support is not as effective
in restraining the radial ground displacements, and as a
result a smaller fraction of the total ground movement
takes place ahead of the face and constant or plane strain
conditions are reached much later. The final radial dis-
placement coefficients in cases 4A - 4E are quite large,
ranging from 0.9 to 6.2, and generally exceed by a sub-
stantial margin the equivalent values in the elastic cases,
which ranged from 0.9 to 1.0 (see Section 3). The effects
of ground yielding on the radial ground displacements can
be seen quite clearly in Figures 5.7 and 5.8. In case 4E,
which has the highest strength, very little yielding
develops and as a result the ground movements are essen-
tially elastic. The additional ground movements that de-
velop in the weaker cases 4A - 4D are due solely to yield-
ing in the ground mass.

The longitudinal ground displacements, $\frac{wE}{PR(1+\nu)}$, at
the centerline of the tunnel also begin at approximately 3
tunnel radii ahead of the face and increase sharply for $\frac{z}{R}$
less than 1. However, whereas in the elastic analyses
the longitudinal and radial ground movements were of roughly
the same magnitudes, the longitudinal displacements in some
of the elasto-plastic analyses are considerably larger than

167

the corresponding radial displacements. This discrepancy
is generally the greatest in the cases which exhibit the
most yielding. An example of this is clearly shown in
Figures 5.7 and 5.8: cases 4A and 4B, the two weakest
rock cases, have much higher ratios of longitudinal to
radial movements than the relatively stronger cases 4C
through 4E.

The variation of the support thrust, $\frac{T}{PR}$, with dis-
tance from the tunnel face is not great in the soft ground
cases 1, 2A, and 2B, as indicated in Figures 5.4 - 5.6.
Most of the thrust develops in the leading support ring
during the first round of advance after installation; sub-
sequent advances of the face increase the support thrust
only slightly. In the relatively less stiff supports of
cases 4A - 4E, (Figures 5.7 and 5.8), however, the support
thrust develops gradually over the first 3 to 4 support
rings, and constant or plane strain conditions are not
reached until a distance of 2 to 3 radii behind the leading
edge of the support. The effects of ground yielding on
support thrust is also quite apparent in Figures 5.7 and 5.8.
Since the relative support stiffness is the same in cases
4A - 4E, the differences in the support thrust for a given
support delay are a function only of the ground strength.
For the short support delay length (L_d = 0.25R), the
thrust in case 4A, the weakest case, is more than 2.5 times
the thrust in case 4E, the strongest case; for the long

168

delay (L_d = 1.25R), the thrust in 4A is nearly 7 times that in 4E.

The final values for the radial ground displacements and circumferential support thrusts from the elasto-plastic analyses are summarized in Table 5.3. These values were calculated after constant (plane strain) conditions had been reached. Also included in Table 5.3 are the values for the thrusts and displacements calculated from the corresponding elastic axisymmetric finite element analyses in Section 3. As expected, the values for the thrusts and displacements from the elasto-plastic analyses are generally greater than or equal to (within the accuracy of the finite element solutions) the values from the elastic cases; in some of the cases, these increases in the elasto-plastic results are quite substantial. However, there are two analyses, case 2A with L_d = 0.25R and 0.75R, that give the opposite result of elasto-plastic thrusts that are smaller than the thrusts from the elastic analyses. This anomalous finding merits further discussion.

Case 2A is unique among all of the cases for two reasons. First, it is by far the weakest ground case considered in the finite element analyses and, with FY = 0.80, it is extremely weak even in absolute terms (recall that FY = 1.0 implies zero strength in the ground mass). Second, it is the only case that corresponds to what is conventionally termed in soil mechanics an "undrained"

169

TABLE 5.3.   RESULTS FROM THE AXISYMMETRIC ELASTO-PLASTIC FINITE ELEMENT ANALYSES

Case	Support Delay $\frac{L_d}{R}$	Elastic[1] $\frac{T}{PR}$	$\frac{uE}{PR(1+\nu)}$	Elasto-Plastic $\frac{T}{PR}$	$\frac{uE}{PR(1+\nu)}$
1	0.25	0.77	0.15	0.75	0.13
	0.75	0.51	0.30	0.50	0.29
	1.25	0.25	0.72	0.24	0.82
2A	0.25	0.84	0.13	0.64	0.38
	0.75	0.61	0.31	0.45	0.56
	1.25	0.27	0.61	0.36	1.15
2B	0.25	0.83	0.12	0.80	0.17
	1.25	0.28	0.69	0.40	1.22
4A	0.25	0.086	0.91	0.24	2.4
	1.25	0.027	0.99	0.17	6.2
4B	0.25	0.086	0.91	0.18	1.8
	1.25	0.027	0.99	0.13	3.3
4C	0.25	0.086	0.91	0.11	1.1
	1.25	0.027	0.99	0.042	1.3
4D	0.25	0.086	0.91	0.088	0.92
	1.25	0.027	0.99	0.027	1.06
4E	0.25	0.086	0.91	0.087	0.91
	1.25	0.027	0.99	0.026	0.95

[1]From the axisymmetric elastic finite element analyses in Section 3.

analysis -- i.e., $\phi = 0$ and ν approaching 0.5. These two factors lead to an exaggerated and atypical pattern of yielding in case 2A.

Looking back at the sketches of the yielded zones in Figure 5.2 and 5.3, the first fact that one recognizes is that the yielded zone in case 2A is much larger than in all of the other cases. This is expected, though, since case 2A is also the weakest of the cases. However, if case 2A is compared with the second weakest case, 4A, some important differences in the yielded zones becomes clear. In 4A with $L_d = 0.25R$, the zone extends to about 1.25R ahead of the face, gradually enlarges nearer the face, and continues to enlarge radially until a maximum, constant radius of 1.75R is reached behind the face. In case 2A with $L_d = 0.25R$, on the other hand, the yielded zone extends further -- 2 full radii -- ahead of the face but it does not enlarge radially very much at points nearer the face; in fact, the yielded zone shrinks and "collapses" behind the face as soon as the support is installed (as it does in all of the soft ground cases). This same yield pattern is observed for the longer delay lengths in case 2A, although now the radial extent of the yielded zone increases.

What seems to be happening in case 2A with $L_d = 0.25R$ is that the extensive yielding ahead of the face causes a "stress relief" in the ground mass. Larger radial ground movements occur ahead of the face and, as a result, more

171

resistance is developed in the surrounding elastic ground region. In essence, the yielded zone in the region ahead of the face acts as a "soft" spot and can be thought of as increasing the "effective" support delay length. This beneficial effect is counterbalanced by the general detrimental aspects of yielding described in Section 4, but these detrimental aspects become important only as the radial extent of the yielded zone increases. In case 2A with L_d = 0.25R (and for L_d = 0.75R), the radius of the yielded zone is small while the longitudinal extent is large, and consequently the yielding of the ground has a net beneficial effect on the support loads.

There are two reasons why this beneficial effect of ground yielding is more pronounced in case 2A than in the other soft ground cases, which also exhibit the same general pattern of yielding. The first is obvious: since case 2A is much weaker than the other cases, its yielded zone extends much farther ahead of the face -- in other words, the "soft" spot ahead of the face is larger. The second reason is a consequence of the plasticity models used in the analyses. Cases 1 and 2B (and 4A - 4E) have a component of frictional strength and therefore, since the associated flow rule is used to compute the plastic strains, the ground in these cases dilates as it yields. Case 2A

has zero frictional strength and therefore no dilation. Thus, the dilating yielded zones in cases 1 and 2B (and 4A - 4E) are less "soft" than the constant-volume yielded zone in case 2A and the stress relieving aspects of the yielding ahead of the face are thereby diminished.

In practical terms, the "constant-volume" yielding occurs only in special cases like a completely undrained clay or a sensitive clay. These types of ground are not common in most tunneling, and as a result the dilating yield behavior exhibited in cases 1, 2B, and 4A - 4E will be the rule.

In order to better isolate the influence of ground yielding on the tunnel performance in the rock cases 4A - 4E, the final values for the radial ground displacements and circumferential support thrusts (given in Table 5.3) are plotted in Figures 5.9 and 5.10 as functions of the first-yield strength index, FY. The ordinates of the graphs show the percentage increases in the displacements and thrusts that result from the ground yielding (i.e., the percentage increase of the elasto-plastic analysis results with respect to the results from the corresponding elastic case). Since cases 4A - 4E differ only in their strength properties, the effects of other variables like the relative support stiffness are eliminated. The figures show quite dramatically the influence of ground yielding.

173
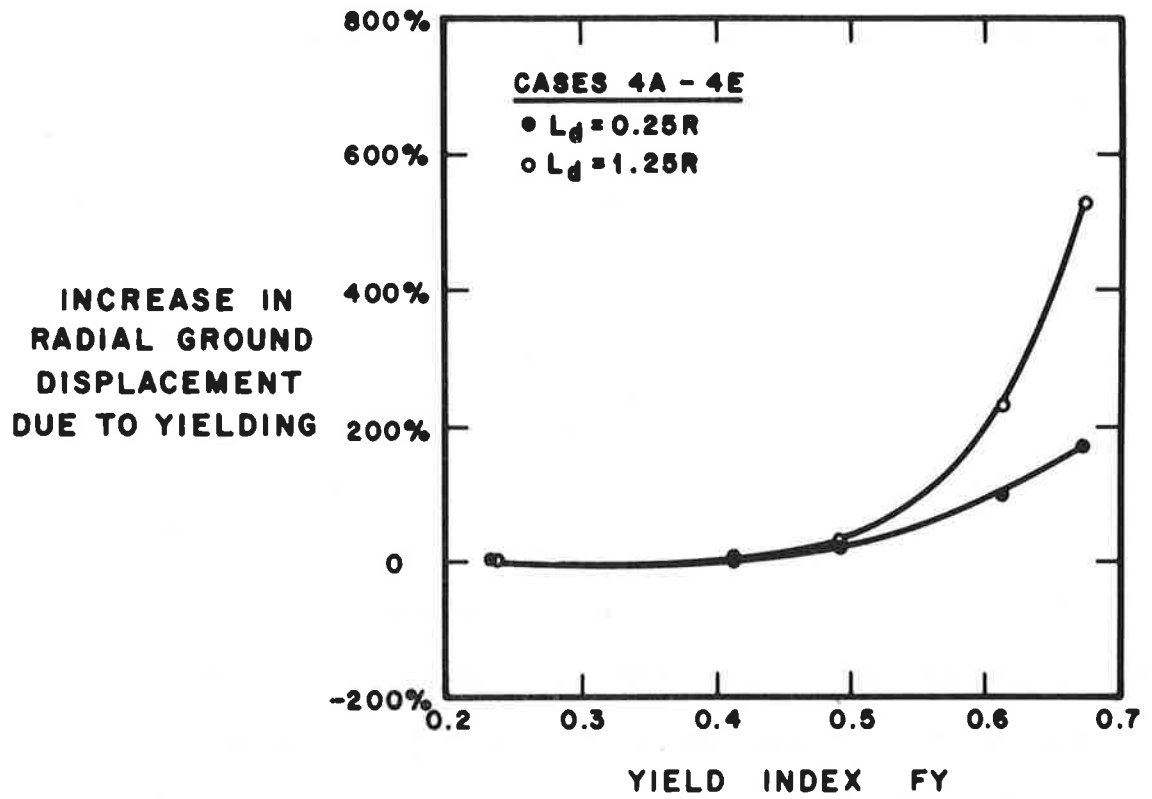
FIGURE 5.9.   INCREASE IN RADIAL GROUND DISPLACEMENT WITH
GROUND YIELDING.

174
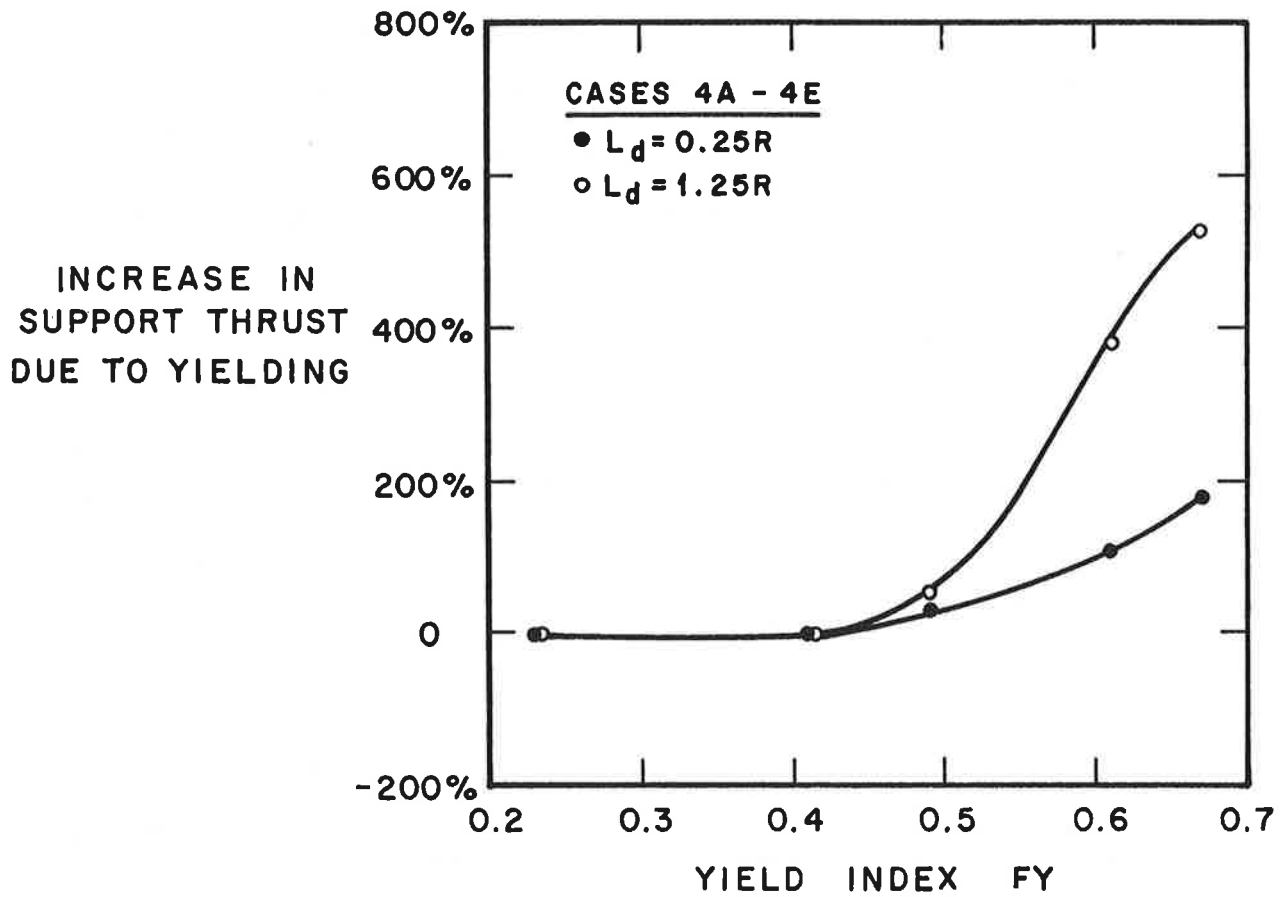
FIGURE 5.10.   INCREASE IN CIRCUMFERENTIAL SUPPORT THRUST
WITH GROUND YIELDING.

175

For a support delay length of 0.25R, a strong ground mass in which little or no yielding occurs -- FY = 0.23 -- produces ground movements and support thrusts essentially equal to the elastic case (i.e., zero percentage increase), while the substantial yielding that develops in a weaker ground mass -- FY = 0.67 -- produces a 165% increase in ground displacements and a 180% increase in support thrust. The coupling between support delay and ground yielding is also evident in the figures. Increasing the support delay length to 1.25R in the weak (FY = 0.67) ground case further increases both the ground displacement and support thrust to values approximately 530% over those from the equivalent elastic analyses.

5.3   APPROXIMATE ANALYSIS FOR GROUND YIELDING UNDER AXISYMMETRIC
      STRESS CONDITIONS

Following the pattern established in Section 3, the results from the axisymmetric elasto-plastic finite element analyses described in the preceding section will be used in the development of simpler analytical procedures more suitable for design calculations. Even more than in the case of elastic ground, three-dimensional finite element analyses (which are what is necessary in the general case) are impractical to use for tunnel support design in yielding ground masses. These materially nonlinear analyses are even more costly than their elastic counterparts, they have

176

an even greater need for high quality input data, and they are technically far more difficult to perform. The more productive approach is to use these nonlinear finite element techniques as research tools to derive or, as will be done in this section, to validate simpler, design-oriented analytical methods that explicitly consider the effects of ground yielding.

5.3.1 Formulation of the Approximate Analysis

Since characteristic curves have proved so valuable in qualitatively describing the various aspects of the ground-structure interaction around a tunnel, it is only natural to use them in the development of a quantitative design tool. Characteristic curves like those in Figure 5.11 model each of the three major variables affecting the tunnel support loads: relative support stiffness is represented by the ratio of the slopes of the ground and support characteristics, support delay is represented by the offset of the origin of the support curve, and ground yielding is represented by the nonlinearity of the ground curve. More important, characteristic curves model the interrelationships among these three variables; it is clear from Figure 5.11 that increasing the support delay or decreasing the support stiffness will not only lead to smaller support loads but will also lead to substantially more ground yielding (these interrelationships among the variables were discussed earlier in Section 5.1). The design

177
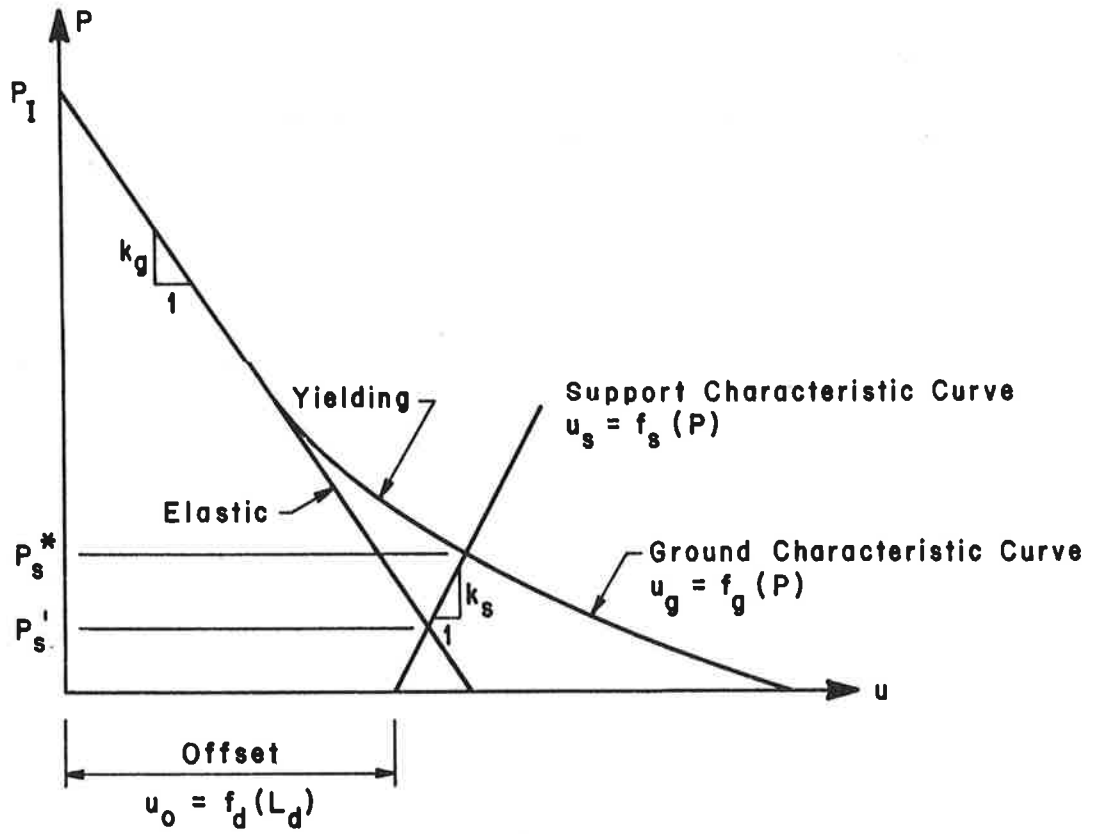
FIGURE 5.11.   CHARACTERISTIC CURVES FOR YIELDING GROUND CASE
WITH SUPPORT DELAY

problem, of course, is to determine P_S^*, the equilibrium

support pressure in the yielding ground mass.

If the ground characteristic, the support characteris-

tic, and the support curve offset were known precisely, it

would be a simple matter to compute P_S^* and P_S' (the cor-

responding support pressure in the linearly elastic case).

178

But, the fact is that these parameters are known precisely, or at least reasonably so. The support pressure P_s' in the elastic case is certainly known, since this was the entire point of the investigations in Sections 2 and 3. It is a simple matter to backfigure the support characteristic curve and its offset from the known support stiffness (in terms of the compressibility ratio, C^*) and the known elastic support load P_s'. The ground characteristic curve is also known, at least approximately, for K = 1 in situ stresses from the plane strain plasticity solutions presented in Section 4. Thus, given the proper mathematical framework it should be possible to directly calculate the support load P_s^* for a tunnel in a yielding ground mass under K = 1 stress conditions.

The mathematical framework for the analyses follows from the relations depicted in Figure 5.11. The ground characteristic curve, the support characteristic curve, and the support curve offset are treated as follows:

(1) The ground characteristic curve is a functional relationship between the radial ground displacement, u_g, and the internal pressure, P:

$$u_g = f_g(P) \qquad\qquad (5.4)$$

For K = 1 in situ stress conditions, $f_g(P)$ can be found from any of the simple plasticity solutions for a cylindrical hole in an infinite medium described in Section 4.

(2)   The support characteristic curve is a functional relationship between the radial support displacement, u_s, and the external pressure, P:

$$u_s = f_s(P) \tag{5.5}$$

If the support behaves linearly elastically, $f_s(P)$ can be found from the definition of the support stiffness used in the derivation of the compressibility ratio in Appendix A (Eq. A.2):

$$\frac{P}{\Delta D/D} = \frac{P}{u_s/R} = \frac{E_s A_s}{(1-\nu_s^2) R} \tag{5.6}$$

Therefore:

$$u_s = f_s(P) = \frac{PR^2 (1-\nu_s^2)}{E_s A_s} \tag{5.7}$$

This essentially is the thin-walled cylinder solution. If the support behaves nonlinearly (see Lombardi, 1973, for examples), the appropriate nonlinear $f_s(P)$ should be used.

180

(3)   The support curve offset u_o, which represents the ground displacements that occur prior to support construction, is primarily a function of the support delay length, L_d (and therefore of the delay factor, λ_d):

$$u_o = f_d(L_d) = f_d'(\lambda_d) \qquad (5.8)$$

Going back to the original treatment of the support delay effect in Section 3, u_o can be derived from the support delay correction factor λ_d, which was defined in Figure 3.13 as:

$$\lambda_d = \frac{u_f - u_o}{u_f} \qquad (5.9)$$

The factor u_f is the radial wall displacement for an unsupported tunnel in an elastic ground mass and is equal to:

$$u_f = \frac{P_I R(1+\nu)}{E} \qquad (5.10)$$

Combining Eqs. (5.8) − (5.10):

$$u_o = f_d'(\lambda_d) = \frac{P_I R(1+\nu)}{E}(1-\lambda_d) \qquad (5.12.a)$$

Also in Section 3, the relationship between λ_d and L_d was determined to be (see Eq. 3.4):

181

$$\lambda_d = 0.98 - 0.57 \left(\frac{L_d}{R}\right) \tag{5.11}$$

Combining Eqs. (5.9) - (5.11) gives the following expression for u_o:

$$u_o = f_d(L_d) = \frac{P_I R(1+\nu)}{E}[0.02+0.57\left(\frac{L_d}{R}\right)] \tag{5.12b}$$

Any pre-support ground movements other than those attributable to the support delay (e.g., from incomplete grouting) must be added to this value of u_o.

Once the functions $f_g(P)$, $f_s(P)$, and $f_d(L_d)$ are known, the support pressure P_s^* can be found by imposing the condition that at equilibrium the support displacement, u_s, plus the support curve offset, u_o, must equal the ground displacement, u_g. Expressed in another way, at equilibrium:

$$f_g(P) - f_s(P) - f_d(L_d) = 0 \tag{5.13}$$

The value of P that satisfies this equation (i.e., the root of the equation) will be the equilibrium support pressure P_s^*. Because of the nonlinearity of $f_g(P)$ (and of $f_s(P)$ in the most general case), iterative methods must be employed to solve Eq. (5.13).

However, these iterative solutions are of a very simple nature and can easily be performed on most programmable

182

desk-top or pocket calculators. Several programs (for different formulations of the ground function $f_g(P)$) based on a Newton-Raphson iteration algorithm have been developed to find the roots of Eq. (5.13) on a Hewlett-Packard Model HP-97 calculator; these programs are fully described and documented in Appendix C.

Equation (5.13) can be used to calculate directly the equilibrium support pressure P_s^* in the yielding ground case. However, for reasons of consistency with the material in Chpater 3 and for other reasons that will become clear in Section 5.4, it is desirable to define a ground yield correction factor, λ_y, that is analogous to the support delay correction factor, λ_d. Recalling that the support delay correction factor was defined in Section 3 as:

$$\lambda_d \equiv \frac{P_s'}{P_s} \qquad (5.14)$$

in which P_s' is the equilibrium support pressure in the elastic case, reduced for the effect of support delay, and P_s is the unreduced support pressure (as calculated from the relative stiffness solution in Section 2, for example), the ground yield correction factor is similarly defined as:

$$\lambda_y \equiv \frac{P_s^*}{P_s'} \qquad (5.15)$$

183

in which $P_s^{'}$ is again the reduced support pressure in the elastic case and P_s^{*} is the equilibrium pressure in the yielding case -- the effects of both support delay and ground yielding are included in P_s^{*} . Both $P_s^{'}$ and P_s^{*} are illustrated in Figure 5.11. In terms of the two correction factors, then, the final equilibrium support pressure is:

$$P_s^{*} = \lambda_d \, \lambda_y \, P_s \qquad\qquad (5.16)$$

This rather circuitous derivation of Eq. (5.16) may not seem to make much sense, since P_s^{*} can be calculated far more easily from the earlier Eq. (5.13). However, the expression of P_s^{*} in terms of the ground yield correction factor λ_y will prove to be very expedient when ground yielding under $K \neq 1$ stress conditions is investigated in Section 5.4

5.3.2 Comparison of Resutls from Approximate and Finite Element Analyses

Up to this point, the derivation of the simplified analysis for the effects of ground yielding has been nothing more than an academic exercise, since no evidence has been offered to verify its accuracy. The best way to validate the simple technique, of course, is to compare its predicted support loads with loads measured in actual tunnels. This will be done in the next section. However, if the simplified analysis is indeed accurate, it should

184

certainly be able to predict the loads calculated in the axisymmetric elasto-plastic finite element analyses described in Section 5.2. This less stringent test simply matches one simple analysis against another more sophisticated one; the variability and uncertainty associated with real tunnels in real ground masses do not muddle the comparison.

At first glance, this comparison of the two analytical methods may seem to involve a bit of circular reasoning. One of the major variables in the approximate analysis, the offset u_o of the support characteristic curve, was backfigured from the elastic axisymmetric finite element analyses; it is tautologically true, then, that the support loads computed from the approximate analysis will be in perfect agreement with those from the elasto-plastic axisymmetric finite element analyses for cases in which the ground is sufficiently strong and does not yield. However, these cases are not being considered here, and consequently the tautology breaks down. The whole point of the comparison between the simple and sophisticated analysis techniques is to investigate their predictions for support loads in cases where the ground does yield, and often quite extensively; the fact that the two analysis techniques are theoretically in perfect agreement for elastic ground behavior does not logically lead to any conclusion about their agreement for the

yielding ground case.

There is one technical complication in the comparison of the two analysis methods, and this is the question of appropriate strength properties. Yielding in the finite element analyses is governed by the Drucker-Prager criterion (Eq. 5.1) and is a function of the strength parameters α and k. Because of the dependence of the Drucker-Prager criterion on the intermediate principal stress σ_2, however, it is difficult if not impossible to incorporate it into a simple plane strain plasticity solution similar to those described in Section 4. The closest yield criterion that can be used in the simple plane strain approximate analysis is the Mohr-Coulomb rule:

$$F_{MC}(\sigma_1, \sigma_3) = \sigma_1 - N_\phi \sigma_3 - \sigma_u = 0 \qquad (5.17)$$

in which
$$N_\phi = \frac{1 + \sin\phi}{1 - \sin\phi} \qquad (5.18a)$$

$$\sigma_u = \frac{(2c)\ \cos\phi}{1 - \sin\phi} \qquad (5.18b)$$

ϕ, c = friction angle and cohesion

= Mohr-Coulomb strength parameters

The Drucker-Prager yield criterion, which considers the effects of the intermediate principal stress σ_2, can be

thought of as the three-dimensional generalization of the
Mohr-Coulomb rule, which is independent of σ_2. However,
it is not generally true that the two criteria are equiva-
lent. The Drucker-Prager criterion reduces to the Mohr-
Coulomb yield function only for special cases with special
stress conditions. One of these cases is the conventional
triaxial test with its uniform and axisymmetric stress dis-
tributions; the relations between α and ϕ and between k
and c for the triaxial compression test were given earlier
in Equations (5.2a) and (5.2b). Another case is any plane
strain limit state in which the stresses remain constant
during continuous yielding.[1] However, the two criteria

_____

[1]As described by Drucker and Prager (1952), limit-state
yielding under constant stress conditions implies that
the total post-yield strain rates are equal to the plastic
strain rate components -- i.e., $\dot{\varepsilon}_{ij} = \dot{\varepsilon}_{ij}^p$, $\dot{\varepsilon}_{ij}^e = 0$.
In the case of plane strain where ε_2 is the total out-of-
plane strain, the plastic component of the out-of-plane
strain rate is derived from the associated plastic flow
rule as:

$$\dot{\varepsilon}_2^p = \frac{\partial F_{DP}}{\partial \sigma_2} \quad , \quad F_{DP} = \text{yield function}$$

and, since for plane strain $\varepsilon_2 = \dot{\varepsilon}_2 = 0$, $\dot{\varepsilon}_2^p = \dot{\varepsilon}_2 = 0$
and therefore $\frac{\partial F_{DP}}{\partial \sigma_2} = 0$; in other words, the yield func-
tion is independent of σ_2 for these failure conditions.
The relations between c and k and between ϕ and α can
then be easily found (see Drucker and Prager's original
paper for more details:

$$c = \frac{k}{(1-12\alpha^2)^{\frac{1}{2}}}$$

$$\phi = \sin^{-1}[\frac{3\alpha}{(1-3\alpha^2)^{\frac{1}{2}}}]$$

These relations do not hold for the tunneling problem be-
cause continued yielding does not take place under constant
stress conditions.

are not equivalent for the plane strain tunneling prob-
blem.

Nevertheless, it is possible to derive an approximate
relation between the Drucker-Prager strength parameters in
the finite element analyses and the Mohr-Coulomb para-
meters needed for the approximate plane strain solution.
The keys to this derivation are the assumptions that, at
the boundary of the yielded zone: (1) the radial, tangen-
tial, and longitudinal stresses (σ_r, σ_θ, σ_z) are the prin-
cipal stresses in the ground mass, and (2) the longitudi-
nal stress σ_z equals the in situ pressure P. Based on
the calculated stresses from the finite element analyses,
these are reasonable assumptions for the ground behind
the face; naturally, these assumptions break down in the
ground region immediately ahead of the face, but then
none of the other assumptions in the plane strain solutions
are valid in this region either. Once these assumptions
are made, though, the stress conditions at the boundary
of the yielded zone are completely defined   (see Figure
5.12). The two yield criteria can now be made roughly
equivalent by requiring that yielding at the boundary
commence under the same stress conditions for both. As
depicted in Figure 5.12, element A, which is at the boun-
dary between the plastic and elastic zones and is there-
fore on the verge of yielding, is acted upon by the prin-
cipal stresses:

188

$$\sigma_1 = \sigma_\theta = P(1+a) \qquad 0 \leq a \leq 1 \qquad (5.19a)$$

$$\sigma_2 = \sigma_z = P \qquad (5.19b)$$

$$\sigma_3 = \sigma_r = P(1-a) \qquad (5.19c)$$

The expression of σ_1 and σ_3 in terms of the (unknown) constant a follows from the condition that , in the elastic zone, $\sigma_r + \sigma_\theta = 2P$ (constant) for $K = 1$ in situ stresses.[1]
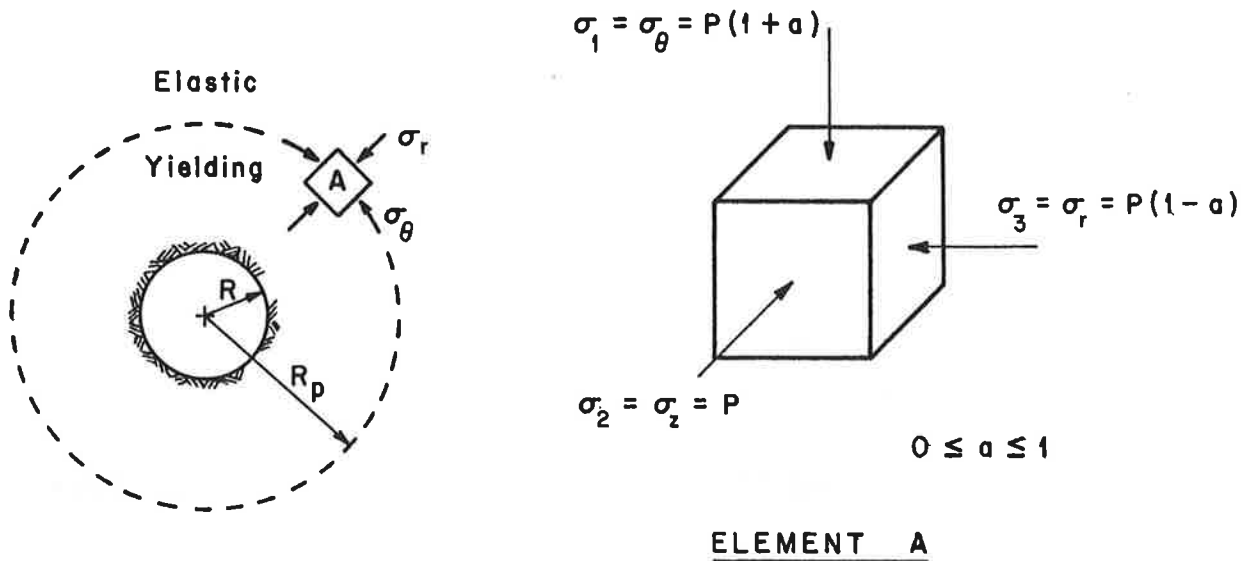
FIGURE 5.12.   GROUND STRESSES AT INSTANT OF YIELD

---

[1]Note that the quantity (1-a) in Eq. (5.19c) is the same as the first-yield index, FY.

189

Substituting these stresses into the Drucker-Prager yield function (Eq. 5.1) gives the following relation:

$$a = 3\alpha + \frac{k}{P}$$ (5.20)

Similarly, the Mohr-Coulomb yield criterion (Eq. 5.17) requires:

$$a = \frac{N_\phi - 1}{N_\phi + 1} + \frac{\sigma_u}{P(N_\phi + 1)}$$ (5.21)

If the Drucker-Prager and Mohr-Coulomb yield rules were equivalent, they would each require the same value for a at yield. Therefore, equating (5.20) and (5.21) and using the definitions for N_ϕ and σ_u given in Eq. (5.18a) and (5.18b) produces the relations:

$$\phi' = \sin^{-1}(3\alpha)$$ (5.22a)

$$c' = \frac{k}{\cos \phi'}$$ (5.22b)

Using these parameters ϕ' and c' makes the ground strength in the plane strain solution roughly equivalent to the strength in the finite element analyses. The two yield criteria will still give different distributions for the stresses and strains within the yielded zone, but

190

considering all of the other simplifications in the approx-
imate analysis -- especially the central assumption of
plane strain behavior near the tunnel face -- the relations
in Eq. (5.22) are adequate for purposes of comparison. The
values of ϕ' and c' for the various cases are summarized in
Table 5.4.

TABLE 5.4 EQUIVALENT PLANE STRAIN STRENGTH PARAMETERS

Case	Drucker-Prager Yield Parameters		Equivalent Mohr--Coulomb Parameters for Plane Strain	
	α	k	ϕ'	c'
1	0.273	0.117 psi	55.0°	0.204 psi
2A	0	19.2	0	19.2
2B	0.189	0.122	34.5	0.148
4A	0.118	10.6	20.7	11.3
4B	0.141	12.8	25.0	14.1
4C	0.118	50.0	20.7	53.5
4D	0.231	20.8	43.9	28.9
4E	0.322	29.1	75.0	112.4

Using the fully dialant plasticity formulation
for the ground characteristic curve (solution B.4 in
Section 4) and the equivalent plane strain strength

191

parameters given in Table 5.4, the approximate analysis
method was used to calculate the values of the support
thrust coefficient $\frac{T}{PR}$ and the ground yield correction
factor λ_y given in Table 5.5 for cases 1, 2A, 2B, and
4A - 4E. The iterative program described in Appendix C
calculates $\frac{T}{PR}$ (which equals $\frac{P_s^*}{P}$ for K = 1) directly; in
order to determine $\lambda_y = \frac{P_s^*}{P_s'}$, P_s' (the support pressure in
an elastic case with support delay) must be computed from
the program by artificially increasing the strength prop-
erties to eliminate yielding (e.g., by setting $c' = P$).
Also summarized in Table 5.5 are the values of $\frac{T}{PR}$ and λ_y
from the axisymmetric elasto-plastic finite element analy-
ses; here λ_y is defined as the thrust from the elasto-
plastic finite element analysis divided by the thrust from
the equivalent elastic analysis in Section 3. Finally,
the last column in the table shows the percentage error
in the thrust coefficient from the approximate analysis
method with respect to the thrust coefficient calculated
from the finite element analysis. A positive error means
the approximate thrust is larger than the finite element
thrust.

As mentioned earlier, the approximate analysis
should give very small errors for cases in which no yield-
ing occurs. Although yielding developed to varying degrees
in all of the finite element solutions, it did not occur

192

TABLE 5.5.   COMPARISON OF THE RESULTS FROM THE APPROXIMATE
AND FINITE ELEMENT ANALYSES (GROUND CHARACTERIS-
TIC CURVE BASED ON FULLY DILATANT RIGOROUS
PLASTICITY FORMULATION)

Case	Support Delay $\dfrac{L_d}{R}$	Approximate Analysis $\dfrac{T}{PR}$	λ_y	Finite Element Analysis $\dfrac{T}{PR}$	λ_y	Error In $\dfrac{T}{PR}$
1	0.25	0.76	1.00	0.75	0.97	1%
	0.75	0.50	1.00	0.50	0.98	0
	1.25	0.24	1.00	0.24	0.96	0
2A	0.25	0.82	1.00	0.64	0.76	28
	0.75	0.61	1.14	0.45	0.74	36
	1.25	0.50	1.93	0.36	1.33	39
2B	0.25	0.81	1.00	0.80	0.96	1
	1.25	0.34	1.31	0.38	1.43	-11
4A	0.25	0.25	2.81	0.24	2.79	4
	1.25	0.23	7.91	0.17	6.30	35
4B	0.25	0.20	2.31	0.18	2.09	11
	1.25	0.18	6.27	0.13	4.81	38
4C	0.25	0.11	1.29	0.11	1.28	0
	1.25	0.068	2.38	0.042	1.56	62
4D	0.25	0.099	1.12	0.088	1.02	12
	1.25	0.058	2.01	0.027	1.00	115
4E	0.25	0.084	1.00	0.087	1.01	-3
	1.25	0.029	1.00	0.026	0.96	12

in all of the approximate analyses, specifically in the cases with λ_y (from the approximate analysis) equal to 1.0. Therefore, one would expect close but not necessarily perfect agreement between the two analyses in these situations. This in fact is the case. Ignoring for the moment the data from case 2A, the approximate analyses with λ_y = 1.0 all give very small errors, ranging from -3% to +12%.[1] For the more strongly yielding cases with λ_y (from the approximate analysis) greater than 1, the average absolute error increases to 33%. The analyses for the two cases with the greatest amounts of yielding (cases 4A and 4B, L_d/R = 1.25, λ_y > 6) are in error by less than 40%. Furthermore, these errors (except for case 2B with L_d/R = 1.25) are positive -- i.e., conservative. Despite the substantial theoretical differences between the two solutions, the errors in the approximate analysis are reasonably small, even for cases in which extensive yielding develops. Given the often gross uncertainties in parameters like the ground modulus, ground strength, and support delay in an actual tunnel, these errors are tolerably small for practical design purposes.

There are some anomalous trends in the data presented in Table 5.5, however. The first inconsistency is that the errors in case 2A are, as a group, much higher than in the other cases. Even case 2A with L_d/R = 0.25R, for which

[1] An error of +5% is inherent in the method even for purely elastic ground behavior because of approximations in the treatment of the support delay variable.

the approximate analysis predicts $\lambda_y = 1.0$ and for which the error should thus be near zero, has an error of 28%. Recall, though, that case 2A also gave inconsistent results in the finite element analyses in Section 5.2. The thrusts from the elasto-plastic analyses were <u>lower</u> than those from the elastic equivalents. It was speculated that this un-expected behavior was due to the very extensive yielding that developed ahead of the face; this extensive yielding relieved the stresses in this region, induced more deforma-tions in the "outer" ground regions, and developed more of the ground's resistance than in the other cases. The effects of this yielding ahead of the face cannot be treated in the approximate analysis, however, so it is only natural that the errors are larger in this case.

Another trend is apparent in the data in Table 5.5, this time for the rock cases 4A through 4E. The errors in the support thrusts calculated from the approximate analy-sis are consistently larger for the long support delay than for the short delay; for $L_d/R = 1.25$, the errors range from 35 to 115% versus a range of only -3 to 12% for $L_d/R = 0.25$. It is difficult if not impossible to rigorously explain the reasons for this pattern in the data, but one very conjectural mechanism can be suggested. In both the finite element and approximate analyses for these cases, the ground dilates as it yields. The effect

195

of this dilation is to increase the ground displacements for a given level of yielding (see Figure 4.2). In the plane strain approximate analysis, these ground displacements are all radial and act to increase the support deformations and the support loads. In the finite element analyses, on the other hand, only part of these dilatancy-related displacements are radial; there will also be a longitudinal component, primarily toward the unsupported sections of the tunnel near the face, and this component will become proportionately larger as the unsupported length increases. In other words, the yielding ground in the finite element analyses expands in part against the tunnel support and in part into the unsupported sections of the tunnel; therefore, the dilatancy-related increase in support deformations and loads is smaller in the finite element analyses -- and especially in those with long unsupported lengths (i.e., support delays) -- than in the approximate plane strain analyses. The plane strain analyses will thus overestimate the support thrusts.

Although this explanation for the discrepancies in the two analyses is highly speculative and ignores all of the other substantial differences in the methods (e.g., the different plastic flow rules), it is plausible and it can be checked in a very approximate fashion. Table 5.6 shows the same comparison between the two analyses as in

196

TABLE 5.6.   COMPARISON OF THE RESULTS FROM THE APPROXIMATE
AND FINITE ELEMENT ANALYSES (GROUND CHARACTER-
ISTIC CURVE BASED ON ASSUMPTION OF CONSTANT
VOLUME OF YIELDED ZONE)

Case	Support Delay $\frac{L_d}{R}$	Approximate Analysis $\frac{T}{PR}$	λ_y	Finite Element Analysis $\frac{T}{PR}$	λ_y	Error In $\frac{T}{PR}$
1	0.25	0.76	1.00	0.75	0.97	1%
	0.75	0.50	1.00	0.50	0.98	0
	1.25	0.24	1.00	0.24	0.96	0
2A	0.25	0.82	1.00	0.64	0.76	28
	0.75	0.61	1.14	0.45	0.74	36
	1.25	0.50	1.93	0.36	1.33	39
2B	0.25	0.81	1.00	0.80	0.96	-1
	1.25	0.30	1.18	0.38	1.43	-21
4A	0.25	0.18	2.01	0.24	2.79	-25
	1.25	0.15	5.12	0.17	6.30	-12
4B	0.25	0.14	1.62	0.18	2.09	-22
	1.25	0.11	3.69	0.13	4.81	-2
4C	0.25	0.099	1.12	0.11	1.28	-10
	1.25	0.045	1.58	0.042	1.56	7
4D	0.25	0.091	1.02	0.088	1.02	3
	1.25	0.036	1.24	0.027	1.00	33
4E	0.25	0.084	1.00	0.087	1.01	-3
	1.25	0.029	1.00	0.026	0.96	12

Table 5.5, but now the ground characteristic curve in the
approximate analysis has been computed assuming the limiting
condition of constant volume in the plastic zone (solution
B.1 in Section 4) -- i.e., the ground is "nondilatant."
The errors in the support thrust for cases 4A - 4E with the
long support delay are now much smaller, ranging from -22
to +33%. The agreement between the analyses for the short
delay length cases has deteriorated somewhat, however; the
errors now range from -25 to +3%. The errors for cases 1,
2A, and 2B are essentially the same regardless of whether
dilatant or nondilatant behavior is assumed in the approxi-
mate analysis; in cases 1 and 2B, this is because little
or no yielding develops ($\lambda_y \cong 1.0$), but in case 2A it is
because the frictionless (i.e., $\phi = 0$) ground mass does
not dilate in either formulation.

Overall, the nondilatant approximate analysis (Table
5.6) gives lower errors than the dilatant solution (Table
5.5); considering only the yielding cases in which λ_y (from
the approximate analysis) is greater than 1.0, the average
absolute error for the data in Table 5.6 is 18% versus an
error of 33% for the numbers in Table 5.5 One bad feature
of the nondilatant formulation is that its errors are fre-
quently negative -- i.e., unconservative. Nevertheless,
the nondilatant formulation is still the better choice
for design use because: (1) real ground masses are not as

198

dilatant as either the finite element analyses or the dilatant approximate analyses would suggest,[1] and (2) the nondilatant formulation gives better results for the longer support delays encountered in real tunnels. To keep matters in perspective, however, it should be remembered that the approximate analysis method is intended to be just that -- approximate. The important point is to include the overall effect of the ground yielding in the analysis.

Although the approximate analysis method can predict with reasonable accuracy the support loads calculated in the more sophisticated axisymmetric finite element analyses, the real test is whether the method can predict the loads measured in actual tunnels. Before this can be checked, however, the restriction that K equal 1 must be relaxed. The effects of ground yielding on support loads for $K \neq 1$ conditions are investigated in the next section.

5.4 EFFECT OF GROUND YIELDING UNDER NONAXISYMMETRIC STRESS CONDITIONS

All of the preceding discussion in this chapter has been limited to cases in which the in situ stresses in the ground are axisymmetric (i.e., $K = 1$). This is a very special condition for tunnels in yielding ground masses. When $K = 1$, the in situ shear stresses ($\tau_{r\theta}$) in the ground

---

[1]For example, Ladanyi and Nguyen Don (1970) found the observed dilatancy of rock specimens in unconfined compression to be much less than theoretical predictions based on associated plastic flow rules.

are zero, and therefore the ground yielding is entirely due to the shear stresses induced by the tunnel excavation. When $K \neq 1$, the in situ shear stresses are added to these excavation-induced stresses, and hence the pattern and extent of the yielding and its effects on the support loads are altered. Before the approximate analysis method described in the preceding section can be used as a general design tool, these effects of K on the ground yielding must be investigated. This is the purpose of this section.

Ground yielding around the face of an advancing tunnel can be quantitatively analyzed using elasto-plastic finite element techniques, but for $K \neq 1$ conditions these analyses are three-dimensional and consequently expensive, time-consuming, and generally impractical even for research. However, for the purpose of checking the validity of the approximate analysis method, a sufficiently accurate picture of the yielding around a tunnel under $K \neq 1$ stress conditions can be gained through much simpler plane strain or plane stress analyses. Finite element techniques will still be required for these two-dimensional analyses since no closed-form plasticity solutions are available.[1] However, these finite element techniques can be used in a parametric study to bring out the salient features of the behavior. Support delay can also be

[1]Savin (1970) does give a solution for $K \neq 1$ yielding governed by the Von Mises criterion, but his derivation is for an unlined opening.

200

simulated in these planar two-dimensional finite element analyses by using the "core modulus reduction" technique described in Section 3 (Section 3.4).

Because of the many variables involved, a complete parametric study of ground yielding under $K \neq 1$ stress conditions would require a large number of finite element analyses. Even if the study only considers 4 values for K, 3 sets of ground strength properties, 3 values for the support delay, 2 values for the relative support stiffness, and the 2 limiting conditions of full-slip and no-slip at the ground-support interface, a total of 144 analyses must be performed. This type of comprehensive study will not be undertaken here. Instead, a more limited investigation will be conducted for the purpose of roughly outlining the nature of the ground yielding under nonaxisymmetric stresses and its effects on the support loads, and an attempt will be made to draw some general conclusions regarding methods for incorporating these effects into the design calculations.

5.4.1 Description of the Analyses

The variables considered in the limited parametric study are: (1) the lateral stress ratio K, (2) the ground strength parameters, (3) the delay of support construction, and (4) the limiting conditions of full-slip and no-slip at the ground-support interface. The relative support

stiffness is the same in all of the analyses; however, the effects of changes in the support stiffness will be discussed in conceptual terms later. Only relatively flexible supports have been analyzed in order to promote yielding in the ground mass, even for short support delays.

The elastic properties in all of the analyses are the same as those in the rock cases 4A through 4E in Section 5.2. For the ground, these properties are: $E = 1.5 \times 10^6$psi, $\nu = 0.15$; for the support: $E_s = 3.0 \times 10^6$ psi, $\nu_s = 0.15$, thickness = 6 inches. The dimensionless compressibility and flexibility ratios equal 10.0 and 48,000. Three sets of properties were considered for the ground strength, which was governed by the Drucker-Prager yield criterion (Eq. 5.1); the strength values for these cases PS1, PS2, and PS3 are given in Table 5.7. These properties, which are not exactly the same as in the axisymmetric cases 4A - 4E but which give roughly the same range of values for the FY strength index, were chosen to give a varied pattern of yielding in the planar analyses.

The mesh used throughout this parametric study is illustrated in Figure 5.13. Because of the symmetry of the problem, it is only necessary to model one quadrant of the ground mass; the vertical and horizontal axes of symmetry are treated as roller boundaries. Forty-four two-dimensional elements are used to discretize the ground

202
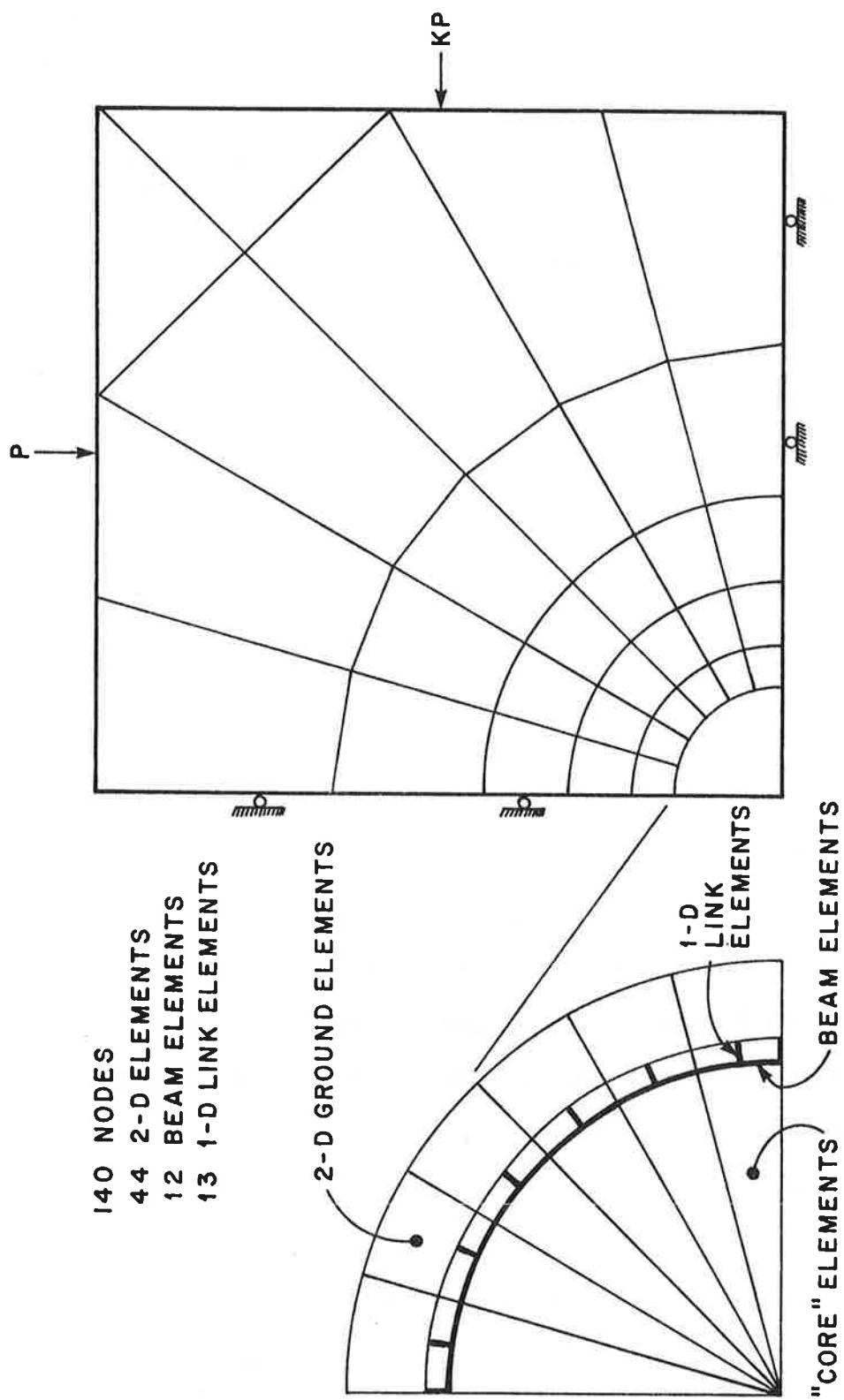
140 NODES
44 2-D ELEMENTS
12 BEAM ELEMENTS
13 1-D LINK ELEMENTS

2-D GROUND ELEMENTS

1-D LINK ELEMENTS

BEAM ELEMENTS

"CORE" ELEMENTS

P

KP

FIGURE 5.13. FINITE ELEMENT MESH FOR K≠1 ELASTO-PLASTIC ANALYSES

TABLE 5.7. STRENGTH PROPERTIES FOR K ≠ 1
ELASTO-PLASTIC ANALYSES

Case	Drucker-Prager Yield Parameters		First-Yield Strength Index[1]
	α	k	FY
PS1	0.25	41.7 psi	0.52
PS2	0.39	9.2	0.40
PS3	0.30	55.6	0.27

[1]Based on Drucker-Prager yield criterion with $\sigma_3 = 0$; see Section 4 for derivation.

mass, and the tunnel support is modeled by 12 rectangular beam elements. Short and very stiff one-dimensional truss elements are used to link the beam elements to the ground elements (see detail in Figure 5.13) in the full-slip analyses; these elements can only transmit normal forces. In the no-slip analyses, the beam elements are directly connected to the ground elements, and both normal and shear forces can be transferred. There are a total of 140 nodes and 229 degrees of freedom in the mesh.

The "construction" of the tunnel is accomplished in two steps. In the first step, the "core" elements (the ground elements within the future perimeter of the tunnel) are active, the support elements are inactive, and the ground

is initially stressed by applying pressure loads at the outer boundaries of mesh; if support delay is to be simulated in the analysis, the core elements will have a lower elastic modulus than the outer ground elements in this step. In the second step, the support elements are activated and the core elements deactivated; the outer ground region then deforms and loads the support.

Plane stress conditions have been assumed for all of the analyses in this parametric study. Although a plane strain analyses would better approximate the displacement fields at locations far behind the face of a real tunnel, the differences between the two formulations are small relative to all of the other approximations in the planar analyses and the plane stress assumption offers certain practical advantages. The out-of-plane stresses are always constant and equal to zero in a plane stress analysis, and, as a consequence, the three-dimensional Drucker-Prager yield criterion reduces to a function of the in-plane stresses only. This aids the interpretation of the results from the finite element solutions.

5.4.2 Results from the Analyses

The quantitative results from the analyses are all expressed in terms of the yield factor, λ_y, which was defined in Section 5.3 as:

$$\lambda_y \equiv \frac{P_s^*}{P_s'} = \frac{T^*}{T'} \tag{5.23}$$

In this equation, P_s^* and T^* are the support load and re-
sulting circumferential thrust from the elasto-plastic
analyses, and P_s' and T' are the load and resulting
thrust from the equivalent elastic analysis (same values
for K, relative support stiffness, and support delay).
Since the supports are relatively flexible in all of the
analyses, the support thrusts for full-slip conditions
are essentially uniform around the ring.

Although bending moments theoretically develop in
the support for K ≠ 1 conditions, they are very small
in all of the parametric analyses. In general, these
bending moments will be negligibly small for all but the
stiffest support systems; they are not considered further
(see Section 3 for additional discussion on this point).

λ_y vs. K for Varying Strengths

The first group of parametric analyses investigated
the effects of the lateral stress ratio K on yielding in
the ground mass for the case of no support delay and full-
slip at the interface. Figures 5.14 - 5.16 show the shape
and extent of the yielded zones for various values of K
in the three cases PS1, PS2, and PS3. Yielding is
greatest at the springlines for K less than one and at
the crown for K greater than one; for K equal to one,

206
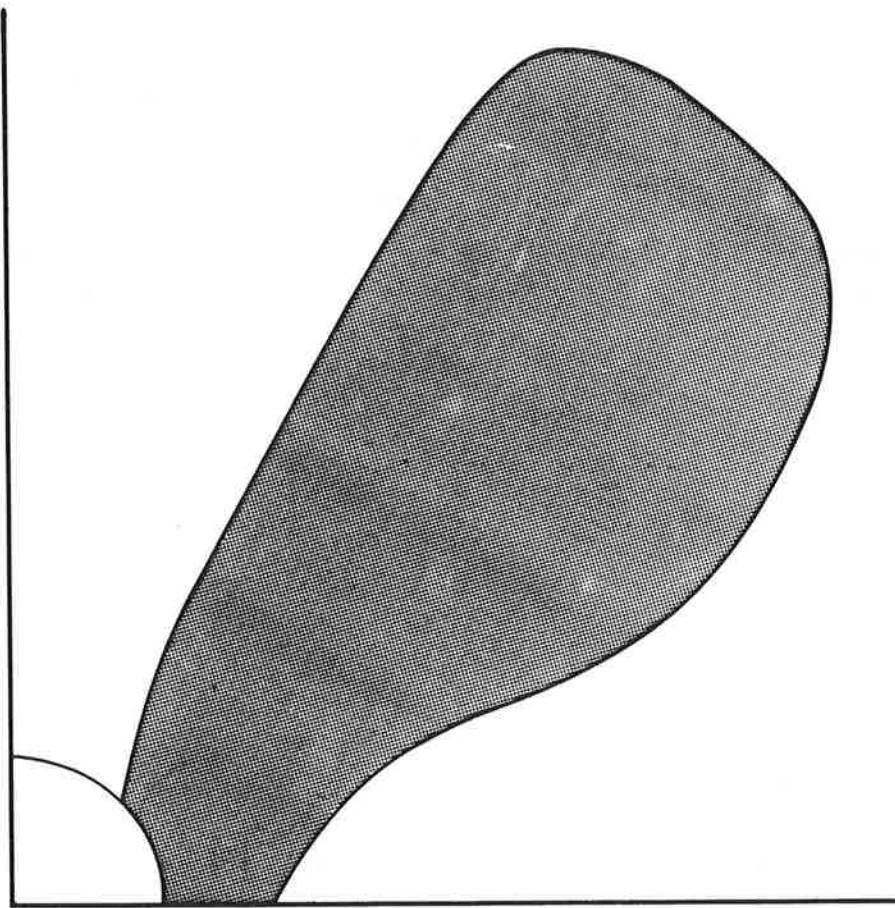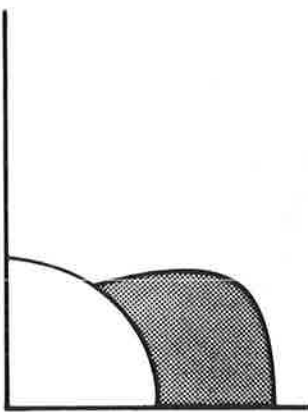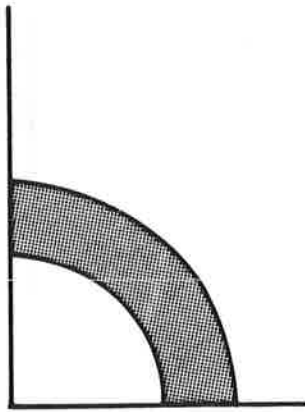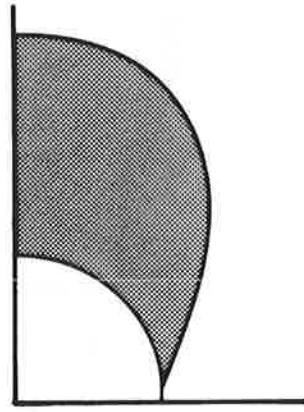
FIGURE 5.14.   EXTENT OF THE YIELDED ZONE--CASE PS1.

207
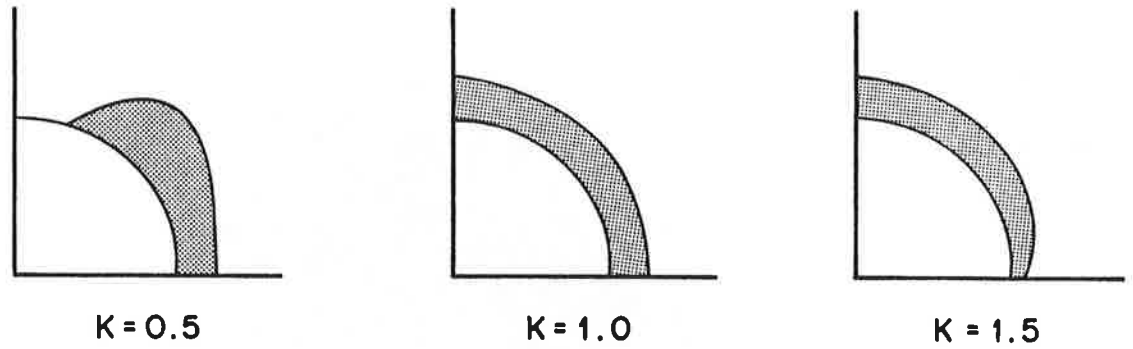
FIGURE 5.15.   EXTENT OF THE YIELDED ZONE--CASE PS2.
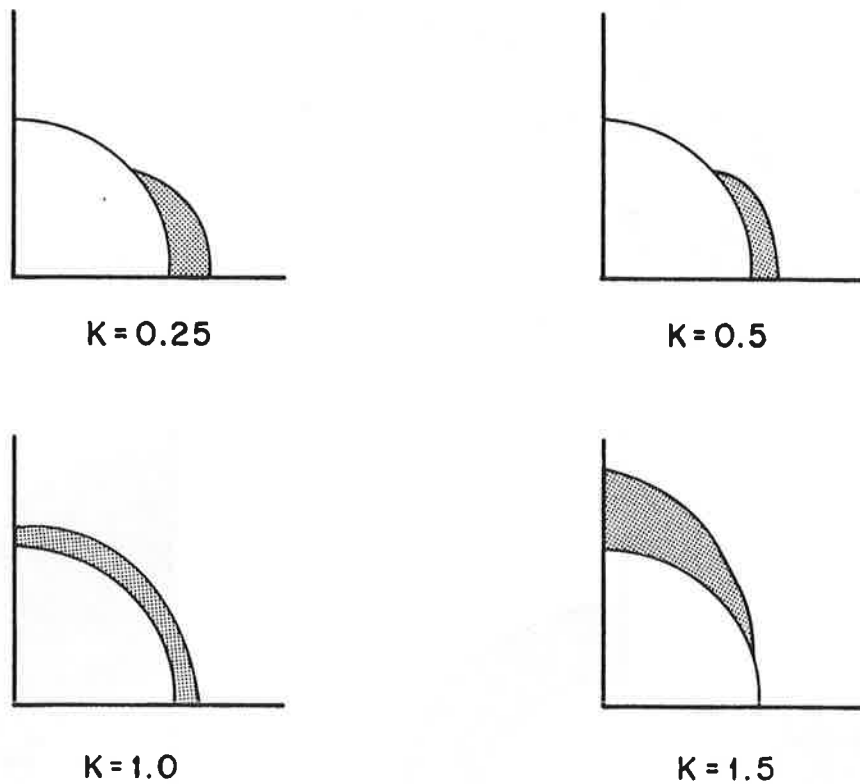
FIGURE 5.16.   EXTENT OF THE YIELDED ZONE--CASE PS3.

the yielded zone is circular. As previously observed by others in the literature (see Reyes and Deere, 1966, for example), the yielded zone takes on a characteristic "butterfly" shape for extensive yielding at very low values of K; this is very clearly shown in case PS1 with K = 0.25. The expected result from increasing the ground strength is also quite evident in Figures 5.14 - 5.16. As the ground strength is increased from case PS1 (FY = 0.52) to case PS3 (FY = 0.27, decreasing FY implies increasing strength), the extent of the yielding correspondingly diminishes.

The relationships between the yield factor λ_y and the lateral stress ratio K for the three different ground strengths are illustrated in Figure 5.17. As expected, for a given value of K the yield factor increases with decreasing strength; λ_y for the weakest case, PS1, is 40 - 130% larger than λ_y for the strongest case, PS3. A more important finding, however, is that the yield factor λ_y for the two strongest cases, PS2 and PS3, is relatively insensitive to variations of K between 0.5 and 1.5. The weakest case, PS1, is more substantially influenced by K, but even here λ_y is reasonably insensitive to variations in K between the narrower limits of 0.5 and 1.0. This limited independence of λ_y from K at low levels of yielding is not too surprising; if the level of yielding is low,
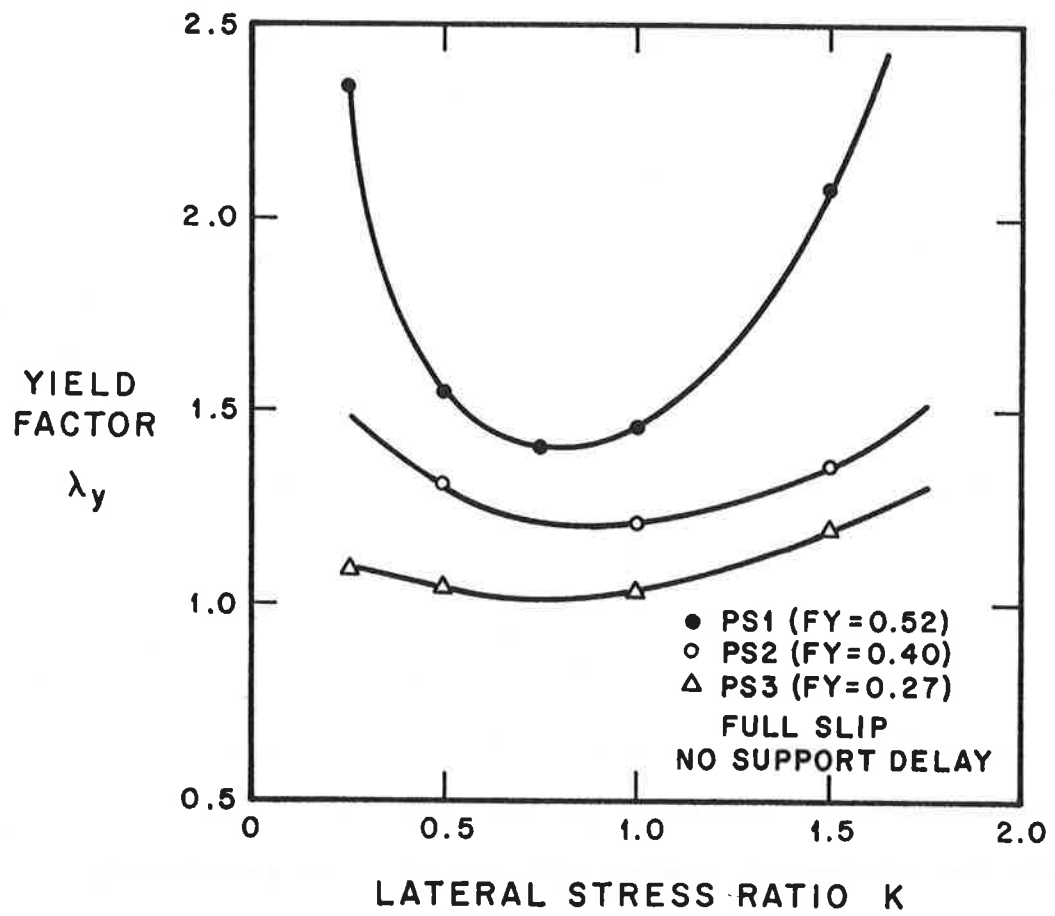
FIGURE 5.17. λ_y VS. K FOR DIFFERENT GROUND STRENGTHS

it will naturally have only a small influence on the sup-
port loads regardless of the lateral stress conditions.
This limited independence of λ_y from K is still very signi-
ficant, though, because it implies that the value of λ_y
calculated from the approximate analysis method for K = 1
conditions (Section 5.3) can be used in cases where
K $\neq$ 1 provided that K is not too different from 1 (i.e.,
0.5 $\leq$ K $\leq$ 1.5) or that the ground yielding is not too
excessive (i.e., λ_y is not too large).

$\underline{\lambda_y \text{ vs. K for Varying Support Delay}}$

The effects of support delay can be approximately
incorporated into the plane stress finite element analyses
through use of the "core modulus reduction" technique
described in Section 3 (Section 3.4). Case PS2 was
analyzed under full-slip conditions for three different
values of the core modulus reduction factor β. Values for
β of 0, 0.67, and 0.9 are equivalent to values for E_{core}
of 1.0, 0.33, and 0.1 times the outer ground modulus E.
These values for β correspond to reasonable values for
the support delay length L_d; as calculated from the inverse
of Eq. (3.11) in Section 3, these values for L_d are approxi-
mately 0, 0.76, and 1.35 times the tunnel radius.

The relationships between λ_y and K for the 3 "support
delay" cases are illustrated in Figure 5.18. These curves
are remarkably similar to those in Figure 5.17 for the
three different ground strengths. For β equal to 0 and

211
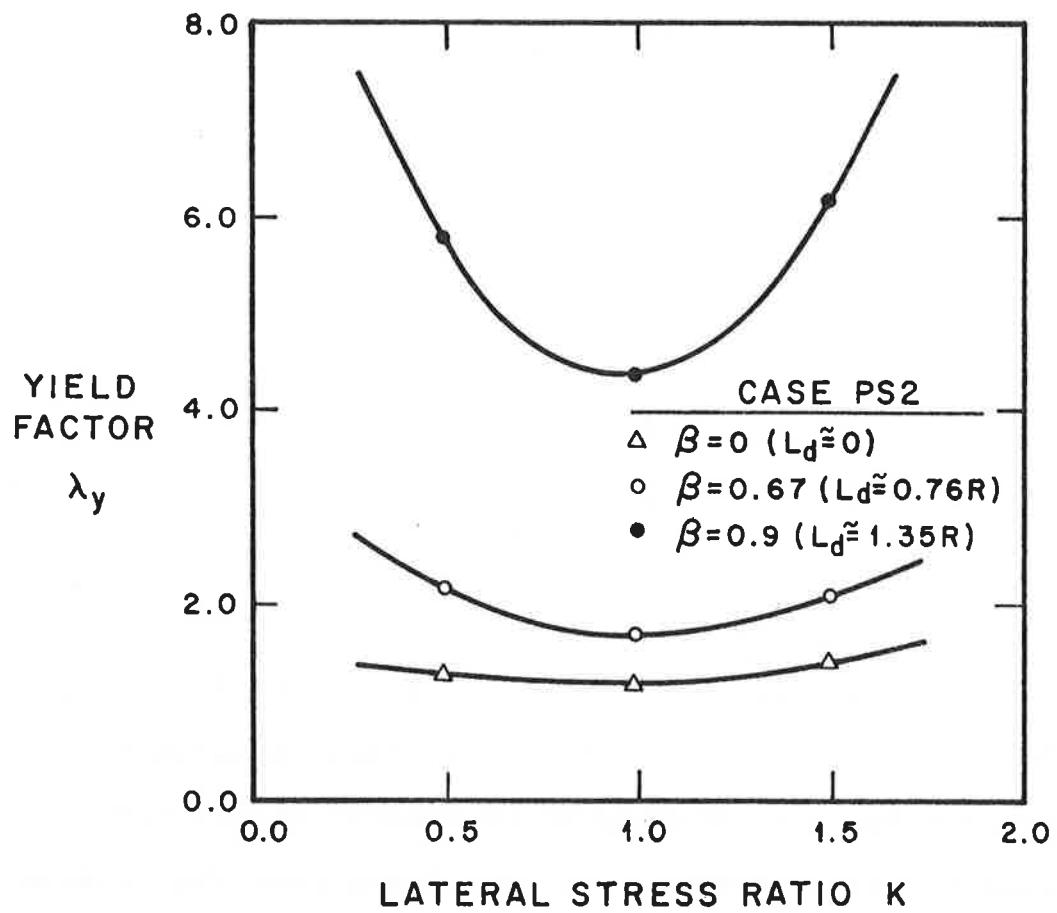
FIGURE 5.18. λ_y VS. K FOR DIFFERENT SUPPORT DELAYS.

0.67 (zero to moderate core modulus reduction), λ_y is relatively small and insensitive to variations of K between 0.5 and 1.5, just as it was in Figure 5.17 for the two higher strength cases; for β equal to 0.9 (large core modulus reduction), λ_y becomes much larger and more dependent on K, as it did in Figure 5.17 for the lowest strength case. The general trend, as expected, is that yielding increases (larger λ_y) at longer support delays (increasing β). It appears that the major variable affecting the λ_y vs. K relationship is the amount of yielding that develops in the ground mass. For small to moderate amounts of yielding (λ_y less than or equal to 2, approximately), λ_y is relatively independent of K, but for larger amounts of yielding -- whether due to low strength properties or long support delay, or both -- λ_y is strongly influenced by K.

No-Slip vs. Full-Slip Conditions

For K ≠ 1 stress conditions, the shear transfer at the ground-support interface theoretically should influence the thrust in the tunnel support. Figure 5.19 illustrates, for cases PS1 and PS2 with no support delay, the relationship between the yield factor at the spring-line and the lateral stress ratio for the two limiting conditions of full-slip and no-slip at the interface. Although there are some small deviations between the curves

213
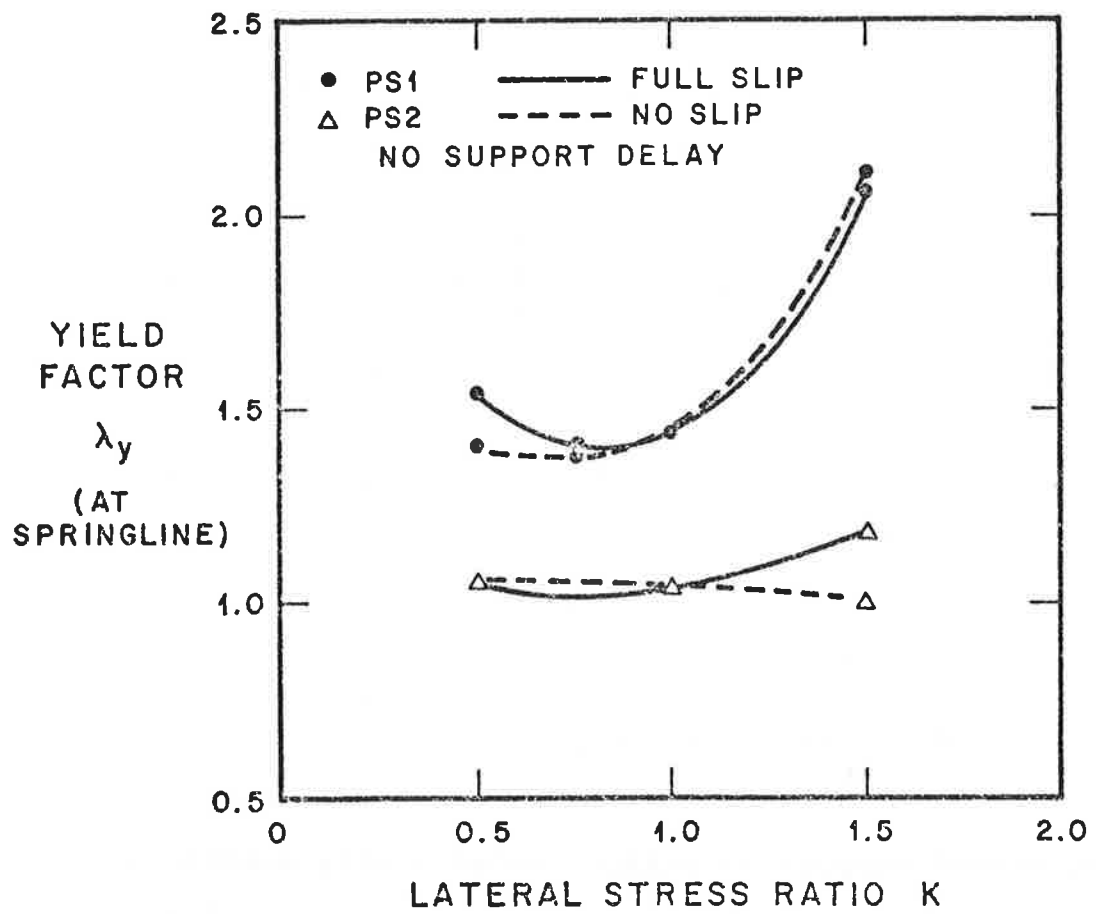
FIGURE 5.19.   NO-SLIP VS. FULL-SLIP FOR NONAXISYMMETRIC
                YIELDING.

214

for the two slip conditions, the general character of the data is the same. Although not shown, there are no discernable differences in the plastic zones for the full-slip and no-slip analyses. It appears that, based on this limited comparison, the shear stresses at the ground-support interface do not significantly affect the yielding in the ground mass.

Effects of Relative Support Stiffness

Although no variation of the relative support stiffness was considered in any of the analyses, some conclusions about its effect on λ_y can still be drawn. The parametric variations of the ground strength and the support delay led to the general conclusion that the principal factor influencing the relationship between λ_y and K is the amount of yielding that develops (as indicated by the magnitude of λ_y) and that it makes little difference whether this yielding is due to low ground strength or a long support delay, or both. This conclusion can be extended to explain the effect of support stiffness on ground yielding.

As long as the flexural stiffness of the support remains small (large flexibility ratio, F^*), the overall character of the support behavior will remain the same for all values of the circumferential stiffness (as expressed by the compressibility ratio, C^*); the initially circular support in the nonaxisymmetric in situ stress field will deform into an ellipse, and at equilibrium the

215

radial support pressure will be uniform around the circumference. The only difference between supports with a high C^* and a low C^* is that the stiffer support will reach equilibrium at smaller displacements. The stiff support will therefore allow smaller ground movements than the flexible support (for the same support delay) and, as a result, will allow only a small amount of ground yielding. Based on the general observations from the parameteric study of flexible support cases (high C^*), this implies that the yield factor λ_y will be small and relatively independent of K for tunnels with stiff (low C^*) supports.

This conclusions will not necessarily be true for cases in which the flexural stiffness of the support is high (low F^*). In these cases, the elliptical deformation of the support is inhibited, the radial support pressure is no longer uniform, and the overall character of the support behavior changes. However, primary supports with very low values for F^* are relatively uncommon. Only very thick concrete supports approach this condition, and even in these cases F^* is usually quite high because of deliberate articulation of the joints (for precast liner elements) or because of longitudinal cracks in the concrete.

5.4.3 Conclusions From Parametric Study of Yielding Under Nonaxisymmetric Stress Conditions

The principal conclusions from this limited parametric study of ground yielding under nonaxisymmetric, plane stress conditions are summarized as follows:

(1) For small to moderate amounts of yielding (λ_y less than or equal to 2, approximately), the yield factor λ_y is reasonably insensitive to variations in the lateral stress ratio K between 0.5 and 1.5

(2) This insensitivity of λ_y to variations in K is the same whether the yielding is due to low ground strength properties or a long support delay, or both.

(3) The analyses are not significantly affected by the shear transfer conditions at the ground-support interface, at least as determined from the very limited data in this study.

In addition to these three conclusions, a fourth conclusion was inferred from (1) and (2) and some additional reasoning. Stiff supports, which permit smaller ground moevements and smaller amounts of yielding than equivalent flexible supports, will generally produce values for λ_y that are small and reasonably independent of K.

217

The implications that these conclusions have for the approximate analysis method in Section 5.3 are significant. The approximate method is surely reaching the limits of its applicability when it is used in the nonaxisymmetric stress case; in general, the magnitude of the equilibrium support load P_s^* calculated from Eq. (5.13) for $K = 1$ stresses will not equal the magnitude of the support load in the $K \neq 1$ case. This was certainly true for linearly elastic ground behavior (see, for example, the relative stiffness solutions in Section 2) and it is no less true when the ground yields. Despite the fact that the total magnitudes of the loads themselves are different, though, conclusions (1) and (2) above indicate that in certain circumstances the yield factor λ_y determined from the analysis for the $K = 1$ case will equal λ_y for $K \neq 1$ stresses. (This limited insensitivity of λ_y to K is analogous to the independence of the support delay factor λ_d from K described in Section 3.) At the limiting values for K of 0.5 and 1.5, λ_y for the nonaxisymmetric case is approximately equal to λ_y for the axisymmetric case provided that yielding is not too extensive and λ_y is less than about 2; as K approaches 1, the approximate analysis can accurately treat larger amounts of yielding and a larger λ_y. This λ_y can then be used to modify the elastic support loads for the effects of ground yielding.

Now the reasons for the circuitous derivation leading to Eq. (5.16) become clear. In terms of support thrusts, for example, Eq. (5.16) states:

$$T^* = \lambda_y \lambda_d T \qquad\qquad (5.23)$$

In this equation, T represents the support thrust calculated from the relative stiffness solution in Section 2; T includes the effects of the relative support stiffness and the lateral stress ratio. The term λ_d is the support delay factor derived in Section 3; this factor, which is independent of the support stiffness and the lateral stress ratio, modifies T for the effects of support delay in an elastic ground mass. The last term, λ_y, is the ground yield factor derived in this chapter; this factor, which is a function of the ground strength, relative support stiffness, and support delay but which is independent of the lateral stress ratio, at least for small amounts of yielding, modifies $\lambda_d T$ for the effects of ground yielding. The term T^* is then the final design thrust for the support.

6. SUMMARY OF SIMPLIFIED ANALYSIS METHOD AND COMPARISON WITH CASE STUDIES

6.1 GENERAL COMMENTS

Sections 2 through 5 have described each of the steps in the development of an approximate, design-oriented method for calculating the loads on tunnel supports. This method, hereafter called the "simplified analysis method", is summarized in its complete form in this section. The simplified analysis method explicitly includes the effects of the three major variables influencing the support loads: the stiffness of the support relative to the ground mass, the spatial lag or delay of support construction behind the tunnel face, and the yielding of the ground mass surrounding the support. In this chapter, the general assumptions underlying this simplified analysis method will be reviewed, and a guide to its application will be outlined. Finally, the accuracy of the simplified method will be verified by comparing its predictions with measured support loads from actual tunnel cases reported in the literature.

Tunnels are constructed throughout the world in a wide variety of geologic formations; as a result, a correspondingly wide variety of excavation and support systems have been devised, each with its own particular set of design problems. The design considerations for a drilled-and-blasted, rockbolt supported tunnel in massive granite,

for example, will be much different from those for a shield-driven, cast-iron supported tunnel in soft river bottom silts. Consequently, no single analytical procedure will be applicable in all cases; any design method must of necessity be limited to a specific class of tunneling problems. The simplified analysis method described here is no exception, and the overall limiting assumptions in its development are itemized as follows:

(1)   The tunnel has a circular cross-section.

(2)   The tunnel is deep enough that

   (a)   the influence of the ground surface on the tunnel behavior is insignificant

   (b)   the variations in the ground stresses over the height of the tunnel are negligibly small relative to the total stress magnitude.

Generally, a centerline depth of 2 tunnel diameters is sufficient for these requirements to be satisfied.

(3)   The ground can be treated as a homogeneous, isotropic continuum. In practical terms, this limitation rules out tunnels in

   (a)   mixed face (soil over rock) conditions

   (b)   rock masses in which the controlling behavior mode is the sliding of large, discrete wedges or blocks into the tunnel

(c)   any situation in which major, discrete discontinuities (e.g., shear zones, faults) transect the ground mass.

(4) Neither the support not the ground mass exhibit any time-dependent behavior. Examples of time-dependent behavior for the support are the curing, creep, and shrinkage of cast-in-place concrete and shotcrete; examples for the ground are squeezing (creep) and swelling or consolidation.

(5) The strength of the ground mass can be realistically modeled using an elastic-perfectly plastic failure rule. (This is not a critical assumption, however. Although the present development is limited to elastic-perfectly plastic behavior, the simplified analysis method can be easily adapted to strain hardening or strain softening failure rules.)

(6) The support is linearly elastic.

(7) The support has a continuous circumference-- i.e., the invert is closed.

(8) The tunnel is excavated full-face, without compressed air.

(9) Any water pressure on a watertight support must be treated as a separate applied load.

223

This simplified analysis is generally intended for circular tunnels in soil, highly jointed rock, or massive rock formations that can for all practical purposes be treated as time-independent homogeneous continua. Only closed-ring primary support systems are considered in the method. Examples of such support systems are circular steel ribs, prefabricated segmented liners, and continuous shotcrete supports. In its present form, the method cannot treat situations like rockbolt support, steel ribs with open inverts, or multiple drift excavation sequences; it also cannot be used to analyze the increase in support loads with time for tunnels in squeezing or swelling ground masses.

Some of the above itemized restrictive assumptions could be relaxed after additional research. For example, assumption (5) concerning the constitutive behavior of the ground mass could easily be relaxed to allow strain softening, provided the ground characterisitic curve for this condition could be analytically determined (see Section 5 for more details). On the other hand, it would be very difficult to eliminate restriction (3) concerning the homogeneity of the ground mass; designs that are controlled by the behavior of discrete discontinuities must in general be treated on a case-by-case basis. The purpose of the limiting assumptions, of course, is to reduce the problem to its essential elements and to render it tractable to solution. The extension of the

basic solution to more esoteric conditions is beyond the scope of this report.

In reality, it is obvious that no practical tunneling situation will satisfy all of the assumptions listed above. Although these assumptions are reasonable in many cases, they are not intended as unequivocally and universally true statements about real tunnels; they merely form the basis for the theoretical development of the simplified analysis method. It is doubtful that the complex interrelationships among the nearly countless variables in any real tunneling problem can ever be rigorously analyzed, even using the most sophisticated numerical techniques. What the simplified analysis method attempts instead is to reduce this very complicated physical problem to its essential elements, to the few major factors that have an overriding influence on the support loads. Naturally, there are potential dangers in this type of severe simplification. As in any practical engineering problem, judgment and ingenuity must be exercised when applying this simplified analysis to an actual tunnel design. This cannot be emphasized too strongly. The engineer must be aware of the deviations between the actual and the assumed conditions. If these deviations are small, he can use the simplified method and simply make adjustments in his design--by adjusting some input parameters or by increasing the factor of safety, for example. On the other hand, if the deviations are large the engineer must consider whether another

225

analytical procedure (e.g., a sliding wedge analysis in a rock tunnel) would be more appropriate. Unfortunately, it is impossible to formulate general guidelines for these decisions and adjustments; each case must be considered individually. The case studies described later in this chapter will give some examples of the practical application of this method. By being aware of the general assumptions explicitly stated above, though, the engineer can exercise his judgement rationally in any situation and will be able to apply the method properly to produce efficient support designs.

6.2 SUMMARY OF THE SIMPLIFIED ANALYSIS METHOD

The simplified analysis method is composed of three major steps, each relating to one of the major variables influencing the ground-structure interaction around tunnels: (1) the stiffness of the support relative to the ground mass, (2) the spatial lag or delay of support construction behind the tunnel face, and (3) the yielding of the ground mass surrounding the support. The method is structured such that each new step builds on all of the preceding steps. A brief summary of each of these steps will now be given, complete with a listing of the required input parameters and a discussion of general applicability and specific limitations.

Step 1.   Relative Stiffness

The effects of relative support stiffness on the

tunnel support loads is incorporated into the simplified
analysis through the relative stiffness solutions derived in
Section 2. These solutions assume: (1) plane strain condi-
tions, (2) elastic behavior for the ground and support, and
(3) simultaneous excavation and support of the tunnel (for
a more detailed description of the assumptions in the deriva-
tion, see Appendix A). As explained in Section 2, the
correct "excavation unloading" condition must be used for
the tunneling problem.

The relative stiffness solutions explicitly consider
the effects of the support stiffness and the ground stress
conditions (the lateral in situ stress ratio, in particular)
on the support thrusts, moments, and displacements at all
points around the circumference of the opening. They do
not consider the effects of support delay and ground yield-
ing, however; these effects are treated in subsequent steps
of the analysis. The loads calculated from the relative
stiffness solutions can be thought of as the "basic" loads
in the simplified method.

The input parameters required for this step of the
simplified analysis method are:

E, ν	Young's modulus and Poisson's ratio for the ground mass (elastic constants)
E_s, ν_s	Young's modulus and Poisson's ratio for the support (elastic constants)
A_s	cross-sectional area of the support, per unit length of tunnel

227

I_s	moment of inertia of support cross-section, per unit length of tunnel
R	radius of tunnel
K	lateral in situ stress ratio

Some of these parameters are used to calculate the dimensionless stiffness ratios for the tunnel. The compressibility ratio, C*, which is a measure of the relative circumferential stiffnesses of the ground and support, is defined as:

$$C^* = \frac{ER(1-\nu_s^2)}{E_s A_s (1-\nu^2)} \qquad (6.1)$$

The flexibility ratio, F*, which is a measure of the relative "flexural" stiffnesses of the ground and support, is defined as:

$$F^* = \frac{ER^3(1-\nu_s^2)}{E_s I_s (1-\nu^2)} \qquad (6.2)$$

Detailed derivations of these two ratios are given in Appendix A. The circumferential support thrusts are primarily related to C* and the support bending moments, to F*; decreasing values for C* and F* imply an increasingly stiffer support (or softer ground).

228

The two limiting conditions of "full-slip" and "no-slip" for the shear transfer at the ground-support interface must be considered. For full-slip, excavation unloading conditions, the relative stiffness solution for the support thrust and moment is:

$$\frac{T}{PR} = \frac{1}{2}(1+K)(1-a_o^*) + \frac{1}{2}(1-K)(1-2a_2^*)\cos 2\theta \qquad (6.3a)$$

$$\frac{M}{PR^2} = \frac{1}{2}(1-K)(1-2a_2^*)\cos 2\theta \qquad (6.3b)$$

in which θ is the angular coordinate measured from the tunnel springline and:

$$a_o^* = \frac{C^*F^*(1-\nu)}{C^* + F^* + C^*F^*(1-\nu)} \qquad (6.3c)$$

$$a_2^* = \frac{(F^*+6)(1-\nu)}{2F^*(1-\nu) + 6(5-6\nu)} \qquad (6.3d)$$

For no-slip, excavation unloading conditions:

$$\frac{T}{PR} = \frac{1}{2}(1+K)(1-a_o^*) + \frac{1}{2}(1-K)(1+2a_2^*)\cos 2\theta \qquad (6.4a)$$

$$\frac{M}{PR^2} = \frac{1}{4}(1-K)(1-2a_2^*+2b_2^*)\cos 2\theta \qquad (6.4b)$$

229

in which:

$$a_o^* = \frac{C^*F^*(1-\nu)}{C^* + F^* + C^*F^*(1-\nu)} \qquad (6.4c)$$

$$\underline{b} = \frac{(6+F^*)C^*(1-\nu) + 2F^*\nu}{3F^* + 3C^* + 2C^*F^*(1-\nu)} \qquad (6.4d)$$

$$b_2^* = \frac{C^*(1-\nu)}{2\{C^*(1-\nu) + 4\nu - 6\underline{b} - 3\underline{b}C^*(1-\nu)\}} \qquad (6.4e)$$

$$a_2^* = \underline{b}b_2^* \qquad (6.4f)$$

The detailed derivation of these solutions in Appendix A also produces equations for the support displacements. These derived displacements are related to the diameter convergences measured in many tunnels; however, they are not treated in the simplified analysis method. Also in Appendix A is documentation for HP-97 calculator programs to compute the thrusts, moments, and displacements from the relative stiffness solutions.

Based on the parametric studies in Section 2, some general conclusions can be drawn about the sensitivity of the thrusts and moments to variations in the input parameters:

(1) $\frac{T}{PR}$ is strongly dependent of C^* only within the range $0.05 < C^* < 50.0$ and is relatively insensitive to variations of F^* (for practical values of F^*)

(2) $\frac{M}{PR^2}$ is near zero for F* > 100 and is insensitive to variations of C*.

(3) For excavation unloading conditions, both $\frac{T}{PR}$ and $\frac{M}{PR^2}$ are insensitive to variations in Poisson's ratio for the ground.

(4) $\frac{T}{PR}$ and $\frac{M}{PR^2}$ vary linearly with K.

(5) Based on theoretical limiting equilibrium considerations, many common tunneling situations will satisfy the full-slip condition at the ground-support interface (see Figure 2.13). Even in cases where perfect no-slip conditions obtain, however, the differences between the support forces calculated from the full-slip and no-slip solutions will be small.

One additional comment is required concerning the support moments expressed by Eqs. (6.3b) and (6.4b). Except for the most rigid concrete supports, these overall bending moments caused by the nonuniform in situ stress field are small. For example, consider a very stiff, 2 ft. thick concrete ($E_s=4.0\times10^6$ psi, $v_s=0.15$) liner in a 10 ft. radius tunnel in soft clay (E=5000 psi, $v=0.4$). The compressibility and flexibility ratios for this situation equal 0.0073 and 2.18; these low values verify the rigidity of the support. Even for this extreme case, though, the eccentricity of the support thrust (as calculated from Eqs. 6.3a and 6.3b) for K=0.5 is only 13% of the tunnel radius. Support moments due

231

to factors like faulty erection, inadequate blocking, or incomplete grouting are usually more critical than this overall bending due to the nonuniform in situ stresses. The tunnel designer must check for these "local" critical moments in his particular support system.

Step 2.   Support Delay

The quantitative reduction of the support load caused by the spatial lag or delay of support construction behind the tunnel face was determined from the numerical and analytical studies described in Section 3. These studies all assumed linearly elastic behavior for the ground. For K=1 in situ stress conditions, axisymmetric finite element analyses that simulated the incremental advance of the tunnel were used to investigate the influence of support delay on ground displacements and support thrusts. The principal findings from these analyses were that the delay of support construction permitted the ground to deform to varying degrees before interacting with the support and that these "pre-support" movements mobilized increased ground resistance and correspondingly reduced the support load. For K≠1 in situ stress conditions, the support delay effects were approximated in a plane strain analysis by reducing the modulus in the "core" region (the ground within the future tunnel circumference) to induce the "pre-support" movements within the ground mass. The findings from these analyses were essentially the same as those from

232

the axisymmetric finite element studies. In both cases, the reduction of the support load due to support delay was represented by a support delay factor λ_d:

$$\lambda_d = \frac{T'}{T} \qquad (6.5)$$

The term T, which ignores the effect of support delay, represents the "basic" thrust calculated from step 1, and T' is the support thrust, reduced for the effects of support delay. The multiplicative factor λ_d is used to modify the support forces calculated in step 1:

$$T_2 = \lambda_d \, T_1 \qquad (6.6a)$$

$$M_2 = \lambda_d \, M_1 \qquad (6.6b)$$

in which the subscripts refer to the step number in the method.

This second step in the simplified analysis explicitly considers only the effects of support delay. The support delay correction factor λ_d is substantially independent of the relative stiffness and in situ stress variables treated in step 1. (The effects of ground yielding are still to be treated in step 3.)

The primary input parameter in this step is the

233

normalized support delay length, L_d/R. The delay length L_d is defined as the distance between the face and the midpoint of the leading active support element; for incremental tunneling operations in which this length changes during a cycle, the longest length should be used for L_d (see Figure 3.4 and the text of Section 3 for more on this point).

The relationship between λ_d and L_d/R was determined from the results of the axisymmetric finite element analyses as:

$$\lambda_d = 0.98 - 0.57(L_d/R) \qquad (6.7)$$

Based on physical considerations, λ_d varies between the extremes of 1.0 (no support delay effect) and 0 (full support delay effect). The analyses from which (6.7) was derived considered values for L_d/R of 0.25, 0.75, and 1.25 only; however, the equation can be used with reasonable accuracy for values of L_d/R greater than approximately 0.15 and less than about 1.5.

If in addition to the ground movements arising from the support delay there are other ground movements that develop before the support contacts the ground (e.g., from an incompletely grouted tailpiece void behind a shield), these must also be incorporated into the delay factor λ_d. Defining u_o' as these additional pre-support ground movements and u_f as the total elastic radial displacement of the wall of an unlined tunnel, the support delay correction factor is expressed as:

234

$$\lambda_d = 0.98 - 0.57\left[\frac{L_d}{R}\right] - \frac{u_o{'}}{u_f} \qquad (6.8)$$

The factor λ_d is still limited to the range $0 \leq \lambda_d \leq 1$.

Based on the analyses for both K=1 and K≠1 in situ stress conditions in Section 3, some general conclusions can be drawn about the sensitivity of λ_d to variations in the other factors affecting the support loads:

1) λ_d can be used with reasonable accuracy to modify both support thrusts and overall bending moments.

2) λ_d is substantially independent of the relative support stiffness, as expressed by C* and F*.

3) λ_d is independent of the lateral stress ratio, K.

The support delay correction factor λ_d is a very important parameter in the analysis. Unfortunately, it is also a parameter that is very difficult to calculate in practice. The support delay length L_d in a real tunnel is usually only approximately known; small variations in blocking or grouting procedures, for example, may significantly move the point at which the support becomes "active"--i.e., comes into contact with the ground. If there is any other component of ground movement prior to support ($u_o{'}$ in Eq. 6.8), the problems are even worse. The case studies in the later sections of this chapter will produce examples of these difficulties in determining L_d and $u_o{'}$ and the ways that these difficulties were

overcome.   It is impossible to state any general guidelines
for circumventing these difficulties; as in many geotechnical
engineering problems, the factors that are most important are
often the ones that are least known. The designer must simply
be aware of this situation and use his judgement accordingly.

Step 3.   Ground Yielding

The increase in support load caused by yielding in the
ground mass surrounding the tunnel was studied in Sections
4 and 5. The precise determination of this support load
increase was somewhat complicated, though, because the effects
of relative support stiffness, support delay, and ground
yielding are all coupled. For the special case of K=1 in
situ stresses, the combined effects of these variables were
analyzed using axisymmetric finite element techniques that
simulated the construction of the tunnel. The principal
findings from these analyses were: (1) significant ground
yielding can develop ahead of the tunnel face, (2) for a
given ground strength, increasing either the support flexibil-
ity or its delay increases the yielding in the ground mass,
and (3) for a given relative support stiffness and delay, the
ground displacements and support thrusts for a tunnel in a
weak ground mass are larger, and often substantially larger,
than those for a tunnel in relatively strong ground. For the
more general case of $K \neq 1$ in situ stresses, the effects of
ground yielding were approximately analyzed using plane stress

236

elasto-plastic finite element techniques; in these analyses, the support delay was simulated by reducing the modulus of the "core" region before excavation. The general findings from a limited set of parametric studies supported the conclusions drawn previously from the axisymmetric analyses.

In both sets of studies, a ground yield factor λ_y was devised to represent the effects of ground yielding:

$$\lambda_y = \frac{P_s^*}{P_s'} = \frac{P_s^*}{\lambda_d P_s} \qquad (6.9)$$

The term P_s' is the equilibrium support pressure in the elastic ground case, reduced for the effect of support delay, and P_s^* is the support pressure in the yielding case; P_s^* includes the effects of both support delay and ground yielding. The yield factor λ_y has a physical lower limit of 1 (corresponding to completely elastic ground behavior) but no upper bound.

The third step in the simplified analysis method, then, is the calculation of λ_y. This factor is primarily a function of the strength parameters of the ground mass, although it is also indirectly dependent upon the support delay and the relative support stiffness. The input parameters required for this step are:

      c   cohesive strength component for the ground mass

      ϕ frictional strength component for the ground mass

E, ν elastic constants for the ground mass (also required in step 1)

E_s, ν_s elastic constants for the support (also required in step 1)

A_s cross-sectional area of the tunnel support, per unit length of tunnel (also required in step 1)

R tunnel radius (also required in steps 1 and 2)

P_I vertical in situ stress at tunnel axis

λ_d support delay factor (from step 2)

The yield factor λ_y is calculated using the approximate plane strain plasticity solution detailed in Section 5.3. The support pressure P_s^* in a yielding ground mass under $K=1$ in situ stress conditions must satisfy the equation:

$$f_g(P) - f_s(P) - f_d'(\lambda_d) = 0 \qquad (6.10)$$

The terms in this equation are defined as follows:

1) $f_g(P)$, the ground characteristic curve, is the functional relationship between the radial ground displacement and the internal pressure for a tunnel in a yielding ground mass under plane strain conditions. It can be found from any of the simple plasticity solutions described in Section 4.

2) $f_s(P)$ is the support characteristic curve. For a linearly elastic support, it is expressed as:

238

$$f_s(P) = \frac{PR^2(1-\nu_s^2)}{E_s A_s} \qquad (6.11)$$

If the support behaves nonlinearly, the appropriate $f_s(P)$ should be used instead.

3) $f_d'(\lambda_d)$ represents the offset of the support characteristic curve corresponding to the support delay. It is expressed as:

$$f_d'(\lambda_d) = \frac{P_I R(1+\nu)}{E} (1 - \lambda_d) \qquad (6.12)$$

Programs for an HP-97 programmable calculator that iteratively determine the root of Eq. (6.10) are documented in Appendix C for various formulations of $f_g(P)$. To calculate the yield factor λ_y, Eq. (6.10) must be solved twice. First, the ground is allowed to yield and the support pressure P_s^* is calculated; second, the ground is prevented from yielding by artificially increasing the strength parameters and the support pressure P_s' is calculated. The yield factor λ_y is then calculated from Eq. (6.9) as P_s^*/P_s'.

Because of the interactions among the relative support stiffness, support delay, and ground yielding variables, λ_y will be indirectly dependent on C* (and F*) and λ_d; this fact was substantiated by the findings from the axisymmetric finite

239

element analyses. The primary purpose of the plane stress finite element analyses was to investigate the sensitivity of λ_y to variations in the lateral stress ratio K. The principal conclusions from these analyses were:

1)   For small to moderate amounts of yielding (λ_y less than or equal to 2, approximately), λ_y is reasonably insensitive to variations in K between 0.5 and 1.5. As the level of yielding increases, this range for K decreases; at very high levels of yielding, Eq. (6.10) can only be used to calculate λ_y for K=1 (the conditions upon which the equation is based).

2)   The insensitivity of λ_y to variations in K is the same whether the yielding is due to low ground strength properties or a long support delay, or both.

3) λ_y is not significantly affected by the shear transfer conditions at the ground-support interface.

4)   Stiff supports will generally produce values for λ_y that are small and reasonably independent of K.

It must be emphasized here that it is only λ_y and not the value of P_s^* itself that is insensitive to K. The value of P_s^* calculated from Eq. (6.10) will equal the true support pressure only for the very special case of K=1; the value of λ_y calculated from the equation will, however, equal the true yield factor for many different values of K (subject to the limitations outlined above). This fact is the key to the

incorporation of the ground yielding effects into the simplified analysis.

The calculation of λ_y represents the final step in the simplified analysis method. The support thrust, which is proportional to the magnitude of the pressure P_s^*, is calculated as:

$$T^* = \lambda_y \lambda_d T \qquad (6.13)$$

In this equation, T is the "basic" thrust from step 1; it includes the effects of <u>relative support stiffness</u> and the <u>lateral stress ratio</u>. The term λ_d is the support delay factor from step 2; this factor, which is independent of the support stiffness and the lateral stress ratio, modifies T for the effects of <u>support delay</u>. The last term, λ_y, is the ground yield factor from step 3; this factor, which is a function of the ground strength, relative support stiffness, and support delay but which is independent of the lateral stress raio, at least for small amounts of yielding, modifies $\lambda_d T$ for the effects of <u>ground yielding</u>. The term T^* is then the final design thrust.

6.3   DESCRIPTION OF THE CASE STUDIES

In order to verify the accuracy of the simplified analysis method, it was applied to five tunnel projects reported in the literature in which the actual support loads were measured during construction. These cases span a representative range of tunneling situations while still satisfying most of the simplifying assumptions in the approximate analysis. The five cases are: (1) the Garrison Dam (North Dakota) outlet tunnels, a series of 8 drilled-and-blasted tunnels in clay shale supported with conventional steel ribs and blocking; (2) the Kielder (England) Experimental tunnel, a machine-excavated tunnel in mudstone supported with segmented steel rings; (3) the Thunder Bay (Ontario) sewer, a machine-excavated tunnel in silty clay lined with precast concrete segments; (4) the Tyne (England) sewer, a hand-mined (no shield) tunnel in stony clay lined with precast concrete segments, and (5) the Victoria Line (England) experimental tunnel, a shield-driven subway tunnel through stiff London clay supported with expanded precast concrete and cast iron liner elements. The general characteristics of these five projects are summarized in Table 6.1.

These cases reasonably satisfy most of the overall assumptions in the simplified analysis method. All of the tunnels are circular, located at depths of more than 2 diameters, and excavated full-face in free air. The ground

242

TABLE 6.1. GENERAL CHARACTERISTICS OF THE FIVE CASE STUDIES

Case	O.D. (meters)	Depth (meters)	Ground Type	Support Type	Method of Construction	Primary References
Garrison Dam Outlet Tunnels (United States)	7.9-10.7	30-55	clay shale	steel ribs	drill-and-blast	Lane (1957, 1960) Burke (1960)
Kielder Experimental Tunnel (England)	3.3	100	strongly jointed mudstone	welded steel segments	road-header type excavator	Ward, Coatts & Tedd (1976) Ward (1978)
Thunder Bay Sewer (Canada)	2.38	10.5	silty clay	precast concrete segments	tunnel boring machine	Belshaw & Palmer (1978)
Tyne Sewer (England)	3.2	12.1	laminated stony clay	bolted precast concrete segments	hand mined w/out shield	Attewell & El Naga (1977)
Victoria Line Subway (England)	4.28	27.9	London clay	expanded precast concrete segments	digger shield	Ward & Thomas (1965)
	4.0	26.1	London clay	expanded cast iron segments	digger shield	

243

masses are reasonably homogeneous and can be adequately modeled by simple constitutive laws. All of the supports are closed rings that are reasonably linearly elastic. The only assumption that is not completely satisfied is the requirement of time-independent ground behavior. In some of the tunnels, the ground movements and support loads do increase slowly with time as the ground consolidates, swells, and/or squeezes (creeps). However, this process is usually so slow that during approximately the first few weeks after construction the ground may be treated as effectively time-independent and the simplified analysis method can be used to calculate the short-term support loads.

The cases in this section were selected not only because they satisfy most of the overall assumptions in the simplified analysis method but also because they have been described in sufficient detail in published reports so that most of the input parameters for the analysis can be determined, at least approximately. The required input data for the simplified analysis can be divided into two broad categories. The first category is comprised of the data on the expected ground properties and the in situ ground stresses. The specific input variables in this category are: the elastic constants for the ground, E and ν; the strength parameters for the ground, ϕ and c or s_u (undrained shear strength); the vertical overburden stress, P; and the

lateral stress ratio, K. Information on the expected
groundwater conditions is also included in this category.
The second group of data pertains to the tunnel excavation
and support details. The specific input variables in this
category are: the support properties, E_s, ν_s, A_s, and I_s
(which, together with the ground properties in the first
category, can be used to compute the dimensionless stiff-
ness ratios C* and F*); the tunnel radius, R; the support
delay length, L_d; any other "pre-support" ground movements,
u_o'. The specific details of the ground excavation and
support erection sequences and of the blocking and/or
grouting procedures have a strong influence on the values
of L_d and u_o' in this category. Once the input parameters
in these two categories have been determined, the "basic"
support thrusts from the relative stiffness solution, the
support delay factor λ_d, and the ground yield factor λ_y
can all be calculated and the simplified analysis can be
used to predict the tunnel support loads.

Even in these case studies, however, there is rarely
enough published information available to permit the precise
calculation of all of the input parameters in the simplified
analysis method. This will often be the case in many actual
design problems as well. The second purpose of the case
studies described in this chapter is to point out some of
the difficulties involved in applying the simplified analysis

245

method--or any other analysis method, for that matter--to actual tunneling situations in which the data on the expected subsurface conditions and the details of the construction procedure are incomplete. In these instances, engineering judgement is required; often a range of values must be considered for the input parameters, and the sensitivity of the design to variations within these ranges must be investigated. The simplified analysis method is particularly well-suited to these parametric and sensitivity analyses. In the case studies that follow, there are several examples of incomplete input information and the techniques employed for dealing with it. In keeping with the approximate nature of the simplified analysis method, these techniques are not rigorous; they are based on material found in standard textbooks (Lambe and Whitman, 1969, for example), on knowledge of other, similar tunneling projects, and on engineering judgement. These techniques are very similar to those that would often be employed by the designer of an actual tunneling project. By carefully following the descriptions of the cases in this section, the reader will get a better idea of how the simplified analysis method can be applied to other practical tunneling situations.

The following detailed descriptions of the individual cases are each divided into four sections: (1) Ground Description, in which the input parameters for the ground

246

stiffness, strength, and in situ stresses are described;
(2) Excavation and Support, in which the construction pro-
cedure is outlined and the support stiffness and delay
parameters are calculated; (3) Instrumentation and Measured
Loads, in which the instrumentation program is briefly out-
lined and the measured support loads are summarized; and
(4) Predicted Support Loads, in which the loads calculated
using the simplified analysis method are compared to the
actual measured loads. The selected values for all of the
input parameters are summarized in Table 6.2. The compar-
isons between the support loads predicted from the simplified
analysis and the support loads actually measured in the
tunnel will be summarized following the detailed descriptions
of the cases. General comments on the accuracy of the
method and its appropriateness for design will also be made
at that time.

TABLE 6.2. INPUT PARAMETERS FOR THE SIMPLIFIED ANALYSIS METHOD

| Case | Section | Ground Properties | | | | In Situ Stress | | Strength Index |
		E (MPa)	ν	ϕ	c or s_u (kPa)	P (kPa)	K	FY
Garrison Dam	4A	192	0.5	32°	0	724[1]	0.5	0.42
	4B$_1$	192	0.5	32°	0	731[1]	0.5	0.42
	4B$_2$	192	0.5	32°	0	731[1]	0.5	0.42
	2B,F[3]	192	0.5	32°	0	647[1]	0.5	0.42
	2E	192	0.5	32°	0	1125[1]	0.5	0.42
	5A-E[3]	192	0.5	32°	0	899[1]	0.5	0.42
Kielder Experimental	–	1200	0.15	36°	0	2510	0.5	0.41
Thunder Bay	–	15.4	0.5	–	35.0	206	0.85	0.83
Tyne Sewer	Sites 1 & 2[3]	64.0	0.5	–	148	286	0.5	0.48
Victoria Line	Concrete	86.3	0.4	–	317	548	1.5	0.42
	Cast Iron	86.3	0.4	–	317	512	1.5	0.38

Notes

1. For all of the Garrison Dam tunnels, the vertical overburden stresses were calculated from an approximate analysis of the stress distributions beneath the toe of the dam (see Lane, 1960, for more details).

2. Equivalent cross-sectional area based on values of E_s and C^*.

3. Similar sections have been averaged.

248

TABLE 6.2. INPUT PARAMETERS FOR THE SIMPLIFIED ANALYSIS METHOD (CONT.)

Case	Section	Support Properties							Stiffness Ratios	
		E_s (GPa)	ν_s	A_s ($\times 10^{-2}$ m^2/m)	I_s ($\times 10^{-5}$ m^4/m)	R (m)	L_d/R	u'_o (cm)	C^*	F^*
Garrison Dam	4A	200	0	0.414^2	–	5.5	1.0	0	1.69	549
	$4B_1$	200	0	0.0146^2	–	5.5	1.0	0	48.2	∞
	$4B_2$	200	0	0.0164^2	–	5.5	1.0	0	42.9	∞
	2B,F	200	0	0.0574^2	–	5.5	1.33	0	12.2	3440
	2E	200	0	0.0673^2	–	5.5	1.17	0	10.4	1340
	5A – E	200	0	0.0792^2	–	5.5	1.00	0	8.85	1150
Kielder Experimental	–	200	0.3	1.27	0.0171	1.65	2.4	0	0.73	150,000
Thunder Bay	–	27.6	0.15	0.226^2	–	1.19	1.68	0–4.5	0.382	∞
Tyne Sewer	Sites 1 & 2	27.6	0.15	6.64	9.35	1.6	0.57	0	0.0728	132
Victoria Line	Concrete	38.0	0.15	22.1	–	2.14	0.43	0.79–1.11	0.0255	∞
	Cast Iron	96.6	0.25	2.86	–	1.98	0.46	0.95–1.27	0.0691	∞

6.3.1 Garrison Dam Outlet Tunnels

Garrison Dam, a 61 m. high rolled fill embankment, is part of the Missouri river control system and is located 120 km. north of Bismark, North Dakota. Its outlet works include eight 370 m. long circular tunnels, ranging from 7.9 m. to 10.7 m.in diameter, that were blasted through the compact Fort Union clay shale formation. Because little was known about the behavior of this clay shale during tunneling, a comprehensive testing program was devised to develop design and construction guidelines. Papers by Lane (1957, 1960) and Burke (1960) describe this testing program in considerable detail.

Ground Description

A cross-section through the dam showing the general layout of the tunnels and the geologic profile is presented in Figure 6.1 . The tunnels lie in the heavily overconsolidated Fort Union clay shale formation at depths of 30-55 meters below the original ground surface. Smith and Redlinger (1953) describe the general characteristics of the Fort Union formation:

> "The Fort Union group makes up the bedrock in a greater portion of the river valley within North Dakota. The dam site and probably the entire reservoir area lie in an upper portion of the group known as the Tongue River formation. This group is of early Tertiary (Paleocene) Age, and except for the lignite beds, sands, and an occasional thin stratum of cemented limestone and sandstone, may be termed an immature (clay) shale. The clay shales can be classified and tested by procedures ordinarily applied to soils. Little cementing material is present,

(a) SECTION THROUGH ℄ DAM LOOKING UPSTREAM

(b) PROFILE OF TUNNEL NO. 4
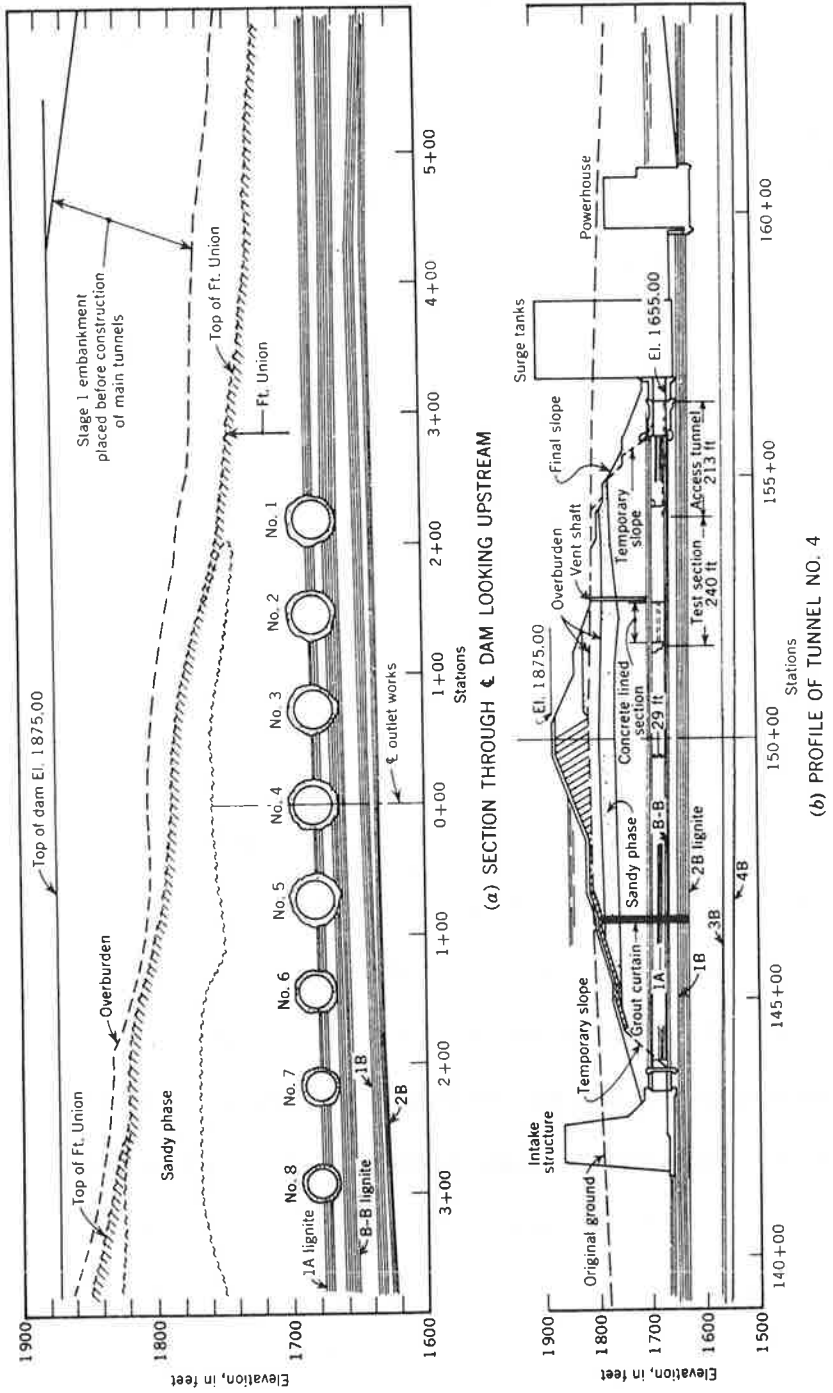
FIGURE 6.1. LOCATION OF TUNNELS--GARRISON DAM (FROM BURKE, 1960)

251

but the formation has been consolidated by super-
imposed loads of similar material up to 1500 feet
in thickness. Repeated consolidation may have been
brought about by at least two ice sheets which pro-
bably covered the dam site area in early Pleistocene
times .... Gradation of the sediments which make up
the Fort Union varies from fine sand to fat clay
with lean clays predominating .... Prominent through-
out the formation and especially at the dam site are
beds of lignite which are jointed and cracked and
are usually water bearing. The thicker beds may
be traced for many miles and are used as correlative
horizons ." (pp. 62-63).

These prominent and very permeable lignite beds were exposed

by the excavations for the powerhouse and intake structures

early during construction; as a result, the clay shale around

the beds was very thoroughly drained before most of the tun-

neling began.

Smith and Redlinger also performed a series of labor-

atory tests, using conventional soil testing equipment, on

the Fort Union clay shale in order to determine its elastic

constants and strength parameters. Based on the results

from triaxial compression tests in which the ratio σ_3/σ_1 was

held constant at 0.5, Smith and Redlinger determined the

elastic modulus to be equal to approximately 192 MPa ;

they also suggest a value of 0.5 for Poisson's ratio. The

strength parameters were obtained from consolidated drained

and consolidated undrained direct shear tests. There was

considerable scatter in the test data; the average values

from the tests are:

Consolidated Drained Tests: $\tau = \sigma_{nc} \tan 32°$

Consolidated Undrained Tests: $s_u = 96.6 + 0.47\sigma_{nc}$ (kPa)

σ_{nc} = consolidation stress

(normal stress)

The strength of the ground mass is essentially the strength of the clay shale; the lignite seams do not appreciably alter the overall strength of the ground mass (except for the effects of improved drainage).

Two questions must be answered when choosing between a drained and undrained short-term analysis for the tunneling problem: 1) which analysis gives the larger support loads? and 2) will drained conditions have been attained by the time the support loads are measured? Considering the second question first, the dissipation of any excess pore pressures will depend upon the permeability, drainage, and stress conditions in the shale surrounding the tunnels and upon the length of time between excavation and the measurement of the support loads. Substantial dissipation of the pore pressures is very likely in the Garrison Dam case for the following reasons:

1) Although the coefficient of consolidation of laboratory specimens of the Fort Union clay shale is very low ($c_v \cong 10^{-4}$ cm^2/sec.), the formation is probably quite fissured and the dissipation of excess pore pressures will be much faster in situ than in the lab.

2)   The tunnels were excavated by drill-and-blast techniques that tend to fracture the shale near the opening. This fracturing aids the dissipation of pore pressures in the very region in which yielding is most likely to occur.

3)   The very permeable lignite seams serve to increase the drainage of the shale.

4)   The "short-term" support loads were measured 2 to 3 months after excavation. Substantial dissipation of pore pressures can occur during this interval, particularly in the critical zone within one radius of the tunnel wall.

Naturally, the question of which condition (drained or undrained) will produce the largest support load can only be answered if the excess pore pressures induced in the ground mass by the excavation are known. If these pressures are positive, the ground yielding and support loads that develop under undrained conditions will be critical; as the pore pressures dissipate with time, the ground mass will get stronger, and there will not be any increase in support loads due to additional yielding. On the other hand, if the pore pressures induced by the excavation are negative, the ground mass will become weaker with time, and the ground yielding and support loads will be largest in the fully drained condition. Unfortunately, the sign of the excess pore pressures around the

tunnel is not generally known, and it probably varies from point to point in the ground mass. All that is known is that, based on items (1) - (4) above, drained conditions had very likely been attained by the time the final support loads had been measured; whether these drained conditions produce the largest predicted support loads is uncertain and must be checked in the analysis.

Since this case study is concerned only with the short-term tunnel support loads, the long-term swelling behavior of the Fort Union clay shale is not important. Smith and Redlinger did conduct some consolidation tests and suggest a value of 0.018 for the swell index. Burke (1960) concludes, based on the observed tunnel performance, that the "Fort Union formation does not exhibit significant swelling nor squeezing properties" (pg. 266).

Because the tunnels are located beneath the toe of the dam embankment, the vertical ground stresses cannot be calculated directly from the overburden depth. Lane (1960) presents the results from an analysis in which the embankment was divided into a series of strip loads that were superimposed using a Boussinesq solution for stresses; the overburden stresses in Table 6.2 were obtained from this analysis.

It is also difficult to determine the value of the lateral stress ratio K in the clay strata surrounding the tunnels. Because of the heavy overconsolidation of the deposit, K would ordinarily be high, perhaps on the order of 2.0. However, the Missouri river has in its past cut a deep valley, deeper than the level of the tunnels. This valley, which has since filled with alluvium, substantially relieved the large horizontal in situ stresses. Based upon the ratio of the measured contact stresses acting at the crown and springline of the very rigid test section 4D, a value of 0.5 is the best estimate of the present lateral stress ratio.[1] This value was used in the analyses for all of the other Garrison dam tunnel sections.

---

[1] This section 4D was mentioned earlier in Section 2. Although the properties of section 4D will be described herein, this tunnel section is not used to verify the simplified analysis method. However, because it is so rigid, it affords a convenient way to determine K, which was not measured in situ.

Excavation and Support

The eight tunnels at Garrison dam were all excavated
by conventional full-face drill-and-blast techniques in
free air. Temporary support was provided by blocked steel
sets and lagging with crown bars, followed much later by a
cast-in-place concrete liner up to 0.9 m thick. Round
lengths ranged from 1.8 to 2.4 m and the rate of advance
after preliminary set-up averaged 6.1 m/day for the 10.7 m
bores and 7.9 m/day for the 7.9 m tunnels. Small amounts
of water seeped into the tunnel from the upper lignite beds,
but the effect on the tunnel behavior was minor and local.

A short length of tunnel 4, subdivided into sections
4A through 4D (see Figure 6.2), was driven initially and
served as a test section for evaluating the performance of
different support configurations. The measured performance
of this test section was used to revise the designs for the
rest of the tunnels. This section was the only length of
tunnel excavated before the dam embankment was built; the
measured incremental support loads induced by the embank-
ment construction ("external loading" condition) have al-
ready been described in Section 2.6. All other tunnel
sections were driven after the embankment construction was
completed.

The support erection procedure was the same for all
of the tunnels. After blasting and mucking a new round,
two steel sets would be erected and lightly blocked. As

257

a) LOCATION OF MEASUREMENTS

- ▨▨▨ DIAMETER AND STRESS MEASUREMENTS ON RIBS
- ││││ DIAMETER MEASUREMENTS ON CONCRETE LINING
- R   MEASUREMENTS ON REINFORCING BARS

b) ARRANGEMENT OF TEST SECTION 4
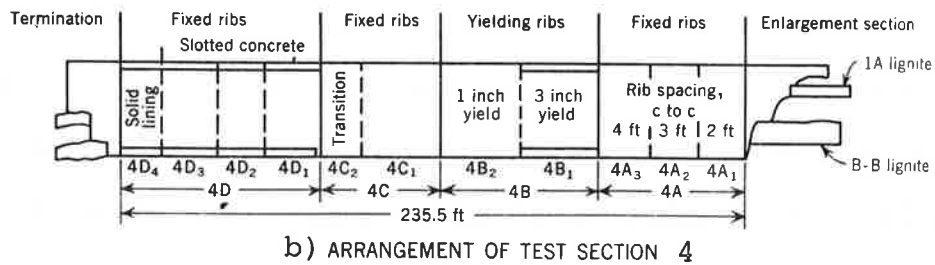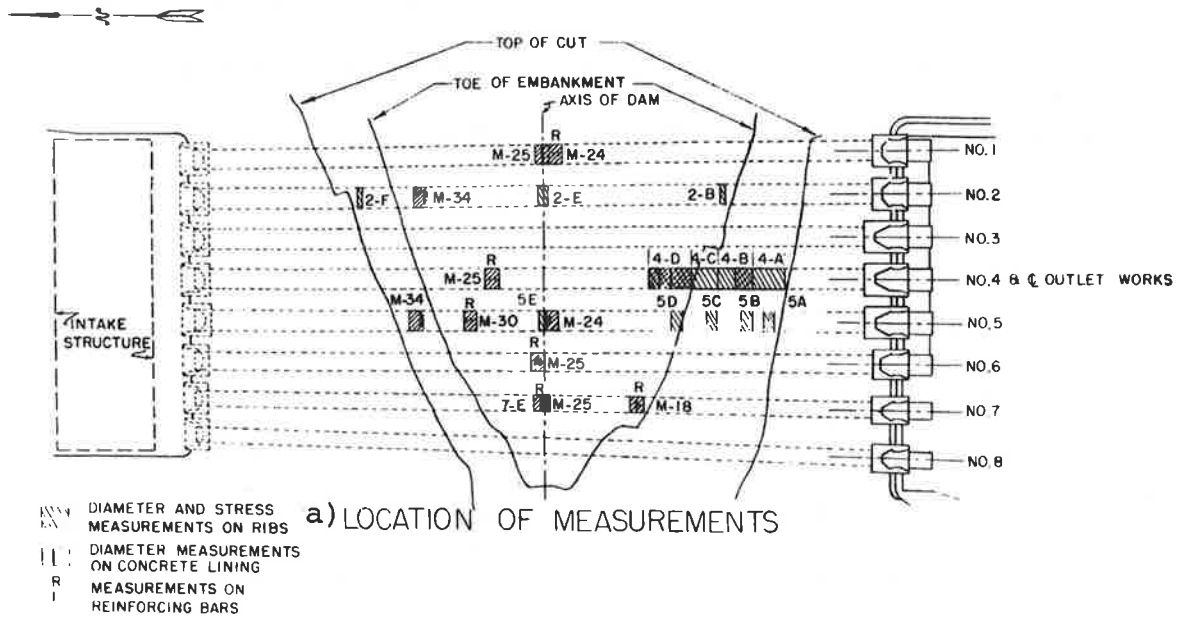
FIGURE 6.2.   LOCATION OF INSTRUMENTED SECTIONS--GARRISON
DAM TUNNELS   (FROM BURKE, 1960)

Burke reports, "only enough blocking was placed to hold the ribs in proper shape and position through the next blast, after which blocking was finished while the blasted material from the next round was being excavated [mucked]" (pg. 234). The support delay length inferred from this erection procedure is shown in Figure 6.3. Lagging was generally open with a maximum center-to-center distance of 1.1 m. A minimum of 16 blocking points per rib was specified; in the test section in tunnel 4, blocking was much closer, covering approximately 75% of the perimeter of the set (about 100 - 25 cm wide blocks). Overbreak averaged 0.18 m outside the outer flanges of the ribs. Well after excavation a very thick (0.8-0.9 m) concrete liner was cast in place.

The steel sets in two lengths ($4B_1$ and $4B_2$) of the test section in tunnel 4 were built with redwood blocks between the rib sections at each joint (see diagram in Figure 6.4). These blocks were designed to crush approximately to one-half of their thickness under the design load of one-half the overburden pressure; section $4B_1$ was designed to allow approximately 7.6 cm of radial yield and section $4B_2$, 2.5 cm. However, when installed in the tunnel these joint blocks were found to be much more flexible than designed. The blocks in the tunnel had crushed enough to allow 3.75 and 2.5 cm (in sections $4B_1$ and $4B_2$, respectively) of radial support movement at measured support loads of only 10-15% of the over-

259

ROUND:
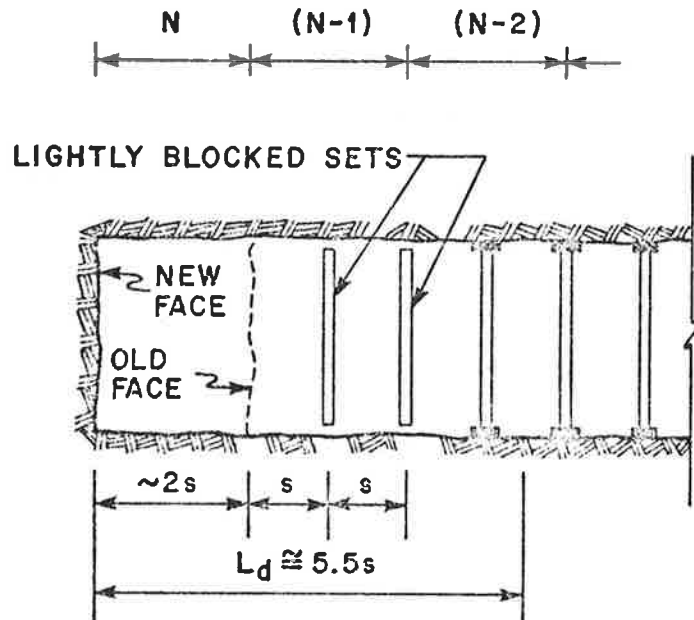
FIGURE 6.3.   SUPPORT DELAY LENGTH--GARRISON DAM TUNNELS

burden pressure.

The only other atypical support in the test tunnel was in section 4D, in which the 0.9 m thick concrete liner was prematurely cast before construction of the dam embankment.

Calculation of the dimensionless compressibility and flexibility ratios for the steel sets requires a modified formulation for the support stiffness. The deformation, and therefore the stiffness, of the support consists of three components:

1)   the strains in the steel rib

2)   the deformation of the wood blocking due to:

a)   axial compression

b)   indentation into the ground mass

3)   the deformation of the compressible blocks at the joints in the rib (if present).

The modified formulations for the compressibility and flexibility ratios are shown in Figure 6.4. The values of C* and F* for the different tunnel sections are given in Table 6.3.

Values of C* and F* for the composite concrete-and-steel support in section 4D can be computed using transformed section techniques, as done in Figure 6.5. These stiffness ratios were used in Section 2.6 to calculate the incremental support loads induced by the embankment construction.
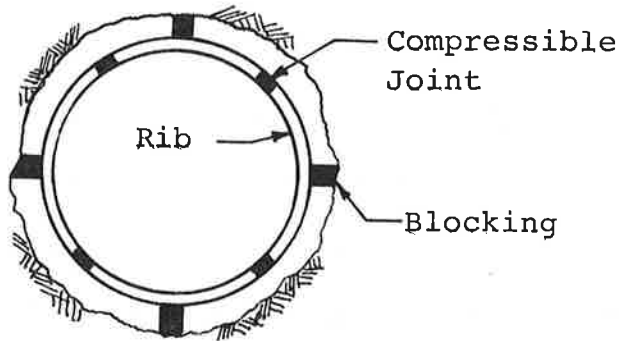
s = rib spacing

n_b = number of blocks

k_b = stiffness of blocks

n_j = number of compressible joints

k_j = stiffness of compressible joints

R,D = tunnel radius, diameter

E,ν = elastic constants

A,L = area, length

ΔD = change in diameter

COMPRESSIBILITY RATIO - COMPONENTS OF SUPPORT DEFORMATION:

1) Rib:

$$\Delta D_R = \frac{PRDs}{E_R A_R}$$

2) Blocking:

$$P_b = \frac{\pi PDs}{n_b}$$
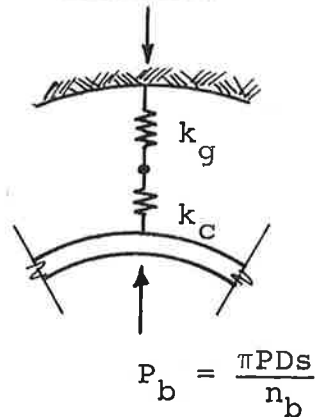
k_c = block stiffness in compression

$$= \frac{E_b A_b}{L_b}$$

k_g = ground stiffness against block indentation

$$\simeq \frac{1.1\sqrt{A_b}\ E}{(1-\nu^2)}$$

(see Poulos and Davis, 1974, pg. 168, for settlement of a square rigid block on an infinite half space)

$$k_b = \left[\frac{1}{k_c} + \frac{1}{k_g}\right]^{-1}$$

$$\Delta D_b = 2\left[\frac{P_b}{k_b}\right] = \frac{2\pi sPD}{n_b k_b}$$

FIGURE 6.4.   COMPRESSIBILITY AND FLEXIBILITY RATIOS FOR STEEL SET SUPPORTS

3) <u>Compressible Joints:</u>
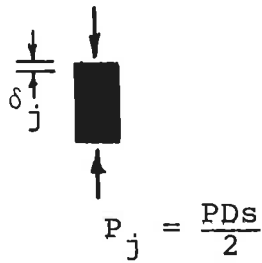
$$k_j = \frac{E_j A_j}{L_j}$$

$$\delta_j = \frac{PDs}{2k_j} \quad \text{for one joint}$$

$$P_j = \frac{PDs}{2}$$

$$(\delta_j)_{Total} = \frac{n_j PDs}{2k_j}$$

$$\Delta D_j = \frac{(\delta_j)_{Total}}{\pi} = \frac{n_j PDs}{2\pi k_j}$$

<u>Total:</u>

$$\Delta D = \Delta D_R + \Delta D_b + \Delta D_j = PDs \left[\frac{R}{E_R A_R} + \frac{2\pi}{n_b k_b} + \frac{n_j}{2\pi k_j} \right]$$

$$\frac{P}{\Delta D/D}_{Set} = \frac{1}{s} \left[\frac{R}{E_R A_R} + \frac{2\pi}{n_b k_b} + \frac{n_j}{2\pi k_j} \right]^{-1}$$

$$C^* = \frac{\left[\frac{P}{\Delta D/D} \right]_{Ground}}{\left[\frac{P}{\Delta D/D} \right]_{Set}} = \frac{\frac{E}{(1-\nu^2)}}{\left[\frac{P}{\Delta D/D} \right]_{Set}}$$

$$C^* = \frac{sE}{(1-\nu^2)} \left[\frac{R}{E_R A_R} + \frac{2\pi}{n_b k_b} + \frac{n_j}{2\pi k_j} \right]$$

FIGURE 6.4. COMPRESSIBILITY AND FLEXIBILITY RATIOS FOR STEEL SET SUPPORTS (CONT.)

FLEXIBILITY RATIO - COMPONENTS OF SUPPORT
DEFORMATION (ALONG VERTICAL DIAMETER):

1) **Rib:**
$$\Delta D_R = \frac{P D s R^3}{6 E_R I_R}$$

2) **Blocking:**
$$\Delta D_b = \frac{2\pi P D s}{n_b k_b} \quad \text{(same as for } C^* \text{)}$$

3) **Compressible Joints:** Consider only the limiting cases; either joints are rigid or $F^* = \infty$.

Total:
$$\Delta D = \Delta D_R + \Delta D_b = P D s \left[\frac{R^3}{6 E_R I_R} + \frac{2\pi}{n_b k_b} \right]$$

$$\left[\frac{P}{\Delta D/D} \right]_{set} = \frac{1}{s} \left[\frac{R^3}{6 E_R I_R} + \frac{2\pi}{n_b k_b} \right]^{-1}$$

$$F^* = \frac{\left[\dfrac{P}{\Delta D/D} \right] \text{Ground}}{\left[\dfrac{P}{\Delta D/D} \right] \text{Set}} = \frac{\dfrac{E}{(1-\nu^2)}}{\dfrac{1}{6} \left[\dfrac{P}{\Delta D/D} \right] \text{Set}}$$

(Factor of $\frac{1}{6}$ in denominator is required for consistency with definition of F^*- see Appendix A)

$$F^* = \frac{sE}{(1-\nu^2)} \left[\frac{R^3}{E_R I_R} + \frac{12\pi}{n_b k_b} \right]$$

FIGURE 6.4.   COMPRESSIBILITY AND FLEXIBILITY RATIOS FOR
STEEL SET SUPPORTS (CONT.)

TABLE 6.3.   COMPRESSIBILITY AND FLEXIBILITY RATIOS FOR GARRISON DAM TUNNELS

Section	Rib	s	A_R	I_R	n_b	k_j	R	C^*	F^*
4A	w12 x 99	91 cm	188.0 cm³	35800 cm⁴	100	–	549 cm	1.69	549
4B$_1$	w12 x 99	91	188.0	35800	100	18200 kN/m	549	48.2	∞
4B$_2$	w12 x 99	91	188.0	35800	100	54600 kN/m	549	42.9	∞
2B,F	w 8 x 48	122	91.0	7650	16	–	549	12.2	3440
2E	w10 x 72	107	53.8	17500	16	–	549	10.4	1340
5A-E	w10 x 72	91	53.8	17500	16	–	549	8.85	1150

Notes

1. Notation as given in Figure 6.4

2. E = 192 MPa, ν = 0.50 throughout

3. Stiffness of Blocks between rib and rock (k_b) is equal to 10900 kN/m.

4. Stiffness of yielding blocks at rib joints (k_j in Sections 4B$_1$ and 4B$_2$) backfigured from observed deformations in tunnel; there are 4 blocks per rib (i.e., n_j = 4)

5. Formulae for C^* and F^* given in Figure 6.4.

265
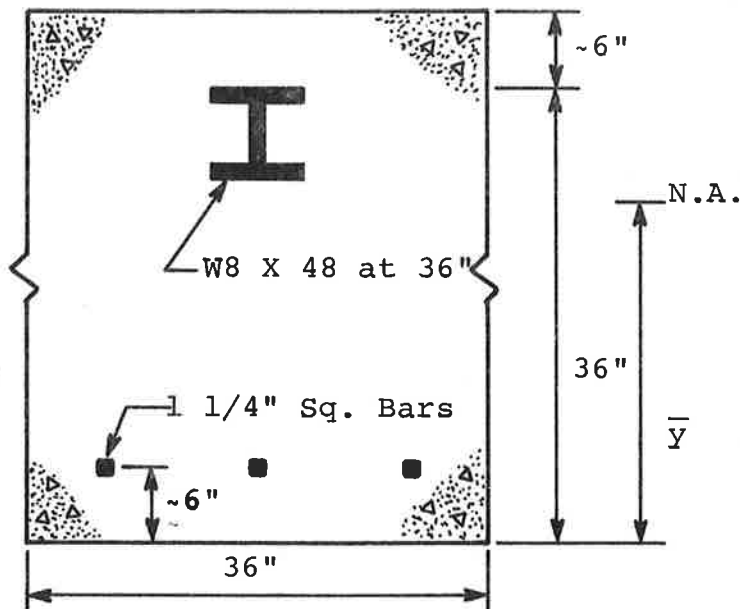
ASSUME:

$E_{CONCRETE}$ = 3600 KSI

E_{STEEL} = 29000 KSI

$n = \dfrac{E_{STEEL}}{E_{CONCRETE}} \cong 8$

FOR W8 X 48:

A = 14.11 in^2
I = 183.7 in^4

FOR TRANSFORMED SECTION:

A_e = (36)(42) + 3(1.25)^2(7) + (14.11)(7) = 1644 in^2/36 in.

A_s = <u>45.7 in^2/in</u>

$\bar{y} = \dfrac{(36)(42)(21) + 3(1.25)^2(7)(6) + (14.11)(7)(31.75)}{1644\ in^2}$ = 21.3 in.

$I_s = \underbrace{\dfrac{(36)(42)^3}{12} + (36)(42)(0.3)^2}_{\text{Concrete}} + \overbrace{(183.7)(7) + (14.11)(7)(10.45)^2}^{\text{W8 X 48}}$

$+ \underbrace{3(1.25)^2(7)(15.3)^2}_{\text{Recar}}$

I_s = 242,000 in^4/36 in = <u>6720 in^4/in.</u>

FIGURE 6.5. COMPRESSIBILITY AND FLEXIBILITY RATIOS FOR CONCRETED
SECTION 4D--GARRISON DAM

266

A_s and I_s must be reduced for the effect of the W30 X 210 "hinges" at the crown, invert, and springlines.
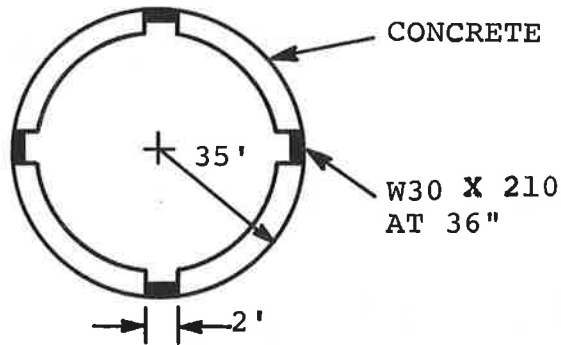
FOR W30 X 210:
$A = 61.8$ in^2
$I = 9870$ in^4

APPROXIMATE OVERALL STIFFNESSES: Consider a section on the liner from the centerline of the "hinge" to the nearest inflection point (at $\theta = 45°$):
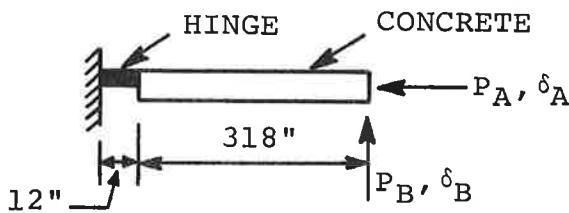
"Overall" stiffness can be approximately determined by considering deformations under this loading system.

$$\frac{P_A}{\delta_A} = \left[\frac{EA}{L}\right]_{OVERALL} = \left\{\sum_i \left[\frac{L}{FA}\right]_i\right\}^{-1} = \left\{\frac{12}{(29000)(61.8)} + \frac{318}{(3600)(1644)}\right.$$

$$\left[\frac{EA}{L}\right]_{OVERALL} = 16500 \qquad A_s = \frac{(16500)(330)}{3600} = 1510 \text{ in}^2/36 \text{ in.}$$

$$A_s = \underline{42.0 \text{ in}^2/\text{in}}$$

FIGURE 6.5. COMPRESSIBILITY AND FLEXIBILITY RATIOS FOR CONCRETED SECTION 4D--GARRISON DAM (CONT.)

$$\frac{P_B}{\delta_E} = \left[\frac{3EI}{L^3}\right]_{\text{OVERALL}} = \left[\frac{L_2^3}{3(FI)_2} + \frac{L_1^3}{3(EI)_1} + \frac{L_2 L_1^2}{(EI)_1} + \frac{L_2^2 L_1}{(EI)_1}\right]^{-1}$$

$$(1 \Longleftrightarrow \text{HINGE}, \quad 2 \Longleftrightarrow \text{CONCRETE})$$

$$\left[\frac{3EI}{L^3}\right]_{\text{OVERALL}} = \left[\frac{318^3}{3(3600)(242000)} + \frac{12^3}{3(29000)(9870)}\right.$$

$$\left. + \frac{(318)(12)^2}{(29000)(9870)} + \frac{(318)^2(12)}{(29000)(9870)}\right]^{-1}$$

$$\left[\frac{3EI}{L^3}\right]_{\text{OVERALL}} = 59.9 \qquad I_s = \frac{(59.9)(330)^3}{3(3600)} = 199{,}000 \ w^4/36 \ \text{in.}$$

$$I_s = \underline{\underline{5530 \ \text{in}^4/\text{in.}}}$$

COMPRESSIBILITY AND FLEXIBILITY RATIOS:

$$C^* = \frac{ER(1-\nu_s^2)}{E_s^- A_s (1-\nu^2)} = \frac{(27.8 \ \text{KSI})(210 \ \text{in.})(0.978)}{(3600 \ \text{KSI})(42.0 \ \text{in}^2/\text{in})(0.75)} = \underline{0.050}$$

$$F^* = \frac{ER^3(1-\nu_s^2)}{E_s I_s (1-\nu^2)} = \frac{(27.8 \ \text{KSI})(210 \ \text{in.})^3(0.976)}{(3600 \ \text{KSI})(5530 \ \text{in}^4/\text{in})(0.75)} = \underline{\underline{16.9}}$$

FIGURE 6.5. COMPRESSIBILITY AND FLEXIBILITY RATIOS FOR CONCRETED
SECTION 4D--GARRISON DAM (CONT.)

Instrumentation and Measured Loads

Strains in the steel sets were measured with Whittemore strain gauges at the crown, invert, and two springlines of the tunnels. The gauges were arranged to measure both axial thrust and bending strains. The concreted section 4D was instrumented with electrical strain gauges in the concrete and on the reinforcing steel and ribs and with earth pressure cells at the ground-concrete interface. The gauges on the rebars and ribs and the earth pressure cells at the interface all gave erratic and unreliable readings.

The support thrusts measured in all of the tunnels are listed in Table 6.5.[1] Due to the flexibility of the supports, the measured thrusts were essentially uniform around the circumference. All of the measured support thrusts given in Table 6.5 are for what Burke and Lane term the "single tunnel case;" that is, the support load measurements were taken before the immediately adjacent tunnels were constructed.

Although the bending moments in the steel sets were measured, the values were erratic and were found to be caused by local irregularities rather than the overall bending of the support. Lane (1960) states:

> The most obvious cause of moment in a ring is the difference between the vertical and horizontal loads [support pressures]. However, on most of the steel ribs the vertical and horizontal loads were so nearly equal that only a small part of the observed moment could be attributed to the small load difference actually measured. Hence, the

---

[1]In Section 6.4.   269

major causes of the rib moment were considered
as irregularities from the blocking loadings,
erection stresses, and similar factors inev-
itable in practical tunnel construction. (pg. 284)

Predicted Support Loads

Given the input parameters summarized in Table 6.2,

the application of the simplified analysis method as described

in Section 6.2 is straightforward. The values for the "basic"

thrust from the relative stiffness solution, the values for

the support delay factor λ_d and the ground yield factor λ_y,

and the values of the final predicted support thrusts are

given in Table 6.4 for both the drained and undrained analy-

ses. Since the blocking points of the steel sets are assumed

incapable of transferring any significant tangential shear

stress, the full-slip relative stiffness solution was used

for the calculations. As a result of this condition and the

extreme flexibility of the steel sets, the support thrusts are

equal at the crown and springlines.

As described earlier, full drainage had very likely

occurred by the time the support loads were measured

(generally 2 to 3 months after excavation). Nevertheless,

both drained and undrained analyses must be performed to

determine which extreme gives the most yielding and the

largest support loads. As shown by the results summarized

in Table 6.4, the drained calculation always gives the larger

support load.

The thrusts predicted from the drained analysis are

270

TABLE 6.4. COMPARISON OF DRAINED AND UNDRAINED ANALYSIS RESULTS -- GARRISON DAM TUNNELS

Section	$\left[\dfrac{T}{PR}\right]$ RSS	λ_d	Undrained Analysis		Drained Analysis	
			λ_y	$\left[\dfrac{T}{PR}\right]$ Predicted	λ_y	$\left[\dfrac{T}{PR}\right]$ Predicted
4A	0.410	0.41	1.05	0.177	1.24	0.208
$4B_1$	0.030	0.41	1.36	0.017	4.95	0.061
$4B_2$	0.033	0.41	1.36	0.018	4.66	0.063
2B,F	0.106	0.22	1.50	0.035	4.33	0.101
2E	0.123	0.31	1.49	0.057	2.95	0.112
5A-E	0.140	0.41	1.25	0.072	2.21	0.127

are compared to the measured support thrusts in Table 6.5
(Section 6.4). Except for the one isolated case in which
the error in the prediction is negative (tunnel section 2E,
error = -15%), the errors are all conservative, ranging from
+10 to +62%. The average error in the predictions is 27%,
which, given the approximate nature of the simplified analysis
and the generally high levels of conservatism in most other
tunnel design methods, is quite acceptably small.

6.3.2 Kielder Experimental Tunnel

The Kielder Experimental Tunnel was constructed in 1974 as part of the Northumbrian Water Authority's Kielder Water Scheme in northern England. The purpose of the experiments was to investigate the performance of various support systems in the Carboniferous rocks common in the area. Although several steel, rockbolt, and shotcrete support systems were tested in both machine-excavated and drilled-and-blasted tunnel sections, only a machine-excavated section supported by a segmented steel liner will be considered here. Further details of the project can be found in papers by Ward, Coats, and Tedd (1976), Farmer (1976), and Ward (1978).

Ground Description

The geology and properties of the Carboniferous mudstones, siltstones, sandstones, and limestones in the general area of the Kielder Water Scheme are described by Carter and Mills (1976). The 3.3 meter diameter experimental tunnel lies in a relatively weak mudstone stratum at depths ranging from 75 to 100 meters and is completely above the ground water table (see Figure 6.6). Access to the experimental tunnel is gained through an inclined adit leading from an adjacent quarry.

The rock at the experimental site is transected by 3 major sets of discontinuities: 1) a set of near-horizontal bedding planes, 2) a near-vertical set of joints striking

273

The image shows a geologic section (top) labeled "Section" with rock layers: Sandstone, Mudstone, Limestone, Sandstone, Limestone, with a Tunnel in mudstone, Inclined adit, Portal, Rogerley quarry face, Mudstone, Limestone, Sandstone, and a scale bar marked 0, 20, 40, 60, 80, 100 m.

The lower image shows a "Plan" view labeled: Tunnel in sandstone, Tunnel in limestone, Tunnel in mudstone, Machine, Drill and blast, Inclined adit, Portal, Rogerley quarry face, with a North arrow (N).

Section and plan of experimental tunnels beneath
Rogerley quarry

FIGURE 6.6.   GEOLOGIC PROFILE--KIELDER EXPERIMENTAL TUNNEL
(FROM WARD, COATTS, AND TEDD, 1976)

at approximately 60° to the tunnel axis, and 3) another near-vertical set of joints striking at approximately 140° to the tunnel axis. The vertical joints in the limestones and sand-stones are wide open, but in the mudstones and siltstones they are closed or only slightly open and are usually oxidized. A lateral extension of the rock mass has very likely occurred at some time in the past, either as the re-sult of valley cutting by the nearby Wear river or because of the intrusion of an extensive quartzite-dolerite sill just below the lower sandstone stratum.

Recovery from diamond NX coring of the mudstone stra-tum at the tunnel's depth ranged from 76-100%; RQD ranged from 0-8%. The mudstone is a highly fissile shale with bed-ding planes every 25-35 mm. Laboratory tests on vertical cores gave the following properties for the intact mudstone:

Bulk Density	2.56 Mg/m^3
Unconfined Compressive Strength	37 MN/m^2
Tangent Young's modulus at 50% ultimate	8.4 GN/m^2
Cohesion, c	5.0 MN/m^2
Friction angle, ϕ	$36°$

The elastic modulus for the jointed rock mass was determined using the modulus ratio vs. RQD correlation suggested by Deere et al. (1968); for RQD less than 10%, the rock mass modulus is approximately 15% of the intact modulus, i.e., $E_{mass} = 1.2$ GN/m^2. Poisson's ratio for the rock mass

275

is assumed to equal 0.15. Unfortunately, it is quite difficult to make correlations between the intact rock's strength and the strength of the jointed rock mass. The friction angle of the closely jointed rock mass is probably very close to the residual friction angle of the intact material; this residual friction angle is approximately equal to the 36° measured in the laboratory tests. The close jointing of the rock mass will also tend to reduce the cohesion to a very small value, or to zero. A zero value for the cohesion is further substantiated by the observed progressive collapse of an unsupported length of the tunnel. Based on these considerations, strength parameters of c = 0 and ϕ = 36° seem reasonable for the rock mass.

The vertical in situ stresses are assumed to equal the overburden weight, ranging from 1880 to 2510 kN/m^2. The open vertical jointing and the likely lateral extension of the rock at some point during its history suggest that the lateral stress ratio K will be low. Since the mudstone is so closely jointed, though, an upper bound for K can be reasonably estimated using Jaky's empirical relation for granular materials, K $\cong$ 1 - sinϕ (see Lambe & Whitman, 1969, pg. 127), giving a value of K $\cong$ 0.5.

The cleft and pore water pressures around the tunnel are vey small. The tunnel is above the nearby river and there are only small perched water tables above some of the rock strata.

Excavation and Support; Instrumentation and Measured Loads

The section of the test tunnel considered herein was excavated in free air using a Dosco road header, a partial-face tunnel excavating machine. The tunnel support was provided by a 12.7 mm thick ($C^* = 0.73$, $F^* = 1.5 \times 10^5$) continuous steel liner, erected in rings 0.7 m long with four segments per ring. The void between the steel liner and the tunnel wall averaged 108 mm in thickness and was filled with grout as soon as possible.

A group of three rings was instrumented with twin-wire vibrating-wire strain gauges. These gauges were positioned to measure the circumferential thrusts at eight different locations around the periphery of each ring. The tunnel face was advanced 2.1 meters by the Dosco road header and the three instrumented rings were installed as a group to within 0.3 m of the face, butt-welded together, and grouted (see Figure 6.7). The face was then advanced 2.7 m, which led to a sudden loading of the support as measured by the strain gauges. Several days later, the face was advanced again, but this induced only slight increases in support load. The short-term support thrust at approximately 2 weeks after construction are indicated in Figure 6.8a. The average thrust in each ring has continued to increase slowly with time; the distributions at 8 months after construction are shown in Figure 6.8b. Some very small bending moments were also measured in the support (Figure 6.8b).
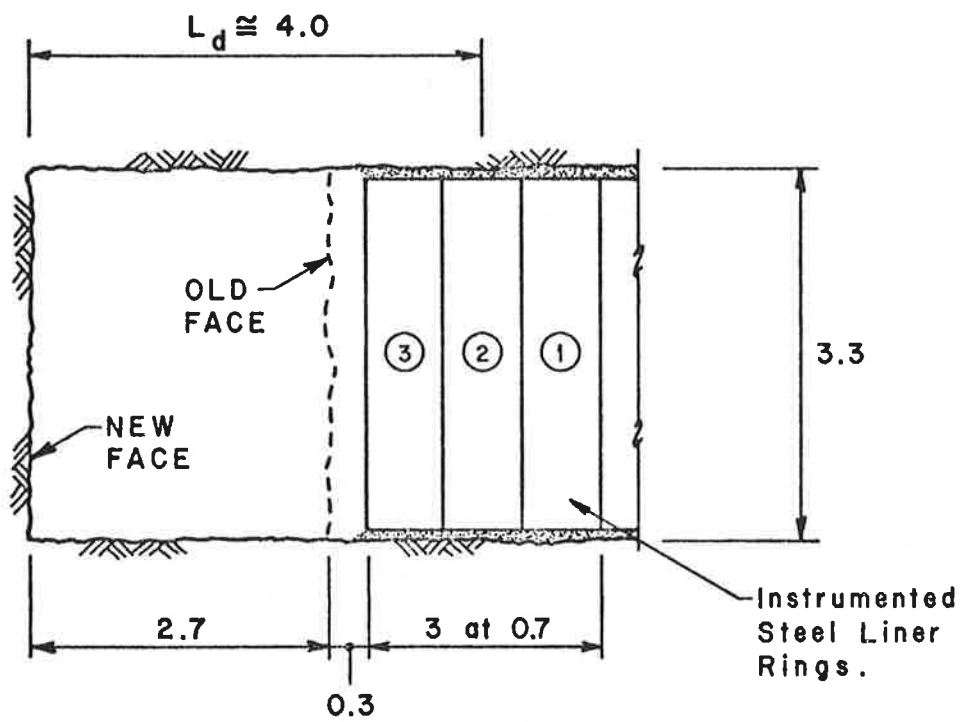
FIGURE 6.7.   SUPPORT DELAY LENGTH--KIELDER EXPERIMENTAL TUNNEL

278
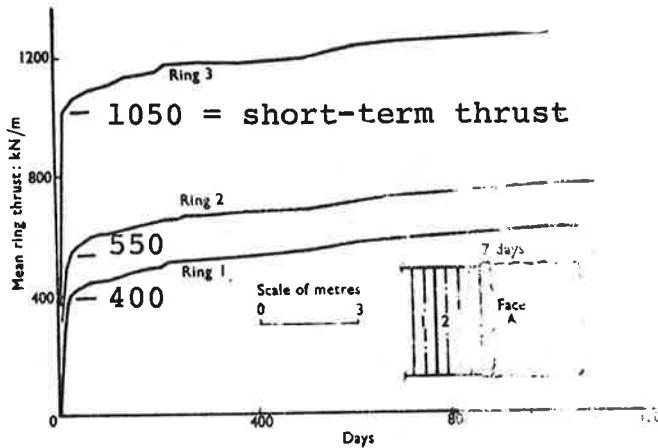
a) Development with time of the mean ring thrust in a steel lining in the Kielder Experimental tunnel

(from Ward, 1978)
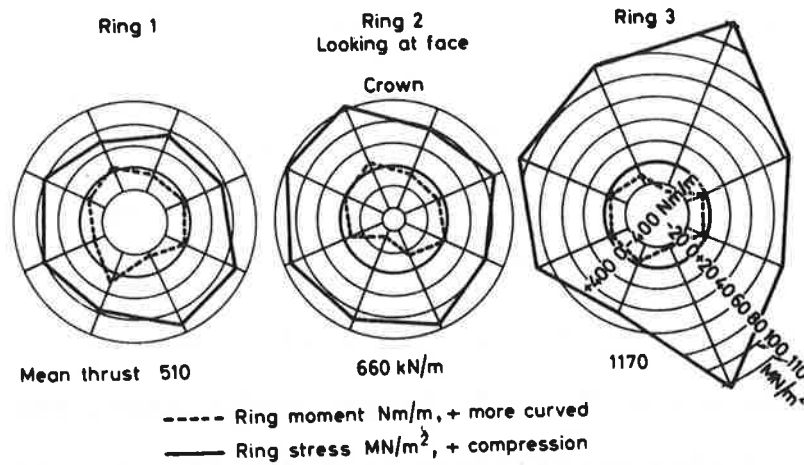
b) Ring stresses and moment distributions in steel liner

(8 months after construction--from Ward, Coatts, and Tedd, 1976)

FIGURE 6.8.   MEASURED SUPPORT LOADS IN THE KIELDER EXPER-
IMENTAL TUNNEL

279

Although the three instrumented rings were installed as a group, Figure 6.8 clearly shows that the ring closest to the face (Ring 3) sustained a much higher loading than those farther away. This result is to be expected, and it reflects the usual longitudinal load distribution in any tunnel support element. For the purpose of computing the support delay length, though, the three simultaneously erected rings should be treated as a single support unit with L_d as shown in Figure 6.7. The input parameter u_o' is zero in this case, since the support ring is completely grouted before the next round of advance.

Predicted Support Loads

The input parameters for the simplified analysis method are listed in Table 6.2. Although the grouting may fully interlock with the rock mass, the friction coefficient between the grout and the smooth segmented steel ring will probably be less than tan 25° and therefore, based on Figure 2.13, the full-slip relative stiffness solution should be used to compute the "basic" thrust coefficient; the calculated value of this coefficient is 0.464 at both the crown and springline. The next step in the simplified analysis is to calculate the support delay factor λ_d. Unfortunately, this step leads to some problems.

The support delay length L_d is known relatively precisely in this case; as indicated in Figure 6.8, $L_d \simeq 4.0$ m. This is a very long support delay and, when combined with the relatively moderate 1.65 m tunnel radius, it yields a normalized delay length L_d/R of 2.4 that far exceeds the limits of Eq. (6.7) for λ_d. This implies that, if the ground were elastic, all of the radial ground displacements would occur before the support is installed and the support loads would therefore be nil. In other words, λ_d equals zero.

Of course, if the ground does not remain elastic, some support loads could still develop. The value of 0.52 for the FY strength index for the mudstone implies that some yielding will probably occur. However, if $\lambda_d = 0$, the yield factor λ_y is no longer defined (see definition of λ_y in Eq. 6.9) and the simplified analysis method cannot be used to predict the support load.

Nevertheless, even though the simplified analysis method cannot be used to predict the exact value of the support load, it can be used after some manipulation to predict an upper bound for it. This upper bound is itself an important quantity to know for design purposes, and its calculation is a good example of how the basic principles underlying the simplified analysis can still be applied to the tunneling problem even when the method itself cannot.

Consider the situation depicted in Figure 6.9.

281
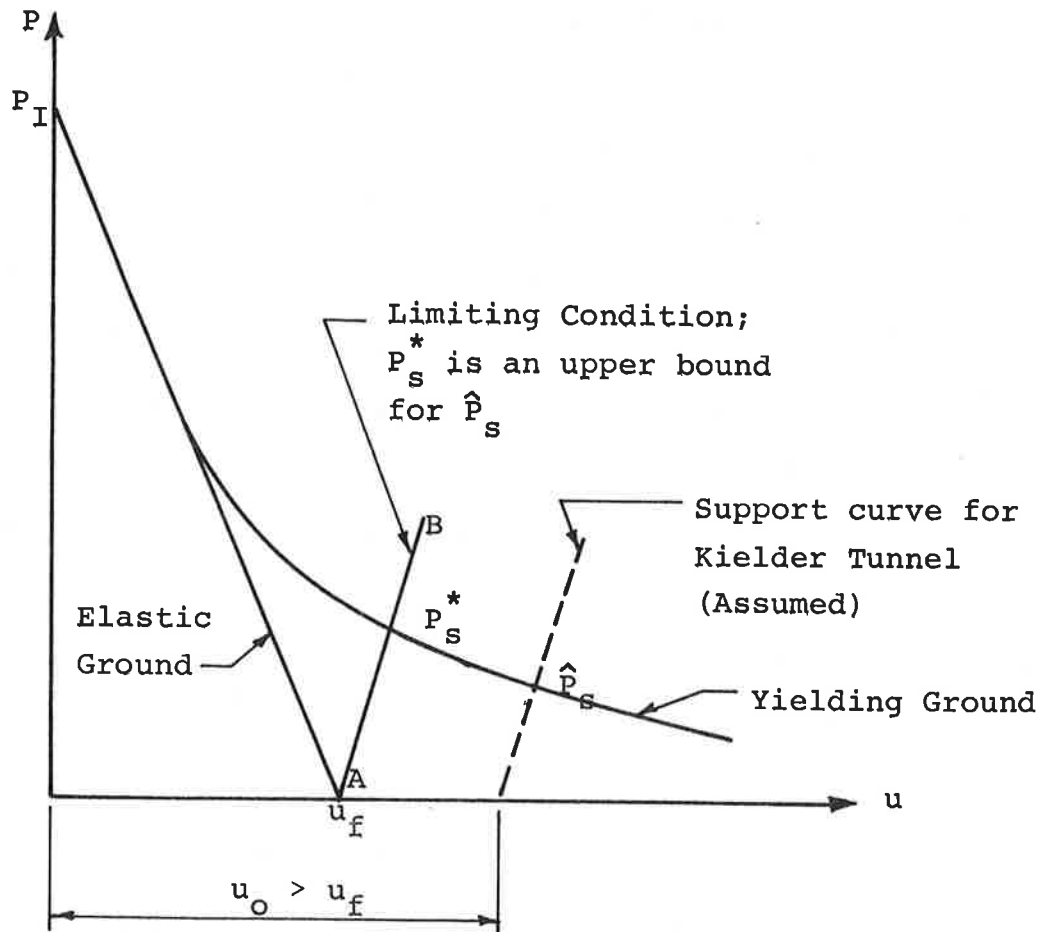
FIGURE 6.9.   UPPER BOUND OF SUPPORT LOAD FOR TUNNEL WITH
LARGE SUPPORT DELAY

The characteristic curves in this diagram are similar to those in Figure 5.11 that were used during the original derivation of the simplified analysis method for K=1 conditions. As described in Section 5 and Section 6.2, the offset u_o of the support characteristic curve is a direct function of the support delay factor λ_d; the exact relationship is given by Eq. (6.12). However, since λ_d has a physical lower limit of zero (corresponding to very long support delays), the offset u_o must have an upper limit of u_f, the maximum elastic radial displacement for an unlined tunnel. The support characteristic curve AB in Figure 6.9 is thus the limiting case that can be treated using the simplified analysis method. In practice, this restriction is generally not too severe since in most common tunneling situations, and particularly in medium to large diameter tunnels with moderate round lengths and especially if the ground mass is relatively weak, the calculated offset will be well below the limiting value of u_f. However, this restriction is a problem when applying the simplified analysis to the Kielder Experimental tunnel.

The restriction on the support curve offset does not imply that no support characteristic curves can lie to the right of curve AB in Figure 6.9; in fact, the actual curve for the Kielder tunnel lies in this range. The restriction only means that the offset cannot be calculated for curves

in this region and that therefore the equilibrium pressure $\hat{P}_s$ for the Kielder tunnel cannot be determined. The equilibrium pressure P_s^* corresponding to the limiting offset of u_f can be calculated, however, and it is clear from Figure 6.9 that this will be an upper bound for $\hat{P}_s$.

Even though the yield factor λ_y is undefined in this limiting case, Eq. (6.10) can still be used to directly calculate the upper bound value P_s^* for K=1 in situ stress conditions. However, some technique must then be found to convert this support pressure to the appropriate support load for K≠1 conditions. A very approximate method for this conversion is outlined below; it makes use of the following notation:

> T = support thrust calculated from relative stiffness solution (no reduction for support delay or increase for ground yielding)
>
> T' = support thrust reduced for support delay
> = λ_d T where, in the general case, λ_d is nonzero
>
> T* = support thrust (in the limiting case of full support delay--i.e., λ_d=0 or u_o=u_f) reduced for support delay and increased for ground yielding
> = P_s^* R   for K=1 conditions

Subscripts are used to denote K=1 or K≠1 conditions. The derivation is based on two assumptions. The first merely states that for the purposes of the derivation the support offset is slightly less than the limiting value of u_f and

284

therefore the values of λ_d and T' are nonzero (but small); this assumption is made for mathematical convenience. The second assumption is that the yield factor λ_y is completely independent of K. Although this assumption is true subject to the restrictions mentioned in Section 6.2, its general validity for the limiting case of full support delay (i.e., $\lambda_d=0$ and λ_y therefore very large) cannot be established. However, this assumption does seem plausible as long as the absolute level of yielding around the tunnel is small, in which case the total effect of the yielding is also small.

For the assumed nonzero but small λ_d, the yield factor λ_y is defined and:

$$\lambda_y \equiv \left[\frac{T^*}{T'}\right]_{K=1} = \left[\frac{T^*}{T'}\right]_{K \neq 1} \tag{6.14}$$

Rearranging:

$$[T^*]_{K \neq 1} = [T^*]_{K=1} \frac{[T']_{K \neq 1}}{[T']_{K=1}} \tag{6.15}$$

From the definition of the support delay factor (see Eq. 3.1):

$$\frac{[\lambda_d]_{K \neq 1}}{[\lambda_d]_{K=1}} = \frac{[T'/T]_{K \neq 1}}{[T'/T]_{K=1}} \tag{6.16}$$

Since in Section 3 it was found that λ_d is independent of K, $[\lambda_d]_{K \neq 1}$ equals $[\lambda_d]_{K=1}$ and Eq. (6.16) therefore equals a constant value of 1. Equation (6.16) can then be rearranged as:

285

$$\frac{[T']_{K \neq 1}}{[T']_{K=1}} = \frac{[T]_{K \neq 1}}{[T]_{K=1}} \qquad (6.17)$$

Equations (6.16) and (6.17) are true for all values of λ_d (including zero in the limit). Substituting (6.17) into (6.15) gives:

$$[T^*]_{K \neq 1} = [T^*]_{K=1} \frac{[T]_{K \neq 1}}{[T]_{K=1}} \qquad (6.18)$$

The quantities $[T]_{K \neq 1}$ and $[T]_{K=1}$ can be calculated directly from the relative stiffness solution (Eqs. 6.3 or 6.4) and $[T^*]_{K=1}$, which equals $P_s^* R$, can be computed from Eq. (6.10). The quantity $[T^*]_{K \neq 1}$ is the upper bound prediction for the support thrust in the tunnel.

Using Eq. (6.18), the upper bound for the predicted average thrust coefficient $\frac{T}{PR}$ in the Kielder tunnel is computed as 0.227. This value is 40% larger than the measured thrust coefficient of 0.162, but since the prediction is only an upper bound this is not surprising. Given all of the other uncertainties in the tunneling problem, this conservative error in the upper bound estimate would be acceptable for design purposes.

The derivation for the upper bound estimate hinges on the assumption that λ_y is independent of K, even as λ_y grows large due to λ_d approaching zero. As mentioned earlier, this

286

assumption is plausible as long as the absolute level of yielding around the tunnel is small. This condition must therefore be checked before the calculated upper bound can be considered even approximately accurate. One measure of the absolute yielding around the tunnel for K=1 in situ stress conditions is the radius of the yielded zone (see Eq. 4.11, for example). For the strength and stress parameters of the mudstone and the condition of full support delay (i.e., $\lambda_d = 0$), this radius is 1.39 times the radius of the tunnel. This represents a moderate amount of yielding (for comparison, see the finite element analyses in Section 5.4), so the assumed independence of λ_y from K will be approximately true.

Besides showing that the upper bound prediction for the support thrust can be reasonably close to the actual measured load, the above derivation illustrates how the basic principles underlying the simplified analysis can be applied to the tunneling problem even when the method itself cannot. In general, the method will be directly applicable to most common tunneling situations. It is only in small to moderate diameter tunnels with long round lengths, like the Kielder, where L_d/R becomes very large and the method breaks down.

6.3.3 Thunder Bay Sewer

This 2.38m O.D. sewer tunnel was constructed in 1976 as part of a larger program to modernize the sewage treatment facilities in the city of Thunder Bay, Ontario, on the shore of Lake Superior. The low bid for the project was based on the then novel combination of a full faced tunnel boring machine (TBM) and segmented precast concrete liner elements. Since this technique had not been used previously in the silty clay deposits in this region, an extensive monitoring program was developed to measure the actual support loads and to evaluate the overall tunnel performance. Belshaw and Palmer (1978) give a detailed description of the tunneling conditions and the instrumentation.

Ground Description

A profile of the subsurface conditions at the instrumented tunnel section is depicted in Figure 6.10. The tunnel lies at a depth of about 10.5 m below the surface in a stratum of layered clay. As described by Belshaw and Palmer (1978):

> The cohesive deposits to a depth of 7.5 m and below a depth of 12.1 m may be classified as a silty clay with a liquid limit of about 40% and a plasticity index of about 20%. Between 7.5 m and 12.1 m the deposit is clay with a liquid limit of about 75-80% and a plasticity index of about 60%. The consistency of the deposit increases with depth from soft above the tunnel to firm below the elevation of the tunnel invert. The stratum is slightly overconsolidated. The amount of layering

288
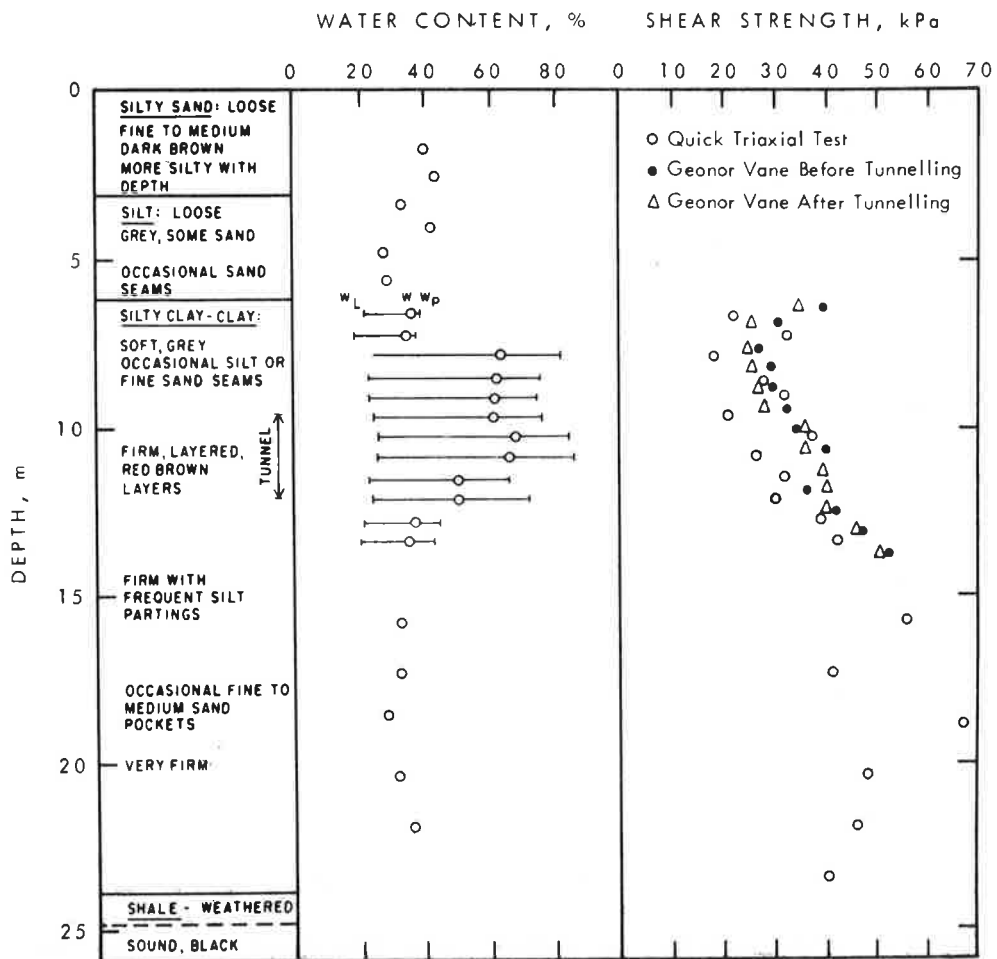
FIGURE 6.10.   SUBSURFACE PROFILE--THUNDER BAY SEWER   (FROM BELSHAW AND PALMER, 1978)

289

increases with depth and occasional thin
silt or sand seams occur. (p. 574)

The only properties (other than index values) that are reported for this clay are the undrained shear strength values summarized in Figure 6.10. At the level of the tunnel, s_u is approximately equal to 35 kPa. The imperviousness of the clay deposit and the short time interval between excavation of the tunnel and measurement of the support loads all suggest that the behavior of the ground around the tunnel can be treated as essentially undrained. There is thus no need for any information on the drained strength parameters for the clay.

The lack of any test data on the elastic properties of the clay deposit is more serious, however. A very crude value for the undrained elastic modulus can be obtained from the relationship between E and $\bar{\sigma}_c$ (the effective consolidation stress) observed for other, similar clays; Lambe and Whitman (1969) give several examples of this relationship (Figures 30.5 and 30.6 on p. 460 in their textbook). In order to use the charts in Lambe and Whitman, the stess level (which they express in terms of the factor of safety) must be known. This stress level unfortunately is not known precisely; moreover, it varies from point to point. However, the overall stress level in the ground mass can be roughly estimated. For s_u = 35 kPa and P $\simeq$ (10.5 m)(19.6 kN/m^3) = 206 kPa at the tunnel axis (although the total unit weight

of this clay is not given, 19.6 kN/m^3 is a reasonable assumption), the "first-yield" index for the tunnel is $\frac{1}{2}$(2 - 70kPa/206kPa) or FY = 0.83; a value of FY this close to 1 implies that the shear stress level will be very high in the clay surrounding the tunnel (in fact, yielding will probably develop at the tunnel wall). This can be alternately thought of as an overall "factor of safety" close to unity. For these conditions, the charts in Lambe and Whitman suggest that the undrained modulus E is very roughly equal to 150 $\bar{\sigma}_c$. Since it is known (based on comments made by Belshaw and Palmer in the text of their paper) that : (1) the clay is only slightly overconsolidated, (2) the water table is near the surface, and (3) the pore pressures are hydrostatic, the effective consolidation stress $\bar{\sigma}_c$ can be approximately calculated as the total vertical stress (206 kPa) minus the hydrostatic pressure (10.45 m x 9.8 kN/m^3 = 103 kPa) or $\bar{\sigma}_c$ = 103 kPa. Finally, E $\simeq$ 150$\bar{\sigma}_c$ = (150)(103 kPa) $\simeq$ 15,400 kPa. The standard assumption can be made that ν = 0.50 for undrained conditions.

The total in situ vertical ground stress has already been calculated above as 206 kPa. The lateral in situ stress ratio can be approximately determined from Brooker and Ireland's chart of K vs. OCR in Lambe and Whitman (1969, p. 300); for an overconsolidation ratio of slightly greater than 1 and a PI of 20 - 60%, the lateral effective

stress ratio is 0.6 - 0.7; in terms of total stresses, K = 0.8 - 0.85.

The water conditions are not a problem in this tunnel. Because the clay is so impervious, there are no large water inflows during tunneling. And, since Belshaw and Palmer state that "the seal at the circumferential joints [in the precast concrete liner] was not entirely effective...and drainage occurred toward the joints" (p. 580), there is no potential for any build-up of water pressure against the tunnel support. As will be discussed later, this was substantiated by piezometers placed in the clay stratum immediately behind the support.

Excavation and Support

The 2.38 m O.D. Thunder Bay sewer tunnel was excavated in free air by a full-face tunnel boring machine (TBM). Since this is a soft ground tunnel, the TBM was enclosed within a shield. Tunnel support was provided by unbolted precast concrete segmented rings 1.37 m long and 11 cm thick, with 4 segments per ring. The support was erected within the tailpiece of the TBM; the machine was then advanced, and a clay grout was injected into the 4.5 cm. thick tailpiece void. Based on surface settlement measurements, it was not certain whether the grouting was completely effective in filling this void; Belshaw and Palmer state that "the initial settlement seemed to be related to the closure of the tailpiece void, and, in spite of the injection of grout,

292

the average volume of the surface settlement troughs was about equal to the volume of the void" (p. 578). The tunnel advance rate averaged 0.5 m/hr initially, increasing to a final production rate of 3 m/hr.

Although the precast concrete support elements had a nominal thickness of 11 cm, the method used for sealing the longitudinal joints made the support stiffness much less than the nominal thickness would suggest. The rubber-like seal in these joints had an initial unstressed thickness of 6 mm but were observed to compress to a thickness of 3 mm in the tunnel. Since no other information is given concerning these seals, the only way that their stiffness can be determined is by backfiguring it from the observed deformations and the measured support thrust. This is not entirely satisfactory because it introduces an element of circular logic into the predictions of the simplified analysis method; however, the stiffness of these seals is only one parameter in the method, so it should not unduly influence the predictions.[1] Based on an observed thrust of 104 kN/m (see Table 6.5) and the observed joint closure of 3 mm, the joint stiffness k_j is 35000 kN/m^2 for each of the four joint seals. Using this stiffness in the

---

[1]The stiffness of the joint seals, which enters into the calculations for C* and F*, has a direct effect only on the "basic" support thrust in the simplified analysis; it has no effect on the support delay factor λ_d and only an indirect influence on the ground yield factor λ_y.

expression for C* derived in Figure 6.4 (and ignoring the middle term involving k_b and n_b, which correspond to the blocking of a steel set) and assuming standard values of $E_s = 27.6$ GN/m^2 and $\nu_s = 0.15$ for concrete:

$$C^* = \frac{sE}{(1-\nu^2)} \left[\frac{R}{E_s A_s} + \frac{n_j}{2\pi k_j} \right]$$

$$C^* = \frac{(1 \text{ m})(15400 \text{ kPa})}{0.75} \left[\frac{1.19 \text{ m}}{(2.76 \times 10^6 \text{ kPa})(.11 \text{m}^2/\text{m})} + \frac{4}{2\pi \ (35000 \text{kN/m}^2)} \right]$$

$$C^* = 0.382$$

Assuming the same values for the support elastic moduli, a compressiblitiy ratio of 0.382 can be thought of as corresponding to an equivalent support cross-sectional area (from Eq. 6.1):

$$(A_s)_{eq} = t_{eq} = \frac{ER(1-\nu_s^2)}{E_s C^*(1-\nu^2)} = 0.00227 \text{ m}^2/\text{m}$$

The seals clearly have a significant effect on the effective circumferential stiffness. In addition, since the joints between the precast concrete segments are unbolted, they have zero flexural rigidity. The flexibility ratio F* may therefore be taken as infinity.

The calculation of the support delay length L_d is

294

at first glance somewhat complicated by the presence of the TBM and shield at the face. Although the locations of the face and the leading support ring are known, the tunnel between these points is not unsupported. The TBM is going to restrain ground movements that ordinarily would mobilize the ground's shearing resistance and reduce the support loads. In fact, the TBM is so much stiffer than the soft clay that it will restrain effectively all radial ground displacements along its length. The magnitude of the radial displacement at the front of the TBM--i.e., at the face of the tunnel-- will be the same as at its tail (see Figure 6.11); therefore, L_d can simply be measured from the tail of the rigid TBM instead of from the face of the tunnel. The support ring immediately behind the tail of the TBM will not be the lead- ing "active" support element, however. The ground will deform behind this ring before it can be grouted after clearing the TBM tailpiece. The second support ring behind the TBM will thus be the first "active" (i.e., grouted) support element, and L_d will be as shown in Figure 6.11. For 1.37 m-long support segments, L_d will equal about 2 m.

There is one more complication at the rear of the TBM, though, and this one is more difficult to resolve. As men- tioned earlier, the measured surface settlements above the tunnel seemed to indicate that the grouting procedure was not effectively filling the tail void between the support elements and the ground. If this void is not filled complete-
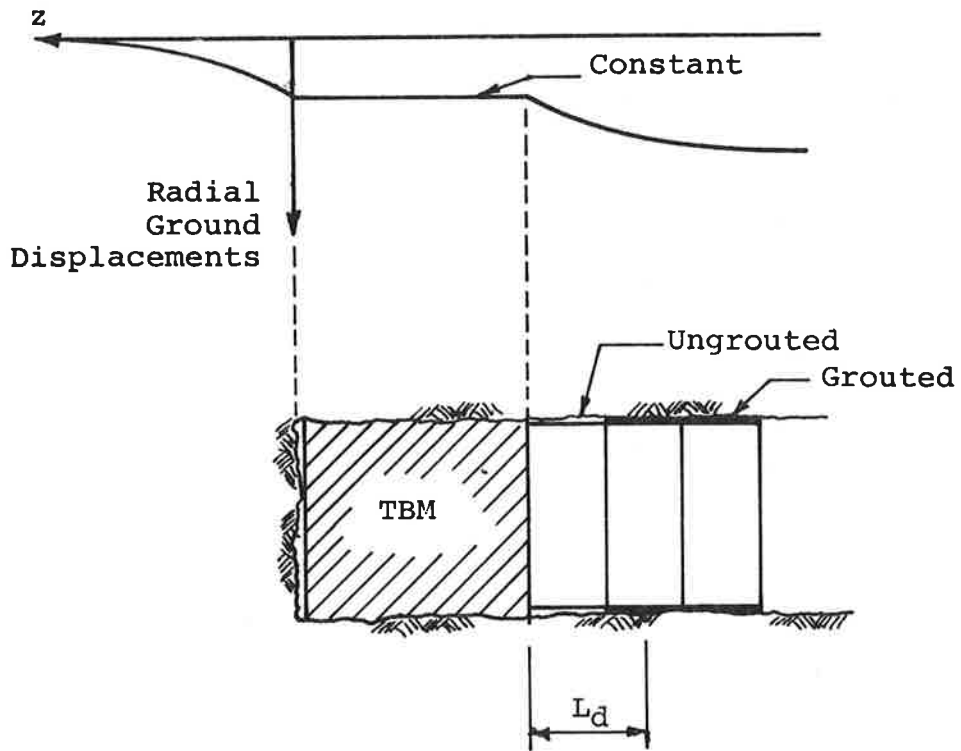
FIGURE 6.11.   SUPPORT DELAY LENGTH--THUNDER BAY SEWER

ly, it introduces another component of "pre-support" ground movements, u_o'. This component can easily be treated in the approximate analysis method, but to do so it must first be known quantitatively. Unfortunately, this is not the case. There is no information available about the degree of completeness of the grouting, except the observation that in some cases the surface settlements were so large that it appeared as if no grouting had been done at all. Hence, the only conclusions that can be drawn about u_o' are that it varies from 0 to 4.5 cm, the maximum thickness of the tail void, and that in some cases it is probably closer to the maximum value.

Instrumentation and Measured Support Loads

The radial support pressure was measured using a set of 12 total pressure cells. These cells were all located on one ring in the configuration illustrated in Figure 6.12a. Although four of these cells (numbers 6,7,8, and 11) were disabled for varying lengths of time during the monitoring program, the performance of the cells was generally quite good. The support pressures measured by these cells are summarized in Figure 6.12b. The average pressure acting on the support during the first month after construction was 87 kPa, which corresponds to a dimensionless thrust ratio $\frac{T}{PR}$ of 0.422. This pressure changed only slightly with time. Although the total pressure acting on the ring is not completely uniform, the variations are within $\pm$ 25% of the

297

(a) LOCATION OF PRESSURE CELLS AND STRESSMETER HOLES
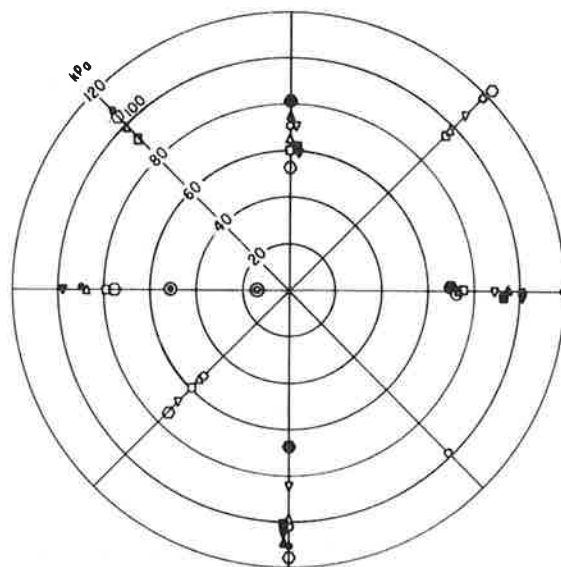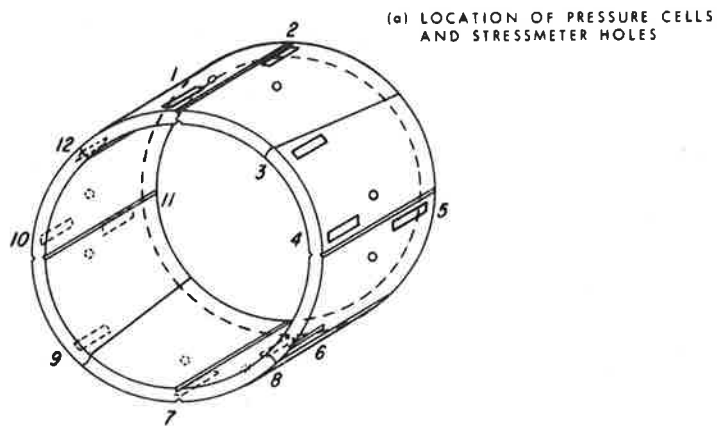
	INSTRUMENT NUMBER 1,3,4,6,7,9,10,12	INSTRUMENT NUMBER 2,5,8,11
APRIL 5/76	o	•
APRIL 12/76	Δ	▲
MAY 12/76	□	■
AUGUST 21/76	▽	▼
APRIL 7/77	O	●
WATER PRESSURE CENTER OF SEGMENT - MAY 10/76 —— ⊚		
- APRIL 7/77 —— ⊚		

b) Data from pressure cells located as shown in (a)

FIGURE 6.12.   MEASURED SUPPORT PRESSURES--THUNDER BAY SEWER (FROM BELSHAW AND PALMER, 1978)

298

average and the only consistent trend is a slightly lower pressure at the crown of the tunnel. A piezometer was also installed between the total pressure cells Nos. 10 and 11 to measure the pore pressure in the clay just behind the support. Five weeks after construction (May 10, 1976), the measured pore pressure of 51 kPa was approximately one-half of the in situ pressure, indicating that some partial drainage toward the tunnel had occurred; at one year after construction (April 7, 1977), this pore pressure had dropped to near zero.

In addition to the total support pressure, accurate measurements were made of the vertical surface settlements, the vertical and horizontal ground movements around the tunnel, and the tunnel convergence. As is expected for a tunnel in clay, the ground movements slowly increase with time as consolidation occurs; the surface settlements at the end of one year, for example, were nearly double the short-term values at the end of the first month. Since the approximate analysis method in its present form does not treat time-dependent (consolidation) ground behavior, it should therefore only be used to predict the short-term tunnel support loads during the first month after construction.

Predicted Support Loads

Given the input parameters described in the preceding sections, the calculation of the basic support thrust from the relative stiffness solution is straightforward; from

299

Eq. (6.3), $\frac{T}{PR} = 0.78$. The calculation of the support delay factor λ_d and the yield factor λ_y is somewhat more complicated, however, because the parameter $u_o{}'$ is not known precisely. Depending on how completely the tail void is grouted, $u_o{}'$ can range from 0 to 4.5 cm. For $u_o{}'$ equal to 0, there is no problem and the procedures described in Section 6.2 can be applied directly to calculate values of 0.022 for λ_d and 28.6 for λ_y. This latter value is very high and at first glance it seems to violate the restrictions on λ_y outlined in Section 6.2 (i.e., that λ_y must be less than about 2 for values of K much different from 1). However, this high value for λ_y can still be used in the simplified analysis of this case for the following two reasons. First, K for the Thunder Bay location is equal to 0.85; this value is sufficiently close to 1 that more yielding (i.e., higher λ_y) can be treated in the simplified analysis (see discussion in Section 6.2). And second, the reason that λ_y is so large is not so much because extensive yielding develops (the radius of the yielded zone for K=1 conditions would only equal 2.5 times the tunnel radius even if the tunnel were completely unsupported) but rather because λ_d is so small. This point was discussed at some length in the Kielder case study. Therefore, the high value for λ_y is acceptable. The simplified analysis gives a predicted thrust coefficient of 0.489, which is 16% larger than the measured value of 0.422.

Note that the Thunder Bay tunnel is very similar to the Kielder Experimental tunnel in that the round length is large relative to the tunnel diameter; thus the normalized support delay length L_d/R is large (in fact, $L_d/R = 2.0$ and is outside of the "safe" limits for Eq. 6.5) and λ_d is near zero. This problem becomes even worse when u_o' equals its extreme value of 4.5 cm. Here λ_d does equal its physical lower limit of zero, and only an upper bound estimate for the support thrust can be determined. Using the derivation presented in the section on the Kielder tunnel, the upper bound estimate for the support thrust coefficient in this case is calculated to equal 0.475, a value 12% greater than the measured thrust coefficient of 0.422.

6.3.4   Tyne Sewer

This 3.20 m O.D. tunnel, constructed in 1976, forms part of the Northumbrian Water Authority's Tyneside Sewage Scheme along the River Tyne in northern England. Very careful measurements of support pressures and displacements were made at two sites along this tunnel in an effort to determine the length of time required for the loads on the primary support to stabilize preparatory to construction of the secondary liner. Details on the tunneling conditions and the measurement program are given by Attewell and El-Naga (1977).

Ground Description

Very little information is provided on the subsurface conditions for this tunnel. Attewell and El-Naga state that the ground at both sites consists of a "stiff stony clay and laminated clay" with the following geotechnical properties:

Material	Unit Weight (Mg/m^3)	Liquid Limit (%)	Plastic Limit (%)	Moisture Content (%)	Undrained Shear Strength s_u (kPa)
Laminated Clay	2.03	63	30	27	89
Stony Clay	2.25	36	18	12	206

No subsurface profile was provided for this case study, so the locations of the different strata relative to the tunnel

and the percentages of each type of clay in the deposit are unknown. Consequently, the overall undrained shear strength for the analysis is taken as the simple average of the values in the table, i.e., s_u = 148kPa.

The undrained elastic modulus for this clay can be approximately determined from test data for other, similar clays. As previously described in the Thunder Bay case study, the E vs. $\bar{\sigma}_c$ relationships given in Figures 30.5 and 30.6 of Lambe and Whitman's (1969) textbook can be used for this purpose once the stresses around the tunnel have been established. The total vertical stress at the axis of the tunnel, 13.6 m below the ground surface, is (13.6 m) (21.0 kN/m^3) = 286 kPa. Although the elevation of the water table is not given, extrapolating the subsurface profile for the nearby Tyne Siphon tunnel (Attewell, et al. 1976) suggests that the sewer tunnel is approximately at the level of the adjacent Wear river. Therefore, the in situ pore pressures around the tunnel will be relatively low; they are considered to be negligible for the purposes of this analysis. Assuming the clay is normally consolidated, the effective consolidation stress $\bar{\sigma}_c$ then equals the total overburden stress P, or 286 kPa. For s_u = 148 kPa and σ_u = 296 kPa, the "first-yield" index equals $\frac{1}{2}$(2 - 296 kPa/286 kPa) or FY = 0.483. A value of FY this low implies that little or no yielding will develop in the clay surrounding the tunnel; the overall "factor of safety"

303

will therefore be relatively high, perhaps between 2 and 3, and the charts in Lambe and Whitman specify that the undrained modulus will be approximately equal to 200 - 250 $\bar{\sigma}_c$. A value of 64000 kPa is selected for the undrained modulus, and Poisson's ratio is assumed equal to 0.5.

Because of the imperviousness of the clay deposit and the short time interval between excavation of the tunnel and measurement of the support loads, the behavior of the ground around the tunnel can be treated as essentially undrained. Thus, there is no need for any drained properties for the clay.

The total in situ vertical ground stress has already been calculated above as 286 kPa. For the assumed normally consolidated state of the clay deposit, the lateral stress ratio K can be reasonably taken as 0.5. The water conditions are not a problem in this tunnel, due both to the imperviousness of the clay stratum and the location of the tunnel at the top of the water table (i.e., at river level).

Excavation and Support

The 3.20 m O.D. Tyne sewer was hand excavated in free air and supported with bolted, precast concrete segments 61 cm. long. Based on partial sketches of the liner segments in Attewell and El-Naga's paper, the support cross-section illustrated in Figure 6.13 was assumed for the analyses; the support properties are A_s = 0.0664 m^2/m,

304

Precast Concrete

E_s = 27.6 GPa

ν_s = 0.15
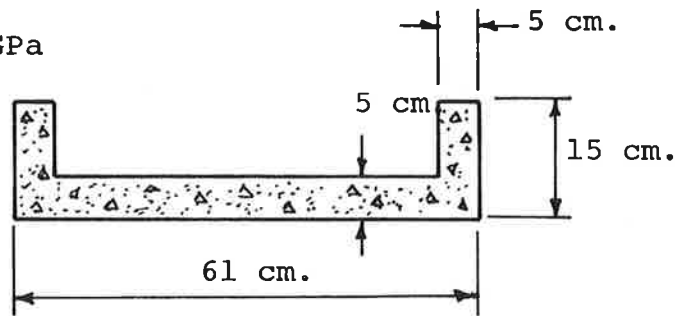
FIGURE 6.13.   SUPPORT CROSS-SECTION--TYNE SEWER.

$I_s = 9.35 \times 10^{-5} \ m^4/m$, $E_s = 2.76 \times 10^7$ kPa, and $\nu_s = 0.15$, producing values of $C^* = 0.0728$ and $F^* = 132.0$. The value F^* is an upper bound value based on the assumption that the bolted joints between segments are perfectly rigid.

Because of the absence of a shield, the support rings were erected tight up to the tunnel face. This was done for two reasons: (1) to minimize the yielding and local instability that might develop in the clay if left unsupported for too long, and (2) to enable the researchers to install their instrumentation and begin measurement as soon as possible after excavation. Very careful construction procedures were employed in this tunnel in order to insure high quality input data from the instruments. The support delay parameters are: $L_d = 0.92$ m, $L_d/R = 0.57$ m, and $u_o' = 0$.

Instrumentation and Measured Support Loads

The radial support pressure was measured using a set of 6 total pressure cells on each of the two instrumented rings. The arrangement of these cells is shown in Figure 6.14a. The development of the radial support pressure with time and its distribution around the support circumference are shown in Figures 6.14b and 6.14c for Site 2; Site 1 gave essentially the same data. The radial support pressure increased rapidly with time, reaching a stable maximum value at 7 - 8 days after erection, and it was uniform around the circumference. The final thrust in the support was 152kN/m

306
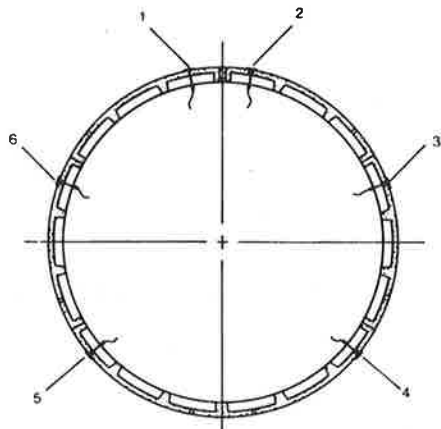
a) Location of cells in the tunnel lining
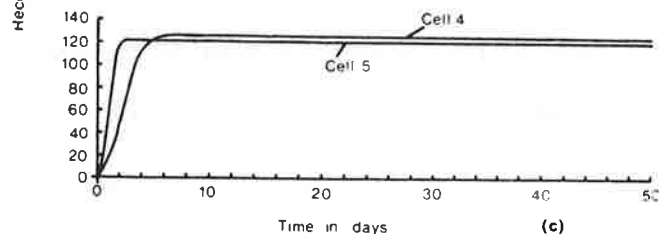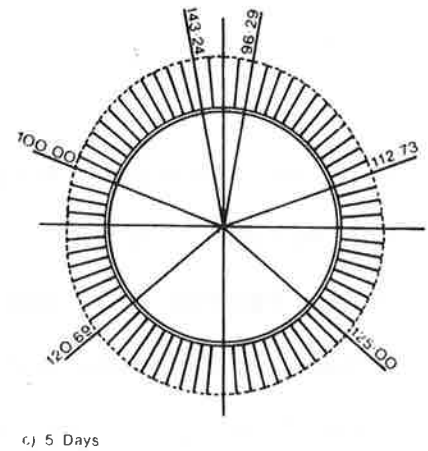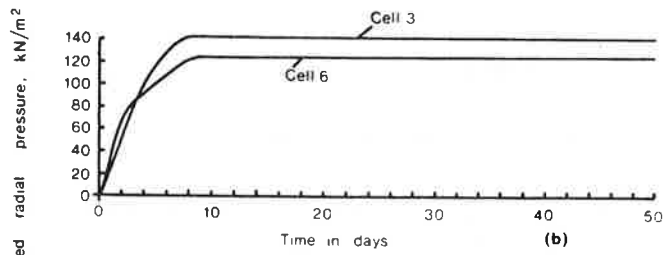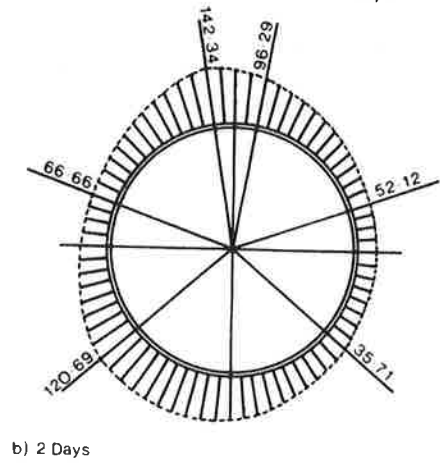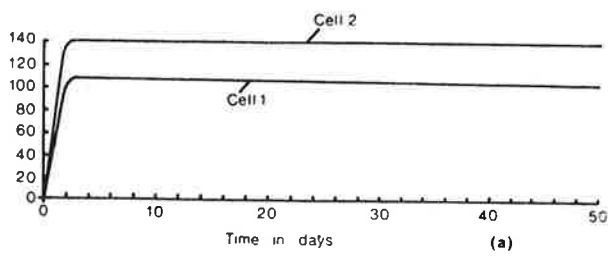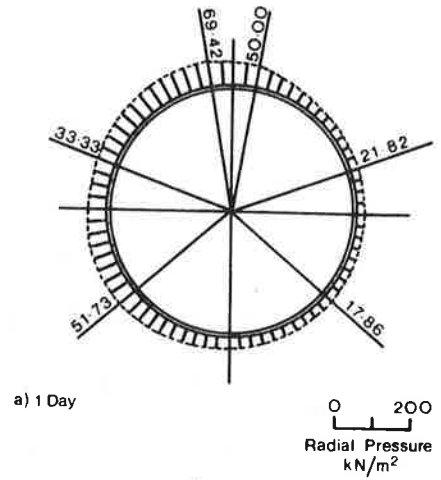
b) Development of radial pressure with time—second test site

a) 1 Day

0   200
Radial Pressure
kN/m²

b) 2 Days

c) 5 Days

c) Distribution of radial pressure around support

FIGURE 6.14.   MEASURED SUPPORT PRESSURES--TYNE SEWER (FROM ATTEWELL AND EL-NAGA, 1977)

307

for Site 1 and 2·02kN/m for Site 2, giving an average thrust of 177 kN/m ($\frac{T}{PR}$ = 0.387) for both.

In addition to the support loads, the diameter changes of the tunnel were precisely measured. These measurements were on the order of a millimeter, with the vertical diameter shortening and the horizontal diameter lengthening as the tunnel "squatted" into the characteristic elliptical shape for K < 1 conditions.

Predicted Support Loads

The input parameters for the simplified analysis method are summarized in Table 6.2. Since Sites 1 and 2 have the same ground and support properties, they have been combined in the analysis. The "basic" support thrust coefficients from the full-slip relative stiffness solution equal 0.734 at the springline and 0.713 at the crown, or an average value of 0.724. (The "basic" moment coefficients were very small, equal to 0.0104 at both the springline and crown). A value of 0.66 was calculated for the support delay factor λ_d. Because of the stiff support and the short delay, the ground surrounding the tunnel does not yield; therefore, λ_y = 1. The final predicted thrust coefficient is 0.478, which is 24% larger than the measured coefficient of 0.387 (average of sites 1 and 2).

308

6.3.5 Victoria Line

The Victoria Line, built in the early 1960's as a
major extension of the London underground railway system,
consists of twin 3.81 m I.D. machine-excavated tunnels in
the stiff clay deposits underlying the city. Examined in
this case study is an experimental tunnel section in which
two novel types of unbolted, expanded precast concrete and
cast iron segmented liners were installed and instrumented.
Details on the measured support loads are given by Ward and
Thomas (1965); background information on the project and the
tunnel designs is provided in papers by Dunton, Kell, and
Morgan (1965) and by Morgan and Bartlett (1969).

Ground Description

The tunnels lie in a thick deposit of London clay at
centerline depths of about 26.1 m for the cast iron section
and 27.9 m for the precast concrete length. The London clay,
a stiff, laminated, fissured, and heavily overconsolidated
deposit, has been extensively tested by many British soils
engineers. Ward, Samuels, and Butler (1959) and Ward,
Marsland and Samuels (1965) have performed a very large
number of unconsolidated undrained triaxial tests on relatively
undisturbed specimens taken from large block samples at
various locations around London; Bishop, Webb, and Lewin (1965)
have performed the corresponding drained tests. The principal
findings from the undrained investigations were that, because
of the horizontal laminations in the deposit, the elastic

309

modulus (E) in the horizontal direction is 1.6 times the vertical modulus, on the average, and the undrained shear strength (s_u) for loads applied parallel to the laminations is about 1.3 times the strength for loads applied perpendicularly. For the simplified analysis, however, only the average E and s_u are required; based on the combined test data for vertically and horizontally oriented specimens taken from the approximate depth of the Victoria Line tunnels, $(E)_{avg.}$ = 86.3 MPa and $(s_u)_{avg.}$ = 317 kPa. The value for the undrained modulus is also consistent with data from in situ plate loading tests reported by Ward, Marsland, and Samuels (1965). A Poisson's ratio of 0.4 was assumed for the analysis.

There is one problem in applying the simplified analysis method to tunnels in the London clay deposit. The London clay swells upon unloading, and, as will be shown later, this swelling causes a significant increase in the tunnel support loads with time. The simplified analysis in its present form cannot treat this time-dependent behavior; it can, however, be used to calculate the short-term loads up to a few weeks after construction, before the swelling becomes important. For this purpose, only the undrained modulus and undraind shear strength are needed in the analysis.

Assuming a total unit weight of 19.6 kN/m^3 for the clay, the total in situ vertical stress at the axis of the concrete section is:

$$P = (27.9 \text{ m})(19.6 \text{ kN/m}^3) = 548 \text{ kPa}$$

and for the cast iron section:

$$P = (26.1 \text{ m})(19.6 \text{ kN/m}^3) = 512 \text{ kPa}$$

Although it is known that the groundwater table is near the surface, the variation of the water pressure with depth is not. If these pressures are assumed hydrostatic, though, the in situ pore pressure at the level of the tunnels will equal 274 kPa for the concrete lined section and 256 kPa for the cast iron length. Bishop, Webb, and Lewin (1965) report a value of 2.0 for the lateral stress ratio, K, in terms of effective stresses; in terms of total stresses, this corresponds to a value of 1.5 for K.

Excavation and Support

The Victoria Line tunnels were machine-excavated full-face in free air using a digger shield (see Figure 6.15). Tunnel support was provided either by precast concrete or cast iron segments that were expanded (using jacks or wedges) as soon as they cleared the tail of the shield. Expanded liners were used in order to take better advantage of the high excavation speed of the digger shield; the liner could be built directly against the clay and held in place by the jacking prestress, thereby eliminating the time-consuming tasks of grouting and bolting (Morgan and Bartlett, 1969).

The support properties for the two sections of the Victoria Line are summarized by Ward and Thomas (1965):

311

CUTTING BEAD

B

A

2'-8"
STROKE

PRESSURE GAUGE
FOR RAMS

DRUM PADDLES

7'-6"

DRUM CONTROL
VALVE

RAM OPERATING
VALVES

13'-1" DIA.

REMOVABLE TINES

SECTION C.C.

PROVISION FOR BOLTING
ON TAIL PLATE

B

8'-11¼" ⅝" THICK SKIN PLATE

A

4"

9'-8¼"

5"

"DRUM DIGGER" SHIELD OF 13'-1" EXTERNAL DIAMETER.
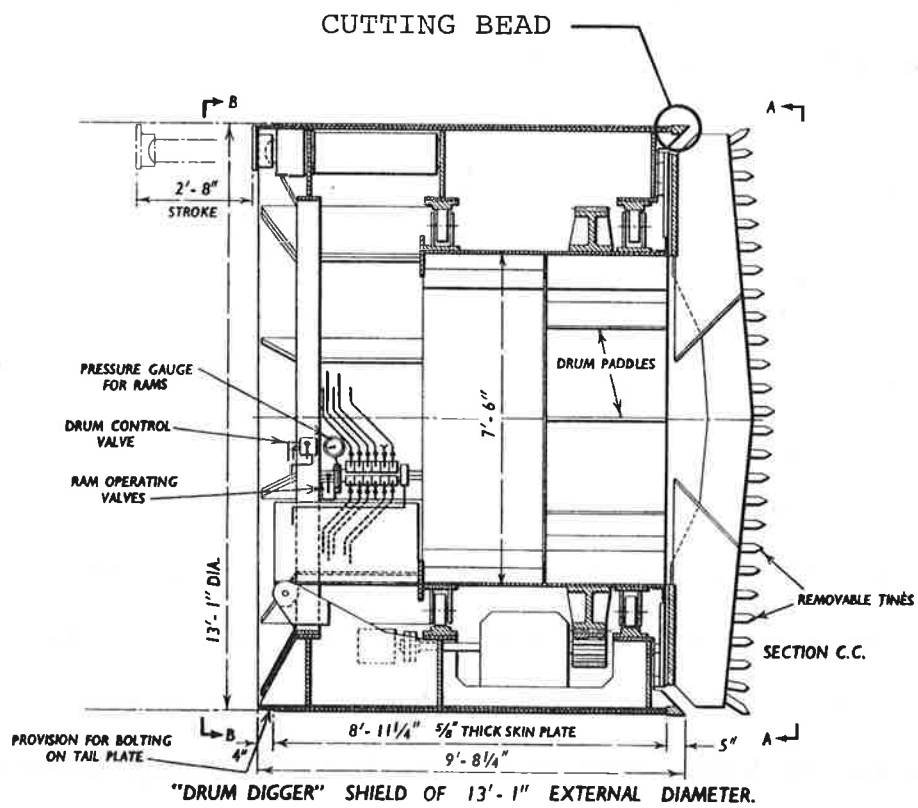
FIGURE 6.15.   DIGGER SHIELD FOR THE VICTORIA LINE TUNNELS
(FROM THE ENGINEER, 1961)

Section	O.R.	Area A_s	Young's Modulus E_s	Circumferential Jacking Force T_j
Concrete	2.13 m	$0.221 m^2/m$	38.0 GPa	294 kN/m
Cast Iron	1.98	0.0286	96.6	196

The support rings are 0.61 m long in both cases. Using values of $\nu_s = 0.15$ for concrete and $\nu_s = 0.25$ for cast iron, the respective values for the compressibility ratio C^* are 0.0225 and 0.0691. Since the joints between the segments are unbolted, the flexibility ratio F^* is infinite.

Using the same reasoning as in the Thunder Bay case study, the support delay length L_d is measured from the tail of the rigid shield instead of from the face of the tunnel. The longest value for L_d occurs just after the shield has advanced a full round but before the new support ring is erected and expanded (similar to the situation depicted in Figure 6.11); L_d therefore equals 1.5 times the ring length, or 0.92 m.

In this case study, there are two components of u_o', the additional ground movements that occur prior to support. The first of these is the ground movement behind the cutting bead at the leading edge of the digger shield. As shown in Figure 6.15, this cutting bead projects beyond the main body of the shield; as the shield is shoved through the clay deposit, a small void forms behind the bead, permitting some small radial movements in the ground. Although no dimensions are given in any of the published reports for the size of

313

this void, the roughly scale drawing in Figure 6.15 suggests values of about $\frac{1}{2} - \frac{5}{8}$ inches (1.27 - 1.59 cm) for this component of u_o'.

The second component of u_o' is actually a negative displacement caused by the expansion of the precast concrete and cast iron segments during erection. This component can be determined, at least approximately, with the aid of the characteristic curves shown in Figure 6.16a. After excavation but before erection and expansion of the support, a total radial ground displacement equal to $(u_o)_A$ has occurred; $(u_o)_A$ consists of the displacements due to the support delay and the displacements due to the void behind the cutting bead on the shield. At $(u_o)_A$, the ground is assumed to be partially yielded--i.e., the ground characteristic curve is nonlinear at $(u_o)_A$. The effect of the erection and expansion of the support is to cause a partial _reloading_ of the ground mass. The initially unstressed support is installed at point F in Figure 6.16a; as the support is then expanded, the jacking pressure P_j causes an elastic reloading of the ground along curve AB in the figure that reduces the ground displacements from $(u_o)_A$ to $(u_o)_B$. Just after expansion of the support, then, the ground is at point B, with an internal pressure of P_B and a displacement of $(u_o)_B$, and the support is at point C, with an internal pressure P_j (the jacking pressure) and the same displacement $(u_o)_B$. It is assumed that point C, which represents the shifted origin of the support charac-

314
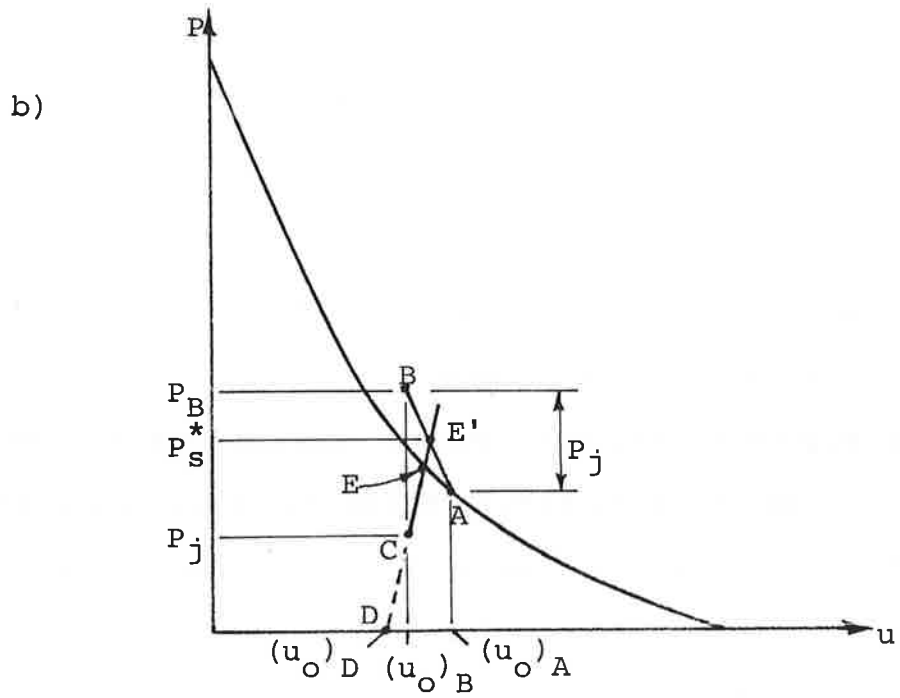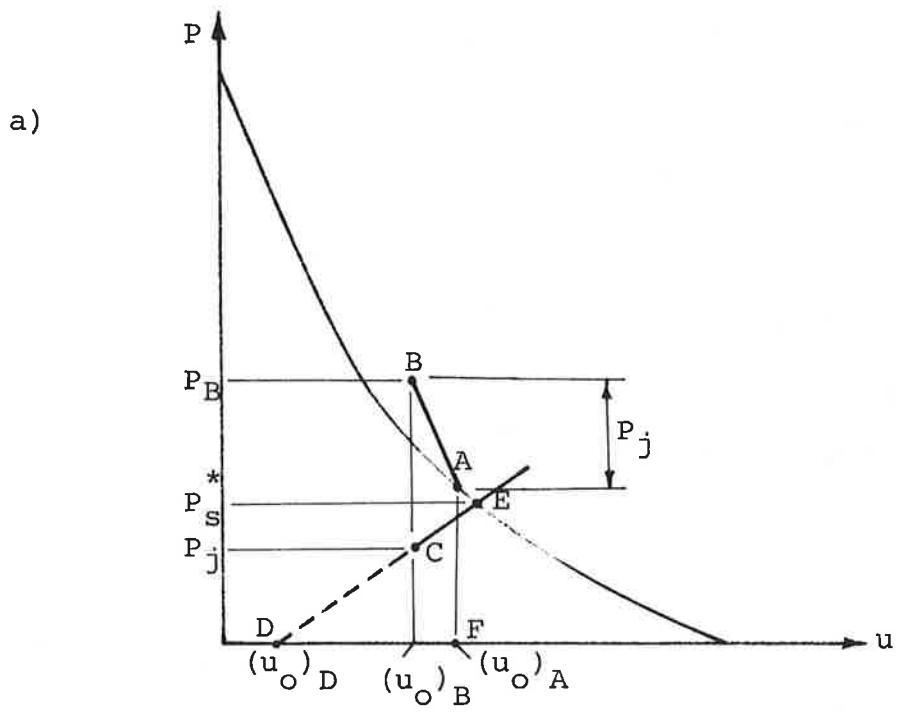
FIGURE 6.16.   ANALYSIS OF EXPANDED SEGMENTED LINERS

315

teristic curve, lies below the ground characteristic curve; this assumption is reasonable as long as the support delay is not excessive and the jacking pressure is small. The pressure differential between points B and C represents the effects of the partial support provided by the shield and by the ground mass ahead of the face. As the tunnel is advanced further, the effect diminishes and the pressure differential decreases; the ground and support proceed along their characteristic curves in the standard way until they cross at point E, the equilibrium point.

It is clear from Figure 6.16a that, if the support characteristic curve is extended back from its shifted origin at point C until it crosses the horizontal axis at point D, the resulting offset $(u_o)_D$ is the value that should be used in the simplified analysis. Everything else in the analysis remains unchanged; the support curve will rise from point D and cross the ground curve at the equilibrium point E as the ground unloads from point B through point A.

If the support curve crosses the ground curve above point A in Figure 6.16a, the problem becomes somewhat more complicated. As shown in Figure 6.16b for this case, the true equilibrium point will be at E' on the elastic reload-unload curve; however, the analysis outlined above would predict point E at equilibrium. Calculating the true equilibrium point E' is difficult and requires analysis beyond that in the simplified method. Fortunately, though, in most

316

practical tunneling situations the jacking pressure P_j will
be relatively small, and therefore the elastic reload-unload
curve AB will be short and the difference between E' and E
will be insignificant.

The calculation of the support curve offset $(u_o)_D$ in
Figure 6.16a is straightforward. The jacking pressure P_j is
calculated from the circumferential jacking thrust T_j (given
by Ward and Thomas, 1965--see table above) as:

$$P_j = \frac{T_j}{R} \qquad \text{(a)}$$

The radial displacement of a cylindrical hole subjected to
an internal pressure is given as (see Jaeger and Cook, 1976,
for example):

$$u = \frac{PR(1+\nu)}{E} \qquad \text{(b)}$$

Therefore, the radial expansion of the ground mass caused by
the jacking pressure is:

$$(u_o)_A - (u_o)_B = \frac{P_j R(1+\nu)}{E} \qquad \text{(c)}$$

The radial displacement of the support due to a radial pres-
sure is given as (see Appendix A, Eq. A.2):

$$u = \frac{PR(1-\nu_s^2)}{E_s A_s} \qquad \text{(d)}$$

Therefore, the offset component $(u_o)_B - (u_o)_D$ corresponding to
the projection of the support curve at point C back to the
horizontal axis at point D (see Figure 6.16) is:

317

$$(u_o)_B - (u_o)_D = \frac{P_j R (1-\nu_s^2)}{E_s A_s} \qquad (e)$$

From (c) and (e), then, the total negative offset due to the expansion of the support is:

$$(u_o)_A - (u_o)_D = P_j R \left[\frac{(1+\nu)}{E} + \frac{(1-\nu_s^2)}{E_s A_s} \right] \qquad (f)$$

For the concrete supports, P_j = 138 kPa and $(u_o)_A - (u_o)_D$ = 0.48 cm; for the cast iron support, P_j = 99.4 kPa and $(u_o)_A - (u_o)_D$ = 0.32 cm. These second components of u_o' must be subtracted from the first component caused by the cutting bead on the shield. Since this first component was determined to range from about 1.27 cm to 1.59 cm, subtracting the second component gives total values for u_o' ranging from 0.79 to 1.11 cm for the concrete lined tunnel and from 0.95 to 1.27 cm for the cast iron supported section.

Instrumentation and Measured Loads

The loads on the supports in the two tunnel sections were measured using sets of vibrating wire strain gauges spaced equally around the circumference. Figure 6.17 summarizes the observed average support stresses (or strains) with time for the concrete and cast iron supports. The increase in the support loads with time as the London clay swells is striking; the compressive stresses in the cast iron doubled during the first 40 months after construction, while the strains in the concrete tripled during the first
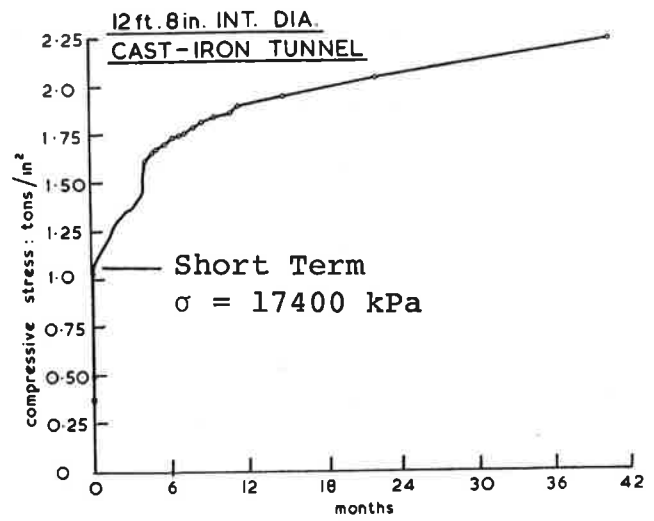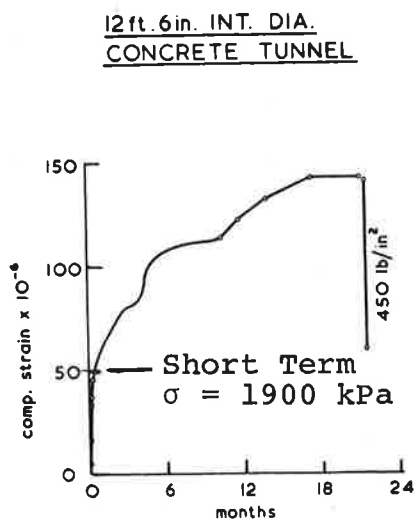
FIGURE 6.17.   MEASURED SUPPORT LOADS--VICTORIA LINE (FROM
WARD AND THOMAS, 1965)

20 months (some of this increase is due to shrinkage and creep of the concrete). Although the simplified analysis method cannot predict these increases in load with time, it can predict the short-term loads within the first few weeks after construction, before swelling becomes significant. The short term loads at approximately two weeks after construction are indicated in Figure 6.17; they correspond to average thrust coefficients of 0.359 for the concrete lined tunnel and 0.490 for the cast iron supported section.

The diametral convergence of the supports was also measured in these two tunnel sections. In both tunnels, the horizontal diameter lengthened by approximately 1.25 cm and the vertical diameter shortened by roughly the same amount. Note that these diameter changes are just the opposite of what would be expected if the ground behaved linearly elastically; for K > 1, the horizontal axis should shorten and the vertical diameter lengthen. Ward and Thomas hypothesize that the observed deformations are largely the result of the fact that the swelling is more agressive across the horizontal laminations of the London clay than it is parallel to them.

Predicted Support Loads

The input parameters required for the simplified analysis are summarized in Table 6.2. Following the procedure outlined in Section 6.2, the "basic" thrust coefficient calculated from the full-slip relative stiffness solution equals an average value of 1.23 for the concrete liner and 1.20 for the cast

320

iron support. This "basic" thrust coefficient is greater than 1 because of the large value for the lateral stress ratio. Since the exact dimensions of the cutting bead on the shield are not known, only a range of values can be given for u_o'; the support delay factor λ_d therefore varies between 0.317 and 0.150 for the concrete lined tunnel and between 0.140 and 0 for the cast iron section. A yield factor ranging from 1.03 to 1.34 for the concrete section leads to final values for the predicted thrust of from 0.401 to 0.247; this represents an error of +12% to -31% relative to the measured coefficient of 0.359. In the cast iron supported tunnel, the extreme of $\lambda_d = 0.140$ leads to a value of 1.29 for λ_y and a predicted thrust coefficient of 0.216, which is 56% lower than the measured value of 0.490; for $\lambda_d = 0$, λ_y is undefined and the method outlined in the Kielder case study leads to an upper bound prediction for the support thrust coefficient of 0.104, which is 79% lower than the thrust measured in the tunnel. These values for the predicted and measured support loads are all summarized in Table 6.5.

6.4 CONCLUSIONS FROM THE CASE STUDIES

The comparisons of the predicted and measured average thrust coefficients for the five cases are summarized in Table 6.5. A total of eleven tunnel sections were analyzed using the simplified method. Also listed in the table are the values for the three primary variables in the analysis. The first of these variables, the "basic" support thrust, $\left[\frac{T}{PR}\right]_{Basic}$, is the thrust coefficient calculated from the relative stiffness solution (Section 2). Since only the average support thrust could be determined from the measurements in many of the case studies, this "basic" thrust is accordingly the average of the calculated thrust values around the ring. For many of the flexible supports in the case studies, however, the calculated thrust is constant around the support (for full-slip conditions) and equal to the average value. The other two fundamental variables in Table 6.5 are the support delay correction factor, λ_d, and the ground yield correction factor, λ_y. These three variables are all multiplied to give the predicted average thrust coefficient, $\left[\frac{T}{PR}\right]_{Predicted}$. As just mentioned, the measured thrust coefficient, $\left[\frac{T}{PR}\right]_{Measured}$, in Table 6.5 corresponds to the average thrust around the circumference of the support. This measured thrust also represents only the short-term component of the support load, generally within the first few weeks after construction. In some of the cases (the Victoria Line, in particular) the support loads were observed

322

TABLE 6.5.   COMPARISONS OF PREDICATED AND MEASURED AVERAGE THRUST COEFFICIENT

Case	Section	$\left[\frac{T}{PR}\right]$ Basic	λ_d	λ_y	$\left[\frac{T}{PR}\right]$ Predicted	$\left[\frac{T}{PR}\right]$ Measured	Error (%)
Garrison Dam	4A	0.410	0.41	1.24	0.208	0.132	58
	4B$_1$	0.030	0.41	4.95	0.061	0.052	17
	4B$_2$	0.033	0.41	4.66	0.063	0.039	62
	2B,F	0.106	0.22	4.33	0.101	0.078	29
	2E	0.123	0.31	2.95	0.112	0.132	-15
	5A – E	0.140	0.41	2.21	0.127	0.115	10
Kielder Experimental	-	0.464	0	—[1]	0.227[2]	0.162	40
Thunder Bay	-	0.714	0.022 – 0	28.6 – —[1]	0.489 – 0.475[2]	0.422	16 to 12
Tyne	Sites 1 & 2	0.724	0.66	1.00	0.478	0.387	24
Victoria Line	Concrete	1.23	0.32-0.15	1.03 – 1.34	0.401 – 0.247	0.359	+12to –31
	Cast Iron	1.20	0.14 – 0	1.29 – —[1]	0.216 – 0.104	0.490	-56 to -79

Notes

1. λ_y is undefined because λ_d = 0

2. Upper bound for long support delay condition

323

to increase with time due to creep, consolidation and/or swelling of the ground mass; the simplified analysis in its present form cannot predict this time-dependent component of the support loads. Lastly, the percentage errors of the predicted thrusts relative to the measured thrusts are presented in the table.

Two sets of questions must be answered when evaluating the simplified analysis method: (1) How easily can it be applied to realistic tunneling situations, and where do any difficulties arise? and (2) How accurate are its predictions, and how accurate do they need to be? Each of these questions will be answered in turn.

6.4.1 Ease of Application of the Method

For the majority of the tunnel sections treated in the case studies, the application of the simplified analysis method was relatively straightforward. It is not too difficult to get rough estimates for the ground properties, the in situ stress levels, and the support geometry. It is, however, somewhat more difficult to get sufficiently precise estimates for the support delay parameters (L_d and u_o'). The values of these parameters usually depend upon very small construction details like the grouting procedure, the size of the cutting bead and tail void on the shield (if used), and the jacking forces during the erection of expanded liner segments (if used). Nevertheless, even in the difficult

324

cases where very few details of the construction method are known, a reasonable range can be estimated for the input parameters and the simplified analysis method can still be applied.

There is only one area in which problems were encountered in the case studies. In the small to moderate diameter tunnels with long round lengths and support delays, λ_d approached or equalled zero, λ_y became very large or undefined, and the simplified analysis could not be applied directly. This was a problem primarily in the Kielder tunnel, although it also occured for certain bracketing conditions in the Thunder Bay and Victoria Line cases. In the other eight tunnel sections studies, this problem did not arise and the calculations of the support thrusts were straightforward. However, even in the cases where this problem did occur, the basic principles underlying the simplified analysis could still be used to calculate an approximate upper bound for the support load (see the Kielder case study, in particular). In most practical tunneling situations, though, the method can be applied directly without these difficulties.

The only limitation on the application of the simplified analysis to actual designs is that in its present form it cannot be used to predict any time-dependent increase in loads (as in the Victoria Line case, for example); in these instances it can only be used to compute the short-term loads

for the first few weeks after construction. If there are
no variations of the ground and support properties with
time, the short-term loads are naturally equal to the long-
term loads and the simplified method can then be used to
predict the final design.

6.4.2 Accuracy of the Simplified Analysis

As shown in Table 6.5, the errors in the predicted
support thrusts ranged between the extremes of -79% (uncon-
servative) and +62% (conservative). However, for 7 of the
11 tunnel sections analyzed, the errors varied between the
more limited bounds of +30%. The average error for all of
the cases is about +15%, and the standard deviation of the
errors is approximately 35 percentage points. On the whole,
there is a slight conservative bias in the predictions,
meaning that the simplified analysis tends to overestimate
the tunnel support loads.

Although this low average error substantiates the
overall accuracy of the simplified analysis, the relatively
large standard deviation implies that the precision of the
predictions is not high--i.e., the method can predict the
support loads only to within a fairly large tolerance.
Nevertheless, with an appropriate factor of safety, both
the accuracy and the precision of the simplified analysis
should be sufficient for design. For example, if it is
assumed that the errors in Table 6.5 are due entirely to

326

the simplifications in the analysis and that these errors are normally distributed with a mean and standard deviation as given above, then a value of 2 for the factor of safety would reduce the probability of an unconservative analysis to less than 4 percent.

Any way of looking at the errors leads to the conclusion that the simplified analysis method is surprisingly accurate, considering its approximate approach to the tunneling problem. Average errors of 15% are certainly comparable to the accuracy of many other types of analytical techniques in geotechnical engineering, and they are certainly lower than the errors in most other types of tunnel design methods. Although the standard deviation of the errors is high, this is only to be expected in view of the large variability inherent in the real tunneling situation. Naturally, these conclusions regarding the accuracy of the simplified method must be tempered somewhat by the fact that only a very limited number of cases were investigated. Nevertheless, although the precise numbers for the average errors may change, it is doubtful that additional case studies will drastically alter the overall conclusions.

7. SUMMARY, CONCLUSIONS, AND
RECOMMENDATIONS FOR FURTHER RESEARCH

A simple, design-oriented analysis method has been
developed for determining the loads for tunnel supports.
It is generally intended for circular tunnels with closed-
ring primary support systems in ground masses that can
for practical purposes be treated as time-independent
continua. The method is also restricted to tunnels that
are excavated full-face under free air at depths greater
than about two tunnel diameters. Examples of practical
tunneling situations suitable for analysis using the simpli-
fied method include--but are not limited to--circular steel
ribs, prefabricated segmented liners, and continuous shot-
crete supports in soil, heavily jointed rock, and massive
rock formations.

It is doubtful that the complex interrelationships
among the nearly countless variables in any real tunneling
problem can ever be rigorously analyzed, even using the
most sophisticated numerical techniques. As an alternative
approach, the simplified method focuses on the essential
elements of very complicated physical phenomena in order
to isolate the few major factors that have an overriding
influence on the support loads. The three major factors
explicitly considered in the simplified method are: (1) the

329

relative stiffnesses of the support and the ground mass,
(2) the spatial lag or delay of support construction behind
the tunnel face, and (3) the yielding of the ground mass as
its shear strength is exceeded. The effects of each of these
variables on the support loads were investigated in detail,
using both closed-form analytical derivations and finite ele-
ment numerical solutions.

Decreasing the relative support stiffness leads to a
reduction of the loads that are "attracted" to it. A
closed-form, plane strain elastic solution was developed
in Section 2 that quantitatively relates the circumferential
support thrusts, the bending moments, and the support dis-
placements to the relative support stiffness. This deriva-
tion incorporates the correct "excavation unloading" con-
dition for tunnels. In the solution, the relative support
stiffness is quantified by two dimensionless ratios: the
compressibility ratio C^*, which is a measure of the circum-
ferential stifness of the ground-support system, and the flex-
ibility ratio F^*, a measure of the "flexural" stiffness of the
system. For practical combinations of ground and support
stiffnesses, it was found that the support thrust is sensi-
tive to variations in the compressibility ratio and that the
overall support moments are usually quite small.

Increasing the support delay decreases the tunnel
support loads, at least for the simple ground behavior
models considered here. The influence of support delay in

330

elastic ground masses was investigated in Section 3 using axisymetric finite element techniques that simulated the step-by-step construction of an advancing tunnel. From the results of these investigations, a support delay correction factor λ_d was determined. This multiplicative correction factor, which ranges from 1 (no support delay) to 0 (full delay), is used to modify the "basic" support forces calculated from the relative stiffness solution (Section 2). An approximate, plane strain solution was also derived to investigate the effects of support delay for nonaxisymmetric (i.e., $K \neq 1$, K = lateral stress ratio) in situ stress conditions; the conclusions from this solution and the finite element studies are that λ_d is essentially the same for both thrusts and moments, and that it is essentially independent of K, C^*, and F^*.

Yielding in the ground mass surrounding the tunnel tends to increase the support loads. The effects of yielding were qualitatively described in Section 4, and some analytical formulations for the nonlinear behavior of the yielding ground mass were summarized. The combined effects of ground yielding, support delay, and relative support stiffness were quantitatively investigated in Section 5 using axisymmetric elasto-plastic finite element techniques. Based on these studies, a ground yield correction factor λ_y was derived. This factor represents the increase in

support load in the yielding ground case over that for an equivalent tunnel in an elastic ground mass. The effects of nonaxisymmetric ($K \neq 1$) in situ stress conditions on the ground yielding were also investigated; a limited set of plane stress elasto-plastic finite element parametric analyses led to the conclusion that λ_y is reasonably indepen- dent of K provided K is not significantly different from 1 (i.e., $0.5 < K < 1.5$) and the level of yielding is not too large (i.e., $\lambda_y < 2$ at extreme values of K).

The derivation of the yield factor λ_y represents the final step in the development of the simplified method. The method (which has been more completely summarized in Sections 6.1 and 6.2) states that the thrust T* in a tunnel support can be calculated as:

$$T^* = \lambda_y \lambda_d \ T \qquad\qquad (7.1)$$

in which T is the "basic" thrust calculated from the relative stiffness solution (Section 2), λ_d is the support delay correction factor (Section 3), and λ_y is the ground yield correction factor (Section 5). The support thrusts cal- culated from Eq. (7.1) were compared with those calculated from the axisymmetric elasto-plastic finite element analyses in Section 5; the similarity of the results from the two approaches is acceptable, with the average difference in the loads calculated by the two techniques less than 20 percent.

In order to verify the accuracy of the simplified

332

analysis method, it was applied to five tunnel projects
(a total of 11 tunnel sections) reported in the literature
in which the actual support loads were measured during con-
struction. These cases span a representative range of
tunneling situations for which the simplified analysis is
applicable. Two of the case studies are tunnels in soft
rock and three are in soil (various types of clay). The
supports in the case studies include steel ribs, precast
concrete segments, and cast iron segments; several hand and
machine excavation systems are also represented.

Since the simplified method requires so few input
parameters, its application to the case studies was quite
straightforward. The published accounts of the cases
generally gave enough information that most of the parameters
could be determined with reasonable precision, and ranges
of values could be estimated for the rest. However, the
application of any approximate technique like this method
requires some care and judgment; the second purpose of the
case studies is to provide examples of how this judgment
should be exercised.

Given the streamlined, approximate nature of the method,
it was surprisingly accurate in predicting the support loads
measured in the case studies. The errors in the predicted
support thrusts ranged between the extremes of -79%
(unconservative) and +62% (conservative). However, for
7 of the 11 tunnel sections analyzed, the errors varied

between the more limited bounds of ±30%. The average error
for all of the cases was about 15%, and the standard devia-
tion of the errors was approximately 35 percentage points.
On the whole, there was a slight conservative bias in the
predictions.

In any approximate analytical technique, there is
always the possibility, through further research, of develop-
ing additional refinements. The simplified analysis method
for tunnel support loads is no exception. Undoubtedly, a
long list of very specific variations and improvements could
be compiled with varying applicability and usefulness. It
would seem more productive, however, to emphasize the follow-
ing four most potentially fruitful recommendations for
the further development and extrapolation of the method:

    (1)   The effects of ground yielding under nonaxisym-
          metric stress conditions should be investigated
          more intensively. Based on the very limited
          parametric study in Section 5.4, it was only
          possible to draw very weak conclusions about
          the variations of λ_y with changes in K and the
          ground strength. These conclusions should be
          strenthened for the simplified analysis method
          to have a wider range of applicability.

    (2)   The effects of ground yielding at long support
          delays could be better formulated. The calcula-
          tions for some of the case studies showed that

334

at long support delays λ_y becomes undefined, allowing only an approximate calculation of an upper bound for the support loads. Although cases like these will generally not be common in practice, provisions could be made in the method for their treatment.

(3) Strain softening strength behavior for the ground could be incorporated into the analysis. Many types of geologic materials do soften and become less strong as they progressively yield; this will tend to increase the support loads. Provided the correct analytical formulation for the characteristic curve of the ground mass can be determined, the strain softening behavior can be easily included.

(4) The effects of time-dependent ground behavior (e.g., swelling/consolidation and squeezing) should be investigated. In some instances (e.g., the Victoria Line case study), the time-dependent component of the load is quite significant and must be considered in the design. Although no time-dependent behavior can be treated in the simplified method in its present form, it could readily be added, perhaps through a "time effect" correction factor λ_t.

Finally, additional case studies could be compiled to substantiate further the accuracy of the simplified analysis.

In all, the simplified analysis method is an appropriate and accurate design technique in many types of tunneling situations. It reduces the tunneling problem to its bare essentials, capturing the fundamental aspects in a few variables. Since the method does require only a few, relatively easily determined input parameters, it is very simple to apply. No large computers are needed, as they are for the more sophisticated numerical techniques; the support loads can be readily computed using simple desk top or pocket programmable calculators. And since the support loads can be computed with so little effort, the simplified analysis is perfectly suited for parametric sensitivity studies when designing for uncertain conditions. This computational ease, coupled with accuracy sufficient for any practical tunnel analysis, makes the simplified analysis method a valuable and effective design tool.

8. REFERENCES

_____ (1961), "Tunneling in London Clay," *The Engineer*, Vol. 211, No. 5486, March 17, pp. 422-425.

Abel, J.F. and Lee, F.T. (1973), "Stress Changes Ahead of an Advancing Tunnel," *International Journal of Rock Mechanics, Mining Sciences and Geomechanical Abstracts*, Vol. 10, pp. 673-698.

Attewell, P.B. and El-Naga, N.M.A. (1977), "Ground-Lining Pressure Distribution and Lining Distortion in Two Tunnels Driven Through Stiff, Stony/Laminated Clay," *Ground Engineering*, Vol. 10, No. 3, April, pp. 28-35.

Attewell, P.B., Farmer, I.W., and Wickson, J.L.(1976), "Measurement of Ground-Lining Interaction Pressures in an Underground Tunnel in Coal-Measures Rock", *Tunnelling '76*, London, pp 255-263, Disc. pp 271-272.

Baligh, M.M. (1976), "Cavity Expansion in Sands with Curved Failure Envelopes," *Journal of the Geotechnical Engineering Division*, ASCE, Vol. 102, No. GT11, November, pp. 1131-1146.

Bathe, K.J. (1976), "Static and Dynamic Geometric and Material Nonlinear Analysis Using ADINA," *Report 82448-2*, Acoustics and Vibration Laboratory, Mechanical Engineering Department, Massachusetts Institute of Technology.

Bathe, K.J. (1977), "ADINA - A Finite Element Program for Automatic Dynamic Incremental Nonlinear Analysis," *Report 82448-1*, Acoustics and Vibration Laboratory, Mechanical Engineering Department, Massachusetts Institute of Technology (Revised May, 1977).

Belshaw, D.J. and Palmer, J.H.L. (1978), "Results of a Program of Instumentation Involving a Precast Segmented Concrete-Lined Tunnel in Clay," *Canadian Geotechnical Journal*, Vol. 15, No.4, November, pp. 573-583.

Bishop, A.W., Webb, D.L., and Lewin, P.I. (1965), "Studies of the Properties of Undisturbed London Clay at the Ashford Common Shaft: Strength-Effective Stress Relationships," *Geotechnique*, Vol. 15, No. 1, pp. 1-31.

Bjorkman, G.S.,Jr. and Richards, R.,Jr. (1976), "Harmonic Holes - An Inverse Problem in Elasticity," *Journal of Applied Mechanics*, ASME, Vol. 43, Series E, No.3, September, pp. 414-418.

Burke, H.H. (1960), "Garrison Dam Test Tunnel - Investigation and Construction," *Transactions*, ASCE, Vol. 125, pp. 230-267 (also published in November 1957 in the *Journal of the Soil Mechanics and Foundations Division*, as Proceedings Paper No. 1438).

Burns, J.Q. and Richard, R.M. (1964), "Attenuation of Stresses for Buried Cylinders," Proceedings, Symposium on Soil-Structure Interaction, Tucson, Arizona, pp. 378-392.

Carter, P.G. and Mills, D.A.C. (1976), "Engineering Geological Investigations for the Kielder Tunnels," Quarterly Journal of Engineering Geology, Vol. 9, No. 2, pp. 125-141.

Curtis, D.J. (1975), Discussion of "The Circular Tunnel in Elastic Ground" by A.M. Muir Wood, Geotechnique, Vol. 25, No. 3, pp. 231-237.

Daemen, J.J.K. (1975), "Tunnel Support Loading Caused by Rock Failure," Technical Report No. MRD-3-75, Omaha District, U.S. Army Corps of Engineers, May (NTIS AD A013405).

Daemen, J.J.K. and Fairhurst, C. (1972), "Rock Failure and Tunnel Support Loading," Proceedings, International Symposium on Underground Openings, Lucerne, pp. 356-369.

Daemen, J.J.K. and Fairhurst, C. (1973), "Tunnel and Shafts in Rock - Part 2, Ground Support Interaction: Fundamentals and Design Implications," Contract No. DACW 45-72C-0018, Missouri River Division, U.S. Army Corps of Engineers.

Dar, S.M. and Bates, R.C. (1974), "Stress Analysis of Hollow Cylindrical Inclusions," Journal of the Geotechnical Engineering Division, ASCE, Vol. 100, No. GT2, February, pp. 123-138.

Deere, D.U., Hendron, A.J., Patton, F.D., and Cording, E.J. (1968), "Design of Surface and Near-Surface Construction in Rock," Proceedings, Eighth U.S. Symposium on Rock Mechanics, Minneapolis, Minnesota, pp. 237-302.

Deere, D.U., Peck, R.B., Monsees, J.E., and Schmidt, B. (1969), "Design of Tunnel Liners and Support Systems," Report to the Office of High Speed Ground Transportation, U.S. Department of Transportation (NTIS No. PB 183799).

Descoeudres, F., "Three-Dimensional Analysis of Tunnel Stability Near the Face in an Elasto-Plastic Rock," Advances in Rock Mechanics, Proceedings, Third Congress, International Society for Rock Mechanics, Denver, 1974, Vol. 2, Part B, pp. 1130-1135 (in French).

Drucker, D.C. and Prager, W. (1952), "Soil Mechanics and Plastic Analysis in Limit Design," Quarterly of Applied Mathematics, Vol. 10, No. 2, pp. 157-165

Dunns, C.S. and Butterfield, R. (1971), "Flexible Buried Cylinders," International Journal of Rock Mechanics, Mining Sciences, and Geomechanical Abstracts, Vol. 8, pp. 577-627.

Dunton, C.E., Kell, J., and Morgan, H.D. (1965), "Victoria Line: Experimentation, Design, Programming and Early Progress," Proceedings, Institution of Civil Engineers, London, Vol. 31, May, pp. 1-15.

Farmer, I. (1976), "Support of Tunnels in Rock," Ground Engineering, Vol. 9, No. 4, May, pp. 29-32.

Fenner, R. (1938), "Untersuchungen Zur Erkenntnis Des Gebirgsdruckes," Glückauf, Technical Translation Report R 700159, pp. 681-695 and 701-715.

Flugge, W. (1966), Stresses in Shells, Springer-Verlag, Inc., New York.

Hendron, A.J. and Aiyer, A.K. (1972), Stresses and Displacements Around a Cylindrical Tunnel in an Elasto-Plastic Material with Dilatancy, Technical Report No. 10, Omaha District, U.S. Army Corps of Engineers, September (NTIS No. AD 748 030).

Heuer, R.E. and Hendron, A.J.,Jr. (1971), Geomechanical Model Study of the Behavior of Underground Openings in Rock Subjected to Static Loads - Report 2, Tests on Unlined Openings in Intact Rock, Contract Report N-69-1, U.S. Army Engineer Waterways Experiment Station, Vicksburg, Mississippi, February.

Hobbs, D.W. (1966), "A Study of the Behavior of Broken Rock Under Triaxial Compression and Its Application to Mine Roadways," International Journal of Rock Mechanics and Mining Sciences, Vol. 3, pp. 11-43.

Hocking, G. (1976), "Three-Dimensional Elastic Stress Distribution around the Flat End of a Cylindrical Cavity," International Journal of Rock Mechanics, Mining Sciences, and Geomechanical Abstracts, Vol. 13, No. 12, pp. 331-337.

Hoek, E. and Bray, J.W. (1974), Rock Slope Engineering, The Institution of Mining and Metallurgy, London.

Hoeg, K. (1968),"Stresses Against Underground Structural Cylinders," Journal of the Soil Mechanics and Foundation Engineering Division, ASCE, Vol. 94, No. SM4, July, pp. 833-858.

Jaeger, J.C. and Cook, N.G.W. (1976), Fundamentals of Rock Mechanics, John Wiley and Sons, Inc., New York.

Kastner, H. (1962), Statik des Tunnel - und Stollenbaues, Springer-Verlag, Inc., New York.

Kennedy, T.C. and Lindberg, H.E. (1978a), "Model Tests for Plastic Response of Lined Tunnels," Journal of the Engineering Mechanics Division, ASCE, Vol. 104, No. EM2, April, pp. 399-420.

Kennedy, T.C. and Lindberg, H.E. (1978b), "Tunnel Closure for Nonlinear Mohr-Coulomb Functions," Journal of the Engineering Mechanics Division, ASCE, Vol. 104, No. EM6, December, pp. 1313-1326.

Laabmayr, F. and Swoboda, G. (1978), "The Importance of Shotcrete As Support Element of the NATM," Proceedings, Engineering Foundation Conference on Shotcrete for Underground Support, St. Anton, Austria.

Labasse, H. (1949), "Les Pressions de Terrains dans les Mines de Houilles," Revue Universelle des Mines, Vol. 9, No. 1, pp. 3-15 and No. 3, pp. 78-88.

Ladanyi, B. (1974), "Use of the Long-Term Strength Concept in the Determination of Ground Pressures on Tunnel Linings," Advances in Rock Mechanics, Proceedings, Third Congress, International Society for Rock Mechanics, Denver, Vol. II, Part B, pp. 1150-1156.

Ladanyi, B. and Nguyen Don (1970), "Study of Strains Associated With Brittle Failure," Proceedings, Sixth Canadian Rock Mechanics Symposium, Montreal, pp. 49-64.

Lambe, T.W. and Whitman, R.V. (1969), Soil Mechanics, John Wiley and Sons, Inc., New York.

Lane, K.S. (1957), "Effect of Lining Stiffness on Tunnel Linings," Proceedings, Fourth International Conference on Soil Mechanics and Foundation Engineering, Vol. 2, pp. 223-227.

Lane, K.S. (1960), "Garrison Dam Test Tunnel - Evaluation of Test Results," Transactions, ASCE, Vol. 125, pp. 268-306 (also published in November, 1957, in the Journal of the Soil Mechanics and Foundations Division as Proceedings Paper No. 1439).

Lombardi, G. (1973), "Dimensioning of Tunnel Linings with regard to Construction Procedure," Tunnels and Tunneling, Vol. 5, No. 4, July-August, pp. 340-351.

Mohraz, B., Hendron, A.J.,Jr., Ranken, R.E., and Salem. M.H. (1975), "Liner-Medium Interaction in Tunnels," Journal of the Construction Division, ASCE, Vol. 101, No. CO1, March, pp. 127-141.

Morgan, H.D. (1961), "A Contribution to the Analysis of Stress in a Circular Tunnel," Geotechnique, Vol. 11, No. 1, pp. 37-46.

Morgan, H.D. and Bartlett, J.V. (1969), "Victoria Line: Tunnel Design," Proceedings, Institution of Civil Engineers, London, Supplemental Volume, pp. 377-395.

Morrison, R.G.K. and Coates, D.F. (1955), "Soil Mechanics Applied to Rock Failure in Mines," Canadian Mining and Metallurgical Bulletin, Vol. 48, No. 523, November, pp. 701-711; see also Transactions, Canadian Institute of Mining and Metallurgy, Vol. 58, pp. 401-411.

Muir Wood, A.M. (1975), "The Circular Tunnel in Elastic Ground," Geotechnique, Vol. 25, No. 1, pp. 115-127.

Newmark, N.M. (1969), "Design of Rock Silo and Rock Cavity Linings," Technical Report to Space and Missile Systems Organization, Air Force Systems Command, Norton Air Force Base, Contract No. FO 4701-69-C-0155.

Panet, M (1976), "Stability Analysis of a Tunnel Driven in a Rock Mass in Taking Account of the Post-Failure Behavior," Rock Mechanics, Vol. 8, pp. 209-223 (in French).

Panet, M. and Guellec, P. (1974), "Contribution to the Problem of the Design of Tunnel Support Behind the Face," Proceedings, Third Congress, International Society for Rock Mechanics, Denver, Vol. 2, Part B, pp. 1163-1168 (in French).

Peck, R.B. (1969), "State-of-the-Art Report: Deep Excavations and Tunneling in Soft Ground," Proceedings, Seventh International Conference on Soil Mechanics, Mexico, State-of-the-Art Volume, pp. 225-290.

Peck, R.B., Hendron, A.J.,Jr., and Mohraz, B. (1972), "State of the Art of Soft Ground Tunneling," Proceedings, American Conference on Rapid Excavation and Tunneling, Vol. 1, pp. 259-286.

Poulos, H.G. and Davis, E.H. (1974), Elastic Solutions for Soil and Rock Mechanics, John Wiley and Sons, Inc., New York.

Proctor, R.V. and White, T.L. (1946), Rock Tunneling with Steel Supports, The Commercial Shearing and Stamping Co., Youngstown, Ohio.

Rabcewicz, L.v. (1962), "Aus Der Praxis Des Tunnelbaues - Einige Erfahrungen Über Echten Gebirgsdruck (From the Practice of Tunneling - Some Experiences of True Rock Pressure)," Geologie Und Bauwesen, Vol. 27, No. 3-4, pp. 153-167.

Rabcewicz, L.v. (1969), "The Stability of Tunnels under Rock Load," Water Power, Part 1, June, pp. 225-229; Part 2, July, pp. 266-273; Part 3, August, pp. 297-302.

Rabcewicz, L.v. and Golser, J. (1973), "Principles of Dimensioning the Support System for the New Austrian Tunneling Method," Water Power, March, pp. 88-93.

Ranken, R.E. (1978), "Analysis of Ground-Liner Interaction for Tunnels," Ph.D. Thesis, University of Illinois, Urbana-Champaign.

Ranken, R.E. and Ghaboussi, J. (1975), Tunnel Design Considerations: Analysis of Stresses and Displacements around Advancing Tunnels, Report No. FRA-ORDD 75-84, Federal Railroad Administration, U.S. Department of Transportation, August.

Ranken, R.E., Ghaboussi, J., and Hendron, A.J. (1978), Analysis of Ground-Liner Interaction for Tunnels, Report No. UMTA-IL-06-0043-78-3, Urban Mass Transit Administration, U.S. Department of Transportation, October.

Reyes, S.F. and Deere, D.U. (1966), "Elastic-Plastic Analysis of Underground Openings by the Finite Element Method," Proceedings, First Congress of the International Society of Rock Mechanics, Lisbon, Portugal, pp. 477-483.

Savin, G.N. (1970), Stress Distribution around Holes, NASA Technical Translation NASA TT F-607, National Aeronautics and Space Administration, Washington,D.C., November.

Schmid, H. (1926), Statische Probleme des Tunnel - und Druckstollenbaus, Springer, Berlin (English translation: U.S. Bureau of Reclamation Technical Memo 262, 1931).

Smith, C.K. and Redlinger, J.F. (1953), "Soil Properties of Fort Union Clay Shale," Proceedings, Third International Conference on Soil Mechanics and Foundation Engineering, Switzerland, pp. 62-66.

Sperry, P.E. and Heuer, R.E. (1972), "Excavation and Support of Navajo Tunnel No. 3," Proceedings of North American Rapid Excavation and Tunneling Conference, No. 1, Chapter 29, AIME, pp. 539-571.

Tattersall, F., Wakeling, T.R.M., and Ward, W.H. (1955), "Investigation into the Design of Pressure Tunnels in London Clay," Proceedings, Institution of Civil Engineers, Vol. 4, Part I, pp. 400-471.

Terzaghi, K. (1943), Theoretical Soil Mechanics, John Wiley and Sons, Inc., New York.

Tse, E. (1979), "Adaptable Method in Tunnel Design and Construction: A Formalized Decision Model," unpublished Master of Science thesis, Massachusetts Institute of Technology, Cambridge, Mass.

Vesic, A.S. (1972), "Expansion of Cavities in Infinite Soil Mass," Journal of the Soil Mechanics and Foundation Division, ASCE, Vol. 98, No. SM3, March, pp. 265-290.

Voellmy, A. (1937), "Eingebettete Rohre," Mitteilung Des Institutes Für Baustatik, Eidgenoessische Technische Hochschule, Zurich, Switzerland, No. 9.

Ward, W.H. (1978), "Ground Supports for Tunnels in Weak Rocks," Geotechnique, Vol. 28, No. 2, pp. 133-171.

Ward, W.H., Coats, D.J., and Tedd, P. (1976), "Performance of Tunnel Support Systems in the Four Fathom Mudstone," Tunneling '76, London, March, pp. 329-340, disc. pp. 348-367.

Ward, W.H., Marsland, A., and Samuels, S.G. (1965), "Studies of the Properties of Undisturbed London Clay at the Ashford Common Shaft: In Situ and Immediate Strength Tests," Geotechnique, Vol. 15, No. 4, pp. 321-344.

Ward, W.H., Samuels, S.G., and Butler, M.E. (1959), "Further Studies of the Properties of London Clay," Geotechnique, Vol. 9, No. 2, June, pp. 33-58.

Ward, W.H. and Thomas, H.S.H. (1965), "The Development of Earth Loading and Deformation in Tunnel Linings in London Clay," Proceedings, Sixth International Conference on Soil Mechanics and Foundation Engineering, Vol. II, pp. 432-436.

Westergaard, H.M. (1940), "Plastic State of Stress around a Deep Well," Journal of the Boston Society of Civil Engineers, Vol. 27, No. 1, pp. 1-5.

APPENDIX A

DERIVATION OF THE RELATIVE STIFFNESS
SOLUTIONS FOR EXCAVATION UNLOADING CONDITIONS

A.1 ASSUMPTIONS IN THE ANALYSIS

The derivation of the relative stiffness solution for
the correct excavation unloading condition (see Chapter 2)
in the tunneling problem follows the original logic of Burns
and Richard (1964). The ground mass is postulated to be an
infinite, elastic, homogeneous, isotropic medium with an ini-
tial vertical stress P equal to the vertical overburden pres-
sure at the centerline of the tunnel and with an initial
horizontal stress KP. The tunnel support is treated as an
elastic shell in which both flexural and circumferential de-
formations are considered (i.e., extensible shell theory is
employed). Both the ground and the support are assumed to
be in a state of plane strain. The notation used in the
solution is illustrated in Figure A.1.

A.2 DIMENSIONLESS STIFFNESS RATIOS

The relative stiffness of the ground mass to the tun-
nel support is incorporated into the solution through the
use of two dimensionless parameters, the compressibility and
flexibility ratios. The compressibility ratio, C*, is a
measure of the relative diametral stiffnesses of the ground
and the support under a symmetric or uniform loading condi-
tion (horizontal ground stresses equal to the vertical ground
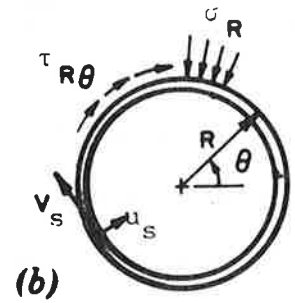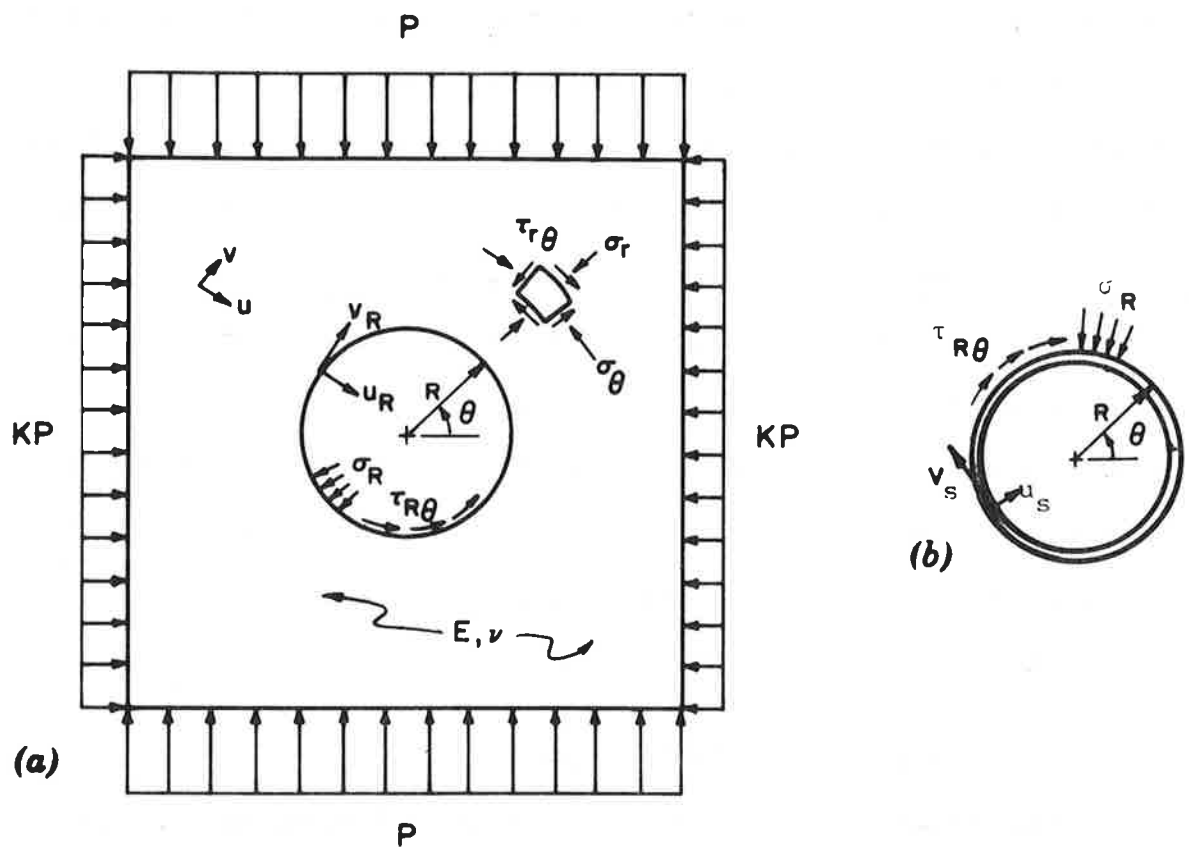
FIGURE A.1.   NOTATION FOR RELATIVE STIFFNESS SOLUTIONS

346

stresses in the free field). The diametral stiffness of the ground is expressed as (see Figure A.2a):

$$\frac{P}{\Delta D/D} = \frac{E}{2(1-\nu^2)} \qquad \text{(A.1)}$$

and for the support:

$$\frac{P}{\Delta D/D} = \frac{E_s A_s}{(1-\nu_s^2)R} \qquad \text{(A.2)}$$

The compressibility ratio is then defined as:

$$C^* = \frac{\left[\dfrac{P}{\Delta D/D}\right] \text{ground}}{\left[\dfrac{P}{\Delta D/D}\right] \text{support}} = \frac{\dfrac{E}{(1-\nu^2)}}{\dfrac{E_s A_s}{(1-\nu_s^2)R}} = \frac{ER(1-\nu_s^2)}{E_s A_s(1-\nu^2)} \qquad \text{(A.3)}$$

where the factor of 2 in the denominator of Eq. A.1 has been dropped for convenience, since C^* is used only as an index parameter.

The flexibility ratio, F^*, is a measure of the relative diametral stiffnesses of the ground and the support under an antisymmetric loading condition (horizontal ground stress equal to but of opposite sign of the vertical ground stress in the free field). The diametral stiffness of the ground for this loading condition is (see Figure A.2b):

347
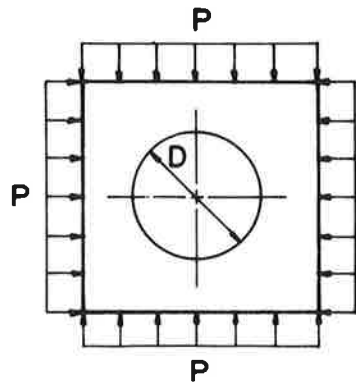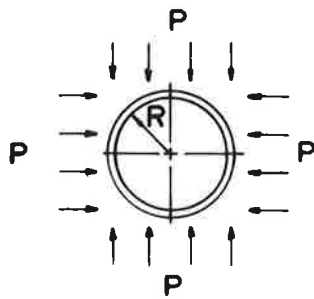
$$\frac{P}{\Delta D/D} \propto \frac{E}{(1-\nu^2)} \qquad \frac{P}{\Delta D/D} = \frac{E_s A_s}{(1-\nu_s^2) R}$$

$$C^* = \text{Compressibility Ratio} = \frac{E R (1-\nu_s^2)}{E_s A_s (1-\nu^2)}$$

E, E_s = Elastic moduli for ground and support

ν, ν_s = Poisson's ratios for ground and support

A_s = Cross-sectional area of support per unit length of tunnel
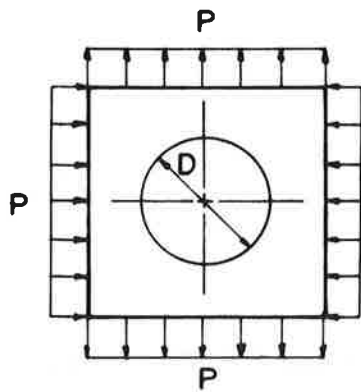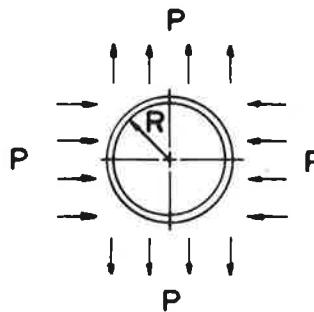
$$\frac{P}{\Delta D/D} \propto \frac{E}{(1-\nu^2)} \qquad \frac{P}{\Delta D/D} \propto \frac{E_s I_s}{(1-\nu_s^2) R^3}$$

$$F^* = \text{Flexibility Ratio} = \frac{E R^3 (1-\nu_s^2)}{E_s I_s (1-\nu^2)}$$

I_s = Moment of inertia of support per unit length of tunnel

FIGURE A.2.   DIMENSIONLESS STIFFNESS RATIOS

348

$$\frac{P}{\Delta D/D} = \frac{E}{4(1-\nu^2)} \qquad (A.4)$$

and for the support:

$$\frac{P}{\Delta D/D} = \frac{6E_s I_s}{(1-\nu_s^2) R^3} \qquad (A.5)$$

The flexibility ratio is then defined as:

$$F^* = \frac{\left[\dfrac{P}{\Delta D/D}\right]\text{ground}}{\left[\dfrac{P}{\Delta D/D}\right]\text{support}} = \frac{\dfrac{E}{(1-\nu^2)}}{\dfrac{E_s I_s}{(1-\nu_s^2) R^3}} = \frac{ER^3 (1-\nu_s^2)}{E_s I_s (1-\nu^2)} \qquad (A.6)$$

where again, since F* will be used only as an index para-
meter, the factors of 4 and 6 in Eq. (A.4) and (A.5) have
been dropped.

It should be noted here that the compressibility and
flexibility ratios defined in Eq. (A.3) and (A.6) are
slightly different from those used by Burns and Richard
(1964), Hoeg (1968), and Peck et al. (1972). In their sol-
utions the calculation of the ground stiffness was based on
the unperforated ground mass existing before the tunnel was
excavated. While this assumption has only a slight effect
on the flexibility ratio, it has a misleadingly extreme ef-
fect on the compressibility ratio. The diametral stiffness

of the unperforated ground mass under a uniform stress condition is:

$$\frac{P}{\Delta D/D} = \frac{E}{(1+\nu)(1-2\nu)} \qquad (A.7)$$

The diametral support stiffness remains unchanged (Eq. A.2), and the compressibility ratio, C, for the unperforated ground case is thus:

$$C = \frac{ER(1-\nu_s^2)}{E_sA_s(1+\nu)(1-2\nu)} \qquad (A.8)$$

The differences between the expressions for C* (Eq. A.3) and C (Eq. A.8) are the terms in the denominator involving Poisson's ratio ν for the ground mass. As ν approaches 0.5 (which might be realistic for a tunnel in undrained soft clay), the compressibility ratio C based on the unperforated ground mass tends toward infinity. From a conceptual viewpoint an infinite compressibility ratio should correspond to zero support thrust. A large compressibility ratio implies that the ground is much stiffer than the support and that the support is therefore "attracting" very little load. But the support thrust for the case of $\nu = 0.5$ does not tend toward zero either in real tunnels or in the relative stiffness solutions by Burns and Richard, Hoeg, and Peck et. al.; thus the expression for C in Eq. (A.8) is misleading.

350

The compressibility ratio C* (Eq. A.3) based on the perforated ground mass better relates the support load to the relative support stiffness for all values of ν. In addition, it is conceptually more correct because it relates the stiffness of the support to the stiffness of the load-carrying component of the ground (the ground outside the tunnel). Therefore, a perforated ground mass has been assumed in the derivation of C* (and F*, for consistency) in the revised relative stiffness solution. The ratios C* and F* in the revised solution are related to the ratios C and F in the original relative stiffness solution by the following expressions:

$$C = \left[\frac{1-\nu}{1-2\nu}\right]C^* \qquad (A.9)$$

$$F = \left[\frac{1-\nu}{6}\right]F^* \qquad (A.10)$$

A.3 DERIVATION OF EXCAVATION UNLOADING SOLUTIONS

The derivation of the revised relative stiffness solution follows three basic steps:

1. Derive the initial displacement field in the ground mass due to the in situ stresses.

2. Derive the total stress and incremental displacement fields in the ground mass after excavation and the contact stresses at the ground-support

351

interface. The incremental displacement field is the displacement field for a circular hole in the ground under an external loading condition minus the displacements due to the in situ stresses. In other words, it is the displacement field induced by the excavation in the initially stressed ground mass. The "full-slip" or "no-slip" boundary conditions at the ground-support interface are also considered in Step 2 and lead to two different solutions.

3. Compute the internal support forces induced by the contact stresses at the ground-support interface.

Details of the derivation for each of the three steps are given below.

Step 1.   Derivation of the initial displacement field in the ground mass due to the in situ stresses.

The stresses existing in the ground before tunneling are given as (see Figure A.1 for notation):

$$\sigma_r = (P/2)[(1+K) - (1-K)\cos 2\theta] \tag{A.11a}$$

$$\sigma_\theta = (P/2)[(1+K) + (1-K)\cos 2\theta] \tag{A.11b}$$

$$\tau_{r\theta} = (P/2)(1-K)\sin 2\theta \tag{A.11c}$$

and the stress-strain-displacement relations in polar co-ordinates are:

$$\varepsilon_r = \frac{\partial u}{\partial r} = \frac{1}{E}\left[(1-\nu^2)\,\sigma_r - \nu(1+\nu)\,\sigma_\theta\right] \qquad \text{(A.12a)}$$

$$\varepsilon_\theta = \frac{u}{r} + \frac{\partial v}{r\partial\theta} = \frac{1}{E}\left[(1-\nu^2)\,\sigma_\theta - \nu(1+\nu)\,\sigma_r\right] \qquad \text{(A.12b)}$$

Substituting (A.11) into (A.12) and integrating yields the expressions for the initial ground displacements, u_I and v_I:

$$u_I = \frac{Pr(1+\nu)}{2E}\left[(1-2\nu)(1+K) - (1-K)\cos 2\theta\right] \qquad \text{(A.13a)}$$

$$v_I = \frac{Pr(1+\nu)}{2E}\,(1-K)\sin 2\theta \qquad \text{(A.13b)}$$

Step 2.   Derivation of the stress and incremental displacement fields in the ground after excavation and the contact stresses at the ground-support interface.
The stresses in the ground mass can be expressed in terms of a stress function, ϕ, as:

$$\sigma_r = \frac{1}{r}\frac{\partial\phi}{\partial r} + \frac{1}{r^2}\frac{\partial^2\phi}{\partial\theta^2} \qquad \text{(A.14a)}$$

$$\sigma_\theta = \frac{\partial^2\phi}{\partial r^2} \qquad \text{(A.14b)}$$

$$\tau_{r\theta} = -\frac{\partial}{\partial r}\left(\frac{1}{r}\frac{\partial\phi}{\partial\theta}\right) \qquad \text{(A.14c)}$$

353

where ϕ in this case is Michell's generalized stress function (see Timoshenko and Goodier, 1934):

$$\phi = a_0 \ln(r) + b_0 r^2 + c_0 r^2 \ln(r) + d_0 r^2 \theta + a_0' \theta$$

$$+ \frac{a_1}{2} r\theta\sin\theta + [b_1 r^3 + a_1' r^{-1} + b_1' r \ln(r)]\cos\theta$$

$$- \frac{c_1}{2} r\theta\cos\theta + [d_1 r^3 + c_1' r^{-1} + d_1' r \ln(r)]\sin\theta$$

$$+ \sum_{n=2,3,4}^{\infty} (a_n r^n + b_n r^{n+2} + a_n' r^{-n} + b_n' r^{-n+2})\cos(n\theta)$$

$$+ \sum_{n=2,3,4}^{\infty} (c_n r^n + d_n r^{n+2} + c_n' r^{-n} + d_n' r^{-n+2})\sin(n\theta)$$

$$(A.15)$$

where a_0, b_0, ... a_1, b_1, a_1', b_1', ... c_n', d_n' are arbitrary constants. This stress function can be simplified somewhat. Considering Eqs. (A.14) and (A.15) together with the symmetry and periodicity requirements of the stress field, one can immediately draw the following conclusions:

a) $d_0 = 0$

b) All terms involving $\sin(n\theta)$ must equal zero for any n and r. Therefore

$$a_1 = d_1 = c_1' = d_1' = c_n = d_n = c_n' = d_n' = 0$$

c) All terms involving $\cos(n\theta)$ must equal zero for any odd n. Therefore

$$b_1 = a_1' = b_1' = c_1 = a_n = b_n = a_n' = b_n' = 0 \text{ for odd n.}$$

354

Additional terms can be eliminated by noting that the stress-
es must approach the in situ values as r approaches infinity.
Considering σ_θ as $r \to \infty$ (using either σ_r or $\tau_{r\theta}$ will give
the same results):

$$\sigma_\theta = \frac{\partial^2\phi}{\partial r^2} = -a_0 r^{-2} + 2b_0 + c_0[2\ln(r) + 3]$$

$$+ \sum_{n=2,4,6}^{\infty}[n(n-1)a_n r^{n-2} + (n+2)(n+1)b_n r^n$$

$$- n(-n-1)a_n' r^{-n-2} + (-n+2)(-n+1)b_n' r^{-n}]\cos(n\theta)$$

$$= \frac{1}{2}P[(1+K) + (1-K)\cos 2\theta] \qquad (A.16)$$

Therefore: $c_0 = 0$; $b_n = 0$ for $n \geq 2$; $a_n = 0$ for $n > 2$
and: $2b_0 + 2a_2 \cos 2\theta = \frac{1}{2} P[(1+K) + (1-K)\cos 2\theta]$
which, when solved at $\theta = 0$ and $\theta = \frac{\pi}{2}$, gives:

$$b_0 = \frac{1}{4} P (1+K)$$

$$a_2 = \frac{1}{4} P (1-K)$$

The general stress function (Eq. A.15) is thus reduced to:

$$\phi = a_0 \ln(r) + \frac{1}{4} Pr^2 (1+K) + a_0'\theta + \frac{1}{4} Pr^2 (1-K)\cos 2\theta$$

$$+ \sum_{n=2,4,6}^{\infty}\left[a_n' r^{-n} + b_n' r^{-n+2}\right] \cos(n\theta) \qquad (A.17)$$

355

Using Eqs. (A.14) and (A.17), the stresses in the ground mass can be expressed as:

$$\sigma_r = a_0 r^{-2} + \tfrac{1}{2}P(1+K) - \tfrac{1}{2}P(1-K)\cos 2\theta$$

$$+ \sum_{n=2,4,6}^{\infty} [(-n^2-n)a_n' r^{-n-2} + (-n^2-n+2)b_n' r^{-n}]\cos(n\theta)$$

$$\text{(A.18a)}$$

$$\sigma_\theta = -a_0 r^{-2} + \tfrac{1}{2}P(1+K) + \tfrac{1}{2}P(1-K)\cos 2\theta$$

$$+ \sum_{n=2,4,6}^{\infty} [-n(-n-1)a_n' r^{-n-2} + (-n+1)(-n+2)b_n' r^{-n}]\cos(n\theta)$$

$$\text{(A.18b)}$$

$$\tau_{r\theta} = a_0' r^{-2} + \tfrac{1}{2}P(1-K)\sin 2\theta$$

$$+ \sum_{n=2,4,6}^{\infty} [n(-n-1)a_n' r^{-n-2} + n(-n+1)b_n' r^{-n}]\sin(n\theta)$$

$$\text{(A.18c)}$$

Substituting Eqs. (A.18) into Eqs. (A.12) and integrating gives the total displacement distribution in the ground mass:

$$u = \frac{1+\nu}{E}\left\{-a_0 r^{-1} + \tfrac{1}{2}Pr(1+K) - \tfrac{1}{2}Pr(1-K)\cos 2\theta \right.$$

$$+ \sum_{n=2,4,6}^{\infty}\left[na_n' r^{-n-1} + (n+2)b_n' r^{-n+1}\right]\cos(n\theta)$$

$$\left. - \nu Pr(1+K) - \nu \sum_{n=2,4,6}^{\infty} 4b_n' r^{-n+1}\cos(n\theta)\right\}$$

$$\text{(A.19a)}$$

356

$$v = \frac{1+\nu}{E} \left\{ \frac{1}{2} Pr(1-K)\sin 2\theta \right.$$

$$\left. + \sum_{n=2,4,6}^{\infty} \left[na_n'r^{-n-1} + (n-4+4\nu)b_n'r^{-n+1} \right] \sin(n\theta) \right\}$$

(A.19b)

The displacements given in Eq. (A.19) correspond to the combined ground movements from both the initial ground stresses and the stress redistribution induced by the excavated circular opening. However, the movements due to the initial ground stresses occur before the tunnel is excavated and do not directly affect the ground-support interaction. These initial displacements, given in Eq. (A.13), must therefore be subtracted from Eq. (A.19) to obtain the incremental displacement field that corresponds to the excavation unloading condition for tunnels. These incremental displacements are:

$$u = \frac{1+\nu}{E} \left\{ -a_0 r^{-1} + \sum_{n=2,4,6}^{\infty} \left[na_n'r^{-n-1} + (n+2-4\nu)b_n'r^{-n+1} \right] \cos(n\theta) \right\}$$

(A.20a)

$$v = \frac{1+\nu}{E} \left\{ \sum_{n=2,4,6}^{\infty} \left[na_n'r^{-n-1} + (n-4+4\nu)b_n'r^{-n+1} \right] \sin(n\theta) \right\}$$

(A.20b)

357

At this point the boundary conditions at the ground-support interface must be introduced. At $r = R$ (see Figure A.1):

Full-slip:

$$\sigma_r = \sigma_R \qquad \text{(A.21a)}$$

$$\tau_{r\theta} = 0 \qquad \text{(A.21b)}$$

$$u = u_s \qquad \text{(A.21c)}$$

No-slip:

$$\sigma_r = \sigma_R \qquad \text{(A.22a)}$$

$$\tau_{r\theta} = \tau_{R\theta} \qquad \text{(A.22b)}$$

$$u = u_s \qquad \text{(A.22c)}$$

$$v = v_s \qquad \text{(A.22d)}$$

Each case must be solved separately.

Full-Slip at Interface

The boundary condition of zero shear stress at $r = R$ requires that:

$$\tau_{r\theta}\bigg|_{r=R} = -\frac{\partial}{\partial r}\left(\frac{1}{r}\frac{\partial\phi}{\partial\theta}\right)\bigg|_{r=R}$$

$$= a_0'R^{-2} + \frac{1}{2}P(1-K)\sin2\theta$$

$$+ \sum_{n=2,4,6}^{\infty}[(-n-1)a_n'R^{-n-2} + (-n+1)b_n'R^{-n}]n\sin(n\theta)$$

$$= 0 \qquad\qquad\qquad\qquad\qquad (A.23)$$

Since this relation must hold for all θ, a_0 must equal zero. In addition, the orthogonality property of sine functions requires that $a_n' = b_n' = 0$ for $n \neq 2$. Therefore, Eq. (A.23) reduces to:

$$b_2' = \frac{1}{4}PR^2(1-K) - 3a_2'R^{-2}$$

The remaining full-slip boundary conditions require consideration of the load-displacement relations for the support. For a compressible shell (extensible shell theory, see Flügge, 1966):

$$\frac{d^2v_s}{d\theta^2} + \frac{du_s}{d\theta} = -\frac{R^2}{D_C}\tau_{R\theta} \qquad\qquad (A.24a)$$

359

$$\frac{dv_s}{d\theta} + u_s + \frac{D_F}{D_C R^2}\left[\frac{d^4 u_s}{d\theta^4} + 2\frac{d^2 u_s}{d\theta^2} + u_s\right] = \frac{R^2}{D_C}\,\sigma_R \qquad \text{(A.24b)}$$

in which:

$$D_C = \frac{E_s A_s}{(1-\nu_s^2)} \qquad \text{(A.24c)}$$

$$D_F = \frac{E_s A_s}{(1-\nu_s^2)} \qquad \text{(A.24d)}$$

Using Eqs. (A.20a) and (A.21c) and integrating Eq. (A.24a) twice:

$$v_s = c\theta + d - \frac{1+\nu}{E}\left\{- a_0 R^{-1}\theta + \frac{1}{2}\left[-2(5-6\nu)a_2' R^{-3} + PR(1-\nu)(1-K)\right]\sin 2\theta\right\}$$

$$\text{(A.25)}$$

The integration constants are evaluated as follows:

At $\theta = 0$: $v_s = 0 = d$

At $\theta = \frac{\pi}{2}$: $v_s = 0 = c\left(\frac{\pi}{2}\right) - \frac{1+\nu}{E}\left\{-a_0 R^{-1}\left(\frac{\pi}{2}\right)\right\}$

$$\therefore \quad c = -\frac{1+\nu}{E}\,a_0 R^{-1}$$

and Eq. (A.25) becomes

$$v_s = \frac{1+\nu}{E}\left[(5-6\nu)a_2' R^{-3} - \frac{1}{2}PR(1-\nu)(1-K)\right]\sin 2\theta \qquad \text{(A.26)}$$

360

Substituting Eqs. (A.18a), (A.21a), and (A.26) into the second
support load-displacement relation, Eq. (A.24b), and using
the identities:

$$\frac{E}{(1+\nu)} \left(\frac{R}{D_C}\right) = C^*(1-\nu) \tag{A.27a}$$

$$\frac{D_F}{D_C R^2} = \frac{C^*}{F^*} \tag{A.27b}$$

gives the following expression:

$$-a_0 R^{-2} + \frac{C^*}{F^*}\{-a_0 R^{-2} + 9[-2(5-6\nu)a_2' R^{-4} + P(1-\nu)(1-K)]\cos2\theta\}$$

$$= C^*(1-\nu)\{a_0 R^{-2} + \frac{1}{2}P[(1+K) - (1-K)\cos2\theta] + [6a_2' R^{-4} - P(1-K)]\cos2\theta\} \tag{A.28}$$

Eq. (A.28) must hold for all θ. At $\theta = \frac{\pi}{4}$:

$$a_0 = -\frac{1}{2}PR^2(1+K)a_0^* \quad ; \quad a_0^* = \frac{C^*F^*(1-\nu)}{C^* + F^* + C^*F^*(1-\nu)} \tag{A.29a}$$

At $\theta = 0$:

$$\tag{A.29b}$$

$$a_2' = \frac{1}{2}PR^4(1-K)a_2^* \quad ; \quad a_2^* = \frac{(F^*+6)(1-\nu)}{6(5-6\nu) + 2F^*(1-\nu)}$$

Combining Eqs. (A.18), (A.20), (A.23),(A.26), and (A.29) for the full-slip case yields the contact stresses:

$$\sigma_R = \tfrac{1}{2}P(1+K)(1-a_0^*) - \tfrac{1}{2}P(1-K)(3-6a_2^*)\cos2\theta \qquad \text{(A.30a)}$$

$$\tau_{R\theta} = 0 \qquad \text{(A.30b)}$$

and the support displacements (in dimensionless form):

$$\frac{u_s E}{PR(1+\nu)} = \tfrac{1}{2}(1+K)a_0^* - (1-K)[(5-6\nu)a_2^* - (1-\nu)]\cos2\theta \qquad \text{(A.31a)}$$

$$\frac{v_s E}{PR(1+\nu)} = \tfrac{1}{2}(1-K)[(5-6\nu)a_2^* - (1-\nu)]\sin2\theta \qquad \text{(A.31b)}$$

in which:
$$a_0^* = \frac{C^* F^*(1-\nu)}{C^* + F^* + C^* F^*(1-\nu)} \qquad \text{(A.32a)}$$

$$a_2^* = \frac{(F^*+6)(1-\nu)}{2F^*(1-\nu) + 6(5-6\nu)} \qquad \text{(A.32b)}$$

C^*, F^* given in Eq. (A.3) and (A.6)

No-Slip at Interface

Using boundary conditions (A.22) and substituting Eqs. (A.18) and (A.20) into the first support load-displacement relation, Eq. (A.24a):

362

$$\frac{1+\nu}{E} \{ - \sum_{n=2,4,6}^{\infty} n^2 [na_n' R^{-n-1} + (n-4+4\nu) b_n' R^{-n+1}] \sin(n\theta)$$

$$- \sum_{n=2,4,6}^{\infty} n [na_n' R^{-n-1} + (n+2-4\nu) b_n' R^{-n+1}] \sin(n\theta) \} \tag{A.33}$$

$$= \quad - \frac{R^2}{D_c} \{ \frac{1}{2} P(1-K) \sin 2\theta + \sum_{n=2,4,6}^{\infty} [n(-n-1) a_n' R^{-n-2} + n(-n+1) b_n' R^{-n}] \sin(n\theta) \}$$

The orthogonality property of the sine functions in Eq. (A.33) requires that n = 2 only. Incorporating the identities given in Eq. (A.27) further simplifies Eq. (A.33) to:

$$12 a_2' R^{-3} + 8\nu b_2' R^{-1} = C^*(1-\nu) [\frac{1}{2} PR(1-K) - 6a_2' R^{-3} - 2b_2' R^{-1}] \tag{A.34}$$

Performing similar operations on the second support load-displacement relation, Eq. (A.24b), yields:

$$[6a_2' R^{-3} + 4\nu b_2' R^{-1}]\cos 2\theta - a_0 R^{-1} + \frac{C^*}{F^*} \{9[2a_2' R^{-3} + 4(1-\nu) b_2' R^{-1}]\cos 2\theta - a_0 R^{-1}\}$$

$$= C^*(1-\nu) \{a_0 R^{-1} + \frac{1}{2} PR(1+K) - [\frac{1}{2} PR(1-K) + 6a_2' R^{-3} + 4b_2' R^{-1}]\cos 2\theta\}$$

$$\tag{A.35}$$

When $\theta = \frac{\pi}{2}$, Eq. (A.35) gives:

$$a_0 = -\tfrac{1}{2}PR^2(1+K)a_0^* \quad ; \quad a_0^* = \frac{C^*F^*(1-\nu)}{C^* + F^* + C^*F^*(1-\nu)} \tag{A.36}$$

Simultaneously solving Eqs. (A.34) and (A.35) when $\theta = 0$ gives $\acute{a}_2$ in terms of $\acute{b}_2$:

$$\acute{a}_2 = -\hat{b}\,\acute{b}_2 R^2 \quad ; \quad \hat{b} = \frac{C^*(F^*+6)(1-\nu) + 2F^*\nu}{3F^* + 3C^* + 2C^*F^*(1-\nu)} \tag{A.37}$$

Substituting this back into Eq. (A.34) gives:

$$\tag{A.38}$$

$$\acute{b}_2 = \tfrac{1}{2}PR^2(1-K)b_2^* \quad ; \quad b_2^* = \frac{C^*(1-\nu)}{2[C^*(1-\nu) + 4\nu - 6\hat{b} - 3\hat{b}C^*(1-\nu)]}$$

Combining Eqs. (A.18), (A.20), and (A.36) – (A.38) for the no-slip case yields the contact stresses:

$$\sigma_R = \tfrac{1}{2}P(1+K)(1-a_0^*) - \tfrac{1}{2}P(1-K)(1-6a_2^* + 4b_2^*)\cos 2\theta \tag{A.39a}$$

$$\tau_{R\theta} = \tfrac{1}{2}P(1-K)(1+6a_2^* - 2b_2^*)\sin 2\theta \tag{A.39b}$$

and the support displacements (again in dimensionless form):

$$\frac{u_s E}{PR(1+\nu)} = \frac{1}{2}(1+K)a_0^* + (1-K)[2(1-\nu)b_2^*-a_2^*]\cos2\theta \qquad \text{(A.40a)}$$

$$\frac{v_s E}{PR(1+\nu)} = -(1-K)[a_2^*+(1-2\nu)b_2^*]\sin2\theta \qquad \text{(A.40b)}$$

in which:

$$a_0^* = \frac{C^*F^*(1-\nu)}{C^* + F^* + C^*F^*(1-\nu)} \qquad \text{(A.41a)}$$

$$\hat{b} = \frac{C^*(F^*+6)(1-\nu) + 2F^*\nu}{3F^* + 3C^* + 2C^*F^*(1-\nu)} \qquad \text{(A.41b)}$$

$$b_2^* = \frac{C^*(1-\nu)}{2[C^*(1-\nu) + 4\nu - 6\hat{b} - 3\hat{b}C^*(1-\nu)]} \qquad \text{(A.41c)}$$

$$a_2^* = \hat{b}b_2^* \qquad \text{(A.41d)}$$

C^*, F^* given in Eq. (A.3) and (A.6)

Step 3   Compute the internal support forces induced by
          the contact stresses at the ground-support inter-
          face.

The differential equations for the axial thrust T and
moment M in the tunnel support under plane strain conditions
are (see Flügge, 1966):

$$R\frac{dT}{d\theta} - \frac{dM}{d\theta} = R^2 \tau_{R\theta} \qquad\qquad (A.42a)$$

$$RT + \frac{d^2M}{d_\theta^2} = R^2 \sigma_R \qquad\qquad (A.42b)$$

In the general case, the expressions for $\tau_{R\theta}$ and σ_R will be
of the form:

$$\sigma_R = B_1 + B_2 \cos2\theta \qquad\qquad (A.43a)$$

$$\tau_{R\theta} = B_3 \sin2\theta \qquad\qquad (A.43b)$$

Eqs. (A.42) and (A.43) will yield the expressions for the
support moments and thrusts in the general case. Differ-
entiating Eq. (A.42b) and adding to Eq. (A.42a) gives:

366

$$\frac{d^3M}{d\theta^3} + \frac{dM}{d\theta} = R^2(B_3 - 2B_2) \sin2\theta \qquad (A.44)$$

for which the solution is:

$$M = \frac{1}{6}R^2(B_3 - 2B_2)\cos2\theta + c \qquad (A.45)$$

The integration constant, c, is independent of θ and re-
presents the second-order moments that arise because of the
difference in the internal and external support radii.
These second-order moments develop even under isotropic
(i.e., $K=1$) stress conditions; however, they are always of
an extremely small magnitude (for practical support thick-
nesses) and may be neglected.

Substituting Eq. (A.45) back into Eq. (A.42a) and
solving gives:

$$T = RB_1 + \frac{1}{3}(2B_3 - B_2)R\cos2\theta \qquad (A.46)$$

The actual expressions for B_1, B_2, B_3 have already been
derived in Step 2; they are given in Eqs. (A.30) for the

367

full-slip case and in Eqs. (A.39) for the no-slip case. The
support forces, in dimensionless form, for the full-slip
case are thus:

$$\frac{T}{PR} = \frac{1}{2}(1+K)(1-a_0^*) + \frac{1}{2}(1-K)(1-2a_2^*)\cos2\theta \qquad\qquad \text{(A.47a)}$$

$$\frac{M}{PR^2} = \frac{1}{2}(1-K)(1-2a_2^*)\cos2\theta \qquad\qquad\qquad\qquad \text{(A.47b)}$$

where a_0^*, a_2^* are given in Eqs. (A.32). Similarly for the
no-slip case:

$$\frac{T}{PR} = \frac{1}{2}(1+K)(1-a_0^*) + \frac{1}{2}(1-K)(1+2a_2^*)\cos2\theta \qquad\qquad \text{(A.48a)}$$

$$\frac{M}{PR^2} = \frac{1}{4}(1-K)(1-2a_2^*+2b_2^*)\cos2\theta \qquad\qquad\qquad \text{(A.48b)}$$

where a_0^*, a_2^*, b_2^* are given in Eq. (A.41).

The solutions in the recent dissertation by Ranken
(1978) generally agree with the above derivations. There
are only two notable differences between the two sets of
solutions: 1) Ranken uses the old formulation for the

368

compressibility ratio C (Eq. A.8), which, as criticized earlier, is based on the stiffness of the unperforated ground mass, and 2) Ranken keeps the small second-order moment terms in Eq. (A.45). In his dissertation, Ranken also derives solutions for the excavation unloading case in which the support is treated as a thick walled cylinder. However, as he points out, "if t/R < 0.10 the two solution types [thin shell vs. thick-walled cylinder solutions] will give essentially the same results." For most practical support systems, a thickness-to-radius ratio of 0.10 is very rarely exceeded.

A.4 SUMMARY OF EXCAVATION UNLOADING SOLUTIONS

The expressions for the support forces and displacements in the full-slip case are:

$$\frac{T}{PR} = \frac{1}{2}(1+K)(1-a_0^*) + \frac{1}{2}(1-K)(1-2a_2^*)\cos2\theta \qquad (A.47a)$$

$$\frac{M}{PR^2} = \frac{1}{2}(1-K)(1-2a_2^*)\cos2\theta \qquad (A.47b)$$

$$\frac{u_s E}{PR(1+\nu)} = \frac{1}{2}(1+K)a_0^* - (1-K)[(5-6\nu)a_2^* - (1-\nu)]\cos2\theta \qquad (A.31a)$$

$$\frac{v_s E}{PR(1+\nu)} = \frac{1}{2}(1-K)\left[(5-6\nu)a_2^* - (1-\nu)\right]\sin2\theta \qquad \text{(A.31b)}$$

in which:

$$a_0^* = \frac{C^* F^* (1-\nu)}{C^* + F^* + C^* F^* (1-\nu)} \qquad \text{(A.32a)}$$

$$a_2^* = \frac{(F^*+6)(1-\nu)}{2F^*(1-\nu) + 6(5-6\nu)} \qquad \text{(A.32b)}$$

C^*, F^* given in Eqs. (A.3) and (A.6)

For the no-slip case:

$$\frac{T}{PR} = \frac{1}{2}(1+K)(1-a_0^*) + \frac{1}{2}(1-K)(1+2a_2^*)\cos2\theta \qquad \text{(A.48a)}$$

$$\frac{M}{PR^2} = \frac{1}{4}(1-K)(1-2a_2^* + 2b_2^*)\cos2\theta \qquad \text{(A.48b)}$$

370

$$\frac{u_s E}{PR(1+\nu)} = \frac{1}{2}(1+K)a_0^* + (1-K)[2(1-\nu)b_2^* - a_2^*]\cos 2\theta \qquad \text{(A.40a)}$$

$$\frac{v_s E}{PR(1+\nu)} = -(1-K)[a_2^* + (1-2\nu)b_2^*]\sin 2\theta \qquad \text{(A.40b)}$$

in which:

$$a_0^* = \frac{C^* F^* (1-\nu)}{C^* + F^* + C^* F^* (1-\nu)} \qquad \text{(A.41a)}$$

$$\hat{b} = \frac{C^*(F^*+6)(1-\nu) + 2F^*\nu}{3F^* + 3C^* + 2C^* F^* (1-\nu)} \qquad \text{(A.41b)}$$

$$b_2^* = \frac{C^*(1-\nu)}{2[C^*(1-\nu) + 4\nu - 6\hat{b} - 3\hat{b}C^*(1-\nu)]} \qquad \text{(A.41c)}$$

$$a_2^* = \hat{b}b_2^* \qquad \text{(A.41d)}$$

C^*, F^* given in Eqs. (A.3) and (A.6)

A.5 SUMMARY OF EXTERNAL LOADING SOLUTIONS

For the sake of completeness, two published relative stiffness solutions incorporating the external loading condition are summarized here. For the full-slip, external loading case, the dimensionless support forces and radial displacement are (after Peck, Hendron, and Mohraz, 1972):

$$\frac{T}{PR} = \frac{1}{2}(1+K)(1-a_1) + \frac{1}{6}(1-K)(1+3a_2-4a_3)\cos2\theta \qquad \text{(A.49a)}$$

$$\frac{M}{PR^2} = \frac{1}{6}(1-K)(1+3a_2-4a_3)\cos2\theta \qquad \text{(A.49b)}$$

$$\frac{u_sE}{PR(1+\nu)} = \frac{1}{2}(1+K)C^*(1-\nu)(1-a_1) - \frac{1}{18}(1-K)F^*(1-\nu)(1+3a_2-4a_3)\cos2\theta$$

$$\text{(A.50)}$$

in which:

$$a_1 = \frac{C^*(1-\nu) - 1 + 2\nu}{C^*(1-\nu) + 1} \qquad \text{(A.51a)}$$

$$a_2 = \frac{F^*(1-\nu) + 3 - 6\nu}{F^*(1-\nu) + 15 - 18\nu} \qquad \text{(A.51b)}$$

372

$$a_3 = \frac{F^*(1-\nu) - 3}{F^*(1-\nu) + 15 - 18\nu} \qquad \text{(A.51c)}$$

C^*, F^* given in Eqs. (A.3),(A.6)

For the no-slip, external loading case the expressions are (after Hoeg, 1968):

$$\frac{T}{PR} = \tfrac{1}{2}(1+K)(1-a_1) + \tfrac{1}{2}(1-K)(1+a_2)\cos2\theta \qquad \text{(A.52a)}$$

$$\frac{M}{PR^2} = \tfrac{1}{4}(1-K)(1-a_2-2a_3)\cos2\theta \qquad \text{(A.52b)}$$

$$\frac{u_s E}{PR(+\nu)} = \tfrac{1}{2}(1+K)(1-2\nu)\left[1+\frac{a_1}{(1-2\nu)}\right] - \tfrac{1}{2}(1-K)\left[1+a_2+4(1-\nu)a_3\right]\cos2\theta$$

$$\text{(A.53)}$$

in which:

$$a_1 = \frac{C^*(1-\nu) - 1 + 2\nu}{C^*(1-\nu) + 1} \qquad \text{(A.54a)}$$

$$\hat{a} = \frac{F^*(1-\nu)}{6} \left[(3-2\nu) + C^*(1-\nu) \right] + \frac{C^*(1-\nu)}{(1-2\nu)} \left[\frac{5}{2} - 8\nu + 6\nu^2 \right] + 6 - 8\nu$$

$$(A.54b)$$

$$a_2 = \frac{1}{\hat{a}} \left\{ \frac{F^*(1-\nu)}{6} \left[(1-2\nu) - C^*(1-\nu) \right] - \frac{1}{2} C^*(1-\nu)(1-2\nu) + 2 \right\}$$

$$(A.54c)$$

$$a_3 = \frac{1}{\hat{a}} \left\{ \frac{F^*(1-\nu)}{6} \left[C^*(1-\nu) + 1 \right] - \frac{1}{2} C^*(1-\nu) - 2 \right\} \qquad (A.54d)$$

C^*, F^* given in Eqs. (A.3), (A.6)

A.6 HP97 PROGRAMS FOR RELATIVE STIFFNESS SOLUTIONS

The relative stiffness solutions derived in this Appendix have been programmed on a Hewlett-Packard Model HP97 desk top calculator. Program listings and documentation are provided in this section for the following four solutions:

1) Excavation Unloading, Full-Slip

2) Excavation Unloading, No-Slip

3) External Loading, Full-Slip (Peck et al., 1972)

4) External Loading, No-Slip (Hoeg, 1968)

374

All of these programs use the same input format. The input
variables are initially stored in the registers as follows:

Register	Variable
1	C^*
2	F^*
3	ν
4	K
5	θ

Generally, Program A calculates the dimensionless thrust
coefficient, Program B the dimensionless moment coefficient,
and Program C the dimensionless displacement coefficient.
The exception to this is the External Loading, Full-Slip
program; here, $\frac{T}{PR}$ and $\frac{M}{PR^2}$ are both calculated using Program A,
and $\frac{u_s E}{PR(1+\nu)}$ is calculated from Program B. For the External
Loading, No-Slip solution, the program is too long for one
card and has been split; the thrusts and moments are calculated
from Programs A and B on the first card, and the displacements
are calculated from Program C on the second.

User Instructions

EXCAVATION UNLOADING, FULL-SLIP

$$\frac{T}{PR} \qquad \frac{M}{PR^2} \qquad \frac{u_s E}{PR(1+\nu)}$$

STEP	INSTRUCTIONS	INPUT DATA/UNITS	KEYS		OUTPUT DATA/UNITS
1	LOAD SIDES 1 AND 2				
2	STORE INPUT DATA	C^*	STO	1	
		F^*	STO	2	
		ν	STO	3	
		K	STO	4	
		θ	STO	5	
3	CALCULATE THRUST COEFFICIENT		A		T/PR
4	CALCULATE MOMENT COEFFICIENT		B		M/PR^2
5	CALCULATE DISPLACEMENT COEFFICIENT		C		$uE/PR(1+\nu)$

STEP	KEY ENTRY	KEY CODE	COMMENTS	STEP	KEY ENTRY	KEY CODE	COMMENTS
001	*LBL1	21 01		057	+	-55	
002	RCL3	36 03		058	x	-35	
003	CHS	-22		059	2	02	
004	1	01		060	÷	-24	
005	+	-55		061	STO8	35 08	
006	RCL2	36 02		062	GSB2	23 02	
007	x	-35		063	2	02	
008	RCL1	36 01		064	y	-35	
009	x	-35		065	CHS	-22	
010	STO6	35 06		066	1	01	
011	RCL2	36 02		067	+	-55	
012	+	-55		068	RCL4	36 04	
013	RCL1	36 01		069	CHS	-22	
014	+	-55		070	1	01	
015	RCL6	36 06		071	+	-55	
016	÷	-24		072	x	-35	
017	1/X	52		073	2	02	
018	RTN	24		074	÷	-24	
019	*LBL2	21 02		075	RCL5	36 05	
020	RCL3	36 03		076	2	02	
021	CHS	-22		077	x	-35	
022	1	01		078	COS	42	
023	+	-55		079	x	-35	
024	RCL2	36 02		080	RCL8	36 08	
025	6	06		081	+	-55	
026	+	-55		082	PRTX	-14	
027	x	-35		083	RTN	24	
028	STO7	35 07		084	*LBLB	21 12	
029	RCL3	36 03		085	GSB2	23 02	
030	CHS	-22		086	2	02	
031	1	01		087	x	-35	
032	+	-55		088	CHS	-22	
033	RCL2	36 02		089	1	01	
034	x	-35		090	+	-55	
035	2	02		091	RCL4	36 04	
036	x	-35		092	CHS	-22	
037	RCL3	36 03		093	1	01	
038	6	06		094	+	-55	
039	x	-35		095	x	-35	
040	CHS	-22		096	2	02	
041	5	05		097	÷	-24	
042	+	-55		098	RCL5	36 05	
043	6	06		099	2	02	
044	x	-35		100	x	-35	
045	+	-55		101	COS	42	
046	RCL7	36 07		102	x	-35	
047	÷	-24		103	PRTX	-14	
048	1/X	52		104	RTN	24	
049	RTN	24		105	*LBLC	21 13	
050	*LBLA	21 11		106	GSB1	23 01	
051	GSB1	23 01		107	RCL4	36 04	
052	CHS	-22		108	1	01	
053	1	01		109	÷	-55	
054	+	-55		110	x	-35	
055	RCL4	36 04		111	2	02	
056	1	01		112	÷	-24	

REGISTERS

0	1 C^*	2 F^*	3 ν	4 K	5 θ	6 USED	7 USED	8 USED	9 USED
S0	S1	S2	S3	S4	S5	S6	S7	S8	S9
A	B		C	D		E		I	

STEP	KEY ENTRY	KEY CODE	COMMENTS	STEP	KEY ENTRY	KEY CODE	COMMENTS
113	ST09	35 09					
114	GSB2	23 02		170			
115	RCL3	36 03					
116	6	06					
117	x	-35					
118	CHS	-22					
119	5	05					
120	+	-55					
121	x	-35					
122	RCL3	36 03					
123	+	-55					
124	1	01		180			
125	-	-45					
126	RCL4	36 04					
127	CHS	-22					
128	1	01					
129	+	-55					
130	x	-35					
131	RCL5	36 05					
132	2	02					
133	x	-35					
134	COS	42		190			
135	x	-35					
136	CHS	-22					
137	RCL9	36 09					
138	+	-55					
139	PRTX	-14					
140	RTN	24					
141	R/S	51					
				200			
150							
				210			
160							
				220			

LABELS

A T/PR	B M/PR²	C u E/PR(HN)	D	E
a	b	c	d	e
0	1 USED	2 USED	3	4
5	6	7	8	9

FLAGS

0
1
2
3

SET STATUS

FLAGS		TRIG	DISP
	ON OFF		
0	☐ ☒	DEG ☒	FIX ☐
1	☐ ☒	GRAD ☐	SCI ☒
2	☐ ☒	RAD ☐	ENG ☐
3	☐ ☒		n 2

EXCAVATION UNLOADING, NO-SLIP

$\dfrac{T}{PR} \qquad \dfrac{M}{PR^2} \qquad \dfrac{U_S E}{PR(1+\nu)}$

STEP	INSTRUCTIONS	INPUT DATA/UNITS	KEYS		OUTPUT DATA/UNITS
1	LOAD SIDES 1 AND 2				
2	STORE INPUT DATA	C^*	STO	1	
		F^*	STO	2	
		ν	STO	3	
		K	STO	4	
		θ	STO	5	
3	CALCULATE THRUST COEFFICIENT		A		T/PR
4	CALCULATE MOMENT COEFFICIENT		B		M/PR^2
5	CALCULATE DISPLACEMENT COEFFICIENT		C		$U E/PR(1+\nu)$

Program Listing I

STEP	KEY ENTRY	KEY CODE	COMMENTS	STEP	KEY ENTRY	KEY CODE	COMMENTS
001	*LBL1	21 01		057	RCL2	36 02	
002	RCL3	36 03		058	x	-35	
003	CHS	-22		059	RCL3	36 03	
004	1	01		060	CHS	-22	
005	+	-55		061	1	01	
006	RCL2	36 02		062	+	-55	
007	x	-35		063	x	-35	
008	RCL1	36 01		064	RCL7	36 07	
009	x	-35		065	÷	-24	
010	2	02		066	RTN	24	
011	x	-35		067	*LBL3	21 03	
012	RCL1	36 01		068	GSB1	23 01	
013	3	03		069	3	03	
014	x	-35		070	x	-35	
015	+	-55		071	RCL1	36 01	
016	RCL2	36 02		072	x	-35	
017	3	03		073	RCL3	36 03	
018	x	-35		074	CHS	-22	
019	+	-55		075	1	01	
020	STO6	35 06		076	+	-55	
021	RCL1	36 01		077	x	-35	
022	RCL2	36 02		078	STO9	35 09	
023	x	-35		079	GSB1	23 01	
024	RCL1	36 01		080	6	06	
025	6	06		081	x	-35	
026	x	-35		082	RCL9	36 09	
027	+	-55		083	+	-55	
028	RCL3	36 03		084	CHS	-22	
029	CHS	-22		085	RCL3	36 03	
030	1	01		086	4	04	
031	+	-55		087	x	-35	
032	x	-35		088	+	-55	
033	RCL2	36 02		089	RCL3	36 03	
034	RCL3	36 03		090	CHS	-22	
035	x	-35		091	1	01	
036	2	02		092	+	-55	
037	x	-35		093	RCL1	36 01	
038	+	-55		094	x	-35	
039	RCL6	36 06		095	+	-55	
040	÷	-24		096	2	02	
041	RTN	24		097	x	-35	
042	*LBL2	21 02		098	STO8	35 08	
043	RCL1	36 01		099	RCL3	36 03	
044	RCL2	36 02		100	CHS	-22	
045	x	-35		101	1	01	
046	RCL3	36 03		102	+	-55	
047	CHS	-22		103	RCL1	36 01	
048	1	01		104	x	-35	
049	+	-55		105	RCL8	36 08	
050	x	-35		106	÷	-24	
051	RCL1	36 01		107	RTN	24	
052	+	-55		108	*LBL4	21 04	
053	RCL2	36 02		109	GSB3	23 03	
054	+	-55		110	STO0	35 00	
055	STO7	35 07		111	GSB1	23 01	
056	RCL1	36 01		112	RCL0	36 00	

REGISTERS

0 USED	1 C*	2 F*	3 ν	4 K	5 θ	6 USED	7 USED	8 USED	9 USED
S0	S1	S2	S3	S4	S5	S6	S7	S8	S9
A USED	B USED	C	D	E	I				

380

STEP	KEY ENTRY	KEY CODE	COMMENTS	STEP	KEY ENTRY	KEY CODE	COMMENTS
113	x	-35		169	COS	42	
114	RTN	24		170	x	-35	
115	*LBLA	21 11		171	PRTX	-14	
116	GSB2	23 02		172	RTN	24	
117	CHS	-22		173	*LBLC	21 13	
118	1	01		174	GSB2	23 02	
119	+	-55		175	RCL4	36 04	
120	RCL4	36 04		176	1	01	
121	1	01		177	+	-55	
122	+	-55		178	x	-35	
123	x	-35		179	2	02	
124	2	02		180	÷	-24	
125	÷	-24		181	STOB	35 12	
126	STOA	35 11		182	GSB4	23 04	
127	GSB4	23 04		183	2	02	
128	2	02		184	x	-35	
129	x	-35		185	CHS	-22	
130	1	01		186	RCL0	36 00	
131	+	-55		187	RCL3	36 03	
132	RCL4	36 04		188	CHS	-22	
133	CHS	-22		189	1	01	
134	1	01		190	+	-55	
135	+	-55		191	x	-35	
136	x	-35		192	4	04	
137	2	02		193	x	-35	
138	÷	-24		194	+	-55	
139	RCL5	36 05		195	RCL4	36 04	
140	2	02		196	CHS	-22	
141	x	-35		197	1	01	
142	COS	42		198	+	-55	
143	x	-35		199	x	-35	
144	RCLA	36 11		200	2	02	
145	+	-55		201	÷	-24	
146	PRTX	-14		202	RCL5	36 05	
147	RTN	24		203	2	02	
148	*LBLB	21 12		204	x	-35	
149	GSB4	23 04		205	COS	42	
150	2	02		206	x	-35	
151	x	-35		207	RCLB	36 12	
152	CHS	-22		208	+	-55	
153	1	01		209	PRTX	-14	
154	+	-55		210	RTN	24	
155	RCL0	36 00		211	R/S	51	
156	2	02					
157	x	-35					
158	+	-55					
159	RCL4	36 04					
160	CHS	-22					
161	1	01					
162	+	-55					
163	x	-35					
164	4	04		220			
165	÷	-24					
166	RCL5	36 05					
167	2	02					
168	x	-35					

LABELS

A T/PR	B M/PR²	C u E/PR(H-U)	D	E
a	b	c	d	e
0	1 USED	2 USED	3 USED	4 USED
5	6	7	8	9

FLAGS

0
1
2
3

SET STATUS

FLAGS ON OFF	TRIG	DISP
0 ☐ ☒	DEG ☒	FIX ☐
1 ☐ ☒	GRAD ☐	SCI ☒
2 ☐ ☒	RAD ☐	ENG ☐
3 ☐ ☒		n 2

381

EXTERNAL LOADING, FULL SLIP

$$\frac{M}{PR^2}; \frac{T}{PR}, \frac{u_s E}{PR(1+\nu)}$$

STEP	INSTRUCTIONS	INPUT DATA/UNITS	KEYS		OUTPUT DATA/UNITS
1	LOAD SIDES 1 AND 2				
2	STORE INPUT DATA	C*	STO	1	
		F*	STO	2	
		J	STO	3	
		K	STO	4	
		θ	STO	5	
3	CALCULATE MOMENT AND THRUST COEFFICIENTS		A		M/PR^2; T/PR
4	CALCULATE DISPLACEMENT COEFFICIENT		B		$uE/PR(1+\nu)$

382

Program Listing 1

STEP	KEY ENTRY	KEY CODE	COMMENTS	STEP	KEY ENTRY	KEY CODE	COMMENTS
001	*LBL1	21 01		057	1	01	
002	RCL3	36 03		058	+	-55	
003	CHS	-22		059	STO0	35 00	
004	1	01		060	RCL8	36 08	
005	+	-55		061	3	03	
006	RCL1	36 01		062	-	-45	
007	x	-35		063	STOA	35 11	
008	STO6	35 06		064	RCL8	36 08	
009	1	01		065	1	01	
010	-	-45		066	5	05	
011	RCL3	36 03		067	+	-55	
012	2	02		068	RCL3	36 03	
013	x	-35		069	1	01	
014	+	-55		070	8	08	
015	STO7	35 07		071	x	-35	
016	RCL6	36 06		072	-	-45	
017	1	01		073	RCLA	36 11	
018	+	-55		074	÷	-24	
019	RCL7	36 07		075	1/X	52	
020	÷	-24		076	4	04	
021	1/X	52		077	x	-35	
022	CHS	-22		078	CHS	-22	
023	1	01		079	RCL0	36 00	
024	+	-55		080	+	-55	
025	RTN	24		081	RTN	24	
026	*LBL2	21 02		082	*LBLA	21 11	
027	RCL3	36 03		083	GSB1	23 01	
028	CHS	-22		084	RCL4	36 04	
029	1	01		085	1	01	
030	+	-55		086	+	-55	
031	RCL2	36 02		087	x	-35	
032	x	-35		088	2	02	
033	STO8	35 08		089	÷	-24	
034	3	03		090	STOB	35 12	
035	+	-55		091	GSB2	23 02	
036	RCL3	36 03		092	RCL4	36 04	
037	6	06		093	CHS	-22	
038	x	-35		094	1	01	
039	CHS	-22		095	+	-55	
040	+	-55		096	x	-35	
041	STO9	35 09		097	6	06	
042	RCL8	36 08		098	÷	-24	
043	1	01		099	RCL5	36 05	
044	5	05		100	2	02	
045	+	-55		101	x	-35	
046	RCL3	36 03		102	COS	42	
047	1	01		103	x	-35	
048	8	08		104	~~CHS~~	~~-22~~	(DELETE)
049	x	-35		105	PRTX	-14	
050	CHS	-22		106	~~CHS~~	~~-22~~	(DELETE)
051	+	-55		107	RCLB	36 12	
052	RCL9	36 09		108	+	-55	
053	÷	-24		109	PRTX	-14	
054	1/X	52		110	RTN	24	
055	3	03		111	*LBLB	21 12	
056	x	-35		112	GSB1	23 01	

REGISTERS

0	1	2	3	4	5	6	7	8	9
USED	C*	F*	ν	K	θ	USED	USED	USED	USED

S0	S1	S2	S3	S4	S5	S6	S7	S8	S9

A	B	C	D	E	I
USED	USED	USED			

383

STEP	KEY·ENTRY	KEY CODE	COMMENTS	STEP	KEY ENTRY	KEY CODE	COMMENTS
113	RCL4	36 04					
114	1	01		170			
115	+	-55					
116	x	-35					
117	RCL1	36 01					
118	x	-35					
119	2	02					
120	÷	-24					
121	STOC	35 13					
122	GSB2	23 02					
123	RCL4	36 04					
124	CHS	-22		180			
125	1	01					
126	+	-55					
127	x	-35					
128	RCL2	36 02					
129	x	-35					
130	1	01					
131	8	08					
132	÷	-24					
133	RCL5	36 05					
134	2	02		190			
135	x	-35					
136	COS	42					
137	x	-35					
138	CHS	-22					
139	RCLC	36 13					
140	+	-55					
141	RCL3	36 03					
142	CHS	-22					
143	1	01					
144	+	-55		200			
145	x	-35					
146	PRTX	-14					
147	RTN	24					
148	R/S	51					

384

EXTERNAL LOADING, NO-SLIP

$\dfrac{T}{PR} \qquad \dfrac{M}{PR^2}$

STEP	INSTRUCTIONS	INPUT DATA/UNITS	KEYS		OUTPUT DATA/UNITS
1	LOAD SIDES 1 AND 2				
2	STORE INPUT DATA	C^*	STO	1	
		F^*	STO	2	
		ν	STO	3	
		K	STO	4	
		θ	STO	5	
3	CALCULATE THRUST COEFFICIENT		A		T/PR
4	CALCULATE MOMENT COEFFICIENT		B		M/PR^2

STEP	KEY ENTRY	KEY CODE	COMMENTS	STEP	KEY ENTRY	KEY CODE	COMMENTS
001	*LBL1	21 01		057	CHS	-22	
002	RCL3	36 03		058	+	-55	
003	CHS	-22		059	RCL6	36 06	
004	1	01		060	+	-55	
005	+	-55		061	RTN	24	
006	RCL1	36 01		062	*LBL2	21 02	
007	x	-35		063	RCL3	36 03	
008	RCL3	36 03		064	CHS	-22	
009	2	02		065	1	01	
010	x	-35		066	+	-55	
011	CHS	-22		067	RCL1	36 01	
012	3	03		068	x	-35	
013	+	-55		069	STO7	35 07	
014	+	-55		070	1	01	
015	RCL3	36 03		071	-	-45	
016	CHS	-22		072	RCL3	36 03	
017	1	01		073	2	02	
018	+	-55		074	x	-35	
019	x	-35		075	+	-55	
020	6	06		076	RCL7	36 07	
021	÷	-24		077	1	01	
022	RCL2	36 02		078	+	-55	
023	x	-35		079	÷	-24	
024	STO6	35 06		080	RTN	24	
025	RCL3	36 03		081	*LBL3	21 03	
026	x^2	53		082	RCL3	36 03	
027	6	06		083	2	02	
028	x	-35		084	x	-35	
029	RCL3	36 03		085	CHS	-22	
030	8	08		086	1	01	
031	x	-35		087	+	-55	
032	CHS	-22		088	RCL7	36 07	
033	+	-55		089	CHS	-22	
034	2	02		090	+	-55	
035	.	-62		091	RCL3	36 03	
036	5	05		092	CHS	-22	
037	+	-55		093	1	01	
038	RCL3	36 03		094	+	-55	
039	CHS	-22		095	x	-35	
040	1	01		096	6	06	
041	+	-55		097	÷	-24	
042	x	-35		098	RCL2	36 02	
043	RCL3	36 03		099	x	-35	
044	2	02		100	STO8	35 08	
045	x	-35		101	RCL3	36 03	
046	CHS	-22		102	2	02	
047	1	01		103	x	-35	
048	+	-55		104	CHS	-22	
049	÷	-24		105	1	01	
050	RCL1	36 01		106	+	-55	
051	x	-35		107	RCL7	36 07	
052	6	06		108	x	-35	
053	+	-55		109	2	02	
054	RCL3	36 03		110	÷	-24	
055	8	08		111	CHS	-22	
056	x	-35		112	2	02	

REGISTERS

0 USED	1 C*	2 F*	3 U	4 K	5 θ	6 USED	7 USED	8 USED	9
S0	S1	S2	S3	S4	S5	S6	S7	S8	S9

A	B USED	C USED	D	E USED	I

STEP	KEY ENTRY	KEY CODE	COMMENTS	STEP	KEY ENTRY	KEY CODE	COMMENTS
113	+	-55		169	CHS	-22	
114	RCLB	36 08		170	1	01	
115	+	-55		171	+	-55	
116	STOB	35 12		172	x	-35	
117	GSB1	23 01		173	2	02	
118	RCLB	36 12		174	÷	-24	
119	÷	-24		175	GSB5	23 05	
120	1/X	52		176	x	-35	
121	RTN	24		177	RCL0	36 00	
122	*LBL4	21 04		178	+	-55	
123	RCL7	36 07		179	PRTX	-14	
124	1	01		180	RTN	24	
125	+	-55		181	*LBLB	21 12	
126	RCL3	36 03		182	GSB4	23 04	
127	CHS	-22		183	2	02	
128	1	01		184	x	-35	
129	+	-55		185	STOE	35 15	
130	x	-35		186	GSB3	23 03	
131	6	06		187	RCLE	36 15	
132	÷	-24		188	+	-55	
133	RCL2	36 02		189	CHS	-22	
134	x	-35		190	1	01	
135	RCL7	36 07		191	+	-55	
136	2	02		192	RCL4	36 04	
137	÷	-24		193	CHS	-22	
138	-	-45		194	1	01	
139	2	02		195	+	-55	
140	-	-45		196	x	-35	
141	STOC	35 13		197	4	04	
142	GSB1	23 01		198	÷	-24	
143	RCLC	36 13		199	GSB5	23 05	
144	÷	-24		200	x	-35	
145	1/X	52		201	PRTX	-14	
146	RTN	24		202	RTN	24	
147	*LBL5	21 05		203	R/S	51	
148	RCL5	36 05					
149	2	02					
150	x	-35					
151	COS	42					
152	RTN	24					
153	*LBLA	21 11					
154	GSB2	23 02		210			
155	CHS	-22					
156	1	01					
157	+	-55					
158	RCL4	36 04					
159	1	01					
160	+	-55					
161	x	-35					
162	2	02					
163	÷	-24					
164	STO0	35 00		220			
165	GSB3	23 03					
166	1	01					
167	+	-55					
168	RCL4	36 04					

LABELS

A T/PR.	B M/PR.²	C	D	E
a	b	c	d	e
0	1 USEL	2 USEL	3 USEL	4 USEL
5 USEL	6	7	8	9

FLAGS

0
1
2
3

SET STATUS

FLAGS		TRIG	DISP
	ON OFF	DEG ☒	FIX ☐
0	☐ ☒	GRAD ☐	SCI ☒
1	☐ ☒	RAD ☐	ENG ☐
2	☐ ☒		n 2
3	☐ ☒		

387

EXTERNAL LOADING, NO-SLIP

$$\frac{u, E}{PR(1+\nu)}$$

STEP	INSTRUCTIONS	INPUT DATA/UNITS	KEYS		OUTPUT DATA/UNITS
1	LOAD SIDES 1 AND 2				
2	STORE INPUT DATA	C^*	STO	1	
		F^*	STO	2	
		ν	STO	3	
		K	STO	4	
		θ	STO	5	
3	CALCULATE DISPLACEMENT COEFFICIENT		C		$uE/PR(1+\nu)$

388

Program Listing I

STEP	KEY ENTRY	KEY CODE	COMMENTS	STEP	KEY ENTRY	KEY CODE	COMMENTS
001	*LBL1	21 01		057	CHS	-22	
002	RCL3	36 03		058	+	-55	
003	CHS	-22		059	RCL6	36 06	
004	1	01		060	+	-55	
005	+	-55		061	RTN	24	
006	RCL1	36 01		062	*LBL2	21 02	
007	x	-35		063	RCL3	36 03	
008	RCL3	36 03		064	CHS	-22	
009	2	02		065	1	01	
010	x	-35		066	+	-55	
011	CHS	-22		067	RCL1	36 01	
012	3	03		068	x	-35	
013	+	-55		069	ST07	35 07	
014	+	-55		070	1	01	
015	RCL3	36 03		071	-	-45	
016	CHS	-22		072	RCL3	36 03	
017	1	01		073	2	02	
018	+	-55		074	x	-35	
019	x	-35		075	+	-55	
020	6	06		076	RCL7	36 07	
021	÷	-24		077	1	01	
022	RCL2	36 02		078	+	-55	
023	x	-35		079	÷	-24	
024	ST06	35 06		080	RTN	24	
025	RCL3	36 03		081	*LBL3	21 03	
026	x^2	53		082	RCL3	36 03	
027	6	06		083	2	02	
028	x	-35		084	x	-35	
029	RCL3	36 03		085	CHS	-22	
030	8	08		086	1	01	
031	x	-35		087	+	-55	
032	CHS	-22		088	RCL7	36 07	
033	+	-55		089	CHS	-22	
034	2	02		090	+	-55	
035	.	-62		091	RCL3	36 03	
036	5	05		092	CHS	-22	
037	+	-55		093	1	01	
038	RCL3	36 03		094	+	-55	
039	CHS	-22		095	x	-35	
040	1	01		096	6	06	
041	+	-55		097	÷	-24	
042	x	-35		098	RCL2	36 02	
043	RCL3	36 03		099	x	-35	
044	2	02		100	ST08	35 08	
045	x	-35		101	RCL3	36 03	
046	CHS	-22		102	2	02	
047	1	01		103	x	-35	
048	+	-55		104	CHS	-22	
049	÷	-24		105	1	01	
050	RCL1	36 01		106	+	-55	
051	x	-35		107	RCL7	36 07	
052	6	06		108	x	-35	
053	+	-55		109	2	02	
054	RCL3	36 03		110	÷	-24	
055	8	08		111	CHS	-22	
056	x	-35		112	2	02	

REGISTERS

0	1 C*	2 F*	3 N	4 K	5 θ	6 USED	7 USED	8 USED	9
S0	S1	S2	S3	S4	S5	S6	S7	S8	S9
A USED	B USED	C USED		D	E USED			I	

389

STEP	KEY ENTRY	KEY CODE	COMMENTS	STEP	KEY ENTRY	KEY CODE	COMMENTS
113	+	-55		169	2	02	
114	RCL8	36 08		170	x	-35	
115	+	-55		171	CHS	-22	
116	STOB	35 12		172	1	01	
117	GSB1	23 01		173	+	-55	
118	RCLB	36 12		174	x	-35	
119	÷	-24		175	2	02	
120	1/X	52		176	÷	-24	
121	RTN	24		177	STOA	35 11	
122	*LBL4	21 04		178	GSB4	23 04	
123	RCL7	36 07		179	RCL3	36 03	
124	1	01		180	CHS	-22	
125	+	-55		181	1	01	
126	RCL3	36 03		182	+	-55	
127	CHS	-22		183	x	-35	
128	1	01		184	4	04	
129	+	-55		185	x	-35	
130	x	-35		186	STOE	35 15	
131	6	06		187	GSB3	23 03	
132	÷	-24		188	RCLE	36 15	
133	RCL2	36 02		189	+	-55	
134	x	-35		190	1	01	
135	RCL7	36 07		191	+	-55	
136	2	02		192	RCL4	36 04	
137	÷	-24		193	CHS	-22	
138	-	-45		194	1	01	
139	2	02		195	+	-55	
140	-	-45		196	x	-35	
141	STOC	35 13		197	2	02	
142	GSB1	23 01		198	÷	-24	
143	RCLC	36 13		199	GSB5	23 05	
144	÷	-24		200	x	-35	
145	1/X	52		201	CHS	-22	
146	RTN	24		202	RCLA	36 11	
147	*LBL5	21 05		203	+	-55	
148	RCL5	36 05		204	PRTX	-14	
149	2	02		205	RTN	24	
150	x	-35		206	R/S	51	
151	COS	42					
152	RTN	24					
153	*LBLC	21 13					
154	GSB2	23 02		210			
155	RCL3	36 03					
156	2	02					
157	x	-35					
158	CHS	-22					
159	1	01					
160	+	-55					
161	÷	-24					
162	1	01					
163	+	-55					
164	RCL4	36 04		220			
165	1	01					
166	+	-55					
167	x	-35					
168	RCL3	36 03					

LABELS

A	B	C uE/FR(H+N)	D	E
a	b	c	d	e
0	1 USED	2 USED	3 USED	4 USED
5 USED	6	7	8	9

FLAGS

0	1	2	3

SET STATUS

FLAGS		TRIG	DISP
	ON OFF	DEG ☒	FIX ☐
0	☐ ☒	GRAD ☐	SCI ☒
1	☐ ☒	RAD ☐	ENG ☐
2	☐ ☒		n 2
3	☐ ☒		

Sketch(es)

Sample Problem(s) A BOLTED, PRECAST CONCRETE LINED TUNNEL IN A STIFF CLAY DEPOSIT, HAVING THE FOLLOWING PROPERTIES:

$$C^* = 0.05 \quad F^* = 100.0 \quad \nu = 0.4 \quad K = 0.5$$

COMPUTE THE THRUST, MOMENT, AND DISPLACEMENT COEFFICIENTS AT $\theta = 30°$ USING THE 4 RELATIVE STIFFNESS SOLUTIONS.

Solution(s)

	$\dfrac{T}{PR}$	$\dfrac{M}{PR^2}$	$\dfrac{u_s E}{PR(1+\nu)}$
EXCAVATION UNLOADING, FULL-SLIP	7.36 −01	7.74 −03	−1.33−01
EXCAVATION UNLOADING, NO-SLIP	8.12−01	7.07−03	−1.19−01
EXTERNAL LOADING, FULL-SLIP	8.87−01	1.33−02	−2.39−01
EXTERNAL LOADING, NO-SLIP	1.02+00	1.21−02	−2.16−01

Reference(s)

APPENDIX B

DERIVATION OF RELATIVE STIFFNESS SOLUTION
INCORPORATING APPROXIMATE EFFECT OF SUPPORT DELAY

B.1 ASSUMPTIONS IN THE ANALYSIS

As described in Section 3, the most important effect of support delay is that movement takes place in the ground mass before the support is constructed. This movement mobilizes some of the resistance of the ground and thereby reduces the load the support must carry. In the axisymmetric finite element analyses in Section 3, these movements were an intrinsic part of the simulation of the incremental tunnel construction. However, it is also possible to arificially incorporate these "pre-support" movements, which are directly related to the support delay length L_d, into a closed-form plane strain analysis.

These "pre-support" ground movements are treated in the present plane strain solution using the method advocated by Laabmayr and Swoboda (1978). In their system, the ground mass is initially unperforated. Before the tunnel is excavated and the support is erected, the elastic modulus within the "core" region—i.e., the region within the eventual tunnel perimeter—is reduced by a fraction β (see Figure B.1) and the ground moves radially inward by an amount u_o at r=R; the support is then activated and the core region is simultaneously "excavated" by reducing the modulus to zero.

Region A
E_A, ν_A

R u

Region B
E_B, ν_B

P

KP

P

$\nu_B = \nu_A$

$E_B = (1-\beta)E_A$
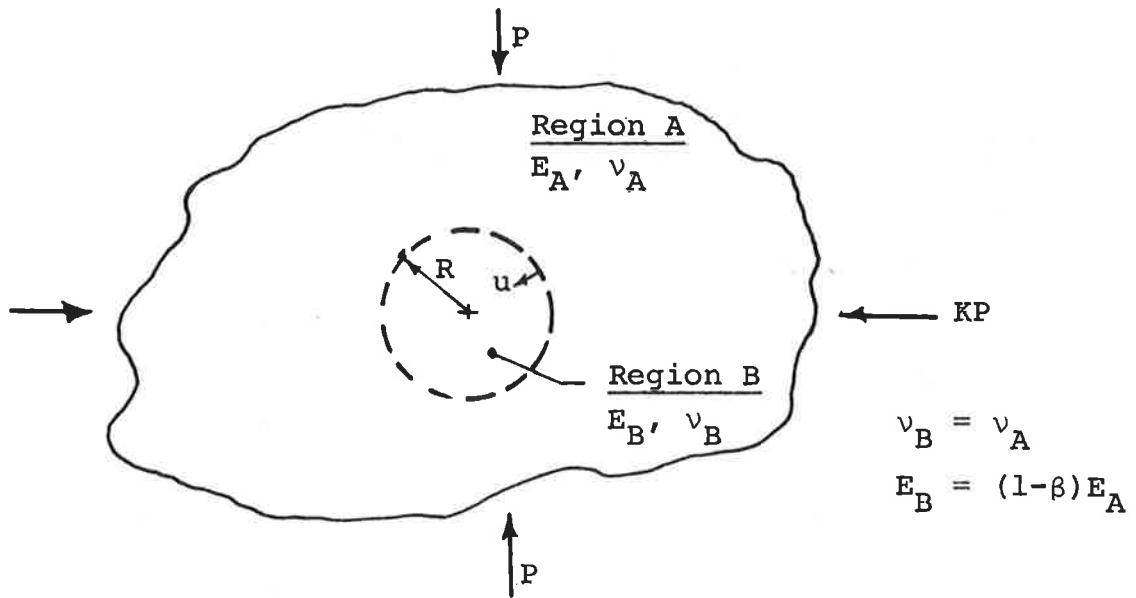
FIGURE B.1.   NOTATION

394

A closed-form plane strain solution that incorporates Laabmayr and Swoboda's approximation for the support delay is developed in this Appendix. This solution is very similar to the relative stiffness solutions derived in Appendix A. The major difference in the new solution is that, instead of deriving the initial ground displacements u_I and v_I from the in situ stresses in the unperforated ground mass, the initial ground movements are now based on the stresses existing in the ground mass after the modulus in the core region has been partially reduced. All subsequent steps in the derivations for the two solutions are the same. For simplicity, only the full-slip boundary condition at the ground-support interface is considered herein; although the no-slip condition may in fact be more appropriate in certain cases, the differences in the support loads calculated from the two (full-slip vs. no-slip) solutions would be small (see Section 2).

As in Appendix A, the ground is postulated to be an infinite, elastic, isotropic medium with initial vertical and horizontal stresses of P and KP. The tunnel support is treated as an elastic shell in which both flexural and circumferential deformations are considered (i.e., extensible shell theory is employed). Plane strain conditions are assumed throughout. The notation used in the solution is illustrated in Figure A.1 in Appendix A and in Figure B.1;

constants with capital subscripts refer to either region A or region B in Figure B.1, and constants with no subscripts apply to both regions.

B.2 DERIVATION

The derivation of the modified solution follows three basic steps:

1) Derive the initial displacement field in the outer ground region A surrounding the soft cylindrical inclusion, region B.

2) Derive the total stress and incremental displacement fields in the ground mass after excavation and the contact stresses at the ground-support interface. The incremental displacement field is the displacement field for a circular hole in the ground under an external loading condition minus the initial displacements calculated in step 1. In other words, it is the displacement field induced by the excavation in the initially stressed ground mass.

3) Compute the internal support forces induced by the contact stresses at the ground-support interface.

Only full-slip conditions at the ground-support interface are considered in the modified solution. Details of the derivation for each of the three steps are given below.

396

<u>Step 1.</u> Derivation of the initial displacement field in the

outer ground region A.

Much of the knowledge gained in the derivation of the

relative stiffness solutions in Appendix A applied equally

well to the present solution. For example, instead of

starting with Michell's generalized stress function (Eq. A.15),

the following much simpler expression, which already incor-

porates the symmetry and periodicity requirements for the

problem, can be used:

$$\phi = a\ln(r) + br^2 + [dr^2 + er^4 + fr^{-2} + g]\cos 2\theta$$

<div align="right">(B.1)</div>

The stresses are then:

$$\sigma_r = \frac{1}{r}\frac{\partial\phi}{\partial r} + \frac{1}{r^2}\frac{\partial^2\phi}{\partial\theta^2}$$

$$= ar^{-2} + 2b - [2d + 6fr^{-4} + 4gr^{-2}]\cos 2\theta$$

<div align="right">(B.2a)</div>

$$\sigma_\theta = \frac{\partial^2\phi}{\partial r^2}$$

$$= -ar^{-2} + 2b - [2d + 12er^2 + 6fr^{-4}]\cos 2\theta$$

<div align="right">(B.2b)</div>

$$\tau_{r\theta} = -\frac{\partial}{\partial r}\left[\frac{1}{r}\frac{\partial\phi}{\partial\theta}\right]$$

$$= -2[d + 3er^2 - 3fr^{-4} - gr^{-2}]\sin 2\theta$$

<div align="right">(B.2c)</div>

The stress-strain-displacement relations in polar co-ordinates are:

$$\varepsilon_r = \frac{\partial u}{\partial r} = \frac{1+\nu}{E} [(1-\nu)\sigma_r - \nu\sigma_\theta] \qquad (B.3a)$$

$$\varepsilon_\theta = \frac{\partial v}{rd\theta} + \frac{u}{r} = \frac{1-\nu}{E} [(1-\nu)\sigma_\theta - \nu\sigma_r] \qquad (B.3b)$$

Substituting (B.2) into (B.3) and integrating gives the general displacement fields:

$$u = \frac{1+\nu}{E} \{-ar^{-1} + 2br - (2dr - 2fr^{-3} - 4gr^{-1})\cos2\theta$$

$$-4\nu[br + (er^3 + gr^{-1})\cos2\theta]\} \qquad (B.4a)$$

$$v = \frac{1+\nu}{E} \{2dr + 2(3-2\nu)er^3 + 2fr^{-3} - 2(1-2\nu)gr^{-1}\}\sin2\theta$$

$$(B.4b)$$

Some of the constants in the stress function can be evaluated by considering the boundary conditions within each region.

Region A (Outer Ground)

The in situ stresses in a homogeneous infinite ground mass are:

$$\sigma_r = \frac{1}{2}P[(1+K) - (1-K)\cos2\theta] \qquad (B.5a)$$

$$\sigma_\theta = \frac{1}{2}P[(1+K) + (1-K)\cos2\theta] \qquad (B.5b)$$

399

$$\tau_{r\theta} = \frac{1}{2}P(1-K)\sin2\theta \qquad\qquad (B.5c)$$

As r approaches infinity, the stresses given by (B.2) must approach these in situ values. Therefore,

$$e_A = 0 \qquad\qquad (B.6)$$

and:

$$\sigma_r = 2b_A - 2d_A\cos2\theta = \frac{1}{2}P[(1+K)-(1-K)\cos2\theta] \qquad (B.7)$$

$$\therefore \quad b_A = \frac{1}{4}P(1+K) \qquad\qquad (B.8a)$$

$$d_A = \frac{1}{4}P(1-K) \qquad\qquad (B.8b)$$

At this point, it is convenient to introduce the following expression for the radial stress distribution at the boundary between regions A and B (i.e., at r = R):

$$\sigma_r = \frac{1}{2}P[(1+K) - (1-K)]\cos2\theta + A + B\cos2\theta \qquad (B.9)$$

This expression is of the same form as (B.2) at r = R with b_A and d_A as given by (B.8). The terms A + Bcos2θ represent the deviation of the radial stresses from the in situ values caused by the soft core region. Combining (B2a), (B.8) and (B.9) at r = R gives:

$$\frac{1}{2}P(1+K) - \frac{1}{2}P(1-K)\cos2\theta + a_A R^{-2} - (6f_A R^{-4} + 4g_A R^{-2})\cos2\theta$$

$$= \frac{1}{2}P[(1+K) - (1-K)\cos2\theta] + A + B\cos2\theta \qquad (B.10)$$

Therefore:

$$a_A = AR^2 \qquad\qquad (B.11a)$$

$$f_A = -[\frac{BR^4}{6} + \frac{2g_A R^2}{3}] \qquad\qquad (B.11b)$$

Region B (Core Region)

At $r = 0$, σ_r, σ_θ and $\tau_{r\theta}$ must all remain finite; therefore, from (B.2):

$$a_B = f_B = g_B = 0 \qquad\qquad (B.12)$$

At $r = R$, the radial stresses are given by (B.2a) and (B.9) as:

$$\sigma_R = 2b_B - 2d_B\cos2\theta = \frac{1}{2}P[(1+K) - (1-K)\cos2\theta]$$

$$+ A + B\cos2\theta \qquad\qquad (B.13)$$

$$\therefore \quad b_B = \frac{1}{4}P(1+K) + \frac{A}{2} \qquad\qquad (B.14a)$$

$$d_B = \frac{1}{4}P(1-K) - \frac{B}{2} \qquad\qquad (B.14b)$$

401

The remaining constants in the stress function must be evaluated by considering the conditions at the boundary between regions A and B itself.

Boundary Between Regions A and B

At the boundary r = R, the shear stresses in the two regions must be equal, i.e. $(\tau_{R\theta})_A = (\tau_{R\theta})_B$. Using (B.2c) for the shear stresses and (B.6), (B.8), (B.11), (B.12) and (B.14) for the constants:

(B.15)

$$\frac{1}{4}P(1-K) + \frac{B}{2} + 2g_A R^{-2} - g_A R^{-2} = \frac{1}{4}P(1-K) - \frac{B}{2} + 3e_B R^2$$

$$\therefore \quad e_B = \frac{BR^{-2}}{3} + \frac{g_A R^{-4}}{3} \qquad (B.16)$$

In addition, $(u_R)_A = (u_R)_B$ at r = R. In core region B, $E_B = (1-\beta)E_A$; using (B.4a) for the displacements, (B.6), (B.8), (B.11-12), (B.14) and (B.16) for the constants, and the definition:

$$\mu \equiv \frac{1}{1-\beta} \qquad (B.17)$$

gives the following expression:

$$-AR + \frac{1}{2}PR(1+K) - [\frac{1}{2}PR(1-K) + \frac{BR}{3} - \frac{8g_A R^{-1}}{3}]\cos 2\theta$$

$$-4\nu[\frac{1}{4}PR(1+K) + g_A R^{-1}\cos 2\theta] =$$

402

$$\mu \{ AR + \tfrac{1}{2}PR(1+K) - [\tfrac{1}{2}PR(1-K) - BR]\cos 2\theta$$

$$-4\nu[\tfrac{1}{2}PR(1+K) + \frac{AR}{2} + \frac{BR}{3} + \frac{g_A R^{-1}}{3}]\cos 2\ \theta\} \qquad (B.18)$$

At $\cos 2\theta = 0$, (B.18) becomes:

$$- AR + \tfrac{1}{2}PR(1+K) - \nu PR(1+K) = \mu\{AR + \tfrac{1}{2}PR(1+K) - \nu PR(1+K) - 2\nu AR\}$$

$$(B.19)$$

Solving (B.19) for A:

$$A = \tfrac{1}{2}P(1+K) \left[\frac{(1-\mu)(1-2\nu)}{2[1+\mu(1-2\nu)]}\right] \qquad (B.20)$$

At $\cos 2\theta = 1$, (B.18) becomes:

$$-[\tfrac{1}{2}PR(1-K) + \frac{BR}{3} - \frac{8g_A R^{-1}}{3}] - 4\nu g_A R^{-1} =$$

$$\mu\{ - [\tfrac{1}{2}PR(1-K) - BR] - 4\nu[\frac{BR}{3} + \frac{g_A R^{-1}}{3}]\} \qquad (B.21)$$

Solving (B.21) for g_A:

$$g_A = \frac{3(1-\mu)[\tfrac{1}{2}PR^2(1-K)] + BR^2[1+\mu(3-4\nu)]}{4[2 + \nu\mu - 3\nu]} \qquad (B.22)$$

403

Lastly, $(v_R)_A = (v_R)_B$ at the boundary $r = R$. Using (B.4b) for the displacements and (B.6), (B.8), (B.11 – 12), (B.14), and (B.16) for the constants:

$$\tfrac{1}{2}PR(1-K) \;-\; \frac{BR}{6} \;-\; \frac{2g_A R^{-1}}{3} \;-\; (1-2\nu)g_A R^{-1} \;=$$

$$\mu\{\tfrac{1}{4}PR(1-K) \;-\; \frac{BR}{2} \;+\; (3-2\nu)[\frac{BR}{3} + \frac{g_A R^{-1}}{3}]\} \qquad (B.23)$$

Collecting terms:

$$(1-\mu)\tfrac{1}{4}PR(1-K) \;-\; \frac{g_A R^{-1}}{3}\,[2+3(1-2\nu) + \mu(3-2\nu)]$$

$$= \frac{BR}{6}\,[2\mu(3-2\nu) - 3\mu + 1] \qquad (B.24)$$

Substituting (B.22) into (B.24), simplifying and collecting terms gives:

$$(1-\mu)\tfrac{1}{2}PR(1-K)\{2[2+\nu\mu-3\nu] - [2+3(1-2\nu) + \mu(3-2\nu)]\}$$

$$= \frac{BR}{3}\{[1+\mu(3-4\nu)][2+3(1-2\nu) + \mu(3-2\nu)]$$

$$+ [2\mu(3-2\nu) -3\mu + 1][4+2\nu\mu-6\nu]\}$$

$$(B.25)$$

Solving for B yields:

$$B = \tfrac{1}{2}P(1-K)\left[\frac{-(1-\mu)[1+\mu(3-4\nu)]}{[(1+\mu)^2(3-4\nu)+4\mu(1-2\nu)^2]}\right] \qquad (B.26)$$

In summary, the initial ground displacements in the outer ground region A can be obtained by combining (B.4), (B.6), (B.8), and (B.11)

$$u_I = \frac{1+\nu}{E}\left[\tfrac{1}{2}PR(1+K) - \tfrac{1}{2}PR(1-K)\cos2\theta\right.$$

$$- AR - (\frac{BR}{3} - \frac{8g_A R^{-1}}{3})\cos2\theta$$

$$\left. - \nu[PR(1+K) + 4g_A R^{-1}]\cos2\theta\right] \qquad (B.27a)$$

$$v_I = \frac{1+\nu}{E}\left[\tfrac{1}{2}PR(1-K) - \frac{BR}{3} - \frac{10g_A R^{-1}}{3} + 4\nu g_A R^{-1}\right]\sin2\theta \quad '$$

$$(B.27b)$$

in which:

$$A = \tfrac{1}{2}P(1+K)\left\{\frac{(1-\mu)(1-2\nu)}{2[1+\mu(1-2\nu)]}\right\} \qquad (B.20)$$

$$B = \tfrac{1}{2}P(1-K)\left\{\frac{-(1-\mu)[1+\mu(3-4\nu)]}{[(1+\mu)^2(3-4\nu) + 4\mu(1-2\nu)^2]}\right\} \qquad (B.26)$$

$$g_A = \frac{3(1-\mu)[\tfrac{1}{2}PR^2(1-K)] + BR^2[1+\mu(3-4\nu)]}{4[2 + \nu\mu - 3\nu]} \qquad (B.22)$$

405

<u>Step 2</u>

Derive the total stress and incremental displacement fields in the ground mass after excavation and the contact stresses at the ground-support interface. From the derivation for the revised relative stiffness solution, for n = 2 only, the stresses are (see Appendix A, Eq. A.18):

$$\sigma_r = a_o r^{-2} + \tfrac{1}{2}P(1+K) - \tfrac{1}{2}P(1-K)\cos2\theta - [6a_2' r^{-4} + 4b_2' r^{-2}]\cos2\theta$$

$$(B.28a)$$

$$\sigma_\theta = -a_o r^{-2} + \tfrac{1}{2}P(1+K) + \tfrac{1}{2}P(1-K)\cos2\theta + 6a_2' r^{-4}\cos2\theta$$

$$(B.28b)$$

$$\tau_{r\theta} = a_o' r^{-2} + \tfrac{1}{2}P(1-K)\sin2\theta - [6a_2' r^{-4} + 2b_2' r^{-2}]\sin2\theta$$

$$(B.28c)$$

The corresponding displacement field is (Appendix A, Eq. A.19):

$$u = \frac{1+\nu}{E}\{-a_o r^{-1} + \tfrac{1}{2}Pr(1+K) - \tfrac{1}{2}Pr(1-K)\cos2\theta \qquad (B.29a)$$

$$+[2a_2' r^{-3} + 4b_2' r^{-1}]\cos2\theta - \nu Pr(1+K) - 4\nu b_2' r^{-1}\cos2\theta\} - u_I$$

$$v = \frac{1+\nu}{E}\{\tfrac{1}{2}Pr(1-K)\sin2\theta + [2a_2' r^{-3} - 4(1-\nu)b_2' r^{-1}]\sin2\theta\} - v_I$$

$$(B.29b)$$

The initial displacements u_I and v_I in this case are given by (B.27) in Step 1. Subtracting these displacements from

(B.29) and using the relations:

$$A = \frac{1}{2}P(1+K)A_1; \quad A_1 = \frac{(1-\mu)(1-2\nu)}{[1+\mu(1-2\nu)]} \tag{B.30a}$$

$$B = \frac{1}{2}P(1-K)A_2; \quad A_2 = -\frac{(1-\mu)[1+\mu(3-4\nu)]}{[(1+\mu)^2(3-4\nu) + 4\mu(1-2\nu)^2]} \tag{B.30b}$$

$$g_A = \frac{1}{2}PR^2(1-K)A_3; \quad A_3 = \frac{3(1-\mu) + A_2[1+\mu(3-4\nu)]}{4[2 + \nu\mu - 3\nu]} \tag{B.30c}$$

gives the incremental (or net) displacement fields at r = R:

$$u = \frac{1+\nu}{E}\{-a_oR^{-1} + [2a_2'R^{-3}+4b_2'R^{-1}]\cos2\theta - 4\nu b_2'R^{-1}\cos2\theta$$

$$+ \frac{1}{2}PR(1+K)A_1 - \frac{1}{2}PR(1-K)[\frac{8A_3}{3} - 4\nu A_3 - \frac{A_2}{3}]\cos2\theta \} \tag{B.31a}$$

$$v = \frac{1+\nu}{E}\{2a_2'R^{-3} - 4(1-\nu)b_2'R^{-1}$$

$$+ \frac{1}{2}PR(1-K)[\frac{10}{3}A_3 - 4\nu A_3 + \frac{A_3}{3}]\}\sin2\theta \tag{B.31b}$$

The full-slip boundary conditions between the ground and the support at r = R are:

$$\sigma_{R,\text{support}} = \sigma_{R,\text{ground}} \tag{B.32a}$$

$$u_s = u \tag{B.32b}$$

407

$$\tau_{r\theta} = 0 \qquad\qquad\qquad\qquad\qquad \text{(B.32c)}$$

Taking the last boundary condition first, (B.28c) for the shear stresses becomes:

$$a_o' R^{-2} + \frac{1}{2}P(1-K)\sin 2\theta - [6a_2' R^{-4} + 2b_2' R^{-2}]\sin 2\theta = 0 \quad \text{(B.33)}$$

$$\therefore \quad a_o' = 0 \qquad\qquad\qquad\qquad\qquad \text{(B.34a)}$$

$$b_2' = \frac{1}{4}PR^2(1-K) - 3a_2' R^{-2} \qquad\qquad \text{(B.34b)}$$

To impose the other two boundary conditions, the differential stress-displacement equations for the liner are required (from Flugge, 1966):

$$\frac{d^2 v_s}{d\theta^2} + \frac{du_s}{d\theta} = -\frac{R^2}{D_c}\tau_{R\theta} \qquad\qquad \text{(B.35a)}$$

$$\frac{dv_s}{d\theta} + u_s + \frac{D_F}{D_c R^2}\left[\frac{d^4 u_s}{d\theta^4} + 2\frac{d^2 u_s}{d\theta^2} + u_s\right] = \frac{R^2}{D_c}\sigma_R$$

$$\text{(B.35b)}$$

$$\text{where:} \quad D_c = \frac{E_s A_s}{(1-\nu_s^2)} \quad D_F = \frac{E_s I_s}{(1-\nu_s^2)} \qquad \text{(B.35c)}$$

408

Substituting (B.32b) and (B.32c) into (B.35a) and integrating gives:

$$v_s = -\frac{1+\nu}{E}\left\{-(5-6\nu)a_2' R^{-3} + \frac{1}{2}PR(1-K)\left[1-\nu-\frac{4A_3}{3}+2\nu A_3+\frac{A_2}{6}\right]\right\}\sin 2\theta$$

(B.36)

Substituting (B.32a), (B.32b), and (B.36) into (B.35b) gives:

$$-a_o R^{-2} + \frac{1}{2}P(1+K)A_1 + \frac{C^*}{F^*}\left[-a_o \bar{R}^{-2} + \frac{1}{2}P(1+K)A_1\right.$$

$$\left. - 9\left[2(5-6\nu)a_2' R^{-4} + \frac{1}{2}P(1-K)(2\nu-2+\frac{8A_3}{3}-4\nu A_3-\frac{A_2}{3})\cos 2\theta\right]\right]$$

$$= C^*(1-\nu)\left\{a_o R^{-2} + \frac{1}{2}P(1+K) - \frac{1}{2}P(1-K)\cos 2\theta + [6a_2' R^{-4} - P(1-K)]\cos 2\theta\right\}$$

(B.37)

At $\theta = \pi/4$, (B.37) can be solved for a_o:

$$a_o = -\frac{1}{2}PR^2(1+K)a_o^*$$

(B.38a)

in which: $\quad a_o^* = \dfrac{C^*(1-\nu) - A_1(1+C^*/F^*)}{C^*(1-\nu) + (1+C^*/F^*)}$

(B.39

At $\theta = 0$, (B.37) can be solved for a_2':

$$a_2' = \frac{1}{2}PR^4(1-K)a_2^*$$

(B.39a)

in which: $\quad a_2^* = \dfrac{(F^*+6)(1-\nu) - 8A_3 + 12\nu A_3 + A_2}{2F^*(1-\nu) + 6(5-6\nu)}$ (B.39b)

Since it can be shown that $A_3 = -A_2$, the above expression for a_2^* can be further simplified to:

$$a_2^* = \frac{(F^*+6)(1-\nu) + A_2[1+4(2-3\nu)]}{2F^*(1-\nu) + 6(5-6\nu)}$$ (B.40)

Combining (B.28), (B.34), (B.38-40) produces the final expression for the contact stresses at $r = R$:

$$\sigma_R = \tfrac{1}{2}P(1+K)(1-a_o^*) - \tfrac{1}{2}P(1-K)(3-6a_2^*)\cos 2\theta$$ (B.41a)

$$\tau_{R\theta} = 0$$ (B.41b)

in which $\quad a_o^* = \dfrac{C^*(1-\nu) - A_1(1+C^*/F^*)}{C^*(1-\nu) + (1+C^*/F^*)}$ (B.42a)

$$a_2^* = \frac{(F^*+6)(1-\nu) + A_2[1+4(2-3\nu)]}{2F^*(1-\nu) + 6(5-6\nu)}$$ (B.42b)

$$A_1 = \frac{(1-\mu)(1-2\nu)}{[1+\mu(1-2\nu)]}$$ (B.42c)

$$A_2 = \frac{-(1-\mu)[1+\mu(3-4\nu)]}{[(1+\mu)^2(3-4\nu) + 4\mu(1-2\nu)^2]}$$ (B.42d)

$$C^* = \frac{ER(1-\nu_s^2)}{E_s A_s(1-\nu^2)}$$ (B.42e)

$$F^* = \frac{ER^3(1-\nu_s^2)}{E_s I_s (1-\nu^2)} \qquad (B.42f)$$

$$\mu = \frac{1}{1-\beta} \quad ; \quad (1-\beta) = \frac{E_B}{E_A} \qquad (B.42g)$$

Note that the form of (B.41) is the same as the equivalent equation (A.30) for the revised relative stiffness solution (Appendix A). Only the constants a_o^* and a_2^* change in the support delay solution.

Step 3

Compute the internal support forces induced by the contact stresses at the ground-support interface.

Since equations (B.41) for the contact stresses in the support delay solution are of the same form as (A.30) for the revised relative stiffness solution, the equations for the support thrust and moment coefficients in the revised relative stiffness solution (A.47) will also hold for the support delay derivation. Only the constants in the equations will change. For full-slip at the interface:

$$\frac{T}{PR} = \frac{1}{2}(1+K)(1-a_o^*) + \frac{1}{2}(1-K)(1-2a_2^*)\cos 2\theta \qquad (B.43a)$$

$$\frac{M}{PR^2} = \frac{1}{2}(1-K)(1-2a_2^*)\cos 2\theta \qquad (B.43b)$$

in which the constants a_o^* and a_2^* are given by (B.42)

411

B.3 HP97 PROGRAM FOR CORE MODULUS REDUCTION SOLUTION

The modified relative stiffness solution incorporating the approximate support delay effect derived in this Appendix has been programmed on a Hewlett-Packard Model HP97 desk top calculator. The operation of this program is very similar to that of the programs for the regular relative stiffness solutions in Appendix A. The input variables are initially stored in the registers as follows:

Register	Variable
0	β
1	C^*
2	F^*
3	ν
4	K
5	θ

Program A calculates the dimensionless thrust coefficient and the dimensionless moment coefficient. Program output consists of the following printed variables: 1) the value for β used in the analysis, and 2) the dimensionless thrust and moment coefficients.
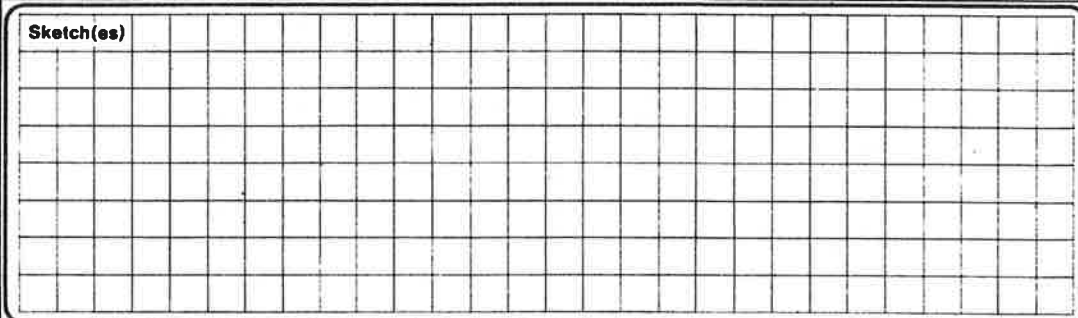
Core Modulus Reduction Solution

$$\frac{T}{PR} ; \frac{M}{PR^2}$$

STEP	INSTRUCTIONS	INPUT DATA/UNITS	KEYS		OUTPUT DATA/UNITS
1	LOAD SIDES 1 AND 2				
2	STORE INPUT DATA	β	STO	0	
		C^*	STO	1	
		F^*	STO	2	
		ν	STO	3	
		K	STO	4	
		θ	STO	5	
3	CALCULATE DIMENSIONLESS THRUST AND MOMENT COEFFICIENTS		A		β $\frac{T}{PR}$ $\frac{M}{PR^2}$

STEP	KEY ENTRY	KEY CODE	COMMENTS	STEP	KEY ENTRY	KEY CODE	COMMENTS
001	*LBLA	21 11		057	1	01	
002	1	01		058	+	-55	
003	ENT↑	-21		059	1	01	
004	RCL3	36 03		060	RCL6	36 06	
005	2	02		061	-	-45	
006	x	-35		062	x	-35	
007	-	-45		063	CHS	-22	
008	STOB	35 12		064	RCLE	36 15	
009	3	03		065	÷	-24	
010	ENT↑	-21		066	STOB	35 08	
011	RCL3	36 03		067	RCL1	36 01	
012	4	04		068	RCLD	36 14	
013	x	-35		069	x	-35	
014	-	-45		070	1	01	
015	STOC	35 13		071	+	-55	
016	1	01		072	RCL1	36 01	
017	RCL3	36 03		073	RCL2	36 02	
018	-	-45		074	÷	-24	
019	STOD	35 14		075	+	-55	
020	RCL0	36 00		076	STOE	35 15	
021	SPC	16-11		077	1	01	
022	PRTX	-14		078	RCL1	36 01	
023	CHS	-22		079	RCL2	36 02	
024	1	01		080	÷	-24	
025	+	-55		081	+	-55	
026	1/X	52		082	RCL7	36 07	
027	STO6	35 06		083	x	-35	
028	1	01		084	CHS	-22	
029	RCL6	36 06		085	RCL1	36 01	
030	-	-45		086	RCLD	36 14	
031	RCLB	36 12		087	x	-35	
032	x	-35		088	+	-55	
033	RCLB	36 12		089	RCLE	36 15	
034	RCL6	36 06		090	÷	-24	
035	x	-35		091	STO9	35 09	
036	1	01		092	2	02	
037	+	-55		093	RCL2	36 02	
038	÷	-24		094	x	-35	
039	STO7	35 07		095	RCLD	36 14	
040	1	01		096	x	-35	
041	RCL6	36 06		097	5	05	
042	+	-55		098	RCL3	36 03	
043	X²	53		099	6	06	
044	RCLC	36 13		100	x	-35	
045	x	-35		101	-	-45	
046	RCLB	36 12		102	6	06	
047	X²	53		103	x	-35	
048	RCL6	36 06		104	+	-55	
049	x	-35		105	STOE	35 15	
050	4	04		106	2	02	
051	x	-35		107	ENT↑	-21	
052	+	-55		108	RCL3	36 03	
053	STOE	35 15		109	3	03	
054	RCLC	36 13		110	x	-35	
055	RCL6	36 06		111	-	-45	
056	x	-35		112	4	04	

REGISTERS

0 β	1 C^*	2 F^*	3 ν	4 K	5 θ	6 USED	7 USED	8 USED	9 USED
S0	S1	S2	S3	S4	S5	S6	S7	S8	S9

A USED	B USED	C USED	D USED	E USED	I

STEP	KEY ENTRY	KEY CODE	COMMENTS	STEP	KEY ENTRY	KEY CODE	COMMENTS
113	x	-35		170			
114	1	01					
115	+	-55					
116	RCL8	36 08					
117	x	-35					
118	RCL2	36 02					
119	6	06					
120	+	-55					
121	RCLD	36 14					
122	x	-35					
123	+	-55					
124	RCLE	36 15		180			
125	÷	-24					
126	STOA	35 11					
127	2	02					
128	x	-35					
129	CHS	-22					
130	1	01					
131	+	-55					
132	1	01					
133	RCL4	36 04					
134	-	-45		190			
135	x	-35					
136	2	02					
137	÷	-24					
138	2	02					
139	RCL5	36 05					
140	x	-35					
141	COS	42					
142	x	-35					
143	STOE	35 15					
144	1	01		200			
145	RCL9	36 09					
146	-	-45					
147	1	01					
148	RCL4	36 04					
149	+	-55					
150	x	-35					
151	2	02					
152	÷	-24					
153	RCLE	36 15		210			
154	+	-55					
155	PRTX	-14					
156	RCLE	36 15					
157	PRTX	-14					
158	RTN	24					
159	R/S	51					
160							
				220			

LABELS

A T/PR; M/PR²	B	C	D	E
a	b	c	d	e
0	1	2	3	4
5	6	7	8	9

FLAGS

0
1
2
3

SET STATUS

FLAGS		TRIG	DISP
	ON OFF		
0	☐ ☒	DEG ☒	FIX ☐
1	☐ ☒	GRAD ☐	SCI ☒
2	☐ ☒	RAD ☐	ENG ☐
3	☐ ☒		n 2

Program Description II

Sketch(es)

Sample Problem(s) A BOLTED, PRECAST CONCRETE LINED TUNNEL IN A STIFF CLAY DEPOSIT, HAVING THE FOLLOWING PROPERTIES:

$$C^* = 0.05 \quad F^* = 100.0 \quad \nu = 0.4 \quad K = 0.5$$

COMPUTE THE THRUST AND MOMENT COEFFICIENTS AT $\theta = 30°$ FOR $\beta = 0.25$

Solution(s)

$$\beta = 2.50 - 01$$

$$\frac{T}{PR} = 6.97 - 01$$

$$\frac{M}{PR^2} = 6.80 - 03$$

Reference(s)

416

APPENDIX C

HP97 PROGRAMS FOR CALCULATING
THE GROUND YIELD FACTOR

The iterative solution of Eq. (6.10) for the equilibrium support pressure for a tunnel in a yielding ground mass has been programmed on a Hewlett-Packard Model HP97 desk top calculator. Program listings and documentation are provided in this Appendix for solutions incorporating the following two formulations for the ground characteristic curve $f_g(P)$:

1) Constant total volume in the yielded zone (Solution B.1 in Section 4)

2) Fully dilatant ground behavior in the yielded zone, governed by the associated plastic flow rule (Solution B.4 in Section 4)

Both of these programs use the same input format. The input variables are initially stored in the registers as follows:

Register	Variable	Description
1	E'	Plane strain elastic modulus for ground
2	ν'	Plane strain Poisson's ratio for ground
3	E'_s	Plane strain elastic modulus for support
4	A_s	Cross-sectional area of support (effective)
5	R	Tunnel radius
6	P	Vertical in situ ground stress
7	u_o	Total offset of support characteristic curve

417

Register	Variable	Description
8	c	cohesion (or undrained shear strength)
9	ϕ	friction angle for ground

To run the program, an initial nonzero guess for the thrust coefficient is entered and Program A is executed. The program iteratively searches for the true thrust coefficient, pausing after each iteration loop to display the current value for the thrust coefficient. When convergence is reached, the program prints the equilibrium thrust coefficient, the normalized radius of the plastic zone (R/R_p), and the total ground displacement, u, at equilibrium.

In order to calculate the ground yield factor λ_y, the program must be run twice. The first time, the correct ground strength properties are used, the ground is allowed to yield, and the thrust coefficient $\frac{T^*}{PR}$ for the yielding ground case is computed. The second time, the ground strength is set artificially high to prevent ground yielding (e.g., by setting c = P), and the thrust coefficient $\frac{T'}{PR}$ for the elastic case is computed. The ground yield factor is then given as:

$$\lambda_y = \frac{T^*/PR}{T'/PR}$$

418

Program Description I

Program Title ANALYSIS FOR YIELDING + SUPPORT DELAY

Contributor's Name _____

Address _____

City _____ **State** _____ **Zip Code** _____

Program Description, Equations, Variables ITERATES TO FIND ROOTS OF THE FOLLOWING FUNCTION:

$$F[P] = f_g[P] - f_s[P] - u_o = 0$$

IN WHICH: $f_g(P) = u_g$ = NET GROUND DISPLACEMENT AS A FUNCTION OF PRESSURE. BASED ON PLANE STRAIN PLASTICITY SOL'NS DERIVED IN CHAPTER 4.

$f_s(P) = u_s$ = SUPPORT DISPLACEMENT AS A FUNCTION OF PRESSURE (FROM THIN WALLED CYLINDER SOL'N)

u_o = OFFSET OF SUPPORT CHARACTERISTIC CURVE

PROGRAM CAN BE USED TO:

a) FIND VALUE OF P_R CORRESPONDING TO THE ROOT OF F(P)

b) FIND $u_g = f_g(P)$ (GROUND CHARACTERISTIC CURVE)

Operating Limits and Warnings CONVERGENCE SPEED IS A FUNCTION OF THE ACCURACY OF THE INITIAL ESTIMATE. IF ERROR OCCURS DURING ITERATION:

1) CHECK THAT PRIMARY REGISTERS ARE ACCESSIBLE TO PROGRAM; IF NOT, $\boxed{P \leftrightarrow S}$

2) ENTER A DIFFERENT INITIAL ESTIMATE; KEY $\boxed{A}$

ANALYSIS FOR YIELDING + SUPPORT DELAY
$\Delta V^T = 0$ (SOL'N B.1 IN CH.4)

◄ 1 $\boxed{I}$ $\boxed{PR}$ GUESS 2 ►

STEP	INSTRUCTIONS	INPUT DATA/UNITS	KEYS		OUTPUT DATA/UNITS
1	LOAD SIDES 1 AND 2				
2	STORE INPUT DATA (CONSISTENT UNITS):	E'	STO	1	
		ν'	STO	2	
		E'_s	STO	3	
		A_s	STO	4	
		R	STO	5	
		P	STO	6	
	$(u_o < u_f)$	u_o	STO	7	
		c	STO	8	
	(NONZERO)	$\emptyset$	STO	9	
3	IF $u_g = f_g(P)$ IS DESIRED, GO TO STEP 6.				
4	ENTER INITIAL ESTIMATE FOR T/PR; PROGRAM ITERATES FOR CORRECT T/PR, PAUSING AND DISPLAYING CURRENT VALUE AFTER EACH CYCLE	T/PR	↑	A	
5	CONVERGENCE; PRINTED RESULTS:				T/PR
					R_p/R
					u_g
6	CALCULATE: $u_a = f_g(P)$ DIRECTLY. INITIALIZE PROGRAM		F	a	
7	ENTER PRESSURE	P	↑		
8	CALCULATE u_g		F	b	u_g

STEP	KEY ENTRY	KEY CODE	COMMENTS	STEP	KEY ENTRY	KEY CODE	COMMENTS
001	*LBLA	21 11	INITIALIZE PROGRAM REGISTERS	057	GTO6	22 06	
002	RCL6	36 06		058	RTN	24	
003	x	-35		059	*LBLC	21 13	PRINT FINAL RESULTS:
004	STO0	35 00		060	SPC	16-11	
005	GSBa	23 16 11		061	RCL0	36 00	$\frac{T}{PR}$
006	RCL0	36 00		062	RCL6	36 06	
007	EEX	-23	$\Delta P = 0.01 P$	063	÷	-24	
008	CHS	-22		064	PRTX	-14	
009	2	02		065	RCLE	36 15	$\frac{R_P}{R}$
010	%	55		066	PRTX	-14	
011	STOC	35 13		067	RCL0	36 00	
012	2	02		068	RCL5	36 05	u_g
013	÷	-24		069	X²	53	
014	-	-45	$F(P_i - \frac{\Delta P}{2})$	070	x	-35	
015	STOA	35 11		071	RCL3	36 03	
016	STO0	35 00		072	÷	-24	
017	GSBB	23 12		073	RCL4	36 04	
018	STOD	35 14		074	÷	-24	
019	RCLA	36 11		075	RCL7	36 07	
020	RCLC	36 13		076	+	-55	
021	+	-55	$F(P_i + \frac{\Delta P}{2})$	077	PRTX	-14	
022	STO0	35 00		078	RTN	24	
023	GSBB	23 12		079	*LBLB	21 12	
024	STOB	35 12		080	GSBb	23 16 12	
025	GTO0	22 00		081	RCL0	36 00	
026	*LBL6	21 06	$F(P_n')$	082	RCL5	36 05	
027	RCL0	36 00		083	X²	53	CALCULATE $F(P_n)$
028	GSBB	23 12		084	x	-35	
029	STOB	35 12		085	RCL3	36 03	
030	*LBL0	21 00	SECANT METHOD CALCULATES CORRECTION FOR P & SETS VALUES FOR NEXT LOOP	086	÷	-24	
031	RCLA	36 11		087	RCL4	36 04	
032	RCL0	36 00		088	÷	-24	
033	STOA	35 11		089	-	-45	
034	-	-45		090	RCL7	36 07	
035	RCLD	36 14		091	-	-45	
036	RCLB	36 12		092	RTN	24	
037	STOD	35 14		093	*LBLa	21 16 11	INITIALIZE PROGRAM REGISTERS FOR $f_g(P)$ CALCULATION
038	-	-45		094	RCL5	36 05	
039	÷	-24		095	RCL1	36 01	
040	x	-35		096	÷	-24	
041	ST-0	35-45 00		097	STOA	35 11	
042	RCL0	36 00	PAUSE AND DISPLAY CURRENT ESTIMATE	098	RCL2	36 02	
043	RCL6	36 06		099	STOB	35 12	
044	÷	-24		100	1	01	
045	PSE	16 51		101	RCL9	36 09	
046	RCL0	36 00		102	SIN	41	
047	RCLA	36 11	ACCURATE TO 0.1 % ?	103	+	-55	
048	-	-45		104	1	01	
049	RCLA	36 11		105	RCL9	36 09	
050	÷	-24		106	SIN	41	
051	ABS	16 31		107	-	-45	
052	EEX	-23		108	÷	-24	
053	CHS	-22		109	STOC	35 13	
054	3	03		110	2	02	
055	X>Y?	16-34		111	RCL8	36 08	
056	GTOC	22 13		112	x	-35	

REGISTERS

0 P_n	1 E'	2 ν'	3 E_s'	4 A_s	5 R	6 P	7 u_a	8 c	9 ϕ
S0 P_n	S1 R/E'	S2 ν'	S3 N_ϕ	S4 USED	S5 P	S6 σ_u	S7	S8	S9
A P_{n-1}	B $F(P_n)$	C ΔP	D $F(P_{n-1})$	E R_P/R	I				

421

STEP	KEY ENTRY	KEY CODE	COMMENTS	STEP	KEY ENTRY	KEY CODE	COMMENTS
113	RCL9	36 09		169	RCL3	36 03	
114	COS	42		170	1	01	
115	x	-35		171	-	-45	$u_g = f_g(P)$
116	1	01		172	x	-35	
117	RCL9	36 09		173	RCL6	36 06	WHEN
118	SIN	41		174	+	-55	
119	-	-45		175	RCL3	36 03	$\dfrac{R_P}{R} \geqslant 1$
120	÷	-24		176	1	01	
121	STOD	35 14		177	+	-55	
122	RCLC	36 13		178	÷	-24	
123	1	01		179	RCLE	36 15	
124	-	-45		180	X²	53	
125	÷	-24		181	x	-35	
126	STOE	35 15		182	1	01	
127	RCL6	36 06		183	RCL2	36 02	
128	P≷S	16-51		184	+	-55	
129	STO5	35 05	STORE VARIABLES	185	x	-35	
130	RCLE	36 15	IN SECONDARY	186	+	-55	
131	STO4	35 04	REGISTERS	187	RCL1	36 01	
132	RCLD	36 14		188	x	-35	
133	STO6	35 06		189	GTOd	22 16 14	
134	RCLC	36 13		190	*LBLc	21 16 13	$u_g = f_g(P)$
135	STO3	35 03		191	RCL5	36 05	
136	RCLB	36 12		192	RCL0	36 00	WHEN
137	STO2	35 02		193	-	-45	
138	RCLA	36 11		194	1	01	$\dfrac{R_P}{R} < 1$
139	STO1	35 01		195	RCL2	36 02	
140	P≷S	16-51		196	+	-55	
141	RTN	24		197	x	-35	
142	*LBLb	21 16 12		198	RCL1	36 01	
143	P≷S	16-51	EVALUATE $f_g(P)$	199	x	-35	
144	STO0	35 00		200	*LBLd	21 16 14	
145	RCL4	36 04		201	P≷S	16-51	
146	+	-55		202	RTN	24	
147	1	01		203	R/S	51	
148	RCL3	36 03					
149	+	-55					
150	x	-35					
151	1/X	52					
152	RCL5	36 05					
153	RCL4	36 04	CALCULATE	210			
154	+	-55					
155	x	-35	$\dfrac{R_P}{R'}$				
156	2	02					
157	x	-35					
158	RCL3	36 03					
159	1	01					
160	-	-45					
161	1/X	52					
162	Yˣ	31					
163	STOE	35 15					
164	1	01		220			
165	-	-45					
166	X<0?	16-45	$\dfrac{R_P}{R} < 1$?				
167	GTOc	22 16 13					
168	RCL5	36 05					

LABELS					FLAGS	SET STATUS		
A ROOT F(P)	B USED	C USED	D	E	0			
a INIT. f_g(P)	b f_g(P)	c USED	d USED	e	1			
0 USED	1	2	3	4	2			
5	6 USED	7	8	9	3			

FLAGS		TRIG	DISP
	ON OFF		
0	☐ ☒	DEG ☒	FIX ☐
1	☐ ☒	GRAD ☐	SCI ☒
2	☐ ☒	RAD ☐	ENG ☐
3	☐ ☒		n 2

ANALYSIS FOR YIELDING + SUPPORT DELAY
FULLY DILATANT GROUND
(SOL'N E.4 IN CHAPTER 4)

◀1   [§] [I PR GUESS]   2▶

STEP	INSTRUCTIONS	INPUT DATA/UNITS	KEYS	OUTPUT DATA/UNITS
	SAME INSTRUCTIONS AS IN PRECEDING PROGRAM			
	(THIS PROGRAM IS BASED ON THE DERIVATION PRESENTED BY HENDRON + AIYER, 1972)			

423

STEP	KEY ENTRY	KEY CODE	COMMENTS
001	*LBLA	21 11	INITIALIZE PROGRAM REGISTERS
002	F2?	16 23 02	
003	P≷S	16-51	
004	RCL6	36 06	
005	x	-35	
006	STO8	35 00	
007	GSBa	23 16 11	
008	RCL0	36 00	$\Delta P = 0.01\, P_1$
009	EEX	-23	
010	CHS	-22	
011	2	02	
012	%	55	
013	STOC	35 13	
014	2	02	$F\left(P_1 - \dfrac{\Delta P}{2}\right)$
015	÷	-24	
016	-	-45	
017	STOA	35 11	
018	STO0	35 00	
019	GSBB	23 12	
020	STOD	35 14	
021	RCLA	36 11	$F\left(P_1 + \dfrac{\Delta P}{2}\right)$
022	RCLC	36 13	
023	+	-55	
024	STO0	35 00	
025	GSBB	23 12	
026	STOB	35 12	
027	GTO8	22 00	EVALUATE $F(P_n)$
028	*LBL6	21 06	
029	RCL0	36 00	
030	GSBB	23 12	
031	STOB	35 12	
032	*LBL0	21 00	SECANT METHOD CALCULATES CORRECTION FOR P AND SETS VALUES FOR NEXT LOOP
033	RCLA	36 11	
034	RCL0	36 00	
035	STOA	35 11	
036	-	-45	
037	RCLD	36 14	
038	RCLB	36 12	
039	STOD	35 14	
040	-	-45	
041	÷	-24	
042	x	-35	
043	ST-0	35-45 00	
044	RCL0	36 00	PAUSE AND DISPLAY CURRENT ESTIMATE
045	RCL6	36 06	
046	÷	-24	
047	PSE	16 51	
048	RCL0	36 00	
049	RCLA	36 11	ACCURATE TO 0.1%?
050	-	-45	
051	RCLA	36 11	
052	÷	-24	
053	ABS	16 31	
054	EEX	-23	
055	CHS	-22	
056	3	03	

STEP	KEY ENTRY	KEY CODE	COMMENTS
057	X>Y?	16-34	
058	GTOC	22 13	
059	GTO6	22 06	
060	RTN	24	
061	*LBLC	21 13	PRINT FINAL RESULTS: $\dfrac{T}{PR}$ $\dfrac{R_p}{R}$ u_g
062	SPC	16-11	
063	RCL0	36 00	
064	RCL6	36 06	
065	÷	-24	
066	PRTX	-14	
067	RCLE	36 15	
068	PRTX	-14	
069	RCL0	36 00	
070	RCL5	36 05	
071	X²	53	
072	x	-35	
073	RCL3	36 03	
074	÷	-24	
075	RCL4	36 04	
076	÷	-24	
077	RCL7	36 07	
078	+	-55	
079	PRTX	-14	
080	RTN	24	
081	*LBLB	21 12	CALCULATE $F(P_n)$
082	GSBb	23 16 12	
083	RCL0	36 00	
084	RCL5	36 05	
085	X²	53	
086	x	-35	
087	RCL3	36 03	
088	÷	-24	
089	RCL4	36 04	
090	÷	-24	
091	-	-45	
092	RCL7	36 07	
093	-	-45	
094	RTN	24	
095	*LBLa	21 16 11	INITIALIZE PROGRAM REGISTERS FOR $f_g(P)$ CALCULATION
096	RCL5	36 05	
097	RCLi	36 01	
098	÷	-24	
099	STOA	35 11	
100	1	01	
101	RCL2	36 02	
102	-	-45	
103	STOB	35 12	
104	1	01	
105	RCL9	36 09	
106	SIN	41	
107	+	-55	
108	1	01	
109	RCL9	36 09	
110	SIN	41	
111	-	-45	
112	÷	-24	

REGISTERS

0 P_n	1 E'	2 ν'	3 E'_s	4 A_s	5 R	6 P	7 u_o	8 c	9 $\emptyset$
S0 P_n	S1 R/E'	S2 $(1-\nu')$	S3 $N\emptyset$	S4 USED	S5 P	S6	S7	S8	S9

A P_{n-1}	B $F(P_n)$	C ΔP	D $F(P_{n-1})$	E R_p/R	I

424

STEP	KEY ENTRY	KEY CODE	COMMENTS	STEP	KEY ENTRY	KEY CODE	COMMENTS
113	STOC	35 13		169	–	-45	$\frac{R_p}{R} \leq 1$?
114	1	01		170	X<0?	16-45	
115	–	-45		171	GTOc	22 16 13	
116	1/X	52		172	RCLE	36 15	
117	2	02		173	2	02	
118	x	-35		174	RCL3	36 03	
119	RCL8	36 08		175	x	-35	
120	x	-35		176	Yˣ	31	
121	RCL9	36 09		177	RCL3	36 03	
122	COS	42		178	1	01	
123	x	-35		179	+	-55	
124	1	01		180	x	-35	
125	RCL9	36 09		181	RCL3	36 03	$\frac{R_p}{R} \geq 1$
126	SIN	41		182	+	-55	
127	–	-45		183	1	01	
128	÷	-24		184	–	-45	
129	STOD	35 14		185	RCL3	36 03	
130	RCL6	36 06		186	1	01	
131	P≷S	16-51		187	–	-45	
132	SF2	16 21 02	STORE VARIABLES	188	x	-35	
133	ST05	35 05	IN SECONDARY	189	2	02	
134	RCLD	36 14	REGISTERS	190	÷	-24	
135	ST04	35 04		191	RCL3	36 03	
136	RCLC	36 13		192	÷	-24	
137	ST03	35 03		193	RCL0	36 00	
138	RCLB	36 12		194	RCL4	36 04	
139	ST02	35 02		195	+	-55	
140	RCLA	36 11		196	x	-35	
141	ST01	35 01		197	GTOd	22 16 14	
142	P≷S	16-51		198	*LBLc	21 16 13	
143	CF2	16 22 02		199	RCL5	36 05	$\frac{R_p}{R} < 1$
144	RTN	24		200	RCL0	36 00	
145	*LBLb	21 16 12		201	–	-45	
146	P≷S	16-51	EVALUATE $f_g(P)$	202	2	02	
147	SF2	16 21 02		203	x	-35	
148	ST08	35 00		204	*LBLd	21 16 14	
149	RCL4	36 04		205	RCL0	36 00	
150	+	-55		206	RCL5	36 05	
151	1	01		207	–	-45	
152	RCL3	36 03		208	RCL2	36 02	$u_g = f_g(P)$
153	+	-55	CALCULATE	209	x	-35	
154	x	-35		210	+	-55	
155	1/X	52	$\frac{R_p}{R}$	211	RCL1	36 01	
156	RCL5	36 05		212	x	-35	
157	RCL4	36 04		213	P≷S	16-51	
158	+	-55		214	CF2	16 22 02	
159	x	-35		215	RTN	24	
160	2	02		216	R/S	51	
161	x	-35					
162	RCL3	36 03					
163	1	01					
164	–	-45		220			
165	1/X	52					
166	Yˣ	31					
167	STOE	35 15					
168	1	01					

LABELS					FLAGS		SET STATUS		
A Root F(P)	B USED	C USED	D	E	0		FLAGS	TRIG	DISP
a Init. $f_g(P)$	b $f_g(P)$	c USED	d USED	e	1		ON OFF		
0 USED	1	2	3	4	2 SECONDARY REGISTERS		0 ☐ ☒	DEG ☒	FIX ☐
5	6 USED	7	8	9	3		1 ☐ ☒	GRAD ☐	SCI ☒
							2 ☐ ☒	RAD ☐	ENG ☐
							3 ☐ ☒		n 2

Program Description II

Sketch(es)

Sample Problem(s)

$E' = 10,000$ $\nu' = 0.67$ $E_s' = 4 \times 10^6$

$A_s = 5.0$ $R = 150$ $P = 200$

$u_\Delta = 3.5$ $c = 10.0$ $\phi = 25°$

a) FIND $\frac{T}{PR}$, GIVEN INITIAL ESTIMATE OF 0.3

b) FIND λ_y

c) CALCULATE u_g FOR $P = 10$

Solution(s)

	SOLUTION B.1	SOLUTION B.4
a)	$T/PR = 3.62-01$ $R_P/R = 1.24+00$ $u_g = 3.58+00$	$T/PR = 3.92-01$ $R_P/R = 1.18+00$ $u_g = 3.59+00$
b)	$\lambda_y = 1.26$	$\lambda_y = 1.36$
c)	$u_g = 1.60+01$	$u_g = 5.38+01$

Reference(s) THESE PROGRAMS ARE BASED IN PART ON THE HEWLETT - PACKARD STANDARD PAC PROGRAM No. 11, "CALCULUS AND ROOTS OF $f(x)$"

426

APPENDIX D

REPORT OF NEW TECHNOLOGY

The work performed under this contract has led to the development of improved practical design tools to provide more accurate representations of the ground-structure interaction in tunneling. In this volume, a simplified analysis for ground-structure interaction in tunneling was developed by isolating the major factors that have an overriding influence on support loads, namely:

1) relative stiffness of support and ground mass,

2) spatial lag or delay of support construction behind tunnel face,

3) yielding of ground mass as its shear strength is exceeded.